INVERSION METHOD FOR
SPECTRAL ANALYSIS OF SURFACE WAVES (SASW)

A Thesis
Presented to
The Academic Faculty

by

M. Catalina Orozco

In Partial Fulfillment of the Requirements for the Degree
Doctor of Philosophy in Civil and Environmental Engineering

Georgia Institute of Technology
November 2003

INVERSION METHOD FOR
SPECTRAL ANALYSIS OF SURFACE WAVES (SASW)

Approved by:

Dr. Glenn J. Rix, Advisor   Dr. Paul Mayne

Dr. Lawrence Jacobs   Dr. Carlos Santamarina

Dr. Tim Long   Date Approved: January 6, 2004

ACKNOWLEDGEMENTS

TABLE OF CONTENTS

LIST OF TABLES

LIST OF FIGURES

LIST OF SYMBOLS OR ABBREVIATIONS

$\Delta \mathbf{c}$ difference between observed and theoretical phase velocities

$\Delta \mathbf{p}$ change in model parameters from one iteration to the next

$\partial^2 S / \partial vs^2$ Hessian of S (S is the cost function used in the maximum likelihood method)

$\partial S / \partial vs$ gradient of S (S is the cost function used in the maximum likelihood method)

λ wavelength for Rayleigh wave (i.e., phase velocity divided by frequency)

Λ diagonal matrix with elements, which are the the singular values of $\mathbf{J}$

$\rho_{i,j}$ correlation coefficient for V_s between layers i and j

σ_vr standard deviations of the experimental phase velocities

σ_vs_f final (i.e., after inversion) standard deviation values of the shear wave velocities

σ_vs_{pr} prior (i.e., before inversion) standard deviation values of the shear wave velocities

c   phase velocity of Rayleigh waves

$\mathbf{C\_vr}$ covariance matrix of the experimental dispersion data

$\mathbf{C\_vs}_f$ posterior covariance matrix (the covariance matrix of $\mathbf{vs}_f$)

$C\_vs_f(\alpha,\beta)$ covariance between layer α and layer β, i.e., the element in row α and column β of matrix $\mathbf{C\_vs}_f$

$C\_vs_f(\alpha,\alpha)$ variance of layer α, i.e., the element in row α and column α of matrix $\mathbf{C\_vs}_f$

$\mathbf{C\_vs}_{pr}$ prior covariance matrix (the covariance matrix of $\mathbf{vs}_{pr}$)

E(k)   "evidence" for Bayesian model selection

$\mathbf{e}_{RMS}$ root mean square error

f	frequency
G_o	shear modulus at the surface
G_∞	shear modulus at infinite depth
$G(z)$	shear modulus at depth z
I	identity matrix
J	matrix of partial derivatives of the phase velocities with respect to the shear wave velocities (i.e., $\partial V_r/\partial V_s$)
J_f	matrix of partial derivatives evaluated at vs_f,
k	wave number
$L(\mathbf{vs}^i)$	likelihood of $\mathbf{vs}^i$
N, N_d or N_{freq}	number of points that describe the dispersion curve
N_p	number of model parameters (i.e., number of layers taking into account the half space)
NP	number of satisfactory V_s profiles,
pdf	probability density function
p	vector of model parameters
R	linearized resolution operator (i.e., resolution matrix)
r(**...**)	forward algorithm applied to the model parameters **vs**
$res(...)$	non-linear resolution operator.
rms	root mean square error (equal to $\mathbf{w\_e_{RMS}}$)
SASW	Spectral Analysis of Surface Waves
S(**vs**)	cost function used in maximum likelihood method
U	matrix whose columns are eigenvectors associated with the columns of **J**
V	matrix whose columns are eigenvectors associated with the rows of **J**
V_p	compressional wave velocity

V_r	Rayleigh wave phase velocity
$\mathbf{vr}_{ex}$	experimental phase velocity vector
$\mathbf{vr}_{th}$	theoretical phase velocity vector
V_s	shear wave velocity
$V_{s\_empirical}$	empirical estimate of shear wave velocity
$\mathbf{vs}$	vector of model parameters (i.e., shear wave velocities)
$\overline{\mathbf{vs}}$	vector of average V_s values
$\mathbf{<vs>}$	vector of mathematical expectations of the V_s values
$\left\langle vs_\alpha \right\rangle$	α component of the vector $\mathbf{<vs>}$ (corresponding to the mathematical expectation of V_s for layer α)
$\mathbf{vs}^i$	vector of V_s values that describe one satisfactory V_s profile
$vs_\alpha{}^i$	α component of the vector $\mathbf{vs}^i$ (corresponding to V_s for layer α)
$\mathbf{vs}_f$	final V_s vector obtained with the maximum likelihood method (maximum likelihood point)
$\mathbf{vs}_n$	model parameter vector at iteration n (for the iterative maximum likelihood inversion algorithm)
$\mathbf{vs}_{n+1}$	model parameter vector at iteration n+1 (for the iterative maximum likelihood inversion algorithm)
$\mathbf{vs}_{pr}$	initial shear wave velocity vector (starting point for the iterative maximum likelihood inversion algorithm)
$\mathbf{W}$	diagonal matrix with elements equal to the inverse of the standard deviations of the experimental phase velocities
$\mathbf{w\_e_{RMS}}$	weighted root mean square error (herein called rms)
Z_{band}	distance over which the layer properties are assumed to be correlated
z_{eq}	equivalent depth for the empirical estimate of the shear wave velocity variation with depth

SUMMARY

This research focuses on estimating the shear wave velocity (V_s) profile based on the dispersion curve obtained from SASW field test data (i.e., inversion of SASW data). It is common for the person performing the inversion to assume the prior information required to constrain the problem based on his/her own judgment. Additionally, the V_s profile is usually shown as unique without giving a range of possible solutions. For these reasons, this work focuses on: (i) studying the non-uniqueness of the solution to the inverse problem; (ii) implementing an inversion procedure that presents the estimated model parameters in a way that reflects their uncertainties; and (iii) evaluating tools that help choose the appropriate prior information.

One global and one local search procedures were chosen to accomplish these purposes: a pure Monte Carlo method and the maximum likelihood method, respectively. The pure Monte Carlo method was chosen to study the non-uniqueness by looking at the range of acceptable solutions (i.e., V_s profiles) obtained with as few constraints as possible. The maximum likelihood method was chosen because it is a statistical approach, which enables us to estimate the uncertainties of the resulting model parameters and to apply tools such as the Bayesian criterion to help select the prior information objectively.

The above inversion methods were implemented for synthetic data, which was produced with the same forward algorithm used during inversion. This implies that all uncertainties were caused by the nature of the SASW inversion problem (i.e., there were no

uncertainties added by experimental errors in data collection, analysis of the data to create the dispersion curve, layered model to represent a real 3-D soil stratification, or wave propagation theory). At the end of the research, the maximum likelihood method of inversion and the tools for the selection of prior information were successfully used with real experimental data obtained in Memphis, Tennessee.

<div align="center">

CHAPTER 1

INTRODUCTION

</div>

1.1 Brief Description of SASW Testing

The surface wave test commonly known as Spectral Analysis of Surface Waves (SASW) is a non-intrusive field method that can be used to evaluate the shear wave velocity (V_s) profile of near-surface soils. The V_s profile is commonly represented by a layered profile with each layer having constant V_s and the last layer being a half-space also with constant V_s (Figure 1.1).

Layer 1 – V_{s1}
Layer 2 – V_{s2}
$\vdots$
Layer n-1 – $V_{s(n-1)}$
Layer n – $V_{s(n)}$
Half-Space – $V_{s(HS)}$

<div align="center">
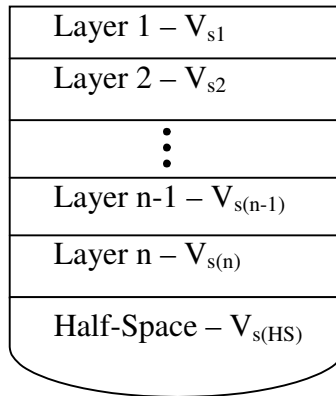
Figure 1.1 Layered V_s profile

</div>

The test consists of measuring vertical ground motions at the surface created by an active source (an impulsive or harmonic force at the surface) or by a passive source (microtremors and/or cultural noise). The sensors are commonly located in a linear array

<div align="center">

1

</div>

with the source when using an active source (Figure 1.2) and in a two-dimensional array when using passive sources (since the locations of these sources are often unknown).
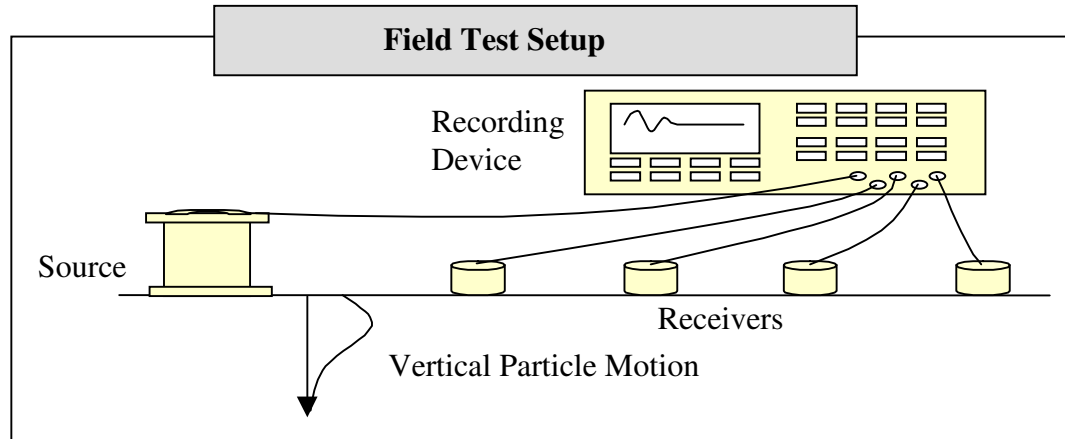
Figure 1.2 Typical field test setup for active surface wave testing

From the SASW test measurements, the dispersion characteristics of the site are calculated and represented with a dispersion curve in which one or more values of phase velocity (V_r) are associated with each frequency (f) (Figure 1.3).

After obtaining the dispersion relation, an inversion algorithm is used to obtain the V_s profile of the site (Figure 1.4). For more detail on the general characteristics of this method see Stokoe et al. (1994), Tokimatsu (1997), and Rix et al. (2001). The focus of this dissertation is the inversion of SASW data.
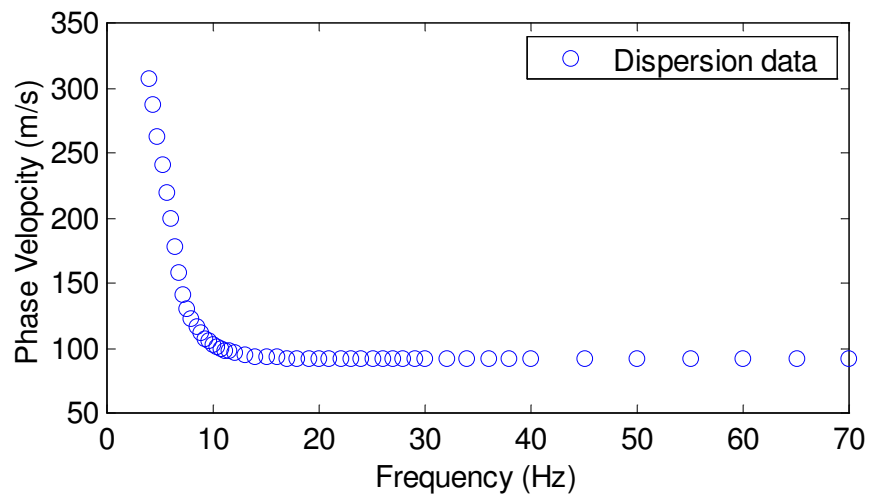
Figure 1.3 Sample dispersion SASW data
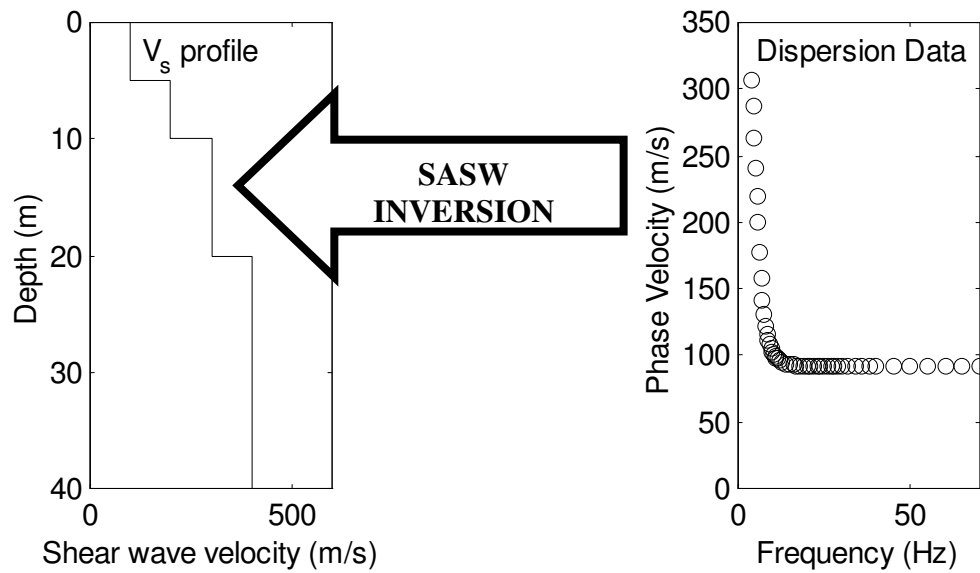
Figure 1.4 SASW Inversion

1.2 Statement of Problem

It is common to present the inverted V_s profile as a unique profile without showing a range of possible solutions or some type of error bars, such as the standard deviation for the V_s of each layer. Additionally, to constrain the problem and reduce the non-uniqueness (i.e., the dispersion curve by itself is insufficient to obtain a unique V_s profile) it is necessary to add some information (such as number of layers, depth to half-space, and initial V_s values) a priori, and it is common for the person performing the inversion to assume the required prior information based on his or her own judgment. For this reason, surface wave inversion is subjective, and potential users of the V_s profiles often have little confidence in its results. Thus, to make the approach as objective as possible, it is important to estimate not only the V_s values but also their related uncertainties, and to have tools to evaluate and choose the prior information that constraints the problem.

The main objectives of this research are:(i) to study the non-uniqueness of the solution to the inverse problem; (ii) to examine and implement inversion procedures that present the estimated model parameters in a way that reflects their uncertainties; and (iii) to evaluate tools that help choose the most appropriate prior information. One global and one local search procedures were chosen to accomplish these purposes: a pure Monte Carlo method and the Maximum Likelihood Method, respectively. The pure Monte Carlo method was chosen to study the non-uniqueness by looking at the range of acceptable solutions (i.e., V_s profiles) obtained with as few constraints as possible. The maximum likelihood

method was chosen because it is a statistical approach, which enables us to estimate the uncertainties of the resulting model parameters and to apply tools such as the Bayesian criterion to help select the prior information objectively.

1.3 Dissertation Outline

Chapter 2 consists of a brief review of inversion methods, presenting a general overview of the basic differences between empirical and theoretical methods and between two types of theoretical methods: global and local search procedures. This chapter also includes a comparison of various local search procedures that have been used for SASW inversion.

Chapter 3 presents the implementation of a global search procedure for SASW inversion using synthetic data. This procedure is a Monte Carlo type algorithm, which is based on the random generation of V_s profiles. Chapter 4 shows the implementation of a local search procedure for SASW inversion using synthetic data. The procedure used is the Maximum Likelihood Method, which is based on the least squares criterion. This method starts from some estimate of the V_s profile and with gradient methods iteratively minimizes the error between theoretical and experimental dispersion curves.

Based on the inversion results obtained in Chapter 4, the influence of various factors on these results is examined in Chapter 5. The factors considered are: (i) number and distribution of points describing the experimental data, (ii) uncertainties of the

experimental data, (iii) depths and thicknesses of the layers of the assumed profile, (iv) depth to half-space, (v) initial estimates of the V_s values, (vi) standard deviations assumed for the intial V_s values, and (vii) correlations assumed for the initial V_s values.

Chapter 6 presents the Bayesian criterion for model selection and its implementation for SASW. This criterion helps rank the layered profiles favoring the one that fits the data well enough with the simplest possible model.

Chapter 7 utilizes real data to evaluate the maximum likelihood inversion method introduced in Chapter 4 and complemented with the Bayesian model selection described in Chapter 6. Finally, Chapter 8 gives the conclusions of the present study and recommendations for future research.

CHAPTER 2

BRIEF REVIEW OF INVERSION METHODS

2.1 Introduction

In general terms, a *forward problem* involves predicting the results of measurements (data) based on some general principle and a set of specific conditions (model parameters), whereas the *inverse problem* addresses the reverse issue: estimating the model parameters based on measured data and a general principle (Menke, 1989). More specifically, as shown in Figure 2.1, for SASW testing the *forward problem* consists of finding a dispersion curve (data) for a specified soil deposit (described by the model parameters) using wave propagation theory (general principle). Conversely, the *inverse problem* consists of estimating the model parameters that represent the soil deposit based on an experimental dispersion curve (data).

This chapter gives a general overview of the various inversion procedures that can be implemented to solve the non-linear inverse problem in SASW. One way to perform the inversion of experimental SASW data is to empirically scale the dispersion curve going from phase velocity versus wavelength to shear wave velocity versus depth (section 2.2). Another way to perform the inversion is with a theoretical inversion method, which is based on wave propagation theory and consequently produces better results for a broader range of cases.
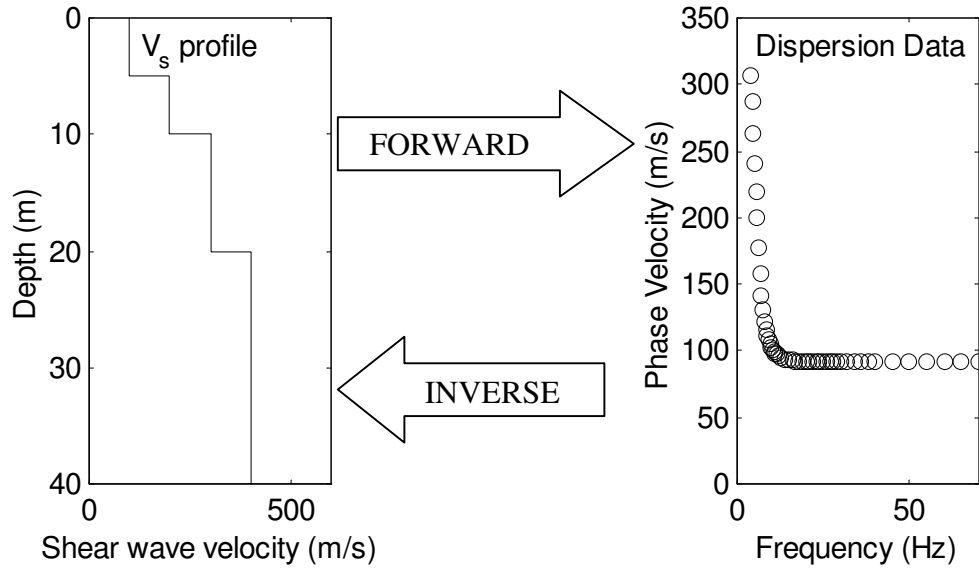
Figure 2.1 SASW forward and inverse problems

Due to the non-linearity of the forward problem in SASW, inversion methods based on wave propagation theory cannot be solved directly and are implemented by iteratively using the solution to the forward problem: for a number of V_s profiles the theoretical dispersion data is obtained ($\mathbf{vr}_{th}$) and compared with the experimental data ($\mathbf{vr}_{ex}$). This comparison is done by calculating an error such as the root mean square error (e_{RMS} = norm[$\mathbf{vr}_{th}$ - $\mathbf{vr}_{ex}$]/$N^{0.5}$, where N is the number of points describing the dispersion curve) and the purpose is to try to find the V_s profile that minimizes that error.

To perform this theoretical inversion there are two different approaches: local search procedures (section 2.3) and global search procedures (section 2.4). Local search procedures are iterative procedures that start at some estimate of the model parameters and with gradient methods minimize the error finding a local minimum in the vicinity of

the initial guess. Global search procedures are usually stochastic-based processes that attempt to search over the entire solution space to find the global minimum for the error. For nonlinear inversion problems such as SASW, finding the global minimum can be a complex problem.

The author is familiar only with theoretical procedures that have been implemented for SASW inversion based on local search procedures and is not informed of the use of global search procedures implemented specifically for SASW inversion. Good references for general inverse theory based on local search procedures are Tarantola (1987) and Menke (1989). For global search procedures see Tarantola (1987) and Sen and Stoffa (1995).

2.2 Overview of the Empirical Inversion Method

The simplest approach to derive the shear wave velocity (V_s) profile from the dispersion curve is the empirical *wavelength method*. This method consists of 'scaling' the phase velocity (V_r) versus wavelength (λ) curve to find the variation of shear wave velocity with depth. The phase velocity is multiplied by a factor of 1.1 to obtain the shear wave velocity (Tokimatsu, 1997). This is based on the fact that for a homogeneous half-space the ratio V_s/V_r is between 1.05 and 1.15, depending on Poisson's ratio. When the profile is not a homogeneous half-space, it becomes necessary to find an equivalent depth (z_{eq}) to which each V_s can be assigned. This can be done for continuously inhomogeneous soil profiles with gradually increasing stiffness with depth. These profiles are commonly

known as normally dispersive because the phase velocity decreases with increasing

frequency. In this case, the fundamental mode of Rayleigh wave propagation is dominant

and the dispersion curve is assumed to represent this mode.

Vrettos (2000) considered profiles with shear modulus increasing with depth as:

$$G(z)=G_o+(G_\infty -G_o)[1-\exp(-\alpha z)] \qquad\qquad (eq.2.1)$$

Where $G(z)$ is the shear modulus at depth z, G_o is the shear modulus at the surface, G_∞ is

the shear modulus at infinite depth, and α is a parameter describing the rate of modulus

increase with depth. He obtained an average scaling factor of 1/3 (i.e., $z_{eq}/\lambda=1/3$). A

scaling factor of 1/2 was considered more appropriate by Leung et al. (1991) for a linear

variation of the shear modulus with depth and by Gazetas (1982) for a shear modulus

variation with depth of the form:

$$G(z)=G_o(1+\beta z)^n \qquad\qquad (eq. 2.2)$$

Where β and n are parameters describing the rate of modulus increase with depth. The

wavelength method may give a reasonable estimate of the shear wave velocity profile for

normally dispersive soil profiles without large discontinuities. However, theoretical

methods based on wave propagation theory give better results for a broader range of site

conditions.

2.3 Overview of Theoretical Inversion Methods: Local Search Procedures

2.3.1 Generalities

Local search procedures are methods that attempt to minimize the error between theoretical and experimental data. To accomplish this, they start at some estimate of the model parameters and with gradient methods iteratively minimize the error. For SASW, these iterative inversion procedures are based on the basic steps shown in Figure 2.2. The first step is to have an initial estimate of the V_s profile. This estimate may be based on the experimental dispersion curve or independently obtained information about the site including penetration data, etc. Then, the theoretical dispersion curve related to the initial profile is estimated and compared with the experimental dispersion curve. If the match between the curves is considered acceptable the problem is solved. If the match is not acceptable, the V_s profile is updated and the new V_s profile is used to find a new theoretical dispersion curve. The iterations continue until an acceptable match is obtained. However, in some cases the algorithm might not converge to an acceptable match. In general, in those cases another initial model may be tried.

A number of methods have been employed to perform this iterative process for SASW inversion (see Table 2.1) with different ways of calculating the theoretical dispersion curve, comparing it with the experimental dispersion curve, deciding if the match is satisfactory, and updating the shear wave velocity profile. The following sections

describe various aspects relevant to these local search procedures and refer to different approaches that have been used in SASW inversion.
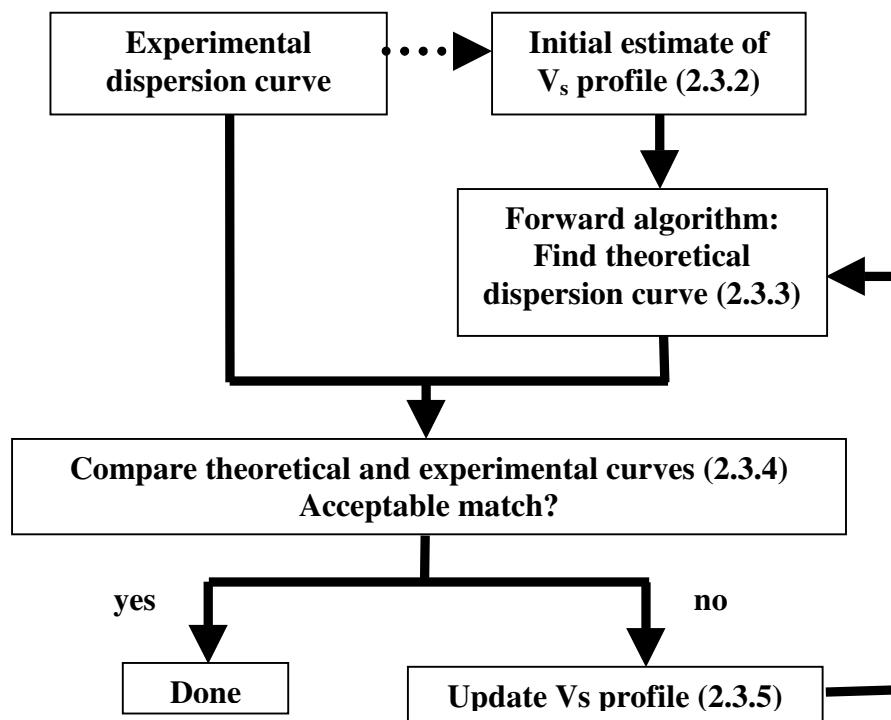
Figure 2.2 Basic flowchart of a Local Search Procedure used for SASW inversion.

Table 2.1 Summary of methods employed for SASW inversion

		Xia, Miller, & Park (1999)
Initial V_s profile (2.3.2)	**Model Parameters**	V_s
	Initial Values	Not specified
Forward algorithm (2.3.3)	**Forward Model**	Knopoff's method: reference to Schwab and Knopoff, 1972
	Type of waves	Rayleigh
	Modes included	Fundamental Mode
Error function (2.3.4)		Not specified
Update V_s profile (2.3.5)	**Method to find change in V_s profile for next iteration**	Linear about values in present iteration ($\Delta c = J\Delta p$)[a] To find Δp: Constrained Weighted least squares using Levenberg-Marquardt method & Singular Value Decomposition
	Partial Derivatives ($\partial V_r / \partial V_s$)	Closed form expressions from finite differences using Ridder's method of polynomial extrapolation

Notes: (a) J: matrix of partial derivatives of the phase velocity with respect to the medium parameters, Δc: difference between observed and theoretical phase velocities, and Δp: change in model parameters to use in next iteration.

(b) c: Rayleigh phase velocity, f: frequency, k: wave number, λ: wavelength.

(c) N:number of frequencies in dispersion curve, W: diagonal matrix with elements equal to the inverse of the standard deviations (σ) of the experimental values ($W_{ii}=1/\sigma_i$).

Table 2.1 (cont'd)

		Ganji, Gucunski, & Nazarian (1998)	Lai & Rix (1998)
Initial V_s profile (2.3.2)	**Model Parameters**	V_s or V_s & Thicknesses	V_s
	Initial Values	Wavelength Method	Not specified
Forward algorithm (2.3.3)	**Forward Model**	Test simulation: based on linearized stiffness matrix (Kausel), with closed form expressions for displacements.	Effective Rayleigh phase velocity (based on harmonic source, and using average over range of receiver offsets)
	Type of waves	Rayleigh and body	Rayleigh
	Modes included	All Modes	All Modes
Error function (2.3.4)		$e_1 = \text{norm}(\Delta c)$	$w\_e_{RMS} = \text{norm}[W \Delta c]/N^{0.5}$ [c]
Update V_s profile (2.3.5)	**Method to find change in V_s profile for next iteration**	Linear about values in present iteration $(\Delta c = J \Delta p)$ [a] To find Δp: Singular Value Decomposition PLUS Non-linear optimization approach (based on Davidon-Fletcher-Powel method) when linear one fails	Linear about values in present iteration $(\Delta c = J \Delta p)$ [a] To find Δp: Constrained non-linear least squares, to find the smoothest profile for Vs, for an acceptable error
	Partial Derivatives $(\partial V_r/\partial V_s)$	Numerical differentiation	Closed form analytical expressions based on Rayleigh variational principle

Table 2.1 (cont'd)

		Tokimatsu (1997)	
		Active SW method	**Passive SW method**
Initial V_s profile (2.3.2)	**Model Parameters** **Initial Values**	V_s or V_s & Thicknesses Not specified	V_s or V_s & Thicknesses Not specified
Forward algorithm (2.3.3)	**Forward Model**	Displacements calculated with compound matrix method (solution separating Rayleigh and body waves) AND Response factors related to the contribution of different modes --------------------- Dispersion curve based on cross-power spectrum like for the displacements measured at the field	Expression for apparent phase velocity that includes all modes; based on simulated dispersion curves like for active method, and on Aki's 1957 study
	Type of waves	Rayleigh and could include body	Rayleigh (and Love if horizontal displacements are measured)
	Modes included	All Modes	All Modes
Error function (2.3.4)		$e_2 = \text{norm}(\Delta c)^2$	$e_2 = \text{norm}(\Delta c)^2$
Update V_s profile (2.3.5)	**Method to find change in V_s profile for next iteration**	Linear about values in present iteration $(\Delta c = J\Delta p)$[a] To find Δp: reference to Dorman and Ewing, 1962, and Wiggins, 1972	Same as for active method
	Partial Derivatives $(\partial V_r / \partial V_s)$	Numerical is too time consuming, use variational technique as in Yuan & Nazarian (1993)	Same as for active method

Table 2.1 (cont'd)

		Joh (1996)	Yuan & Nazarian (1993)
Initial V_s profile (2.3.2)	**Model Parameters**	V_s	V_s or V_s & Thicknesses
	Initial Values	Based on exper. disp. curve	Not specified
Forward algorithm (2.3.3)	**Forward Model**	Test simulation: based on dynamic stiffness matrix (Kausel) with closed form expressions for displacements --------------------- Dispersion curve based on cross-power spectrum like for the displacements measured at the field --------------------- global dispersion curve (doesn't account for real test setup) OR array dispersion curves	Wave propagation theory based on transfer matrix (Thomson, Haskell) --------------------- Dispersion curve created from wavenumber with $c=2\pi f/k$ and $\lambda=2\pi/k$ [b]
	Type of waves	Rayleigh and body	Rayleigh
	Modes included	All Modes	Fundamental Mode
Error function (2.3.4)		Cost function, maximum likelihood method: see Chapter 4	$e_{RMS} = norm[\Delta c]/N^{0.5}$ [c]
Update V_s profile (2.3.5)	**Method to find change in V_s profile for next iteration**	Initial profile based on dispersion curve. Refined with depth resolution and layer sensitivity analyses Maximum likelihood method using Newton-Raphson to minimize cost function (forward problem linear around maximum likelihood point)	Linear about values in present iteration $(\Delta c=J\Delta p)$ [a] To find Δp: Singular Value Decomposition with Marquardt's factor to eliminate effect of small singular values
	Partial Derivatives $(\partial V_r/\partial V_s)$	Numerical differentiation	Expression found based on energy integral equation

Table 2.1 (cont'd)

		Roësset, Chang, & Stokoe (1991)	
		2-D	3-D
Initial V_s profile (2.3.2)	**Model Parameters**	V_s or V_s & Thicknesses	V_s or V_s & Thicknesses
	Initial Values	Wavelength Method	Wavelength Method
Forward algorithm (2.3.3)	**Forward Model**	Wave propagation theory based on transfer matrix (Thomson, Haskell) OR dynamic stiffness matrix (Kausel & Roësset) --------------------- Dispersion curve created from wavenumber with c=2πf/k and λ=2π/k[b]	Expressions for radial and vertical displacements with cylindrical coordinates AND discrete formulation to expand terms in dynamic stiffness matrix (Kausel & Roësset) --------------------- Dispersion curve based on cross-power spectrum like for the displacements measured at the field
	Type of waves	Rayleigh	Rayleigh
	Modes included	Fundamental Mode	All Modes
Error function (2.3.4)		Not specified	Not specified
Update V_s profile (2.3.5)	**Method to find change in V_s profile for next iteration**	Not specified	Not specified
	Partial Derivatives ($\partial V_r/\partial V_s$)	Not specified	Not specified

Table 2.1 (cont'd)

		Gucunski & Woods (1991)
Initial V_s profile (2.3.2)	**Model Parameters**	V_s or V_s & Thicknesses
	Initial Values	Not specified
Forward algorithm (2.3.3)	**Forward Model**	Numerical simulation of test based on stiffness matrix OR Weighted average phase velocity, with weighting factors based on modal displacements
	Type of waves	Rayleigh (and body if numerical simulation is used)
	Modes included	All Modes
Error function (2.3.4)		Not specified
Update V_s profile (2.3.5)	**Method to find change in V_s profile for next iteration**	Not specified
	Partial Derivatives ($\partial V_r / \partial V_s$)	Not specified

2.3.2 Initial Estimate of the Shear Wave Velocity Profile

For inversion methods employing local search procedures, convergence is guaranteed only if the initial guess is sufficiently close to the solution. Furthermore, for SASW inversion, having a good initial estimate of the shear wave velocities improves the convergence of the inversion algorithm and also reduces the number of iterations required. For this reason, Joh (1996) proposes a procedure to obtain the initial estimate of the V_s profile based on the dispersion curve.

The first step to have an initial estimate of the parameters that describe the shear wave velocity profile is to decide which parameters are going to be the unknowns found through the inversion process and which are going to be assumed as known and fixed during inversion. For example, the soil deposit is generally represented by a profile with horizontal layers overlying a half-space with the model parameters including layer thickness, density, P-wave velocity (V_p) and S-wave velocity (V_s). The effect of a change in density and P-wave velocity on the dispersion curve is negligibly small (Tokimatsu et al., 1991), and these parameters are normally assumed as known. Thus, the unknown model parameters are reduced to layer thicknesses and shear wave velocities. However, in many cases the layer thicknesses are assumed known to simplify the problem and the shear wave velocities are viewed as the only unknown parameters.

Yuan and Nazarian (1993) suggested that more layers be used when the thicknesses are fixed during inversion because having more layers gives more flexibility to the profile

and reduces the chance of emphasizing false layer interfaces. Conversely, having too many layers may result in thin layers that do not affect the resulting theoretical dispersion curve enough for it to constrain their V_s values.

For some methods, such as the maximum likelihood method (see Chapter 4), the initial guess also includes uncertainties related to the V_s profile, which reflect how much is known about the initial estimates of the shear wave velocities. These uncertainties are given by standard deviations and correlations assembled in a covariance matrix and described in detail in Chapter 4.

2.3.3 Theoretical Dispersion Curve

Different techniques may be used to solve the forward problem and find the theoretical dispersion curve for a given soil model. The most commonly used approach is the Haskell-Thomson method (Thomson, 1950; Haskell, 1953), which describes wave propagation in a layered medium. This approach is also known as the *transfer matrix method* and is only applicable to profiles that can be represented as a stack of homogeneous layers overlying a homogeneous half–space (see Figure 2.3). Other methods commonly used for wave propagation that are likewise only applicable in layered profiles include: (i) the *dynamic stiffness matrix method* derived by Kausel and Roësset (1981), and (ii) the *method of reflection and transmission coefficients* derived by Kennett (1983).

From the results obtained from wave propagation theory in layered media, it can be noted that Rayleigh waves contain several modes of propagation where each mode travels with a different phase velocity (Figure 2.4). This implies that for an assumed shear wave velocity profile the resulting theoretical dispersion data may include several dispersion curves, one for each propagation mode considered. On the other hand, experimental data usually represents the combined effect of all modes, resulting in a single curve of phase velocity varying with frequency. This phase velocity can then be viewed as an apparent phase velocity since it includes all modes of propagation and could include the effect from body waves.

Many iterative inversion methods like the one presented by Yuan and Nazarian (1993) consider only the fundamental mode of Rayleigh wave propagation. These procedures are useful for soil profiles in which the shear wave velocity generally increases with depth (i.e., normally dispersive) because for these profiles the fundamental mode is the dominant mode of propagation. For inversely dispersive soil profiles in which the variation of shear wave velocity with depth is more irregular, the effect of higher modes may be significant (Tokimatsu et al.,1992a; Gucunski and Woods, 1991). As noted by Tokimatsu (1997), the participation of each mode varies depending on soil stratification and frequency, and in some cases the observed dispersion characteristics may correspond to a higher mode or multiple modes. Consequently, the estimated V_s profiles may have significant errors if the effects of higher modes are neglected during the inversion process.
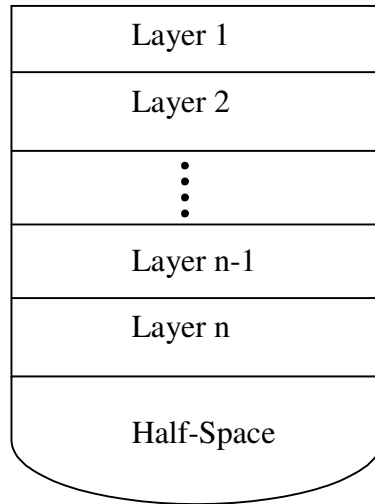
Figure 2.3 Layered Model
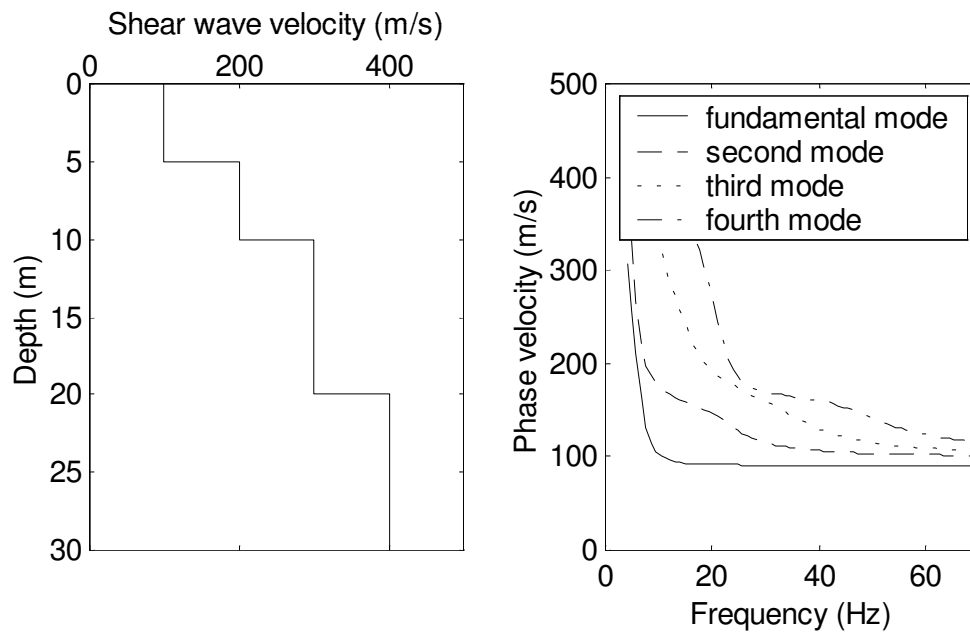
Figure 2.4 Sample wave propagation modes for Rayleigh waves

Recent inversion methods (Lai and Rix, 1998; Tokimatsu, 1997) compare the experimental dispersion curve to an apparent dispersion curve, which includes the effect of higher modes. Lai and Rix (1998) calculate what they call the effective Rayleigh phase velocity. They noted that for sources that are harmonic in time, Rayleigh modes are superimposed, resulting in an effective phase velocity which is a function of frequency and spatial position from the source. The effective phase velocity presents one dispersion curve for each receiver position. These curves form a dispersion surface and they are averaged over the range of receiver spacings to obtain a single "effective" dispersion curve for comparison with the experimental dispersion curve.

Tokimatsu (1997) presents a method to calculate simulated dispersion curves for both vertical and horizontal displacements that include the effect of higher modes. He suggests that in addition to the dispersion data for the vertical motions, the dispersion curve for the horizontal motions or the amplitude ratio of the particle motions (i.e., vertical/horizontal) should be used to reduce the ambiguity of the inversion. Methods that include the effect of higher modes have the capability of inverting normally and inversely dispersive soil profiles more reliably.

The influence from body waves is usually neglected by assuming that the receivers are sufficiently far away from the source because body waves attenuate with distance more quickly than Rayleigh waves. Tokimatsu (1997) studies the effect of body waves on layered profiles. He demonstrates that Rayleigh waves generally dominate over the frequency range of interest for SASW method and he determines under what conditions

the effect of body waves is negligible. By considering different types of layerings, he shows that for some layered media, the effects of body waves may be neglected if the distance from the source exceeds ¼ of the wavelength measured. However, for a case with a stiff surface layer overlying a soft layer, the effect of body waves is minimized only if using f-k spectrum analysis to create the dispersion curve. The description and use of f-k spectrum analysis can also be found in Zywicki (1999) and Rix et al (2002).

Some recent inversion methods include body waves by numerically simulating the field test. This is done by using wave propagation theory to calculate the displacements for each receiver for a source-receiver configuration the same as the one used during the field test (Joh, 1996; Ganji et al., 1998). The theoretical dispersion curve is found based on the calculated displacements in the same way that the experimental dispersion curve is obtained from the displacements measured at the field. This theoretical curve, like the experimental one, represents an apparent phase velocity that includes the effect of body waves and all modes of Rayleigh wave propagation. It is beneficial to calculate the theoretical and the experimental dispersion curves in the same way to eliminate any differences caused by the method of obtaining these curves.

The methods using this approach have capabilities of inverting normally and inversely dispersive soil profiles. The disadvantage of this approach is that in most cases the partial derivatives must be obtained numerically (not analytically). The derivatives must be calculated for each iteration (see section 2.3.4) and performing a numerical calculation of these significantly increases the time of inversion compared to performing this

calculation based on closed-form expressions (Yuan and Nazarian, 1993, and Tokimatsu, 1997).

2.3.4 Convergence Criteria and Constraints

Once the theoretical dispersion curve is obtained, it is necessary to compare it with the experimental dispersion curve. Generally, the difference between the theoretical and the experimental dispersion curves is measured using the Root Mean Squares (RMS) error:

$$\mathbf{e_{RMS}} = \mathbf{norm[\Delta c]/N^{0.5}} \qquad\qquad \text{(eq. 2.3)}$$

where, $\mathbf{\Delta c}$ is the vector of the differences between experimental and theoretical phase velocities, and N is the number of elements in vector $\mathbf{\Delta c}$ (i.e., the number of experimental data points). In general, inversion methods attempt to minimize an error function such as $\mathbf{e_{RMS}}$ (Yuan and Nazarian, 1993), $\mathbf{e_1 = norm(\Delta c)}$ (Ganji et al., 1998), or $\mathbf{e_2 = norm(\Delta c)^2}$ (Tokimatsu, 1997). Note that minimizing $\mathbf{e_1}$ or $\mathbf{e_2}$ is equivalent to minimizing $\mathbf{e_{RMS}}$, but the value of $\mathbf{e_{RMS}}$ is often more useful because it does not depend on the number of data points.

Additionally, Tokimatsu et al. (1991) recommended the use of either the dispersion data of the horizontal motions or the amplitude ratio of particle motions to reduce the non-uniqueness of the problem. Most field methods measure only the vertical displacements,

but Tokimatsu (1997) recommends simultaneous measurement of vertical and horizontal displacements to reduce ambiguity.

Lai and Rix (1998) minimize a weighted RMS error, which includes a weighting matrix based on the uncertainties assigned to the experimental data:

$$w\_e_{RMS} = norm[W\ \Delta c]/N^{0.5} \qquad \text{(eq. 2.4)}$$

Where W is a diagonal matrix with elements equal to the inverse of the standard deviations (σ) of the experimental values ($W_{ii}=1/\sigma_i$). Additionally, their inversion algorithm chooses the smoothest profile within the trial profiles that meet the w_e_{RMS} by minimizing the roughness of the profile.

Joh (1996) employs the maximum likelihood method, which minimizes a cost function that includes two terms: one for Δc and one for the difference between the vector of model parameters p and its initial guessed value. This cost function is described in detail in Chapter 4.

2.3.5 Updating the Shear Wave Velocity Profile

When the match between the theoretical and the experimental dispersion curves is not satisfactory, it is necessary to update the shear wave velocity profile (by updating the

model parameters) to improve the match. The vector **p** of model parameters is updated for the next iteration as:

$$\mathbf{p}_{\text{(iteration i+1)}} = \mathbf{p}_{\text{(iteration i)}} + \mathbf{\Delta p} \qquad (\text{eq. 2.5})$$

In general, for local search procedures the equation to determine **Δp** is based on a linearization of the problem near the values in the present iteration, as shown in the expression below:

$$\mathbf{\Delta c} = \mathbf{J}\,\mathbf{\Delta p} \qquad (\text{eq. 2.6})$$

where, **Δc** is the vector of the differences between experimental and theoretical phase velocities and **J** is the matrix of partial derivatives (i.e., the element in row m and column n of J is $j_{mn} = \delta c_m / \delta p_n$).

The calculation of the partial derivatives of the phase velocity respect to the medium parameters is a very important part of the inversion process and is usually calculated for each iteration and each shear wave velocity profile. As mentioned previously, the use of closed-form expressions for the partial derivatives is less time consuming than estimating these numerically. These closed-form expressions can be derived based on energy integral equation (or Rayleigh variational principle) as presented by Yuan and Nazarian (1993), Tokimatsu (1997), and Lai and Rix (1998).

After obtaining the partial derivatives, there are different ways of solving equation 2.6 to estimate $\Delta\mathbf{p}$ and use it in equation 2.5 to find the parameters ($\mathbf{p}$) for the next iteration. Yuan and Nazarian (1993) employ singular value decomposition of $\mathbf{J}$

$$\mathbf{J=U\Lambda V^T} \qquad\qquad (eq.\ 2.7)$$

Where $\mathbf{U}$ is a matrix whose columns are eigenvectors associated with the columns of $\mathbf{J}$,

$\mathbf{V}$ is a matrix whose columns are eigenvectors associated with the rows of $\mathbf{J}$, and

$\mathbf{\Lambda}$ is a diagonal matrix with elements, which are the nonnegative square roots of

the symmetric matrix $\mathbf{J^TJ}$ and are known as the singular values of $\mathbf{J}$.

With the singular value decomposition, the solution for $\Delta\mathbf{p}$ becomes:

$$\mathbf{\Delta p= (V\Lambda^{-1}U^T)\ \Delta c} \qquad\qquad (eq.\ 2.8)$$

In addition, Yuan and Nazarian (1993) employ Marquardt's factor to eliminate the effect of small singular values. Ganji et al. (1998) also apply singular value decomposition. Furthermore, they implement a non-linear optimization approach based on Davidson-Fletcher-Powel method when the linear one fails. Xia et al. (1999) use constrained weighted least squares to search for a solution that minimizes the error and the change in the model parameters to have a stable convergence procedure. They solve for $\Delta\mathbf{p}$ with the Levenberg-Marquardt method and singular value decomposition of $\mathbf{J}$ obtaining:

$$\Delta p = [V(\Lambda^2 + \alpha I)^{-1}\Lambda \; U^T \; L] \; \Delta c \qquad \qquad \text{(eq. 2.9)}$$

where **L** comes from a weighting matrix $W = L^T L$ and α is a damping factor.

Lai and Rix (1998) used the constrained non-linear least squares algorithm proposed by Constable et al. (1987). This algorithm finds a solution that minimizes the roughness of the V_s profile (i.e., maximizes the smoothness) subject to the constraint that the error be equal to a value considered acceptable. Joh (1996) employs the maximum likelihood method, which favors the shear wave velocity profile that maximizes the probability that the corresponding dispersion curve is the experimental dispersion curve and is described in more detail in Chapter 4.

2.3.6 Uncertainty

Most methods do not address the evaluation of the uncertainty of the inverted V_s profile. This profile presented without error bars may give the interpreter a false sense of certainty of the V_s values. Lai and Rix (1998) recognize that only approximate results can be obtained for the variances of V_s due to the non-linearity of the forward problem. They describe how to find an estimate of the covariance matrix (i.e., the diagonal terms of this matrix are the variances of the estimated V_s values, see Chapter 4) when Occam's inversion algorithm is used to find V_s. The basic idea is to map the uncertainty of the measurements into uncertainty of the estimated model parameters in a manner similar to the mapping of the measurements into model parameters. Yuan and Nazarian (1993) and

Ganji et al. (1998) also evaluate the uncertainty in the profile by mapping the statistics of the data errors into a variance associated with each parameter. Yuan and Nazarian (1993) found that the variances usually underestimate the real uncertainties because they only include the effect from random data errors (i.e., errors in the assumed properties of the profile) and systematic data errors are not included.

Joh (1996) gives a solution to calculate the covariance matrix related to the estimated model parameters. He uses the results presented by Tarantola (1987) for the maximum likelihood method, which are described in detail in Chapter 4. In this method, the covariance matrix of the estimated parameters depends not only on the uncertainty of the measurements but also on the uncertainties of the initial estimate of the model parameters. The reason for this dependence is that the maximum likelihood method attempts to minimize the differences between the model parameters and their initial estimates in addition to minimizing the error between experimental and theoretical data.

2.4 Overview of Theoretical Inversion Methods: Global Search Procedures

2.4.1 Generalities

Global search procedures are processes that attempt to search the entire solution space and find the global minimum by successive forward simulations. The advantage of a global search procedure is that the problem can be solved in a fully non-linear form (i.e.

without any type of linearization of the forward algorithm). The basic steps of a global search procedure are given below:

(i)   Assume values for the model parameters;

(ii)   Find the related theoretical data;

(iii)   Calculate the error between theoretical and experimental data;

(iv)   Save the values of the model parameters if the error is considered satisfactory, and repeat steps (i) to (iv) until the model space has been fully explored;

(v)   Present the range of values for the model parameters corresponding to satisfactory errors (e.g., by calculating the mean and the standard deviation or some other measures considered appropriate);

The main difference among global search procedures is the way of choosing the parameter values in step (i). Enumerative or grid search methods of inversion find the best fit models from a complete search over each point of a predefined model space (Sen and Stoffa, 1995). For a model space with a large number of parameters this might become an unbearable task requiring unreasonable amounts of time and computer resources. In this case, it is more economical to randomly select points in the model space than to define a grid dense enough to ensure that at least one point will be in the best possible area (Tarantola, 1987). Inversion methods that employ a random or pseudo-random generator are called Monte Carlo methods.

2.4.2 Pure Monte Carlo Methods

For any Monte Carlo method it is necessary to constrain the values of the model parameters that will be randomly generated. For a pure Monte Carlo method the constraint is done by choosing the value of each model parameter from an interval determined a priori, where all values within the interval are equally probable (Sen and Stoffa, 1995). Thus, for each model parameter p_i the only condition is:

$$p_i^{min} \leq p_i \leq p_i^{max}$$ (eq. 2.10)

Another way of constraining the values of the randomly generated model parameters and reduce the solution space is to use prior information to define a probability distribution to sample the models from. For instance a Gaussian distribution could be assumed and described by a mean and a standard deviation for each parameter. If the limits of the predefined interval or the standard deviations defining the probability distribution are too wide, the number of forward simulations necessary to explore the model space might be extremely large and require an unreasonable amount of time and computer resources. On the other hand, if the limits or the standard deviations are chosen too small they may control the results obtained (Tarantola, 1987).

Sen and Stoffa (1995) note that if no prior information is available, the search can be performed within a discrete solution space using relatively large increments and

accepting low resolution results. For example for each model parameter p_i an increment Δp_i is defined and the possible values for p_i will be limited to:

$$p_i = p_i^{min} + integer * \Delta p_i \qquad\qquad (eq.\ 2.11)$$

Where the integer is a random number between 1 and $(p_i^{max} - p_i^{min}) / \Delta p_i$. For small values of Δp_i the resolution is better but the computer time might be too large, whereas for large values of Δp_i the resolution is poor but it may be easier to reach a solution near the global minimum. Another important issue with Monte Carlo methods is that it is difficult to determine whether the model space has been adequately explored to consider that the range of satisfactory models represents the solution. It is common to stop the computations based on the total number of models with an acceptable error (Tarantola, 1987, Sen and Stoffa, 1995). Sen and Stoffa (1995) describe how to estimate the resolution matrix for a Monte Carlo inversion method and how this matrix helps decide if enough acceptable models have been found to stop the search.

2.4.3 Directed Monte Carlo Methods

Another type of procedure that employs random generation of the model parameters is called directed Monte Carlo methods. Two procedures that fall into this category are simulated annealing and genetic algorithms and are described by Sen and Stoffa (1995). These methods use random generation of the model parameters but they guide their search using a transition probability rule. The idea is that these methods should not bias

the results, and for this reason they need to keep a large degree of randomness. However, at the same time these methods should direct the search toward sampling the better models (Sen and Stoffa, 1995). Other good references that address these methods are Tarantola (1987) for simulated annealing and Santamarina and Fratta (1998) for genetic algorithms.

2.4.4 Uncertainty

When the model space has been conveniently explored and the number of acceptable models found using the global search procedure is considered satisfactory, the values and uncertainties of the model parameters can be estimated within a statistical framework. Tarantola (1987) and Sen and Stoffa (1995) describe the calculation of the mathematical expectation and covariance matrix for Monte Carlo methods. The covariance matrix presents the uncertainties of the model parameters and the correlations between them.

CHAPTER 3

SASW INVERSION BASED ON RANDOM GENERATION OF V_S PROFILES

3.1 Introduction

In this chapter, a Monte Carlo algorithm is described and implemented for SASW inversion. The purpose of this is to look at the range of V_s values that fit the dispersion curve and obtain an estimate of their uncertainties using a minimum number of constraints. The forward algorithm used to obtain the simulated experimental data is the same one used to find the theoretical dispersion curves in the Monte Carlo inversion process. Thus, in this case, the experimental data and the forward algorithm are ideal, i.e., without any errors added by: (i) noise from data measurement, (ii) analysis of the data to create the dispersion curve, (iii) use of a simplified model attempting to represent the real world, or (iv) wave propagation theory. Consequently, the uncertainties are the ones caused by the nature of the SASW inversion problem alone.

Herein, a theoretical normally dispersive profile is used to obtain a synthetic dispersion curve, which is treated as "experimental" data. To perform the inversion, V_s profiles are randomly generated and tested to choose the ones with theoretical dispersion curves that present a satisfactory match to the "experimental" curve. The generation of the V_s profiles is done with a predefined number of layers and fixed thicknesses. The layers chosen are thinner than the "real" layers with interfaces that match the "real" ones, so the

assumed layering is able to match the "real" one with the appropriate V_s values. The V_s value for each layer is randomly chosen within an interval where all values are equally probable. The interval of possible V_s values is based on an empirical estimate of the V_s profile multiplied by a factor <1 to establish the lower limit and a factor >1 to establish the upper limit.

3.2 Global Search Procedure applied to SASW

3.2.1 Pure Monte Carlo Inversion applied to SASW

In this section the main issues regarding the implementation of a pure Monte Carlo inversion method for SASW inversion are discussed. As mentioned in Chapter 2, the soil deposit is generally represented with horizontal layers overlying a half-space, and described by layer thickness, density, P-wave velocity (V_p) and S-wave velocity (V_s). Since the effects of density and P-wave velocity on the soil deposit are small (Tokimatsu et al., 1991), these values are fixed and the unknown model parameters are reduced to thickness and V_s. Herein, the density (ρ) and the Poisson ratio (υ) are assumed as known for each layer and V_p is calculated as (Kramer, 1996):

$$V_p = V_s \sqrt{\frac{2 - 2\upsilon}{1 - 2\upsilon}}$$

(eq. 3.1)

In some cases the number of layers and their thicknesses may be fixed and the only model parameters randomly generated are the shear wave velocities. Fixing the layer

thicknesses reduces the number of unknown parameters and consequently the size of the model space being searched.

The unknown model parameters are chosen for each randomly generated profile by giving each parameter a value from a predefined interval, using a uniform distribution to give the same probability to any value between (and including) the interval limits (Figure 3.1). The disadvantage of using a uniform distribution is that the lower and upper limits for the model parameters need to be fixed and no values can be outside these limits. The advantage is that within the limits all values are equally probable. If the limits are too wide the process of exploring possible profiles might be excessively time consuming, but if the limits are too narrow they could control the solution.

Another possibility for choosing the parameter values is to use a distribution such as the normal distribution (Figure 3.1). In this case, the random generation of the profile would favor values closer to the mean and there would be no absolute maximum and minimum limits. For this project the purpose of using the random algorithm is to find a number of V_s profiles that fit a set of experimental data without favoring any V_s values, thus a uniform distribution was chosen.

For each randomly generated profile the theoretical dispersion curve is estimated using a forward algorithm such as the one proposed by Lai and Rix (1998). This algorithm provides separately the first ten modes of propagation and an apparent dispersion curve that includes the effect of multiple surface wave modes. The fundamental mode may be

37

used for normally dispersive profiles and the apparent dispersion curve for inversely

dispersive profiles (see Chapter 2).
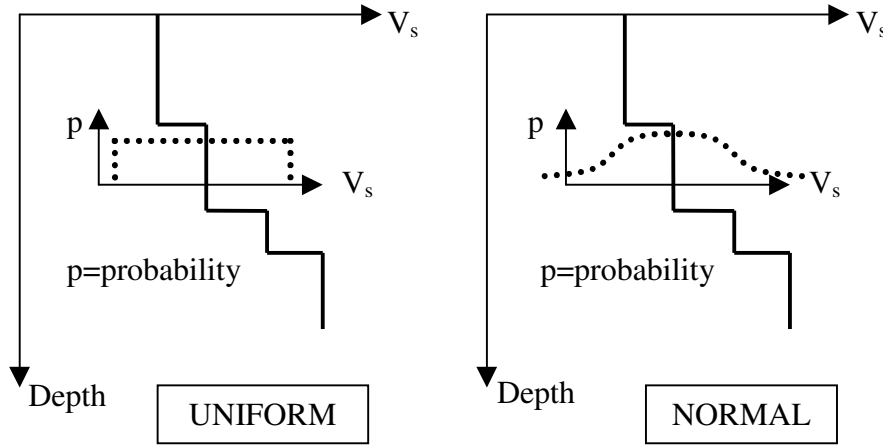
**Figure 3.1 Comparison of uniform and normal distributions to choose
the values of the parameters for the randomly generated V_s profile**

The theoretical dispersion curve is compared with the experimental curve by calculating

the root mean square (rms) error as:

$$rms = \frac{\text{norm}(\mathbf{Wvr}_{ex} - \mathbf{Wvr}_{th})}{\sqrt{N_{freq}}} \qquad (eq.\ 3.2)$$

where

$\text{norm}(\mathbf{x})$ is $\sqrt{\sum_{i=1}^{n}(x_i)^2}$, for a vector $\mathbf{x}$ with elements x_i with i=1...n

$\mathbf{vr}_{ex}$ is the experimental phase velocity vector,

$\mathbf{vr}_{th}$ is the theoretical phase velocity vector,

N_{freq} is the number of points that describe the dispersion curve,

W is the diagonal N_{freq} by N_{freq} matrix with elements $W_{i,i}=1/\sigma\_vr_i$, and

σ_vr_i is the uncertainty in the ith experimental phase velocity.

Thus, the rms value is directly affected by the assumed uncertainties for the experimental phase velocities: the more uncertain the experimental dispersion data the lower the rms error, which results in a less constrained solution with a larger number of V_s profiles satisfying a specified rms criterion. Constable et al. (1987) discuss the issue of establishing an rms criterion, concluding that if the noise in the data can be represented by a zero-mean Gaussian process with σ_vr_i representing the standard deviations, a reasonable value for the rms is 1.0. Tuomi and Hiltunen (1997) presented two SASW experimental cases showing that the phase angle data (which is directly related to the phase velocity in the dispersion curve) seems to be normally distributed. Thus, using a Gaussian model for the data uncertainties appears to be a reasonable assumption for SASW. Additionally, if there is little knowledge about the noise it is not appropriate or justified to use more refined statistical models (Constable et al., 1987).

Tuomi and Hiltunen (1997) showed that there is a low uncertainty in the experimental dispersion data. They presented values for the coefficient of variation (= standard deviation / mean) of the phase angle data which were between 0.2 % and 6.4 %. Based on this information, the dispersion data of the numerical simulation used herein is assumed to have a standard deviation equal to 3% of the phase velocity.

3.2.2 Mathematical Expectation and Covariance Matrix

Tarantola (1987) describes how to find the unbiased estimators of the mathematical expectation and the covariance matrix for a set of NP satisfactory models found using a Monte Carlo simulation. The equations given by Tarantola (1987) are adapted here in terms appropriate for SASW inversion. The mathematical expectation of the shear wave velocities is:

$$\langle vs_\alpha \rangle = \frac{\sum_{i=1}^{NP} vs_\alpha{}^i \cdot L(\mathbf{vs}^i)}{\sum_{i=1}^{NP} L(\mathbf{vs}^i)} \qquad \text{(eq. 3.3)}$$

where

NP is the number of satisfactory V_s profiles,

$\langle vs_\alpha \rangle$ is the α component of the vector **<vs>** (corresponding to V_s for layer α)

<vs> is the vector of the mathematical expectations of the V_s values and describes the expected V_s profile),

$vs_\alpha{}^i$ is the α component of the vector $\mathbf{vs}^i$,

$\mathbf{vs}^i$ is a vector of V_s values that describe one satisfactory V_s profile, with i=1,2,...,NP, and

$L(\mathbf{vs}^i)$ may be called the likelihood, and assuming a Gaussian error distribution for the data it can be calculated as:

$$L(\mathbf{vs}^i) = \exp\left(-\frac{1}{2}\left(\mathbf{vr}_{th}{}^i - \mathbf{vr}_{ex}\right)^T (\mathbf{C\_vr})^{-1}\left(\mathbf{vr}_{th}{}^i - \mathbf{vr}_{ex}\right)\right) \qquad \text{(eq. 3.4)}$$

where

$\mathbf{vr}_{th}{}^{i}$ is the theoretical phase velocity vector,

$\mathbf{vr}_{ex}$ is the experimental phase velocity vector, and

$\mathbf{C\_vr}$ is the covariance matrix of the phase velocity data.

The components of the covariance matrix of the shear wave velocity vector are calculated as:

$$C\_vs_{\alpha,\beta} = \frac{\sum_{i=1}^{N} vs_{\alpha}{}^{i} vs_{\beta}{}^{i} \cdot L(\mathbf{vs}^{i})}{\sum_{i=1}^{N} L(\mathbf{vs}^{i})} - \langle vs_{\alpha} \rangle \langle vs_{\beta} \rangle \qquad \text{(eq. 3.5)}$$

where

$C\_vs_{\alpha,\beta}$ is the component of the α row and the β column of the V_s covariance matrix $\mathbf{C\_vs}_f$. The subindex f is used to indicate that this is the matrix describing the uncertainties and correlations on the *final* shear wave velocities found through the inversion process (i.e., on the estimated mathematical expectation of the V_s values).

It can be noted that the mathematical expectation is a weighted average in which the weights are given to each satisfactory V_s profile based on the likelihood (which is a measure of how well the theoretical dispersion data of the V_s profile matches the experimental data). If the user considers that all profiles that produce a dispersion curve with an rms error under a certain criterion (for example rms<1) are equally satisfactory, then it might be better to use the traditional average without weights (i.e., $L(\mathbf{vs}^{i})=1$ in equation 3.3). The reason is that in the case where the weights are used, the mathematical

41

expectation will produce a V_s profile with values very close to the profile with lowest rms, and might vary insignificantly when satisfactory profiles with a higher rms are added.

If the expected V_s profile is calculated with the traditional average without weights (i.e., $L(\mathbf{vs^i})=1$ in equation 3.3), the covariance matrix should also be calculated without the weights given by the likelihood (i.e., $L(\mathbf{vs^i})=1$ in equation 3.5). Additionally, if a normal distribution is assumed for the V_s values the covariance matrix terms can be found as:

$$C\_vs_{\alpha,\beta} = \frac{1}{N-1} \sum_{i=1}^{N} \left(vs_{\alpha}^{\,i} - \overline{vs_{\alpha}}\right)\left(vs_{\beta}^{\,i} - \overline{vs_{\beta}}\right)$$ (eq. 3.6)

The standard deviations are the square roots of the diagonal terms of the covariance matrix, thus the standard deviation of V_s for layer α can be calculated as:

$$\acute{o}\_vs_{\alpha} = \sqrt{\frac{1}{N-1} \sum_{i=1}^{N} \left(vs_{\alpha}^{\,i} - \overline{vs_{\alpha}}\right)^2}$$ (eq. 3.7)

The assumption of a normal distribution for the V_s values used in equations 3.6 and 3.7 may be evaluated using a normal probability plot to verify that the V_s data for each layer plot as a straight line.

3.2.3 Satisfactory Number of Random V_s Profiles

After establishing an rms criterion, it is necessary to find a sufficient number of V_s profiles to accurately show the range of V_s values and profile shapes that can be associated with the experimental dispersion curve. The profiles that meet the rms criterion are called *satisfactory*. In order to determine if the number of satisfactory profiles can be considered sufficient, a methodology for Monte Carlo inversion proposed by Kennet and Nolet (1978) and presented by Sen and Stoffa (1995) may be used. This methodology is based on estimating the resolution matrix as new satisfactory models (i.e., V_s profiles) are obtained, and stopping the algorithm when the estimate of this matrix does not change with the use of additional models.

The first step is to find a matrix **P** defined as:

$$\mathbf{P} = \frac{1}{NP} \sum_{i=1}^{NP} \left(\mathbf{vs}^i - \overline{\mathbf{vs}} \right) \left(\mathbf{vs}^i - \overline{\mathbf{vs}} \right)^T \qquad \text{(eq. 3.8)}$$

where

NP is the number of satisfactory V_s profiles,

$\mathbf{vs}^i$ is a vector of V_s values that describe one satisfactory V_s profile, with i=1,2,...,NP, and

$\overline{\mathbf{vs}}$ is the vector of average V_s values that describe the average V_s profile and is calculated as:

$$\overline{\mathbf{vs}} = \frac{1}{NP} \sum_{i=1}^{NP} \mathbf{vs}^i \qquad \text{(eq. 3.9)}$$

After constructing matrix $\mathbf{P}$, the eigenvectors ($\mathbf{e}_1$, $\mathbf{e}_2$, ..., $\mathbf{e}_K$,) of this matrix are used to estimate the resolution matrix $\mathbf{R}$ as:

$$\mathbf{R} = \sum_{k=1}^{K} \mathbf{e}_k \mathbf{e}_k^{T} \qquad \text{(eq. 3.10)}$$

where

K is the number of eigenvalues of $\mathbf{P}$

The resolution matrix can be calculated based on more satisfactory profiles as they are found and the algorithm can be stopped when the estimate of this matrix does not change significantly (Kennet and Nolet, 1978).

Another possible way of finding if more satisfactory profiles give additional information is to check if the mean for the V_s values changes with additional trials. Additionally, it is valuable to confirm that the range of profiles that meet the rms criterion is narrower than the range of all randomly generated profiles, to make sure that the limits used to constrain the V_s values do not control the solution. Lastly, the uncertainties of the final profile are expected to be less than the uncertainties of the initial profile.

3.3 Example based on numerical simulation

3.3.1 Theoretical V_s Profile and Related Dispersion Data

Synthetic data is used to evaluate the type of results that may be obtained with Monte Carlo inversion. The V_s profile created to obtain the simulated experimental data has the characteristics shown in Table 3.1. The shear wave velocity increases regularly with depth, which results in a normally dispersive profile. The corresponding dispersion curve was found using the forward algorithm implemented by Lai and Rix (1998). In this case the synthetic dispersion curve used as the "experimental" data includes only the fundamental mode because this is the dominant mode of propagation for a normally dispersive profile like the one presented here.

The forward algorithm used to obtain the simulated experimental data is the same one used to calculate theoretical dispersion curves in the Monte Carlo inversion process. Thus, in this numerical simulation the uncertainties that will be observed are caused solely by the nature of SASW inversion, since there are no errors caused by: (i) noise from data measurement, (ii) analysis of the data to create the dispersion curve, (iii) model attempting to represent the real world, or (iv) wave propagation theory. For a real experimental case these sources of error would result in additional uncertainties.

Table 3.1 Normally dispersive profile ND1

Layer No.	Layer Thickness (m)	Mass Density (g/cm^3)	Shear Wave Velocity (m/s)	Poisson's Ratio
1	5	1.8	100	0.2
2	5	1.8	200	0.45
3	10	1.8	300	0.45
	-	1.8	400	0.45

Figure 3.2 Simulated dispersion curve for profile ND1

The fundamental mode "experimental" dispersion curve is described by 50 points as presented in Figure 3.2. The data points are distributed in frequency in such a way that there are more points in the lower frequency range. This is done because lower frequencies correspond to longer wavelengths, which test deeper soils (i.e., surface waves do not have significant particle motion at depths greater than approximately one wavelength (Tokimatsu, 1997)).

3.3.2 Layered Profile Used to Perform the Inversion

The layered profile used to perform the inversion has ten, 2.5-meter layers on top of a half-space. This configuration has more layers than the real profile used to obtain the synthetic data and a larger depth to the half-space. The layers chosen are thinner than the real layers, but have interfaces that match the real ones. This assures that the assumed layering is able to match the real one if the appropriate V_s values are found. Of course there are many other possible configurations, but only one was chosen due to the time constraints associated with the Monte Carlo algorithm. With this single configuration the main purpose is to determine the expected V_s values that fit the dispersion curve and to obtain an estimate of the uncertainties associated with these values.

3.3.3 Limits Established for V_s Values

An initial estimate of the shear wave velocity profile is used as the basis of randomly generating V_s profiles for the Monte Carlo inversion. The initial estimate of the shear

wave velocities is obtained with the wavelength method, which is used to scale the dispersion curve as described in Chapter 2. The dispersion curve (Figure 3.2) formed by experimental points that relate phase velocity (V_r) with frequency (f) can equivalently be expressed as phase velocity (V_r) vs. wavelength λ (where $\lambda=V_r/f$). Herein, V_r is multiplied by a factor of 1.1 to obtain V_s and λ is multiplied by a factor of 0.33 to obtain the depth (z). For each layer, V_s is then obtained as an average of the scaled data points falling within the layer (Figure 3.3). If no points fall within the layer, V_s is obtained from the closest point to the top and/or the closest point to the bottom of the layer. The empirical estimate obtained using ten, 2.5-meter layers is presented in Table 3.2.

Based on this empirical estimate of the V_s values ($V_{s\_empirical}$), minimum and maximum values are set for each layer as (min_vs_factor)* $V_{s\_empirical}$ and (max_vs_factor)* $V_{s\_empirical}$, respectively. The factors that define the limits are chosen with min_vs_factor <1 and max_vs_factor >1. A V_s profile is formed by multiplying each empirical V_s value by a random number between min_vs_factor and max_vs_factor. The random number is generated using a uniform distribution so any number within (and including) the established limits is equally probable. The factors used to establish the limits are presented in Table 3.3. For the cases proposed, case 1 presents the widest interval and case 3 the narrowest one.
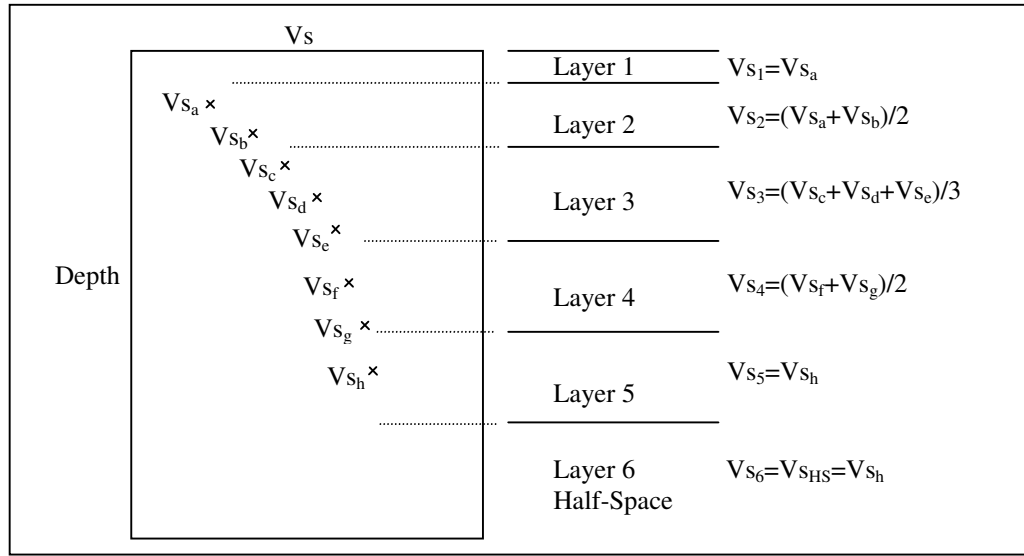
Figure 3.3 Calculation of V_s for layered profile based on V_s versus z points obtained from scaling the dispersion curve.

Table 3.2 Empirical Estimate of the V_s Profile

Layer Thickness (m)	Empirical Estimate of V_s (m/s)
2.5	100.7
2.5	113.7
2.5	144.2
2.5	184.3
2.5	219.4
2.5	241.9
2.5	264.5
2.5	289.1
2.5	314.8
2.5	326.3
Half-Space	337.7

Table 3.3 Factors Used to Establish V_s limits

	min_vs_factor	max _vs_factor
case 1	0.01	6
case 2	0.33	3
case 3	0.50	2

3.4 Results and Comments

3.4.1 V_s profiles obtained with Monte Carlo Inversion

The random algorithm is used to perform the inversion and find V_s profiles with

theoretical dispersion curves that match the "experimental" dispersion curve. The

theoretical dispersion curves are found using the forward algorithm implemented by Lai

and Rix (1998) and formed using only the fundamental mode. This is the same method

used to find the simulated dispersion curve (i.e., the "experimental" data) described in the

previous section. For different factors that establish the limits of V_s values, Table 3.4

shows the total number of trial profiles evaluated in the Monte Carlo inversion during the

time shown. This table also presents the number of the trial profiles with rms errors less

than 1.0, 1.5, 2.0, 2.5, and 3. This is done to give an idea of the amount of profiles that

had rms errors with relatively low values compared to how many profiles were tried. For

example the table shows that for case 1, only 2 of the 25,643 trial profiles had rms values

less than 3, and no profiles had rms values less than 2.

Table 3.4 Number of satisfactory profiles obtained with Monte Carlo Inversion for different V_s limits and different rms criteria

Min & max factors for V_s limits	Trial profiles	Min rms	Number of profiles with rms below [1]:					Time (hours)
			1.0	1.5	2	2.5	3	
0.01 & 6	25,643	2.36	0	0	0	1	2	388
0.33 & 3	44,014	0.94	1	10	25	50	108	376
0.5 & 2	92,053	0.68	14	85	301	658	1154	602
[1] rms values calculated using $\sigma\_vr=3\%*V_r$								

To obtain a large number of profiles with low rms the number of trial profiles and the time required are considerable. A 500 MHz, Pentium II computer was used to perform the Monte Carlo inversion and in the best case scenario it took twenty five, 24-hour days to generate only 14 profiles with rms<1 (Table 3.4). These 14 profiles were obtained out of 92,053 trial profiles. Thus, on average for V_s limits based on factors of 0.50 and 2, it would take 43 hours to run 6,575 profiles and obtain only one profile with rms<1. For the case with V_s limits based on factors of 0.33 and 3, it took 376 hours to run 44,014 profiles and obtain only one profile with rms<1. For the least constraining V_s limits (based on factors of 0.01 and 6) no profiles with rms < 1 were obtained out of 25,643 trial profiles, and the lowest rms found was 2.36.

By scaling the results for the different V_s limits to the same number of trial profiles (Table 3.5) it can be noted that as the limits imposed on V_s are narrowed the, number of profiles with low rms increases and the running time decreases. For wider V_s limits the model space is enlarged increasing the possible V_s values for each layer, and

consequently increasing the number of possible combinations of these values. Thus, more profiles are needed in order to adequately explore the model space, resulting in a smaller ratio of satisfactory profiles per trial profiles. Additionally, the wider limits result in the production of profiles with higher contrasts between layers (i.e., rougher profiles), which increases the computer time needed to run the forward algorithm, and therefore the time to run the Monte Carlo inversion increases significantly.

**Table 3.5 Number of satisfactory profiles for different V_s limits
scaled to the same number of trial profiles**

Min & max factors for V_s limits	Trial profiles	Estimated number of profiles with rms below [1]:					estimated time (hours)
		1.0	**1.5**	**2**	**2.5**	**3**	
0.01 & 6	25,643	0.0	0.0	0.0	1.0	2.0	388
0.33 & 3	25,643	0.6	5.8	14.6	29.1	62.9	219
0.5 & 2	25,643	3.9	23.7	83.8	183.3	321.5	168
[1] rms values calculated using $\sigma\_vr = 3\% * V_r$							

Table 3.6 shows in more detail the number of profiles obtained for different rms criteria (for V_s limits of $0.5 \& 2 * V_{s\_empirical}$). The profiles that meet the rms criterion selected (i.e., a reasonable value is 1.0 as discussed at the beginning of this chapter) can be used to examine the type of profiles that fit the experimental data and the uncertainties that are introduced by the inversion process itself (since no uncertainties are added herein by experimental errors in data collection, analysis of the data to create the dispersion curve, layered model to represent a real 3-D soil stratification, or wave propagation theory).

**Table 3.6 Number of profiles obtained with
Monte Carlo Inversion for different rms criteria.**

rms < than	# of profiles
0.75	1
0.8	2
0.85	4
0.9	6
0.95	11
1	14
1.05	19
1.1	26
1.15	31
1.2	38
1.25	45
total number of trial profiles= 92,053	
min & max factors for V_s limits= 0.5 & 2	

Figure 3.4 presents all the V_s profiles and the related dispersion curves with rms < 1. For the narrower V_s limits (0.5&2 * $V_{s\_empirical}$), the range of profiles with rms<1 covers most of the range of trial profiles (shown by the V_s limits), especially for the layers with depths between 5 and 25 meters. This implies that the limits might be constraining the solution, i.e., that there might be profiles outside the limits that have a satisfactory rms value. For the wider limits (0.33&3 * $V_{s\_empirical}$) it can be noted that the one of the satisfactory profiles falls outside the narrower limits, which confirms that it is possible to find profiles with rms<1 that are outside the range given by the narrower limits. Unfortunately, due to time constraints, it was not possible to generate a sufficient number of profiles with the wider limits to obtain a good representative sample of profiles with rms<1.

Figure 3.5 shows separate plots for the 14 profiles with rms<1 obtained with the narrower limits (0.5&2 * $V_{s\_empirical}$). These plots illustrate that profiles with very different shapes and very different V_s contrasts provide an equally satisfactory match (rms<1) to the experimental dispersion curve. Thus, based on the dispersion curve alone it is not possible to resolve specific velocity contrasts between layers.
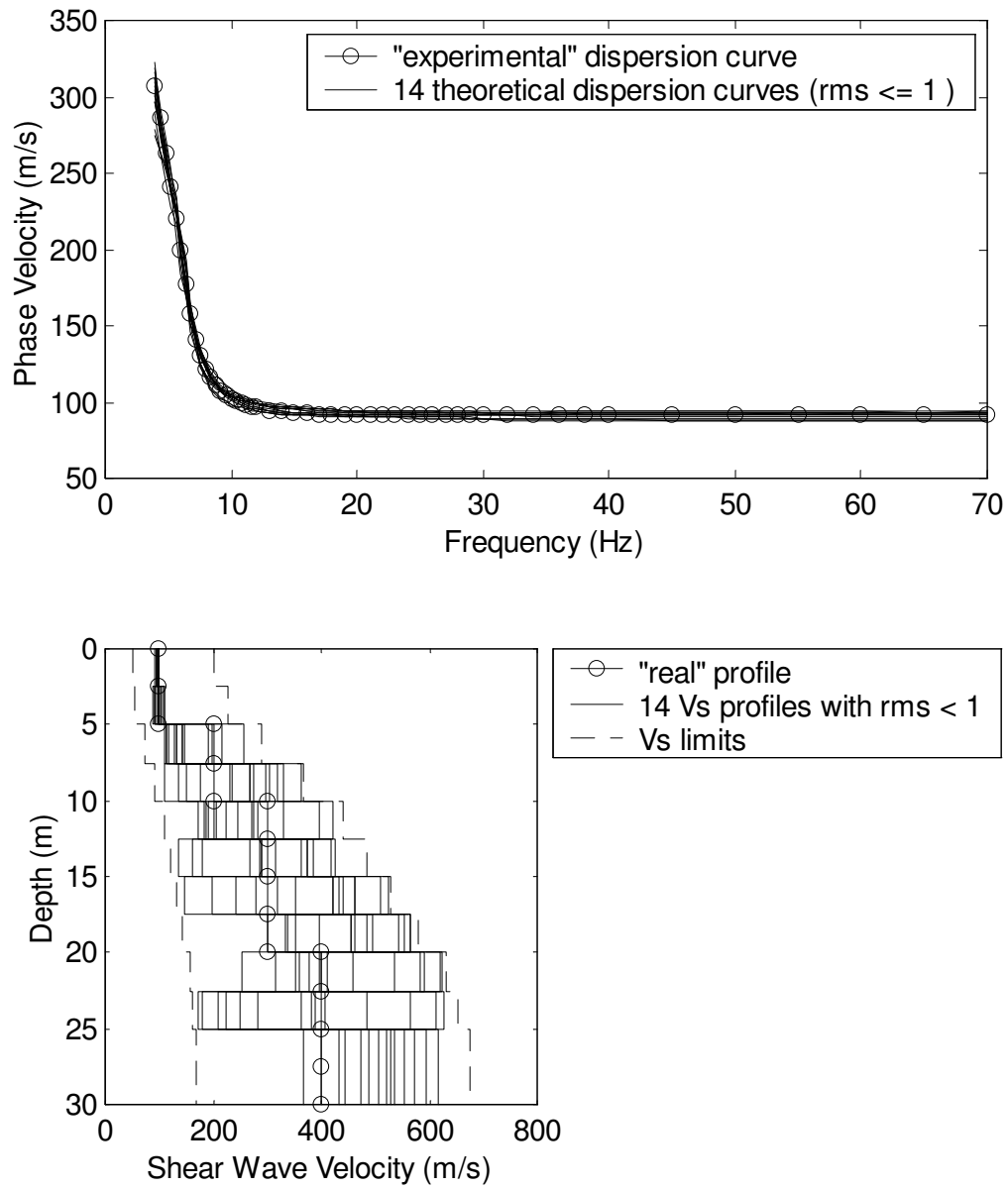
Figure 3.4(a) V_s profiles with rms<1, for V_s limits = 0.5 & 2 * $V_{s\_empirical}$
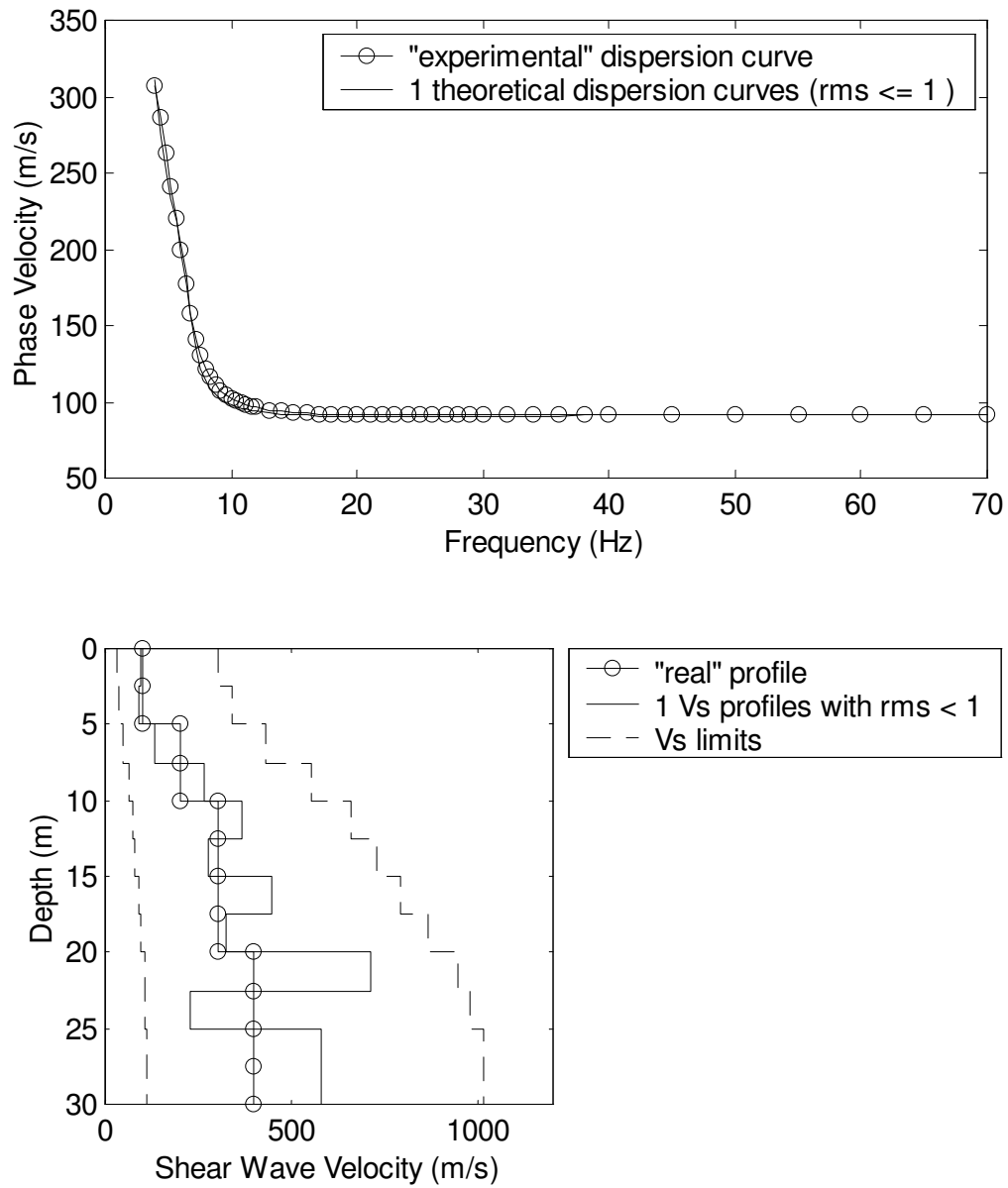
Figure 3.4(b) V_s profiles with rms<1, for V_s limits = 0.33 & 3 * $V_{s\_empirical}$
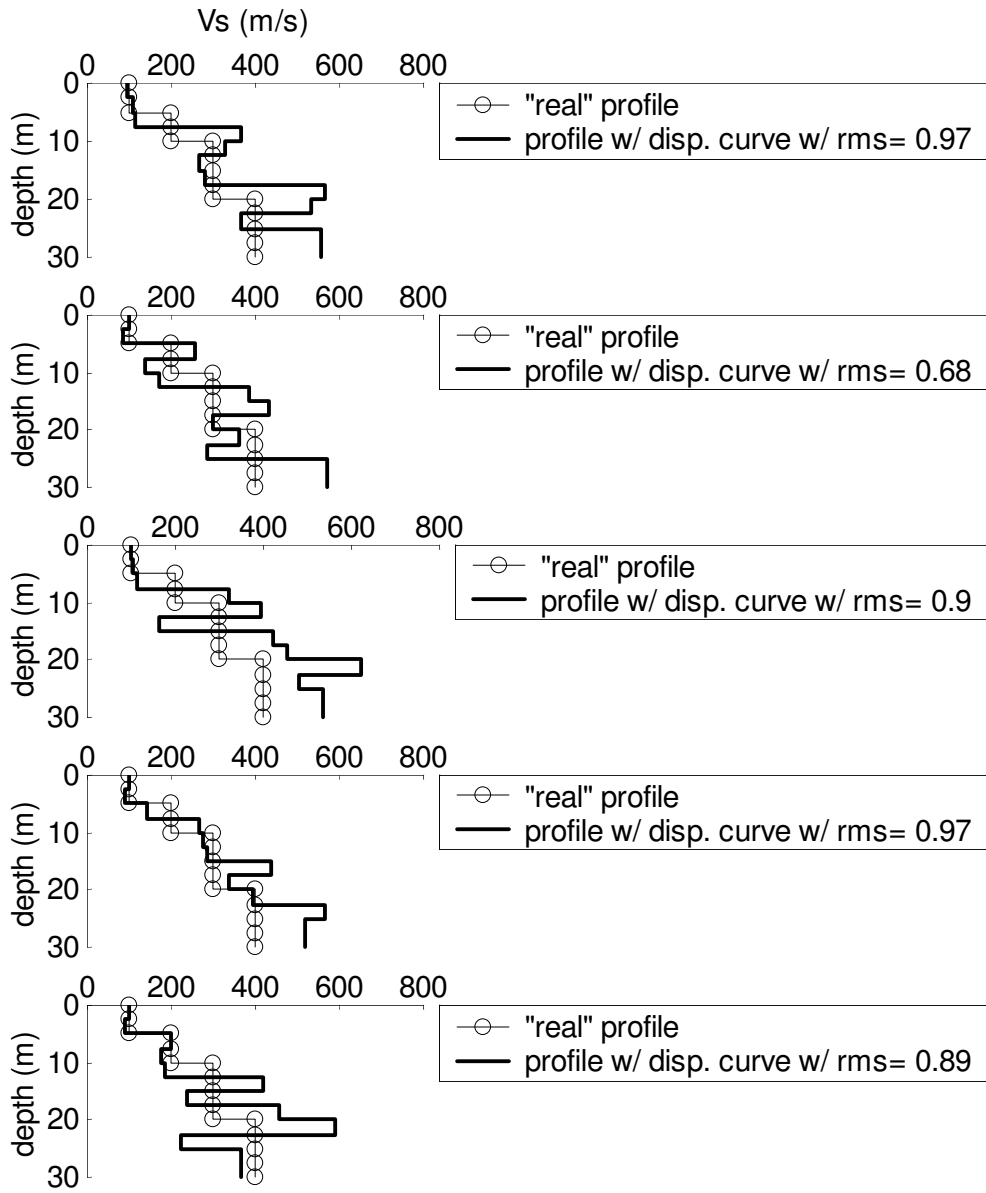
Figure 3.5 Separate plots of V_s profiles with rms<1, for V_s limits=0.5&2*$V_{s\_empirical}$
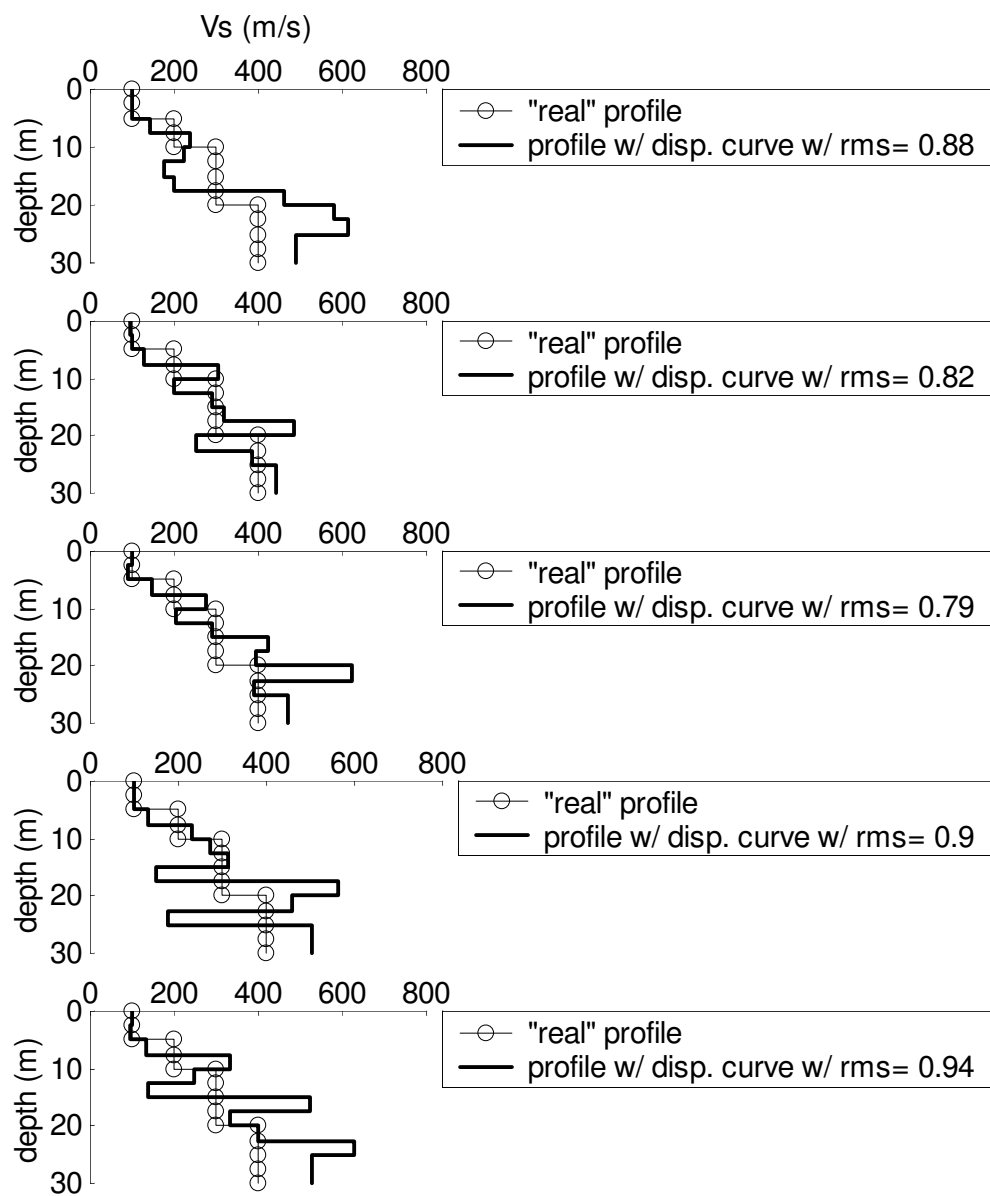
Figure 3.5 (Cont'd)
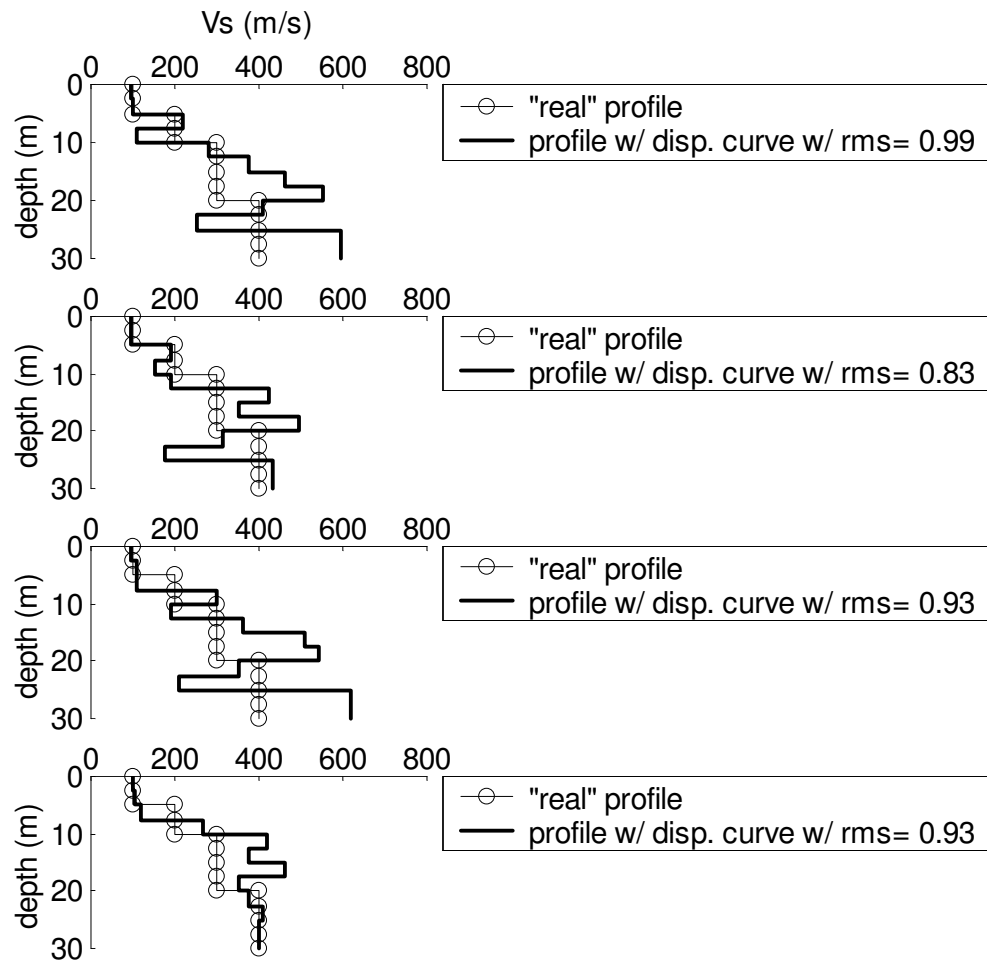
Figure 3.5 (Cont'd)
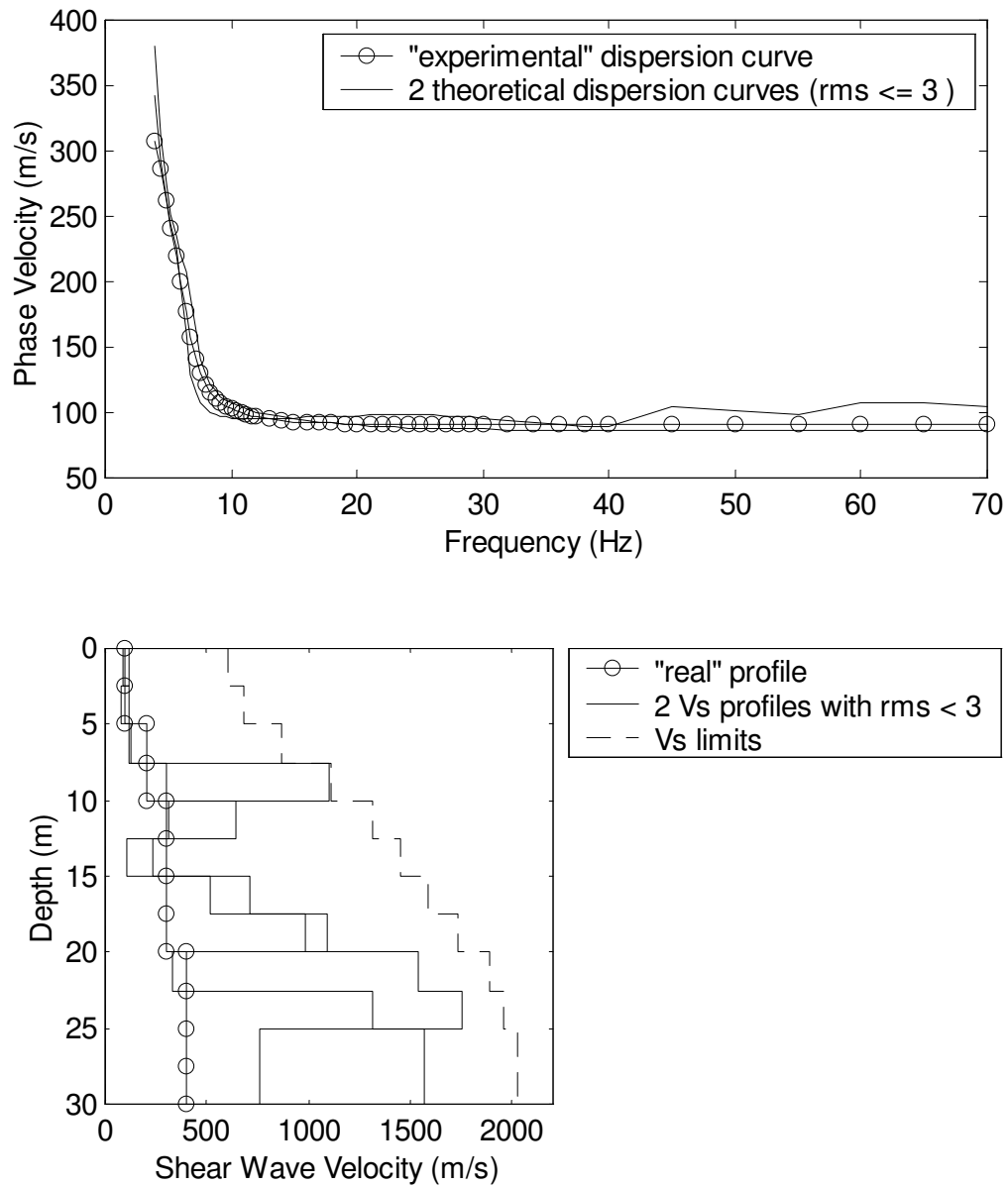
Figure 3.6 Two best fitting profiles obtained for V_s limits=0.01&6*$V_{s\_empirical}$

Figure 3.6 presents the two best profiles for the widest V_s limits used (0.01&6 * $V_{s\_empirical}$), which have rms values of 2.4 and 2.9. These profiles were found out of 25,643 trial profiles that took sixteen, 24-hour days of running time. Profiles with lower rms values (such as those found for narrower V_s limits) could potentially be found with the wider limits, since these limits define a larger model space that includes these profiles. Thus, in this case, the V_s limits of 0.01&6 * $V_{s\_empirical}$ gave too much flexibility to the solution for the amount of time and computer resources that were available, and the model space was not searched thoroughly enough to find a satisfactory number of trial profiles.

3.4.2 Analysis of Results

Given that for the rms criterion of 1.0 there are very few satisfactory profiles, an rms criterion of 1.5 is adopted in order to have a considerably larger number of profiles to analyze the results of the Monte Carlo inversion. This new criterion is considered appropriate, since it results in a reasonable match between theoretical and experimental dispersion curves as shown in Figure 3.7. Figure 3.7 shows the plots of 85 V_s profiles with rms<1.5 obtained for V_s limits of 0.5 & 2 * $V_{s\_empirical}$ and 10 profiles with rms<1.5 obtained for V_s limits of 0.33 & 3 * $V_{s\_empirical}$. It is important to note that the rms value also depends on the assumed uncertainties of V_r, and not only on the match between experimental and theoretical dispersion curves. For instance if the assumed value for the uncertainties of V_r is changed from (3%)$\mathbf{vr}_{ex}$ to (5%)$\mathbf{vr}_{ex}$, the maximum rms value of the 85 profiles presented in Figure 3.7(a) changes from 1.5 to 0.9. Thus, a change in the

uncertainties of V_r from (3%)$\mathbf{vr}_{ex}$ to (5%)$\mathbf{vr}_{ex}$ would actually make all 85 profiles meet the rms criterion of 1.0.

The profiles presented in Figure 3.7 will be used as the basis for the figures that follow, where normal probability plots, expected V_s values and variances are derived. The wide range of profiles that meet the rms<1.5 criterion shows that the limits given to V_s are constraining the range of V_s values obtained. Unfortunately, as discussed previously, widening the V_s limits excessively increases the number of trial profiles needed to find satisfactory profiles. In any event, the profiles observed here are still valuable, since they were found using the fewest possible constraints to the solution space by starting from a large range of possible V_s values for each layer that were all equally probable and independent.

Figure 3.8 presents the normal probability plots for each layer of the 85 profiles with rms<1.5 that were found for V_s limits of 0.5&2*$V_{s\_empirical}$. Normal probability plots can be interpreted as follows: for a specified shear wave velocity (call it V_{s1}) on the horizontal axis, the "probability" given by the vertical axis means the probability that the shear wave velocity will be less than V_{s1}. For example, the V_s value that corresponds to a cumulative probability of 0.5 (i.e., 50%) is commonly called the mean value. The log normal distribution was also considered in order to have a distribution that mathematically restricts V_s to non-negative values. However, the normal distribution resulted in a better representation for the distribution of the available data, and consequently normal probability plots are presented here.
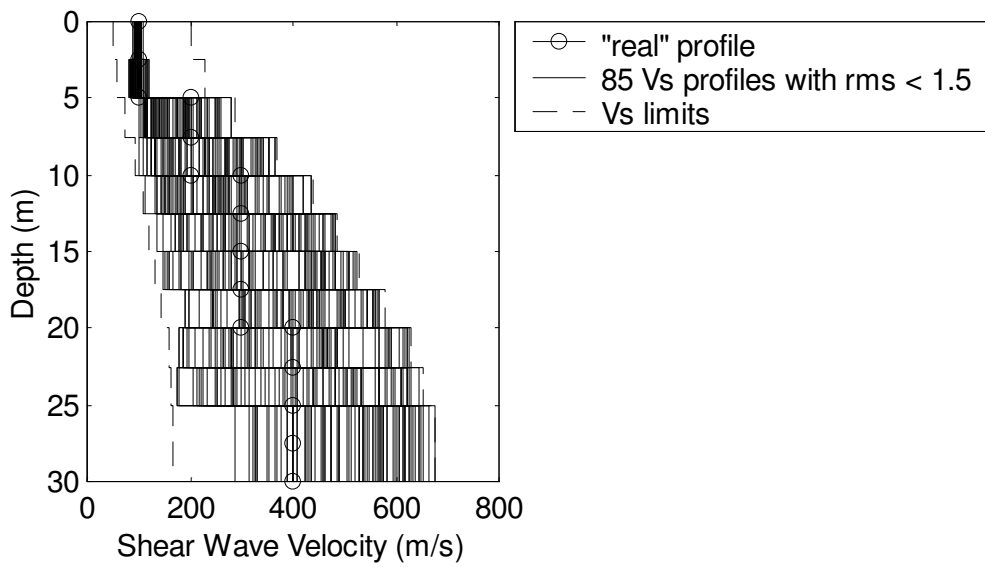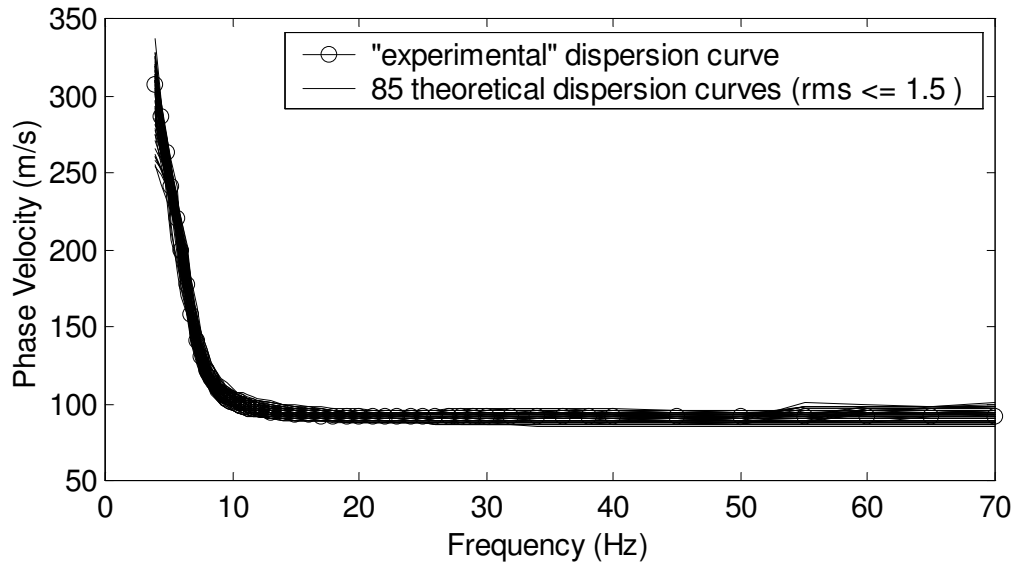
Figure 3.7(a) V_s profiles with rms<1.5, for V_s limits = 0.5 & 2 * $V_{s\_empirical}$
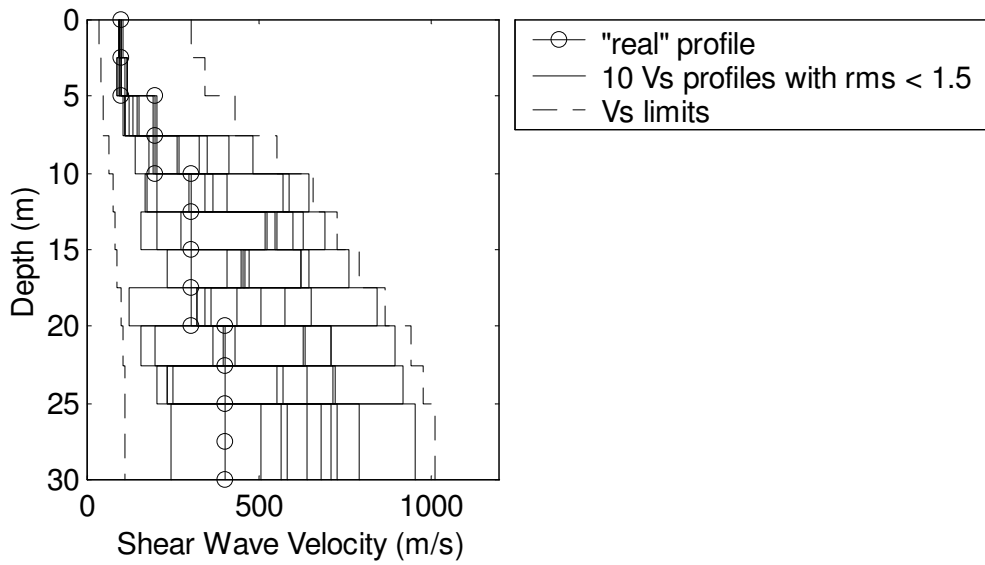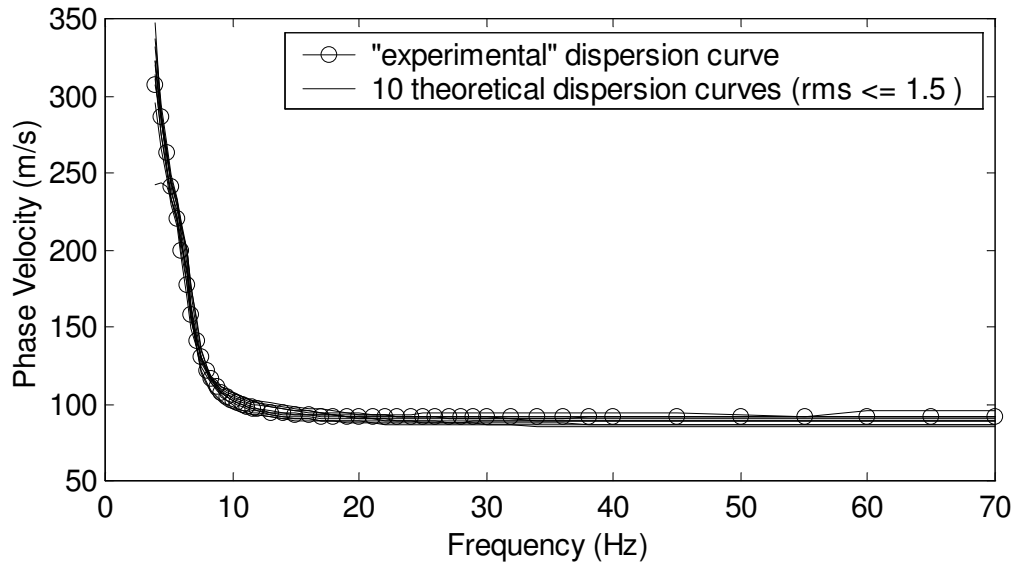
Figure 3.7(b) V_s profiles with rms<1.5, for V_s limits = 0.33 & 3 * $V_{s\_empirical}$
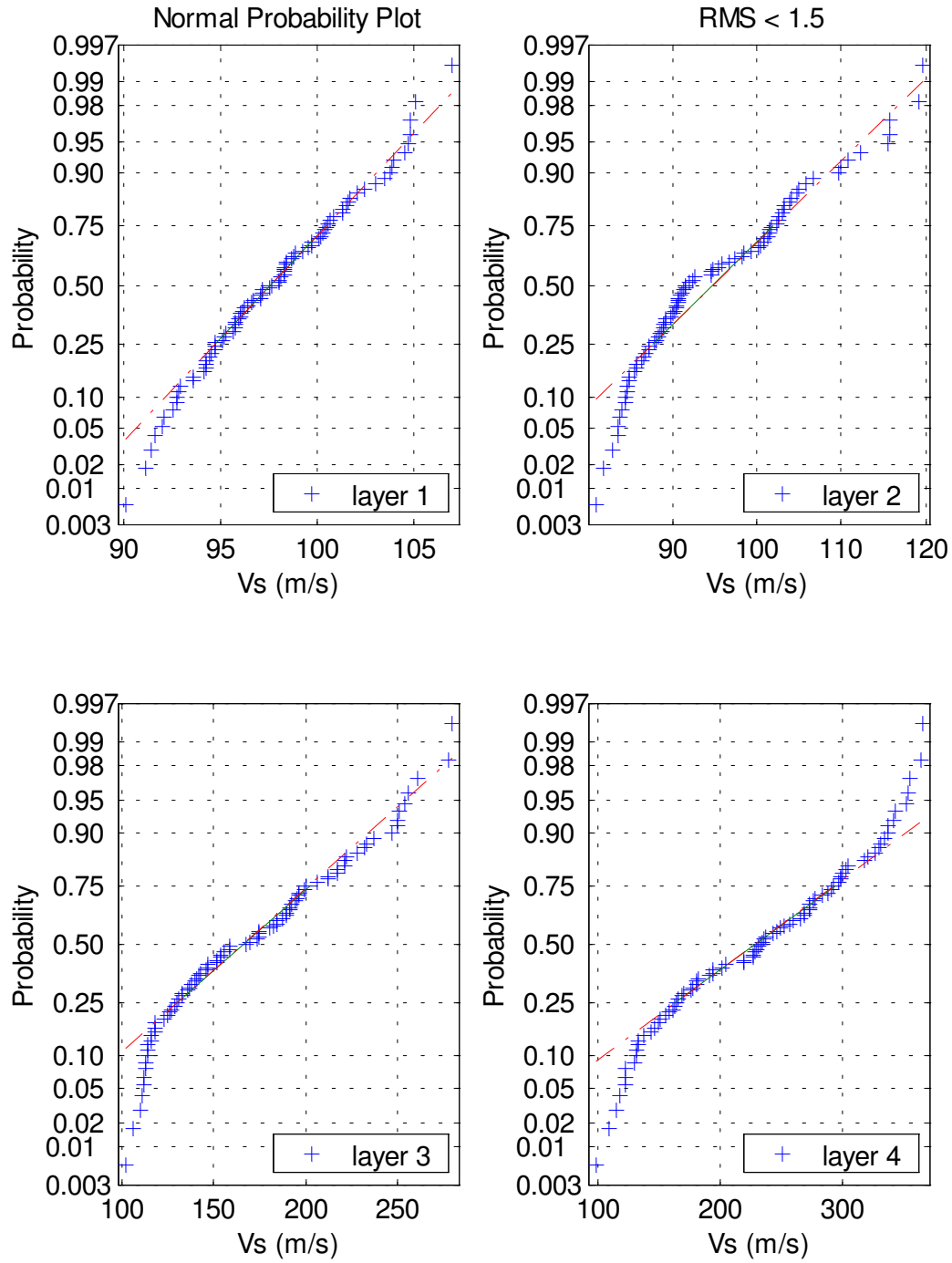
Figure 3.8(a) Normal probability plots for layers 1 to 4, for V$_s$ limits=0.5&2*V$_{s\_empirical}$ and rms<1.5
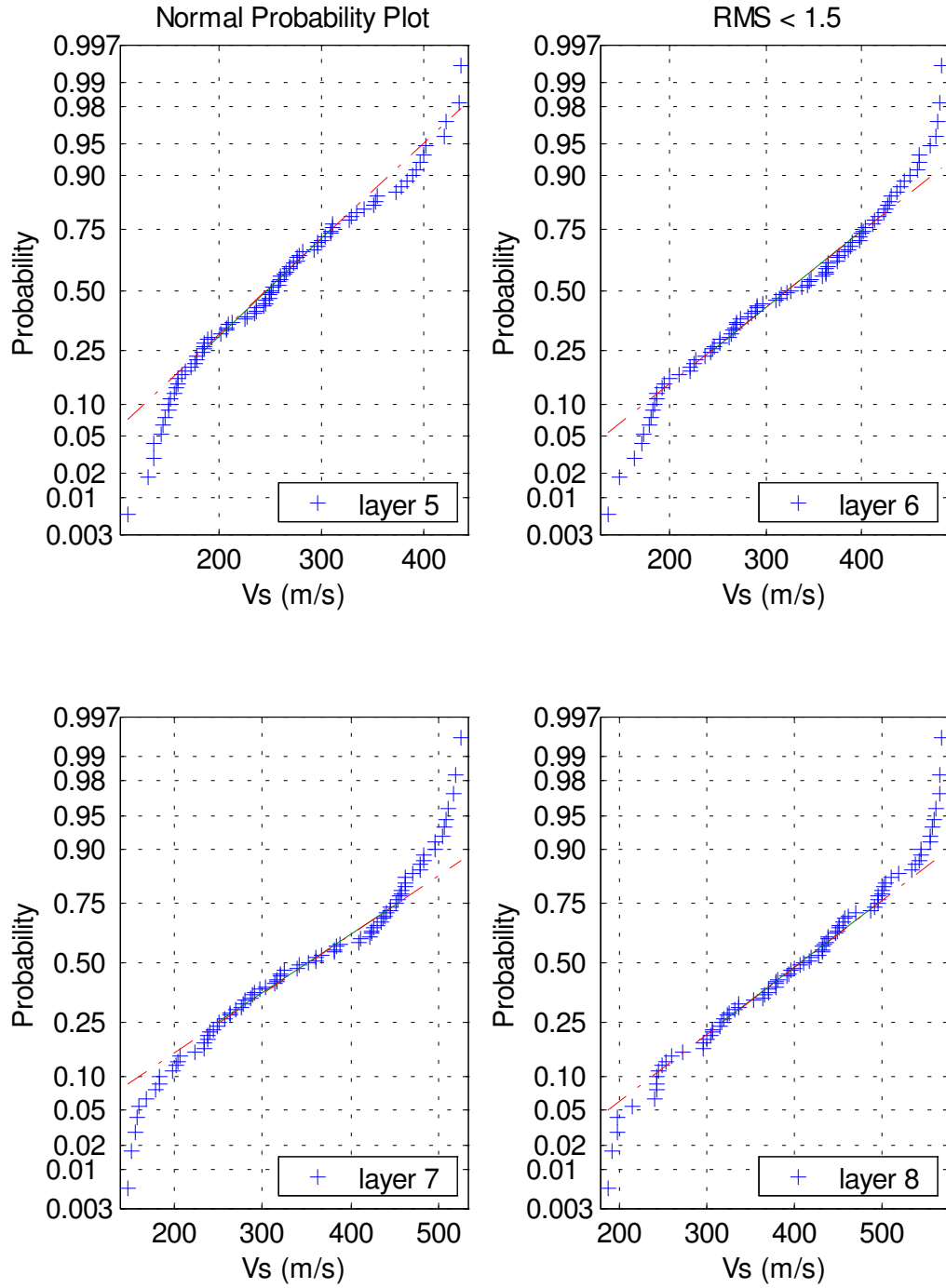
Figure 3.8(b) Normal probability plots for layers 5 to 8, for V_s limits=0.5&2*$V_{s\_empirical}$ and rms<1.5
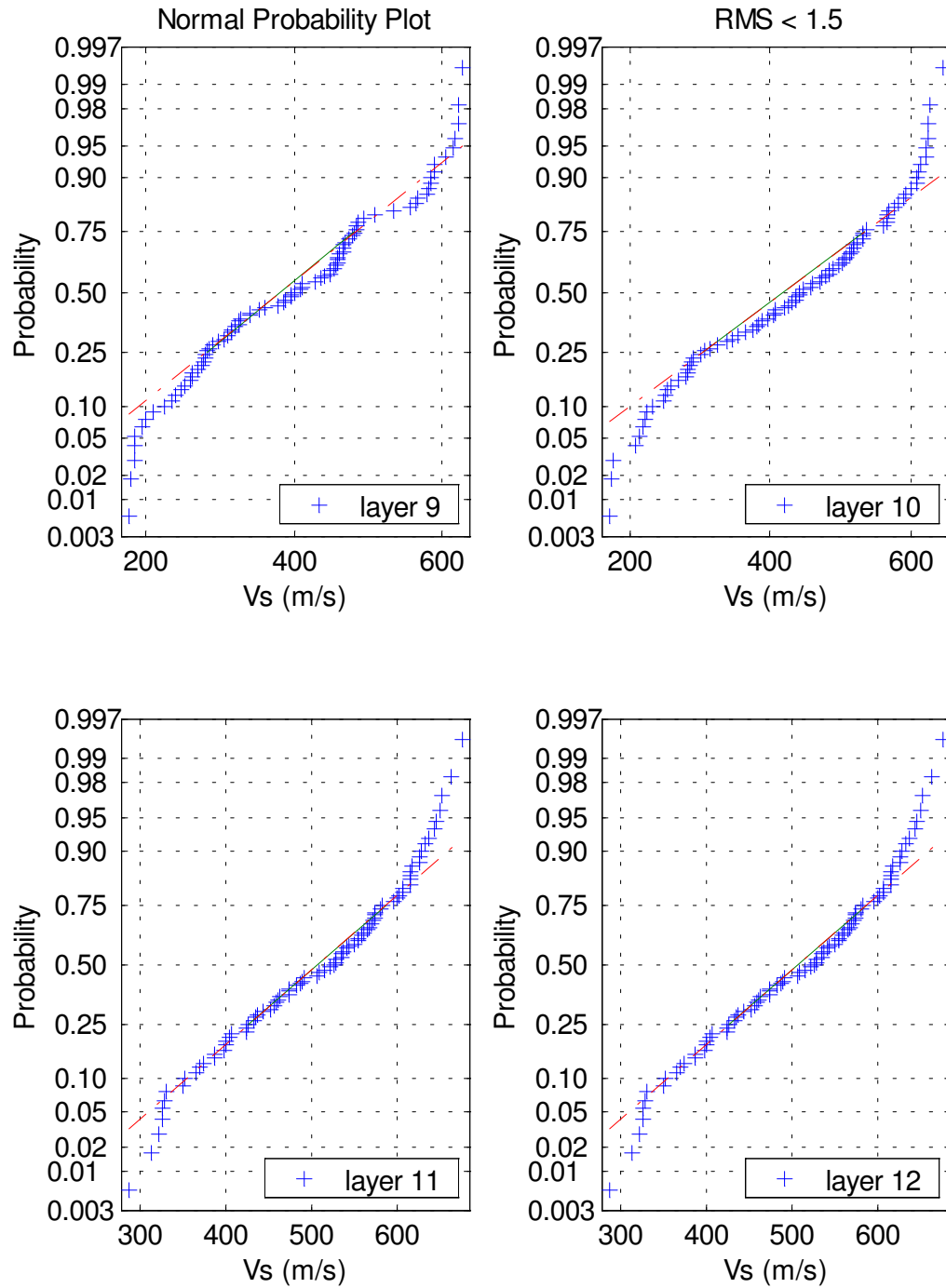
Figure 3.8(c) Normal probability plots for layers 9 to 12, for V_s limits=0.5&2*$V_{s\_empirical}$ and rms<1.5

The normal probability plots in Figure 3.8 show that for a wide interval around the mean, the distribution of the data closely follows a straight line corresponding to a normal distribution. The main difference between the actual distribution of the V_s values obtained and the normal distribution is that the actual distribution has shorter tails. This is most likely caused by the V_s limits constraining the solution and not allowing for very large or very low V_s values. Thus, the plots show that the normal distribution is a reasonable statistical representation for the V_s values obtained, and using the mean and covariance matrix as described by equations 3.6 and 3.9 is justified.

Figure 3.9 shows the mean and standard deviation for the V_s profiles with rms<1.5. The standard deviations are calculated using equation 3.7, which is equivalent to calculating the square roots of the diagonal terms of the covariance matrix described by equation 3.6. Comparing Figures 3.9(a) and 3.9(b), it is clear that both mean and standard deviation vary significantly depending on the V_s limits assumed. For the limits of 0.5&2* $V_{s\_empirical}$ the mean more closely approximates the real profile than for the limits of 0.33&3* $V_{s\_empirical}$, Furthermore, the standard deviation is significantly higher for the latter. Figure 3.9 shows that for the narrower limits the rms error related to the mean profile is 2.21, and for the wider limits, the rms error related to the mean profile is 2.33. Thus, both mean V_s profiles produce dispersion curves with higher rms errors than the maximum rms error of 1.5 of the profiles used to calculate them.

Another option to find a representative profile and its related uncertainties to summarize all the satisfactory V_s profiles is to calculate the mathematical expectation and the

covariance matrix as suggested by Tarantola (1987) and described in equations 3.3 and 3.5. The standard deviations are equal to the square roots of the diagonal terms of the covariance matrix. Figure 3.10 shows the mathematical expectation found using this approach compared to the mean previously presented in Figure 3.9.

As described earlier in this chapter, the mathematical expectation used herein is a weighted average with the weights given by the likelihood, which like the rms error is a measure of the fit between theoretical and experimental data. In this case, the resulting "expected" profile is very close to the profile with the highest likelihood, i.e., lowest rms error (shown in Figure 3.5 for the limits of 0.5&2* $V_{s\_empirical}$ and in Figure 3.4b for the limits of 0.33&3* $V_{s\_empirical}$). This result is highly dependent on the number of satisfactory profiles found since it is very close to the profile with the lowest rms error. As shown in Figure 3.5 the best fitting profiles have different shapes with different V_s contrasts, and following a specific shape with V_s contrasts unnecessary to fit the experimental data may mislead the user of the V_s profile to believe in those contrasts. This also means that if more trial profiles are evaluated and a lower rms error is found, the shape of the "expected" V_s profile may change significantly. On the other hand, a new profile with a lower rms error would not significantly affect the mean presented in Figure 3.9 since this mean is already based on a reasonable number of profiles (see discussion below for Figure 3.11). Thus, in this case the mean of the V_s profile is considered a better alternative to summarize the results than the expectation, because it gives all the profiles with satisfactory rms error the same weight, producing a profile with no large V_s contrasts.
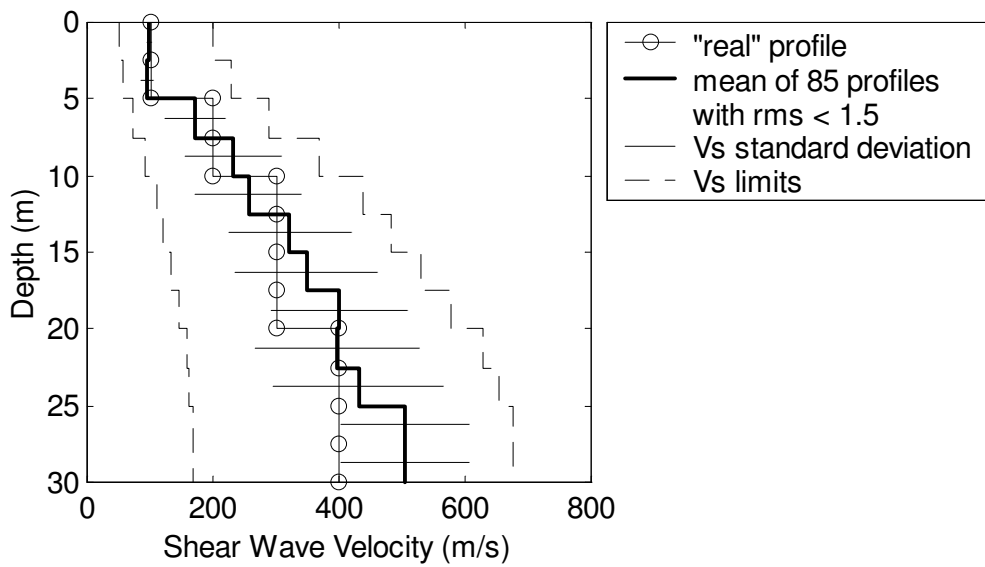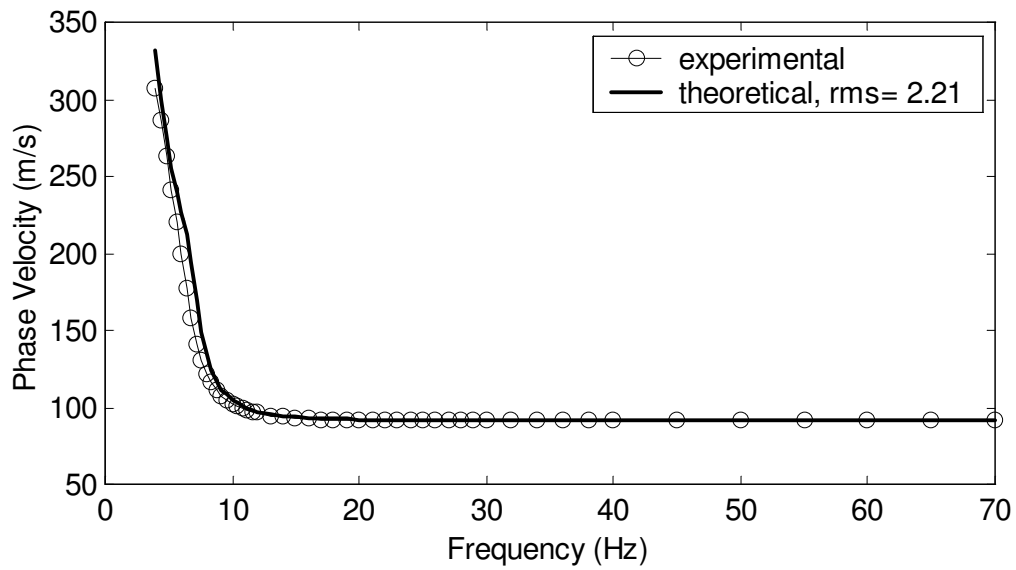
Figure 3.9(a) V_s mean and standard deviations for profiles with rms<1.5, for V_s limits = 0.5 & 2 * $V_{s\_empirical}$
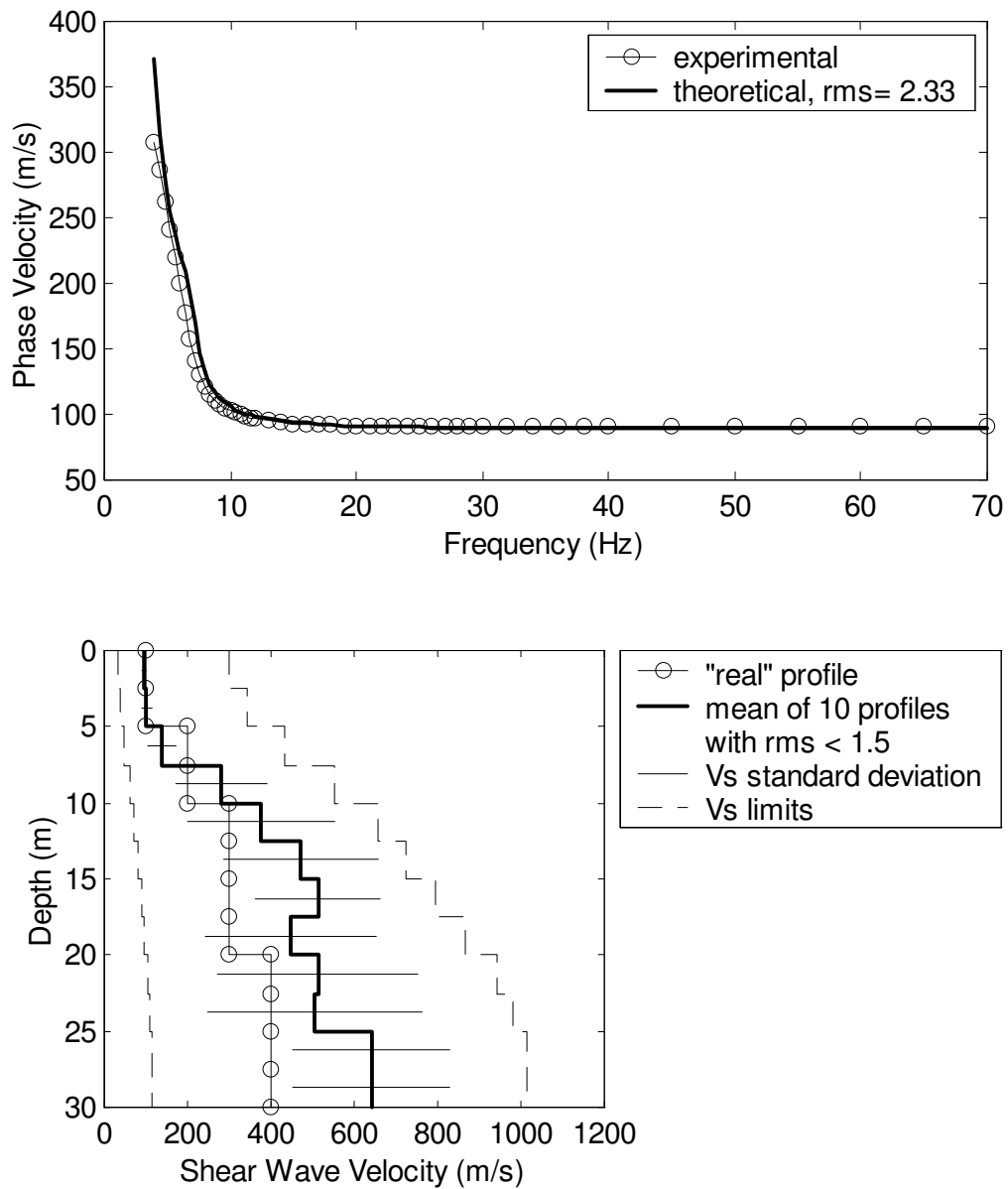
Figure 3.9(b) V_s mean and standard deviations for profiles with rms<1.5, for V_s limits = 0.33 & 3 * $V_{s\_empirical}$
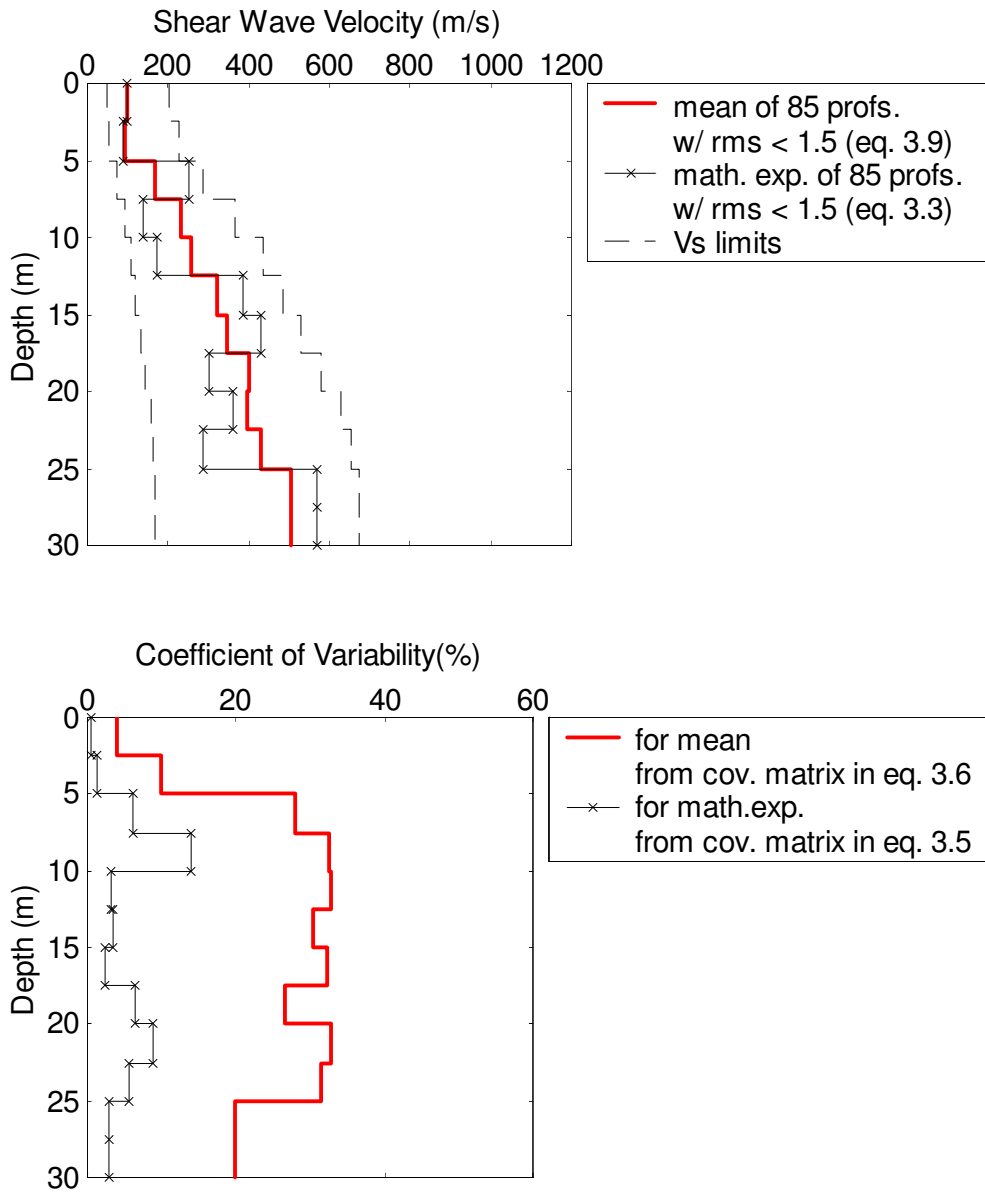
Figure 3.10(a) Comparison of V_s mean, mathematical expectation, and their respective uncertainties, for V_s limits = 0.5 & 2 * $V_{s\_empirical}$
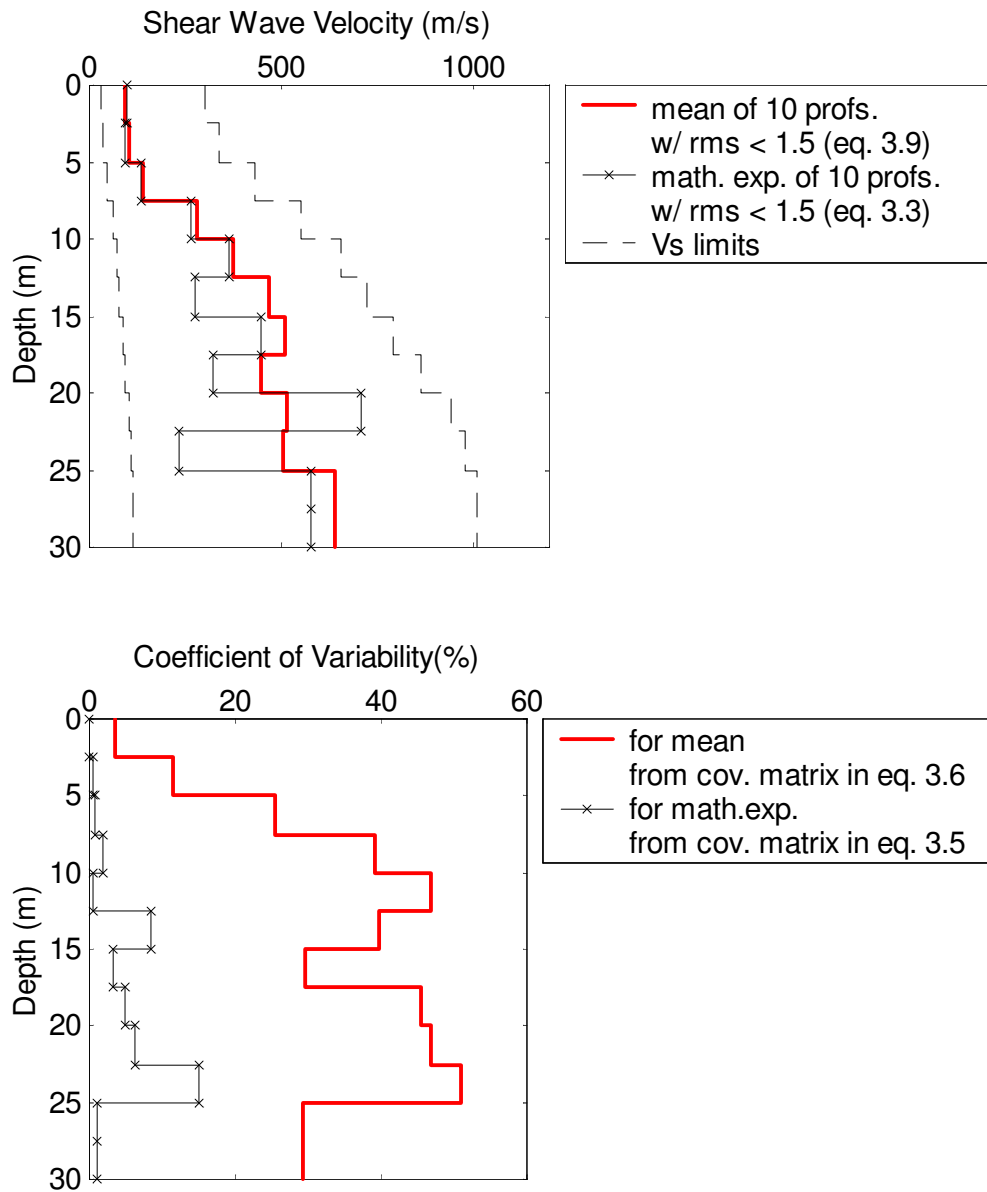
Figure 3.10(b) Comparison of V_s mean, mathematical expectation, and their respective uncertainties, for V_s limits = 0.33 & 3 * $V_{s\_empirical}$

Figure 3.10 also presents results for the uncertainties with plots of the coefficient of variation versus depth. This coefficient is calculated as the standard deviation divided by the value of the shear wave velocity:

$$\text{Coefficient of Variation} = \sigma\_vs / V_s \quad \text{(eq. 3.11)}$$

The standard deviations calculated from the covariance matrix in equation 3.6 correspond to the common "sample" standard deviations as given by equation 3.7, and are the uncertainties related to the mean profile. The standard deviations from the covariance matrix in equation 3.5 include some weighting given by the likelihood, and are the uncertainties related to the "expected" profile (i.e. mathematical expectation). It is clear that the uncertainties for the mean profile result in significantly higher coefficients of variation than the uncertainties for the "expected" profile. The uncertainties for the mean profile better reflect the wide range of profiles that meet the rms criterion (Figure 3.7). Additionally, these uncertainties are based on a normal distribution for the V_s values, which as discussed above is an appropriate distribution for the results obtained. Thus, the mean with its related uncertainties will be used as the representative profile of all the satisfactory V_s profiles that meet the rms error criterion imposed.

To check that the number of satisfactory V_s profiles is sufficient to be a representative sample of the possible solutions, the mean of all of the satisfactory profiles is compared with the mean of only 60% of the satisfactory profiles. The value of 60% was chosen since it results in integer numbers for both 60% of 85 (=51) and 60% of 10 (=6). In this

way, a relatively high number of profiles are removed and the percentage of profiles kept is exactly the same for both cases. Figure 3.11 shows the two means for profiles with rms<1.5, using 85 and 51 profiles for V_s limits of $0.5\&2*V_{s\_empirical}$, and using 10 and 6 profiles for V_s limits of $0.33\&3*V_{s\_empirical}$. Comparing the means, it is noted that the number of profiles used was sufficient for the narrower V_s limits, since the mean does not vary significantly with an important increase in the number of profiles (from 51 to 85 profiles). For the wider V_s limits, there are larger changes in the mean when increasing the number of profiles (from 6 to 10 profiles), and more satisfactory profiles are needed to improve confidence.

The issue of whether the number of profiles is sufficient to have confidence in the solution obtained can be addressed in a more refined way with the resolution matrix (equation 3.10). As mentioned earlier in this chapter, when the estimate of the resolution matrix remains constant, the number of satisfactory profiles is considered sufficient. The change of the resolution matrix was calculated after every other additional profile. For the case with V_s limits of $0.5\&2*V_{s\_empirical}$ it was found that after 13 profiles the resolution matrix does not vary (Table 3.7). For the case with V_s limits of $0.33\&3*V_{s\_empirical}$ there were not enough profiles and the resolution matrix did not stabilize (Table 3.8).
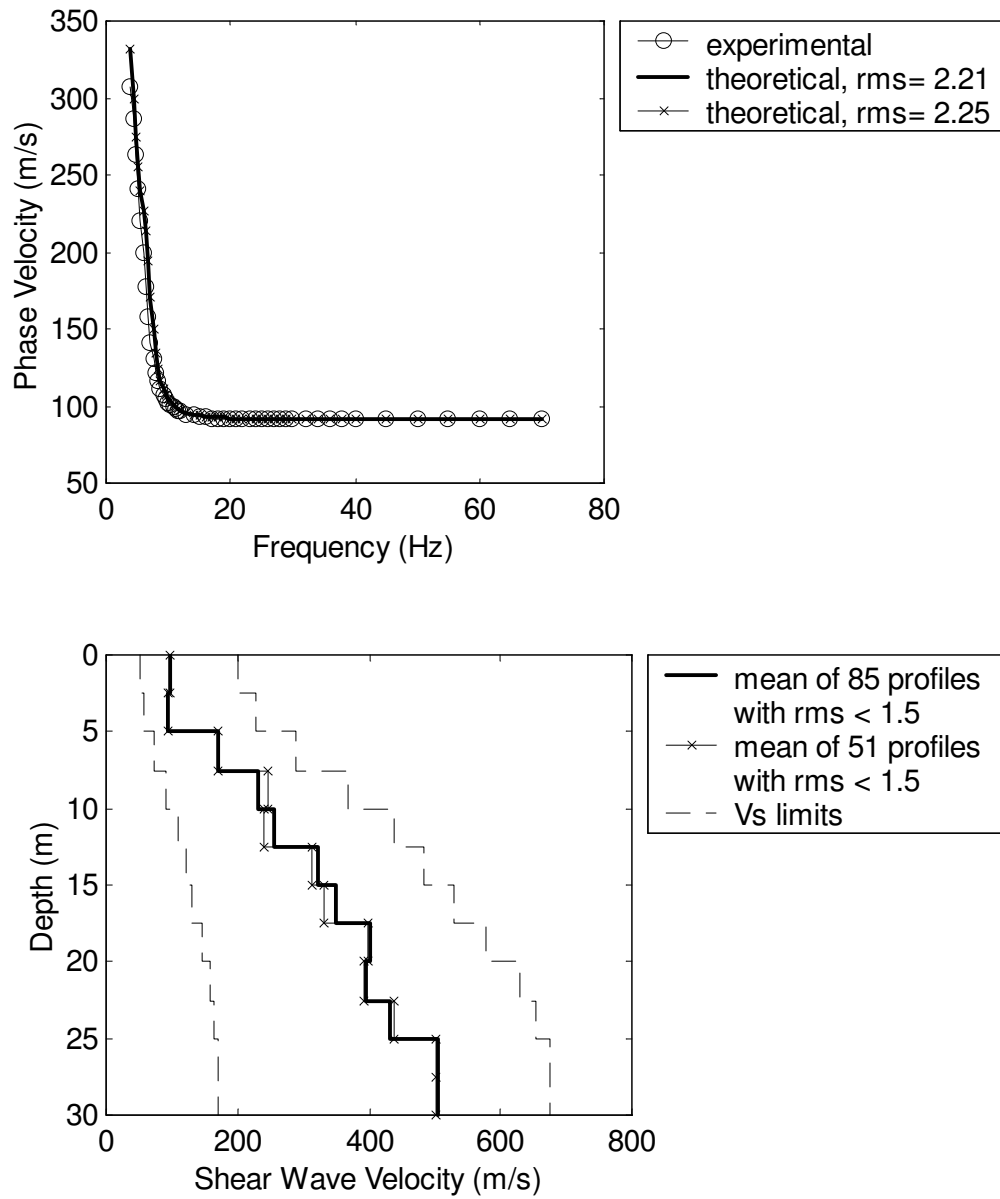
Figure 3.11(a) Changes to the V_s mean when the number of profiles is reduced, for V_s limits = 0.5 & 2 * $V_{s\_empirical}$
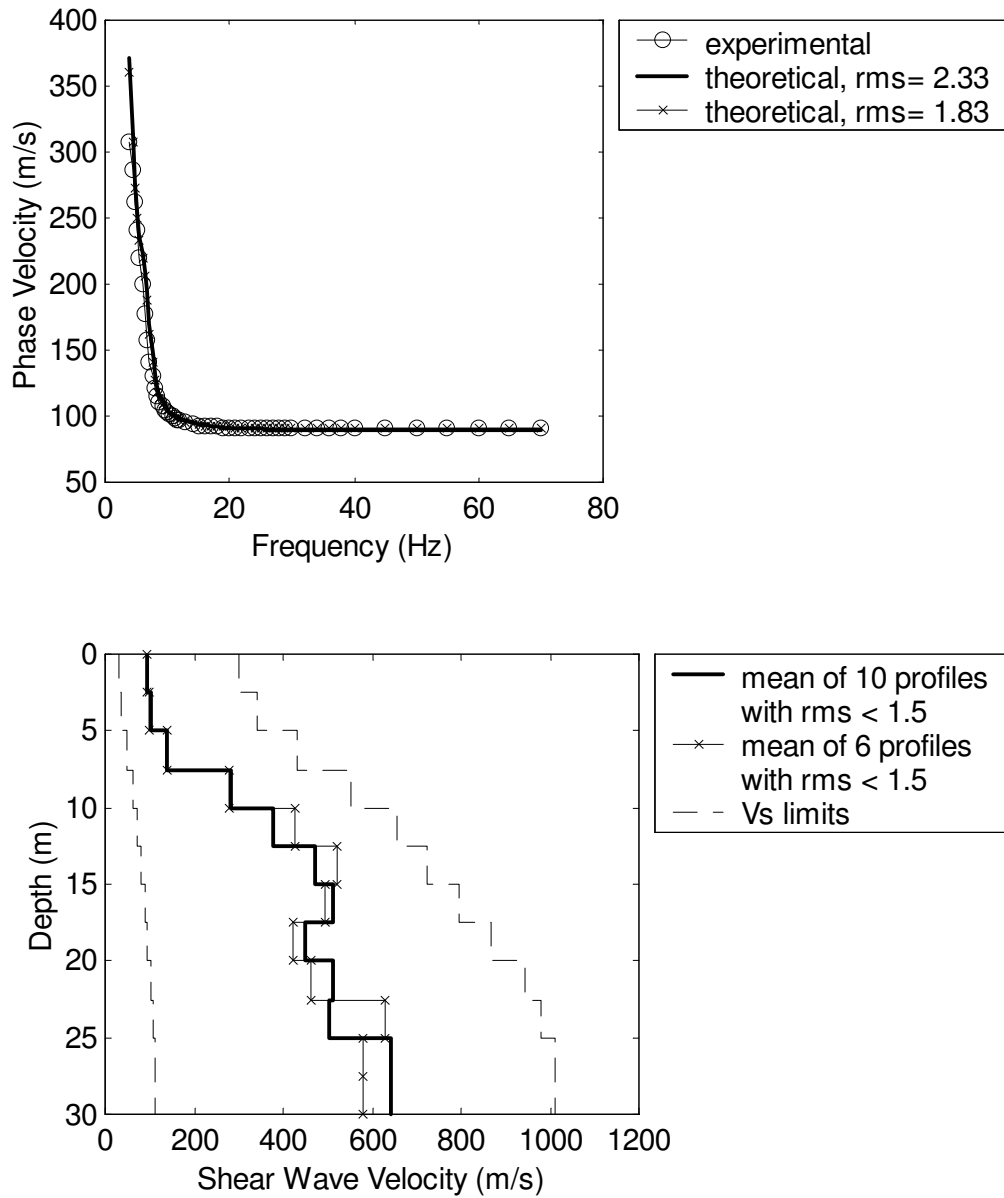
Figure 3.11(b) Changes to the V_s mean when the number of profiles is reduced, for V_s limits = 0.33 & 3 * $V_{s\_empirical}$

Table 3.7 Changes in resolution matrix for V_s limits of 0.5&2*$V_{s\_empirical}$

from: # of profiles	to: # of profiles	Sum of absolute differences in resolution matrix
3	1	12.53
5	3	11.27
7	5	10.39
9	7	8.27
11	9	1.97
13	11	0.00
15	13	0.00
17	15	0.00
…	…	…
85	83	0.00
V_s limits = 0.5&2* $V_{s\_empirical}$		

Table 3.8 Changes in resolution matrix for V_s limits of 0.33&3*$V_{s\_empirical}$

from: # of profiles	to: # of profiles	sum of absolute differences in resolution matrix
3	1	11.55
5	3	8.93
7	5	10.34
9	7	5.41
11	9	-
V_s limits = 0.33&3* $V_{s\_empirical}$		

3.5 Conclusions

The Monte Carlo algorithm provides a valuable technique to examine possible solutions to the inverse problem with minimal contraints. Although the thicknesses of the layers describing the V_s profile were fixed and the depths of the layer interfaces were the same as those of the real profile, the shapes of satisfactory V_s profiles vary significantly. Based on the variety of shapes found it is clear that the dispersion curve does not constrain the solution sufficiently to be able to find a unique V_s profile or to resolve specific velocity contrasts between layers. Consequently, the final layered V_s profile should be interpreted as a discrete model, which is one possible representation of the real V_s profile, and should include uncertainties for the estimated V_s values.

The V_s profiles were found adding very few constraints to the solution space, by starting from a large range of possible V_s values for each layer, which were all equally probable and independent. When no V_s is favored, a good idea of the range and shapes of profiles that fit the data is obtained. Herein, the limits established for V_s constrain the range of results obtained, but it is difficult to explore enough possibilities if more flexibility is given with larger limits. If the limits for V_s are too wide, the number of trials necessary to explore the model space is extremely large, and consequently the inversion requires an unreasonable amount of time and computer resources. In the best case scenario (i.e., most constraining V_s limits) it took twenty five, 24-hour days to generate only 14 profiles with rms<1 with a Pentium II 500MHz processor. For the wider V_s limits (i.e., 0.01&6 * $V_{s\_empirical}$) the model space could not be searched sufficiently to find any satisfactory

profiles within a reasonable time frame. Due to the fast improvement in computers the processing time could be highly reduced in the future and a thorough search of a large model space could become feasible

The profiles meeting the criterion of rms<1.5 for the most constraining V_s limits were used to examine the type of profiles that fit the experimental data and their related uncertainties. The estimated coefficients of variation were between 20% and 30%, except for the very top layers, where the values are lower. These uncertainties are caused by the nature of the SASW inversion problem alone since in this case no uncertainties are added by experimental errors in data collection, analysis of the data to create the dispersion curve, layered model to represent a real 3-D soil stratification, or wave propagation theory.

The V_s profiles with a satisfactory rms error have variable shapes and reporting only the best fitting V_s profile obtained may mislead the user to believe in large V_s contrasts that are unnecessary to fit the experimental data. For this reason, normal probability plots were used to show that the range of V_s values obtained could be reasonably represented by the normal distribution, and consequently the mean and the standard deviation are valid parameters to characterize all the satisfactory V_s profiles that meet a particular rms error criterion.

CHAPTER 4

SASW INVERSION BASED ON THE MAXIMUM LIKELIHOOD METHOD

4.1 Introduction

In this chapter, the maximum likelihood method is described and implemented for SASW inversion assuming Gaussian distributions for the dispersion data and the a priori model parameters (i.e., values given to the shear wave velocities as a starting point for the inversion). These are reasonable assumptions for SASW inversion as discussed in Chapter 3; if desired, other distributions may be used in conjunction with the maximum likelihood method as noted by Menke (1989).

Two normally dispersive V_s profiles are used to obtain synthetic dispersion curves based on the fundamental mode only, and these curves are treated as "experimental" data. The forward algorithm used to obtain the simulated experimental data is the same one used to find the theoretical dispersion curves during the inversion process. Thus, as in Chapter 3, the experimental data and the forward algorithm are ideal, i.e., there is no noise from data measurement errors or any errors induced by using a simplified model attempting to represent the real world.

One of the main characteristics of a local search procedure like the maximum likelihood method is that it needs some information a priori (i.e., before performing the inversion),

which is fixed during inversion and may have an important influence on the solution. These prior assumptions are:

(a) uncertainties of the experimental dispersion data,

(b) number of layers and their thicknesses,

(c) initial shear wave velocities,

(d) standard deviations of the initial shear wave velocities, and

(e) correlations between the initial shear wave velocities.

Prior information (b), (d), and (e) in the above list is varied in this chapter to study the effect on the inversion results. The uncertainties of the experimental data (a) are fixed at 3% of the phase velocity values, which is an appropriate value as discussed in Chapter 3. The effect of varying this value is examined in Chapter 5. The initial V_s values (c) are found based on empirically scaling the dispersion curve because the convergence of the algorithm is improved if the initial shear wave velocities are not too far from the final, unknown values. This approach does not give fixed initial V_s values for all layered profiles but it is a consistent means of calculating an initial estimate. The effect of using other initial V_s values such as a constant V_s for the entire profile is studied in Chapter 5.

The results obtained from this theoretical inversion algorithm may not only be affected by the prior information but also by the number and distribution of points used to describe the dispersion curve. For this reason, these parameters are varied in one of the synthetic examples presented here, creating three different sets of synthetic data to represent the dispersion curve of the same V_s profile.

In summary, the objective of this chapter is to present the maximum likelihood inversion theory applied to SASW and to implement it with two synthetic examples. This chapter introduces the sets of synthetic data, the prior information, and the resulting V_s profiles that are used in Chapter 5 with some additional results to study the factors that influence the inversion outcome.

4.2 Local Search Procedure applied to SASW

4.2.1 Maximum Likelihood Inversion applied to SASW

The following is a brief description of the maximum likelihood method that summarizes the method as presented by Tarantola (1987). Herein, all equations are presented in terms of variables appropriate for SASW inversion.

Maximum likelihood inversion is based on the least squares criterion, which is a good option when there are no large errors associated with the data (i.e., because the criterion is sensitive to even a small number of large errors). For SASW this appears to be a valid assumption, since uncertainties associated with the experimental dispersion data have been found to be low, with standard deviations typically less than 7% of the phase velocity values (Tuomi and Hiltunen, 1997). Additionally, least squares methods are justified when the errors can be modeled using Gaussian functions and, as discussed in Chapter 3, using a Gaussian model for the data uncertainties is a reasonable assumption

for SASW. The least squares criterion is popular due to the relatively straightforward computations that are derived from it (Tarantola, 1987).

For a non-linear relationship between model parameters and data, the posterior probability density function (pdf) can be be complicated and difficult to represent. However, in this case where the model parameters are the shear wave velocities and the data are the Rayleigh phase velocities, the posterior pdf can be assumed to be Gaussian. This is based on the results obtained in Chapter 3, where normal probability plots showed that the normal distribution is a reasonable statistical representation for the estimated model parameters (**vs**). Thus, the model parameters obtained with the inversion may be represented by central estimates and related covariances. The easiest central estimator to compute is the maximum likelihood point (**vs**= **vs**$_f$) where the posterior pdf is maximum (Tarantola, 1987). As described by Tarantola (1987), the maximum likelihood point (**vs**$_f$) is found as the point that minimizes the cost function S(**vs**) defined as:

$$S(\mathbf{vs})=\frac{1}{2}\left[\begin{array}{c}\left(\mathbf{vr}_{th}-\mathbf{vr}_{ex}\right)^{T}\mathbf{C\_vr}^{-1}\left(\mathbf{vr}_{th}-\mathbf{vr}_{ex}\right)\\+\left(\mathbf{vs}-\mathbf{vs}_{pr}\right)^{T}\mathbf{C\_vs}_{pr}^{-1}\left(\mathbf{vs}-\mathbf{vs}_{pr}\right)\end{array}\right] \qquad \text{(eq. 4.1)}$$

where **vr**$_{th}$ is the vector of theoretical data (obtained with the forward algorithm r(**...**) applied to the model parameters **vs**),

vr$_{ex}$ is the vector of experimental data,

C_vr is the covariance matrix of the data, which is defined to combine experimental and theoretical uncertainties:

C_vr=C_vr*ex*+C_vr*th*

where **C_vr***ex* is the covariance matrix of the experimental data obtained at the field and **C_vr***th* is the covariance matrix of the data calculated theoretically, since the forward model is only an approximation to reality,

vs is the vector of the model parameters for which the cost function is being calculated,

vs$_{pr}$ is the initial vector of model parameters (starting point for the iterative inversion algorithm), and

C_vs$_{pr}$ is the covariance matrix of **vs**$_{pr}$.

Gradient and Newton methods can be used for minimizing S if at any point **vs**$_n$ the partial derivatives can be defined and computed (Tarantola, 1987). **J**$_n$ is the matrix of partial derivatives evaluated at **vs**$_n$ and has components $J_n(i,\alpha)$:

$$J_n(i,\alpha) = \left[\frac{\partial r_i}{\partial vs_\alpha} \right]_{\mathbf{vs}=\mathbf{vs_n}}$$

(eq. 4.2)

where r represents the forward algorithm ($\mathbf{vr}_{th} = r(\mathbf{vs})$),

subindex $i = 1,2,...,N_d$ where N_d is the total number of dispersion data points, and

subindex $\alpha = 1,2,...,N_p$ where N_p is the total number of model parameters (=length of vector **vs**).

The gradient of S will be zero at a minimum point, but not every point where the gradient is zero is a minimum. Thus, it is necessary to verify that a point is in fact a minimum by

checking that the sequence $S(\mathbf{vs}_1)$, $S(\mathbf{vs}_2)$,..., obtained with the iterative method decreases. As described by Tarantola (1987), a common way of finding the minimum of a function is the Newton method:

$$\mathbf{vs}_{n+1} = \mathbf{vs}_n - \left[\frac{\partial^2 S}{\partial \mathbf{vs}^2}\right]^{-1}_{\mathbf{vs}=\mathbf{vs}_n} \left[\frac{\partial S}{\partial \mathbf{vs}}\right]_{\mathbf{vs}=\mathbf{vs}_n} \qquad \text{(eq. 4.3)}$$

where $\mathbf{vs}_n$ is the model parameter vector at iteration n,

$\mathbf{vs}_{n+1}$ is the model parameter vector at iteration n+1,

$\partial^2 S/\partial \mathbf{vs}^2$ is called the Hessian of S, and

$\partial S/\partial \mathbf{vs}$ is the gradient of S.

The components of the Hessian of S are:

$$\left[\frac{\partial^2 S}{\partial \mathbf{vs}^2}\right]_{\alpha,\beta} = \frac{\partial^2 S}{\partial vs_\alpha \partial vs_\beta} \qquad \text{(eq. 4.4)}$$

A common approximation in least-squares is to neglect the second-order derivatives of $\mathbf{vr}_{th}$, when calculating the Hessian of S. With this, Tarantola (1987) shows that the minimum of $S(\mathbf{vs})$ can be obtained with a Quasi-Newton algorithm:

$$\mathbf{vs}_{n+1} = \mathbf{vs}_n - \begin{pmatrix} \mu_n \left[\mathbf{J_n}^T \mathbf{C\_vr}^{-1} \mathbf{J_n} + \mathbf{C\_vs}_{pr}^{-1} \right]^{-1} \\ \left[\mathbf{J_n}^T \mathbf{C\_vr}^{-1} \left(r(\mathbf{vs}_n) - \mathbf{vr}_{ex} \right) + \mathbf{C\_vs}_{pr}^{-1} \left(\mathbf{vs}_n - \mathbf{vs}_{pr} \right) \right] \end{pmatrix} \qquad \text{(eq. 4.5)}$$

There are alternative forms of the above formula presented by Tarantola (1987, p.244). The constant μ_n can be equal to one, as long as at each iteration $S(\mathbf{vs}_{n+1}) < S(\mathbf{vs}_n)$. Since it cannot be assured that the algorithm will converge when this condition is not fulfilled, the optimum value for μ_n has to be obtained by linear search with $\mu_n < 1$. This was implemented by calculating $\mathbf{vs}_{n+1}$ and $S(\mathbf{vs}_{n+1})$ for μ_n values of 1.0, 0.95, 0.9, 0.85, .., 0.1, 0.05, 0.0, and the choosing $\mathbf{vs}_{n+1}$ that produced the lowest $S(\mathbf{vs}_{n+1})$.

Due to the nature of local search procedures such as the one described here, the only way to determine if the point reached is the absolute minimum and not a secondary minimum is to start the iterations at different points. Iterations are stopped when the change in **vs** is insignificant or when the difference between theoretical and experimental dispersion data is acceptable.

4.2.2 Posterior Covariance Matrix

The posterior pdf can be evaluated using a linear approximation if the non-linear relation r(**vs**) is linearizable in the region near the maximum likelihood point (Tarantola, 1987). This is possible for SASW inversion, because the posterior pdf of **vs** can be represented with a normal distribution, especially near the mean values. This indicates that the non-

linearity is not too strong, and the posterior covariance matrix of the model parameters can be written as (Tarantola, 1987):

$$\mathbf{C\_vs}_f = \left[\mathbf{J}_f^{\ T} \mathbf{C\_vr}^{-1} \mathbf{J}_f + \mathbf{C\_vs}_{pr}^{\ -1} \right]^{-1} \qquad \text{(eq. 4.6)}$$

or

$$\mathbf{C\_vs}_f = \mathbf{C\_vs}_{pr} - \mathbf{C\_vs}_{pr} \mathbf{J}_f^{\ T} \left[\mathbf{J}_f \mathbf{C\_vs}_{pr} \mathbf{J}_f^{\ T} + \mathbf{C\_vr} \right]^{-1} \mathbf{J}_f \mathbf{C\_vs}_{pr} \qquad \text{(eq. 4.7)}$$

where $\mathbf{C\_vs}_f$ is the posterior covariance matrix (the covariance matrix of $\mathbf{vs}_f$),

$\mathbf{J_f}$ is the matrix of partial derivatives evaluated at $\mathbf{vs}_f$,

$\mathbf{C\_vs}_{pr}$ is the covariance matrix of $\mathbf{vs}_{pr}$, and

$\mathbf{C\_vr}$ is the covariance matrix of the data

The diagonal terms of $\mathbf{C\_vs}_f$ are the variances of the model parameters, and their square roots are the standard deviations. The off-diagonal terms of $\mathbf{C\_vs}_f$ are the covariances and are better interpreted by calculating the correlations between parameters as:

$$\rho_f(\alpha,\beta) = \frac{C\_vs_f(\alpha,\beta)}{\left(C\_vs_f(\alpha,\alpha)\right)^{\frac{1}{2}} \left(C\_vs_f(\beta,\beta)\right)^{\frac{1}{2}}} \qquad \text{(eq. 4.8)}$$

where $\rho_f(\alpha,\beta)$ is the correlation between layer α and layer β,

$C\_vs_f(\alpha,\beta)$ is the covariance between layer α and layer β, i.e., the element in row α and column β of matrix C_vs_f, and

$C\_vs_f(\alpha,\alpha)$ is the variance of layer α, i.e., the element in row α and column α of matrix C_vs_f.

The correlations have values between -1 and 1 (included). The closer a value is to 1 (or -1) the highest the correlation (or anticorrelation) of the uncertainties of the two parameters. A strong correlation means that the two parameters are not independently resolved.

4.2.3 Resolution of Model Parameters

The resolution operator relates the unknown true model parameters ($\mathbf{vs}_{true}$) with the calculated ones ($\mathbf{vs}_f$):

$$\mathbf{vs}_f = res(\mathbf{vs}_{true}) \qquad\qquad (\text{eq.4.9})$$

where res(...) is a non-linear resolution operator. For the maximum likelihood method a linearized version of res(..) can be writen as (Tarantola, 1987):

$$\mathbf{vs}_f - \mathbf{vs}_{pr} = \mathbf{R}(\mathbf{vs}_{true} - \mathbf{vs}_{pr}) \qquad\qquad (\text{eq.4.10})$$

where $\mathbf{vs}_{pr}$ contains the initial model parameters, and the linearized resolution operator $\mathbf{R}$ can be calculated as

$$\mathbf{R} = \mathbf{I} - \mathbf{C\_vs}_f \, \mathbf{C\_vs}_{pr}^{-1} \qquad\qquad\qquad\qquad \text{(eq.4.11)}$$

A perfectly resolved model would have a resolution matrix equal to the identity matrix (**I**). One possible way to measure the goodness of the resolution is based on the spread of the off-diagonal terms, sometimes called Dirichlet spread (Menke, 1989):

$$Dirichlet\_spread(\mathbf{R}) = \sum_i \sum_j \left[R_{i,j} - I_{i,j} \right]^2 \qquad\qquad \text{(eq.4.12)}$$

In order to penalize nonzero elements according to their distance from the diagonal, a weighting factor such as $w(i,j)=(i-j)^2$ can be added. The new spread function is often called the Backus-Gilbert spread (Menke, 1989)

$$Backus\_Gilbert\_spread(\mathbf{R}) = \sum_i \sum_j w(i,j) \left[R_{i,j} - I_{i,j} \right]^2 \qquad \text{(eq.4.13)}$$

The spreads can be used to compare different parameterizations, but they need to be normalized so that they do not depend on the size of the resolution matrix (e.g. on the number of parameters). The Dirichlet spread is normalized by dividing it by the total number of terms in **R**, and the Backus-Gilbert spread is normalized by dividing it by the sum of all the weights used. Comparing the resolution matrix to the identity matrix can help evaluate how different parameters are resolved by the data and can be useful to change depths, thicknesses, and/or number of parameters.

4.2.4 Forward Algorithm and Partial Derivatives

For each trial shear wave velocity profile in the iterative inversion process, the theoretical dispersion curve is estimated using the forward algorithm proposed by Lai and Rix (1998). The algorithm as implemented by Lai and Rix provides the first 10 individual modes of propagation and an "effective" dispersion curve that reflects the superposition of the modes. As mentioned in Chapter 2, Lai and Rix (1998) noted that Rayleigh modes are superimposed for sources that are harmonic in time, resulting in an effective phase velocity which is a function of frequency and spatial position from the source. Thus, the effective phase velocity yields one dispersion curve for each receiver spacing and these curves are averaged over the range of receiver spacings to form a unique effective dispersion curve.

Additionally, the forward algorithm implemented by Lai and Rix provides closed form expressions for both modal and "effective" partial derivatives of Rayleigh phase velocity with respect to the shear wave velocity of each layer in the profile. Based on the variational principle of Rayleigh waves, Lai and Rix (1998) derived the closed form expressions for the partial derivatives of both modal and effective Rayleigh phase velocities with respect to the body waves of the medium. The Rayleigh variational principle was obtained by Lai and Rix (1998) from the application of Hamilton's principle to the solution of the Rayleigh eigenvalue problem.

4.3 Example 1 based on numerical simulation

4.3.1 Theoretical V_s profile ND1 and Related Dispersion Data

Synthetic data is used to illustrate the results that may be obtained with the Maximum Likelihood inversion method. The V_s profile created to obtain the simulated experimental data has the characteristics shown in Table 4.1. This is the same profile used in Chapter 3 and presented in Table 3.1. As mentioned before, this is a normally dispersive profile, and the corresponding synthetic dispersion curve used as the "experimental" data includes only with the fundamental mode. This curve was found using the algorithm by Lai and Rix (1998), which is the same algorithm used to find the theoretical dispersion curves during the inversion process. Thus, as in Chapter 3, the numerical simulation does not include errors caused by the use of simplified models to represent the real world. For a real experimental case there would be more uncertainties, and the effective dispersion curve that includes all modes of propagation may be a better choice.

The "experimental" dispersion curve is described by a specified number of points with a certain frequency distribution. Figure 4.1 presents 3 possible sets of data that could be employed as the experimental dispersion curve. Frequency distribution f1 presented in Figure 3.1 consists of the same 50 data points used in Chapter 3 and is the primary "experimental" dispersion curve used herein. Frequency distributions f2 and f3 are used as alternative experimental dispersion curves where the frequency distribution was changed in one case and the number of points was reduced in the other case. Distribution

f2 contains 50 data points equally spaced in the frequency domain. Distribution f3 contains only 9 data points that attempt to describe the main characteristics of the dispersion curve. These additional curves were employed for comparison purposes because the data points used to represent a dispersion curve may have an effect on the inversion results. Experimentally the distribution and number of points depends on the location of the receivers and on the frequencies selected for measurement and analysis.

Table 4.1 Normally dispersive profile ND1

Layer No.	Layer Thickness (m)	Mass Density (g/cm^3)	Shear Wave Velocity (m/s)	Poisson's Ratio
1	5	1.8	100	0.2
2	5	1.8	200	0.45
3	10	1.8	300	0.45
	-	1.8	400	0.45

The experimental dispersion curve is compared with a theoretical dispersion curve by calculating the root mean square (rms) error as defined in Chapter 3 with equation 3.2. As discussed in Chapter 3, it is reasonable to expect a value for the rms error of about 1.0.
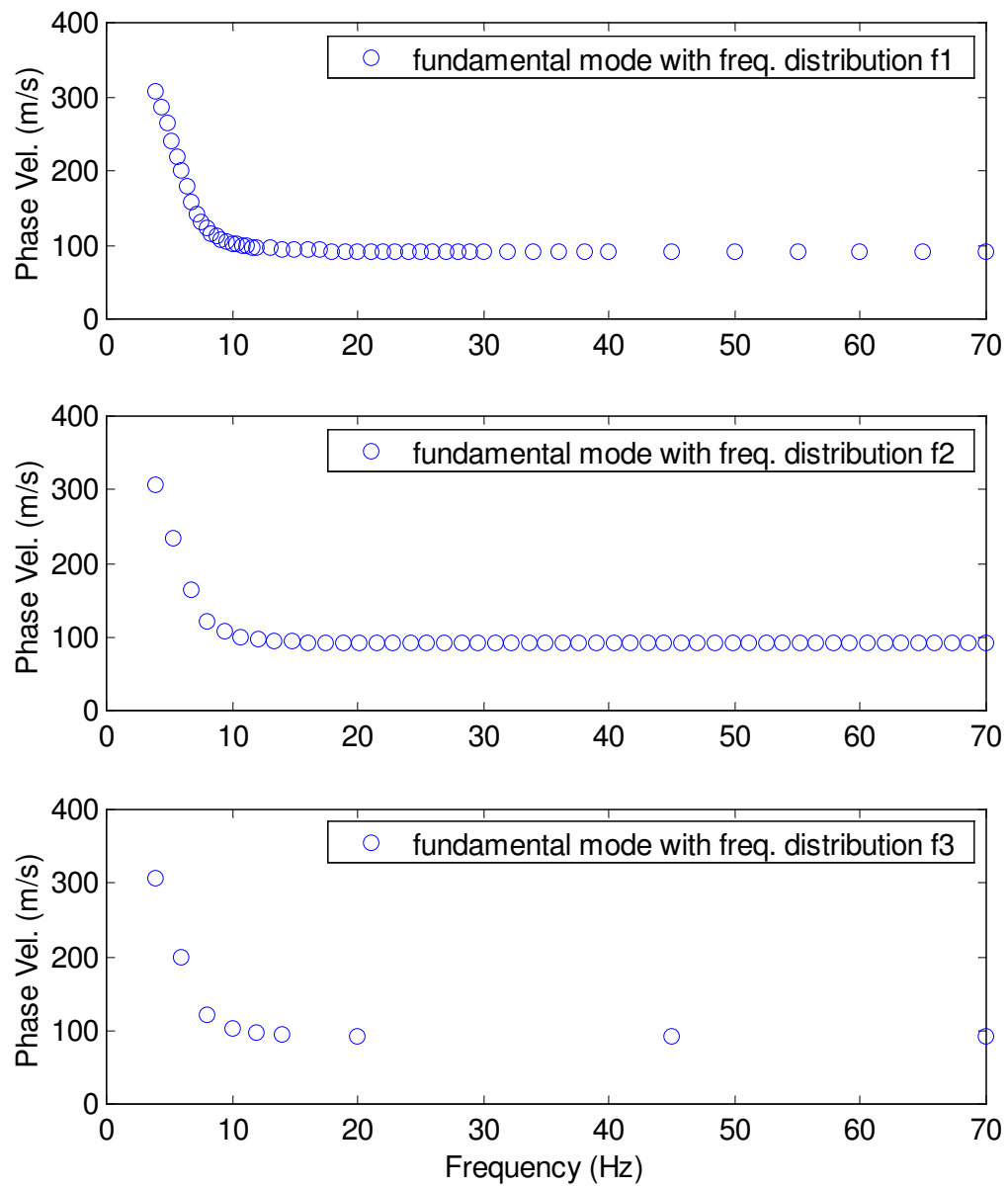
**Figure 4.1 Simulated dispersion curves for profile ND1
- varying distribution and number of points.**

4.3.2 Layered Profiles Used to Perform the Inversion

There are an infinite number of layered profiles that may be used in the inversion process. In this study, trial profiles are formed by varying three parameters: depth to the half-space, number of layers, and layer thicknesses. Some of the configurations implemented have layers that coincide with the real layer interfaces because it is interesting to observe if matching the real layer interfaces makes the inversion process more reliable by improving the estimated V_s profile. However, note that using real layer interfaces would not be possible for most real data. Resolving a specific thickness becomes more difficult at large depths because the surface wave phase velocity is more sensitive to shallow layers than deep layers (Joh, 1996). This is because the particle motion associated with Rayleigh waves is small at depths greater than about one wavelength (Tokimatsu, 1997). Consequently, a long wavelength that penetrates a deep layer also penetrates the layers above it, and there is always a larger number of waves passing through the shallower layers. Accordingly, increasing the thicknesses of the layers with depth agrees with the nature of SASW tests, and the configurations presented below that do not have constant-thickness layers have layer thicknesses that increase with depth. The following options were examined:

- fixed 30-meter depth to half-space, dividing this depth in layers of equal thickness, and varying the number of layers from 1 to 15 (e.g. profile 1 had one 30-m layer, profile 2 had two 15-m layers, ..., profile 15 had fifteen 2-m layers) (Figure 4.2)

Profile #	1	2	3	4	5	6	...	10	...	15
layer thicknesses in meters	30	15 / 15	10 / 10 / 10	7.5 / 7.5 / 7.5 / 7.5	6 / 6 / 6 / 6 / 6	5 / 5 / 5 / 5 / 5 / 5		3 / 3 / 3 / 3 / 3 / 3 / 3 / 3 / 3 / 3		2 / 2 / 2 / 2 / 2 / 2 / 2 / 2 / 2 / 2 / 2 / 2 / 2 / 2 / 2

Figure 4.2 Layered profiles 1 to 15, example 1

- fixed 20-meters depth to half-space, varying the number of layers and their thicknesses, (thicknesses were limited to 1.25, 2.5, 5, 7.5, and 10 meters, with the thinner layers closer to the surface) (Figure 4.3)

Profile #	21	22	23	24	25	26	27	28
layer thicknesses in meters	2.5	2.5	2.5	5	1.25 / 1.25	2.5	5	1.25 / 1.25
	2.5	2.5	2.5		2.5	2.5		2.5
	2.5	2.5	5	5	2.5	5	5	2.5
	2.5	2.5			5			2.5
	2.5	5	10	10		5	5	2.5
	2.5							2.5
	2.5	5			7.5	5	5	5
	2.5							

Figure 4.3 Layered profiles 21 to 28, example 1

96

- fixed 50-meters depth to half-space, varying the number of layers and their thicknesses, (thicknesses were limited to 2.5, 5, and 10 meters, with the thinner layers closer to the surface) (Figure4.4)

Profile #	31	32	33	34	35	36	37	38
	2.5	2.5	2.5	2.5	2.5	2.5	2.5	5
	2.5	2.5	2.5	2.5	2.5	2.5	2.5	
	2.5	2.5	2.5	2.5	2.5	5	5	5
	2.5	2.5	2.5	2.5	2.5			
	2.5	5	5	5	5	5	5	5
	2.5							
	2.5	5	5	5	5	5	5	5
	2.5							
layer	2.5	5	5	5	10	5	10	10
thicknesses	2.5							
in meters	2.5	5	5	5		5		
	2.5							
	2.5	5	5	10	10	10	10	10
	2.5							
	2.5	5	5					
	2.5							
	2.5	5	10	10	10	10	10	10
	2.5							
	2.5	5						
	2.5							

Figure 4.4 Layered profiles 31 to 38, example 1

- all layers 2-meters thick, varying the number of layers, thus varying the depth to the half space (Figure4.5)

97

Profile #	46	47	48	49	50	51	52	53	54	55	56
	2	2	2	2	2	2	2	2	2	2	2
	2	2	2	2	2	2	2	2	2	2	2
	2	2	2	2	2	2	2	2	2	2	2
	2	2	2	2	2	2	2	2	2	2	2
	2	2	2	2	2	2	2	2	2	2	2
	2	2	2	2	2	2	2	2	2	2	2
layer		2	2	2	2	2	2	2	2	2	2
thicknesses			2	2	2	2	2	2	2	2	2
in meters				2	2	2	2	2	2	2	2
					2	2	2	2	2	2	2
						2	2	2	2	2	2
							2	2	2	2	2
								2	2	2	2
									2	2	2
										2	2
											2

Figure 4.5 Profiles number 46 to 56, example 1

4.3.3 Initial V_s Values and Uncertainties

A theoretical inversion algorithm such as the maximum likelihood method requires an initial estimate of the solution that is not too far from the solution to assure convergence. A good approach is to obtain an empirical estimate of the shear wave velocities ($V_{s\_empirical}$) versus depth from the dispersion curve, which relates phase velocity (V_r) with frequency (f). Herein, V_r is multiplied by a factor of 1.1 to obtain V_s as suggested by Tokimatsu (1997). The equivalent depth (z) is found from the wavelength (λ, where $\lambda=V_r/f$). As discussed in Chapter 2, the best scaling factor to determine z depends on the variation of the shear modulus with depth. Thus, the approach taken here is to find a number of empirical estimates of z by multiplying λ by different scaling factors: 0.2, 0.25, 0.3…, 0.8.

For each scaling factor a different empirical V_s profile is obtained as described below and used in the forward algorithm to calculate the theoretical dispersion curve. The best scaling factor and the corresponding V_s profile are the those related to the theoretical dispersion curve closer to the experimental one (i.e., the one with the lowest rms error).

As described in Chapter 3, $V_{s\_empirical}$ is obtained for each layer as an average of the scaled data points falling within or close to the layer. The empirical estimate varies depending on the data points that describe the dispersion curve (Figure 4.1) and the layers that form the profile (Figures 4.2 thru 4.5).

The uncertainties of the initial V_s values are expressed with the prior covariance matrix $\mathbf{C\_vs}_{pr}$. To create this matrix, it is necessary to assume standard deviation values σ_vs_{pr} for each V_s. For the examples presented here, σ_vs_{pr} was assumed constant and four different values were used: 30, 60, 120, and 240m/s. $\mathbf{C\_vs}_{pr}$ is created based on the assumed standard deviations as shown below:

$$\mathbf{C\_vs}_{pr_{i,j}} = \rho_{i,j} \cdot \sigma\_vs_{pr_i} \cdot \sigma\_vs_{pr_j} \qquad\qquad \text{(eq. 4.14)}$$

Where $\rho_{i,j}$ is a correlation coefficient. For the diagonal terms (i.e., i=j), $\rho_{i,i}$ is equal to one and the square of the standard deviation is the variance of each parameter. For the off-diagonal terms it is assumed that there is some correlation between layer properties which is higher for neighboring layers than for layers far from each other. Although it is difficult to determine the correlation between the different layers, this is a means to

99

impose some level of smoothing to the resulting shear wave velocity profile. This means that a profile with layers that are highly correlated will tend to have smaller V_s contrasts (i.e., be smoother) than a profile with uncorrelated layers. Assuming values for $\rho_{i,i}$ implies that if two profiles match the experimental data equally well, the profile with correlations close to the initial assumed correlations is considered a better choice.

The correlation coefficient $\rho_{i,j}$ was obtained with the methodology used by Joh (1996). He assumed $\rho_{i,j}$ to be inversely proportional to the exponential of the squared normalized distance $Z_{i,j}$, as defined below:

$$\rho_{i,j} = e^{-\frac{1}{2}Z_{i,j}^{2}} \qquad \text{(eq. 4.15)}$$

$$Z_{i,j} = 3 \cdot \frac{\left| d_i - d_j \right|}{Z_{band}} \qquad \text{(eq. 4.16)}$$

where $\left| d_i\text{-}d_j \right|$ is the distance between the midpoint of layers i and j, and

Z_{band} is the distance over which the layer properties are assumed to be correlated (for $\left| d_i\text{-}d_j \right|$=$Z_{band}$ the correlation coefficient $\rho_{i,j}$ is 0.0111).

Figure 4.6 presents the magnitude of $\rho_{i,j}$ for layer i when using Z_{band}=5. The Z_{band} values used for the examples presented here are 1, 5, 10, and 15m.

The values used for σ_vs_{pr} and Z_{band} were combined to form the prior covariance matrix and a total of seven cases were observed as shown in Table 4.2.

Table 4.2 Seven cases of prior information used to form the prior covariance matrix

(1) σ_vs_{pr} =30m/s, Z_{band}=5m
(2) σ_vs_{pr} =60m/s, Z_{band}=5m
(3) σ_vs_{pr} =120m/s, Z_{band}=5m
(4) σ_vs_{pr} =240m/s, Z_{band}=5m
(5) σ_vs_{pr} =120m/s, Z_{band}=1m
(6) σ_vs_{pr} =120m/s, Z_{band}=10m
(7) σ_vs_{pr} =120m/s, Z_{band}=15m
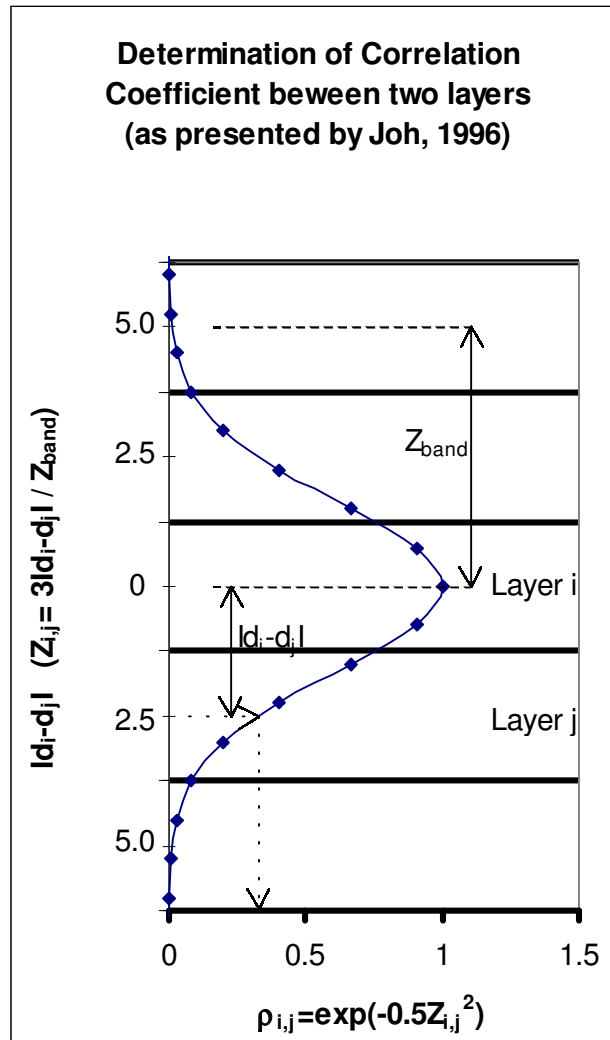
Figure 4.6 Correlation coefficient (Joh, 1996)

4.4 Example 2 based on numerical simulation

4.4.1 Theoretical V_s profile ND2 and Related Dispersion Data

A second set of synthetic data is used to illustrate the results that may be obtained with the Maximum Likelihood inversion method. The V_s profile used to calculate the simulated experimental data has characteristics that differ from the previous example as presented in Table 4.3. This new profile (ND2) has a higher V_s contrast between the second and the third layer than the previous profile (ND1) presented (i.e., a contrast of 200m/s compared to a contrast of 100m/s). Additionally, the thicknesses of the layers do not increase with depth, with the second layer being 10 meters thick and the third being 5 meters thick. Profile ND2 is also a normally dispersive profile and produces additional information to help study the diverse factors that affect the results obtained from the inversion of SASW data.

The "experimental" dispersion curve is described by a 25 data points with the frequency distribution shown in Figure 4.7. This synthetic dispersion curve used as the "experimental" data contains only with the fundamental mode. This curve was found using the algorithm by Lai and Rix (1998), which is the same algorithm used to find the theoretical dispersion curves during the inversion process. Thus, as for example 1, the numerical simulation does not include modeling errors.

The frequency distribution shown in Figure 4.7 has half the number of points of frequency distribution f1 shown in Figure 4.1. Fewer high-frequency points were used to reduce the running time, because the data points for higher frequencies correspond to shorter wavelengths and consequently give information only on the shallower layers.

Table 4.3 Normally dispersive profile ND2

Layer No.	Layer Thickness (m)	Mass Density (g/cm^3)	Shear Wave Velocity (m/s)	Poisson's Ratio
1	5	1.8	100	0.2
2	10	1.8	200	0.45
3	5	1.8	400	0.45
	-	1.8	500	0.45
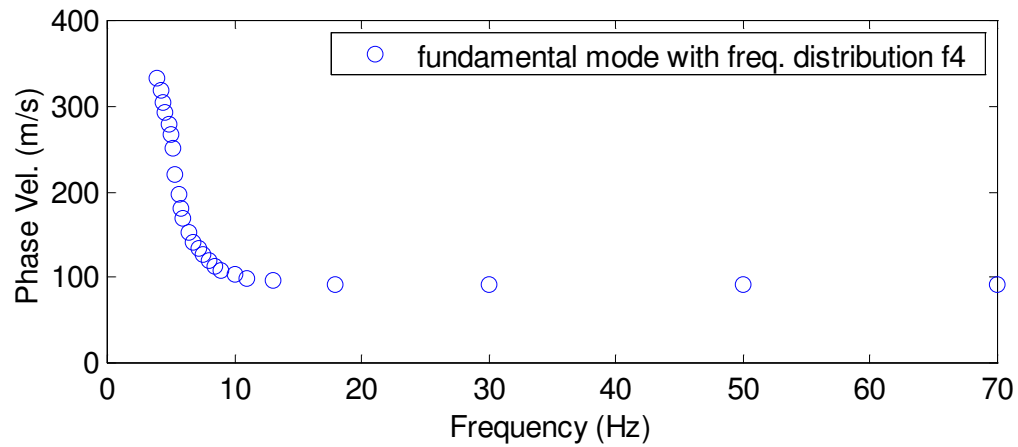
Figure 4.7 Simulated dispersion curve for profile ND2

4.4.2 Layered Profiles Used to Perform the Inversion

As mentioned in section 4.3.2, an infinite number of trial profiles are possible. For Profile ND2, trial profiles are formed by considering two different depths to the half-space and varying the number of layers and their thicknesses. As for Profile ND1, some of the configurations implemented have layers that match the real layer interfaces, and most configurations have their layer thicknesses increasing with depth. This agrees with the nature of SASW tests where layer resolution decreases with depth as discussed in section 4.3.2. The following options were examined:

- fixed 25-meters depth to half-space, varying the number of layers and their thicknesses, (thicknesses were limited to 1.25, 2.5, 5, 7.5, and 10 meters) (Figure4.8)

Profile	21	22	23	24	25	26	27	28	29
	2.5	2.5	2.5	5	1.25	2.5	5	1.25	5
					1.25			1.25	
	2.5	2.5	2.5		2.5	2.5		2.5	
	2.5	2.5	5	5	2.5	5	5	2.5	10
layer thicknesses in meters	2.5	2.5			5			2.5	
	2.5	5	10	10		5	5	2.5	
	2.5				7.5			2.5	
	2.5	5				5	5	5	5
	2.5								

Figure 4.8 Profiles number 21 to 29, example 2

- fixed 50-meters depth to half-space, varying the number of layers and their thicknesses, (thicknesses were limited to 2.5, 5, 10, and 15 meters) (Figure4.9)

Profile #	31	32	33	34	35	36	37	38	39	40	41
	2.5	2.5	2.5	2.5	2.5	2.5	2.5	5	10	5	15
	2.5	2.5	2.5	2.5	2.5	2.5	2.5				
	2.5	2.5	2.5	2.5	2.5	5	5	5		10	
	2.5	2.5	2.5	2.5	2.5						
	2.5	5	5	5	5	5	5	5	10		15
	2.5										
	2.5	5	5	5	5	5	5	5		5	15
	2.5										
layer	2.5	5	5	5	10	5	10	10	10	10	
thicknesses	2.5										
in meters	2.5	5	5	5		5					
	2.5										
	2.5	5	5	10	10	10	10	10	10	10	10
	2.5										
	2.5	5	5								
	2.5										
	2.5	5	10	10	10	10	10	10	10	10	10
	2.5										
	2.5	5									
	2.5										

Figure 4.9 Profiles number 31 to 41, example 2

4.4.3 Initial V_s Values and Uncertainties

The initial V_s values and the covariance matrix for example 2 were obtained with the same method used for example 1 and described in section 4.3.3.

4.5 Results obtained with the Maximum Likelihood Method

4.5.1 V_s profiles obtained for Example 1

The maximum likelihood method was used to perform the inversion and find V_s profiles with theoretical dispersion curves that matched the "experimental" dispersion curve of profile ND1. Figure 4.10 shows 259 V_s profiles obtained for 259 different initial models, which correspond to 37 layered configurations with 7 prior covariance matrices (Although 42 configurations were presented in Figures 4.2 thru 4.5, profiles 1 to 4 resulted in large rms errors and are not included and profile 15 is actually the same as profile 55). The experimental dispersion curve used for these cases corresponds to the fundamental mode with frequency distribution f1. The standard deviations estimated for each V_s value are not presented in this figure for clarity. The purpose of showing all the final V_s profiles in the same plot is to have an overview of the range of V_s values due to a variation of the initial model.

As described previously the initial models were varied by changing the number and thicknesses of the layers, and the standard deviations and correlations of the initial V_s profile. The maximum likelihood method converged to a different final V_s profile in each case. Herein, it was considered that the algorithm had converged when the change in the V_s profile was insignificant as defined by equation 4.17.

$$\sqrt{\frac{1}{N_p} \sum_{i=1}^{N_p} \left(\frac{vs_{n+1}(i) - vs_n(i)}{vs_n(i)} \right)^2} < 0.01$$

(eq.4.17)

where N_p is the total number of layers (taking into account the half space), and

$vs_n(i)$ is the V_s value for layer i obtained after iteration n.

All the profiles shown in Figure 4.10 were found to have final rms errors of less than 0.75. Profiles based on configurations 1 thru 4 had rms values that were significantly higher than for the profiles presented (rms>1.7 for configuration 4 and rms>5.0 for profiles 1 thru 3). As described previously, the theoretical dispersion curves for all profiles were found with the same forward algorithm used to simulate the 'experimental" data. Thus, the ambiguity of the solution is caused solely by the assumed prior information, which has an important influence on the final result obtained from the inversion as seen with the variety of profiles in Figure 4.10.

The range of V_s profiles in Figure 4.10 illustrates that many different V_s profiles can match the experimental dispersion curve with a satisfactory rms, which means that many different V_s profiles are solutions to the inversion problem. Thus, the solution to the inversion problem is non-unique. Since the experimental dispersion data does not constrain the solution to a unique answer, it can be said that the dispersion curve by itself is insufficient to find a unique V_s profile, and it is the information added a priori that constrains the problem to find one V_s profile.
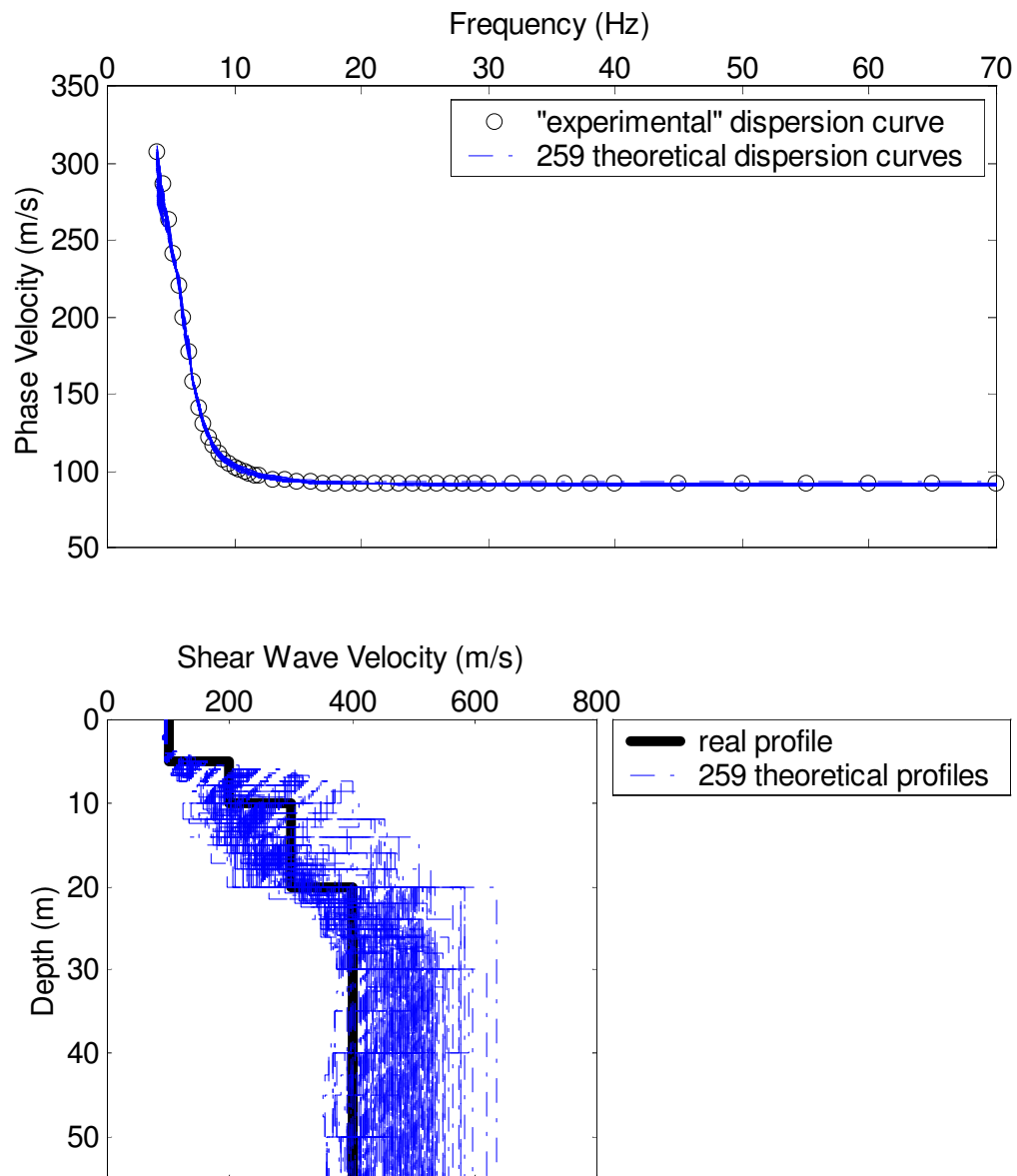
Figure 4.10 Shear wave velocity profiles obtained for example 1 (rms errors< 0.75) (case ND1, frequency f1)

Consequently, it is important to study how the variation of this information changes the V_s profile obtained from the inversion and to find ways to choose this information objectively. The first is addressed in Chapter 5, where the influence of various factors on the inversion results is analysed based on the maximum likelihood results presented herein. The latter is addressed in Chapter 6, where the use of a Bayesian criterion to select the prior information is presented and utilized also with the maximum likelihood results presented herein.

4.5.2 V_s profiles obtained for Example 2

The maximum likelihood method was used to perform the inversion and find V_s profiles with theoretical dispersion curves that matched the "experimental" dispersion curve of profile ND2. Figure 4.11 shows 126 V_s profiles obtained for 126 different initial models, which correspond to 18 layered configurations with 7 prior covariance matrices (Although 20 configurations were presented in Figures 4.8 and 4.9, profiles 39 and 41 resulted in higher rms errors than the others and are not included). The experimental dispersion curve used for these cases corresponds to the fundamental mode with frequency distribution f4. As before, the purpose of showing all the final V_s profiles in the same plot is to have an overview of the range of V_s values caused by the variation of the initial model. As noted for example 1, the maximum likelihood method converged to a different V_s profile in each case.

Even though the convergence criterion was the same as that used for example 1 (equation 4.17), for example 2 the algorithm converged to V_s profiles with higher rms errors. The profiles presented in Figure 4.11 were found to have rms errors between 0.32 and 3.3. Profiles with configurations 39 and 41 did not have enough layers to be able to represent the real profile and resulted in higher rms errors (rms>3.7 for configuration 39 and rms>9.5 for configuration 41). It is important to note that the rms values found for example 2 cannot be directly compared with the values found for example 1 since the frequency distributions used were not the same. Even the same theoretical V_s profile would have different rms errors for different frequency distributions. For example, profile 29 has the same layers as the 'real'' profile ND2 and for σ_vs_{pr} =120m/s and Z_{band}=5m the inversion algorithm converged to V_s values that produce a dispersion curve with an rms error of 1.93 (Figure 4.12). This rms value changes to 1.19 if it is calculated using frequency distribution f1 instead of frequency distribution f4. This is caused by the representation of the dispersion curve by discrete points, where the points chosen are used to calculate the rms error and affect its value. This issue will be examined more closely in Chapter 5.

For example 2, like for example 1, the prior information necessary to constrain the solution was found to have a significant influence on the final result obtained from the inversion. This can be observed in Figure 4.11, where a variety of V_s profiles were obtained for different prior information. The maximum likelihood results obtained herein are used in Chapter 5, with the results of example 1, to analyse the influence of various factors on the inversion result
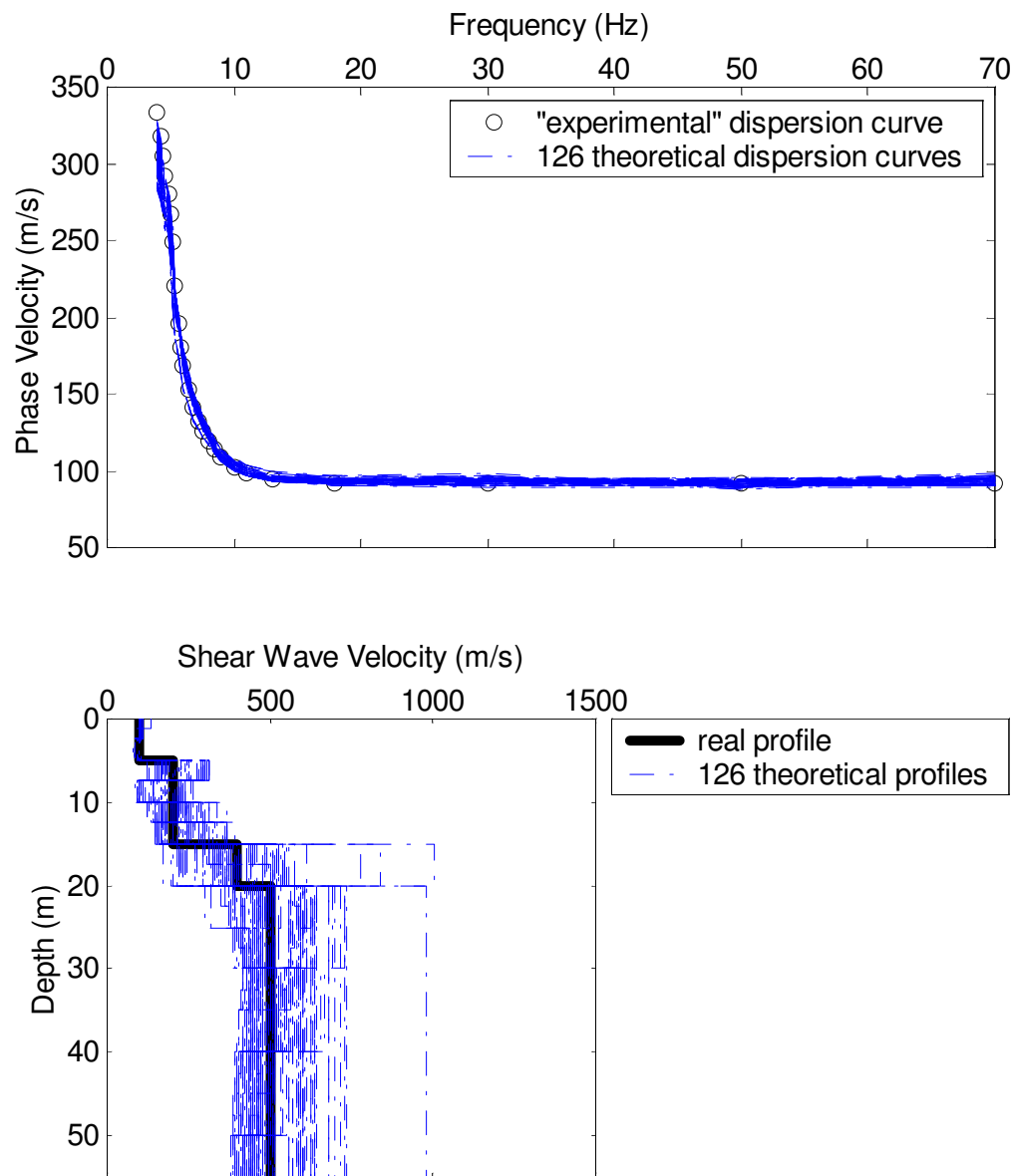
Figure 4.11 Shear wave velocity profiles obtained for example 2 (0.32 < rms errors < 3.3) (case ND2, frequency f4)
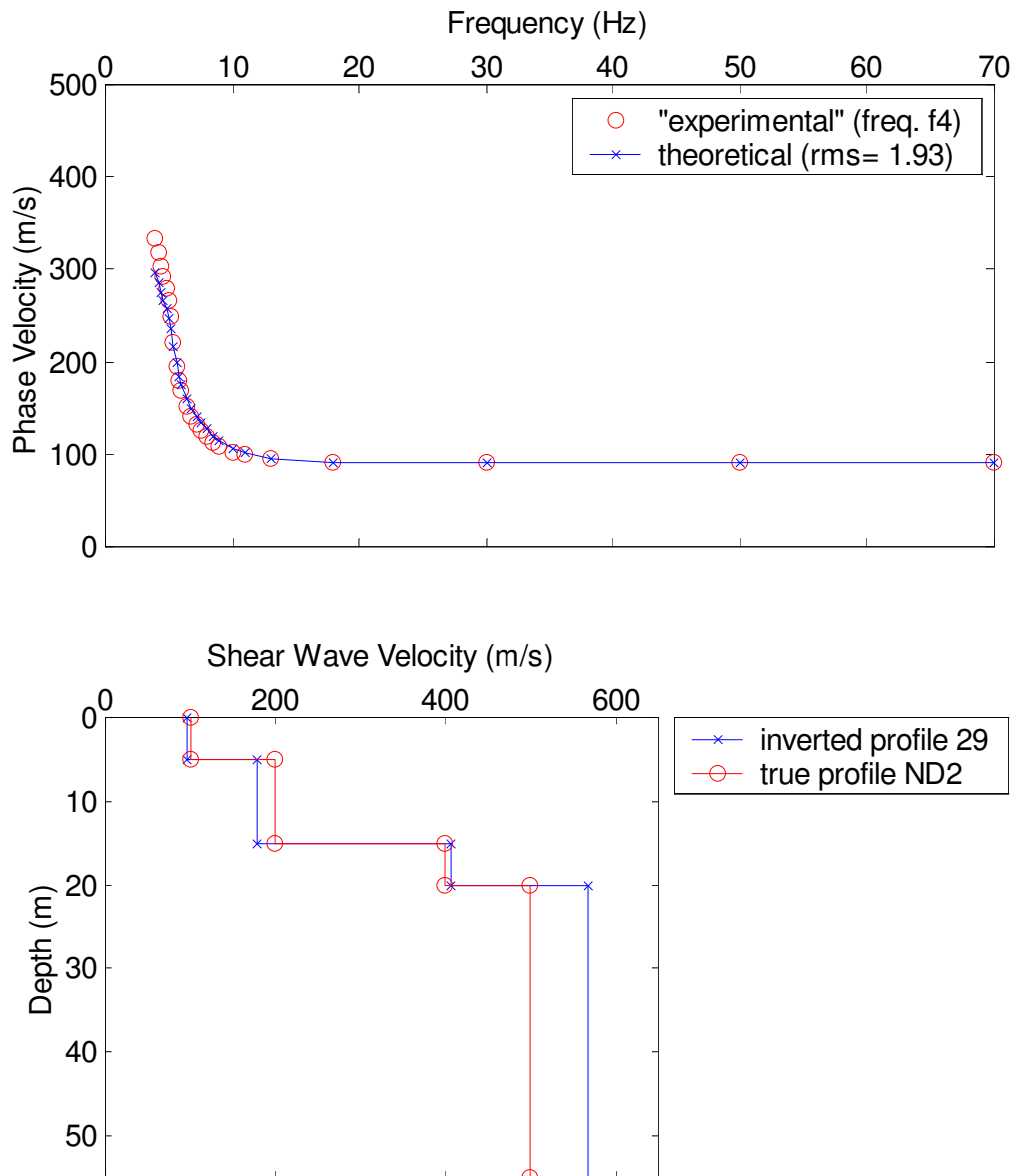
Figure 4.12 Inverted V_s profile for layered configuration 29 (σ_vs_{pr} =120m/s, Z_{band}=5m)

4.6 Conclusions

In this chapter, the application of the maximum likelihood method to SASW inversion was described, and two synthetic examples were presented. The examples were implemented for various frequency distributions of the dispersion curve and for different initial models by varying the number and thicknesses of the layers, and the prior standard deviations and correlations of the initial estimates of the shear wave velocities. An overview of the results obtained showed that the inversion converged to different estimates of the V_s profiles for different initial models, and that a close match to the experimental dispersion curve can be obtained with a large number of V_s profiles. Thus, a V_s profile estimated with this local search procedure is highly dependent on the prior information added to constrain the solution. For this reason, it is important to recognize that the dispersion curve by itself does not have the information to choose among layered configurations that result in equally satisfactory rms errors. Consequently, the estimated V_s profile should be seen as one possible discrete representation of the true V_s variation with depth, with the V_s values including standard deviations or some type of error bar. The details and analyses of the results obtained herein are presented in Chapter 5, where the different factors that affect the inversion are studied.

CHAPTER 5

INFLUENCE OF VARIOUS FACTORS ON THE INVERSION RESULTS

5.1 Introduction

There are a number of assumptions required to perform the inversion that affect the shear wave velocity profile obtained from the inversion process. This chapter utilizes results obtained with the maximum likelihood method as presented in Chapter 4, to discuss the effects that this prior information required to constrain the problem may have on the solution (i.e., V_s values and related uncertainties).

From all the data presented in Chapter 4, it is important to clarify that the main example presented is profile ND1 with frequency distribution f1, assuming: (i) standard deviations for the phase velocities (σ_vr) of 3% of the phase velocities, (ii) initial V_s values based on the empirical method for the corresponding layered profile, (iii) initial V_s standard deviation (σ_vs_{pr}) of 120 m/s and (iv) correlations based on Z_{band} of 5m. The variations in frequency distribution, uncertainties of the phase velocities, initial V_s values, prior uncertainties and correlations for the V_s values, were performed one at a time. Thus, for example, when looking at the effect of σ_vs_{pr}, all other assumptions are fixed in their main values.

5.2 Factors Related to the Experimental Dispersion Curve

5.2.1 Effect of Number and Distribution of Points Describing the Experimental Data

The points describing the dispersion curve represent the frequencies measured at the field, and give information on the wavelengths of the surface waves that sampled the soils. As mentioned by Tokimatsu (1997): "*The particle velocities of Rayleigh waves in either half or layered medium decay with depth, being negligibly small at depths greater than their propagating wavelengths*". Thus, it can be considered that a layer was not sampled by wavelengths shorter that the depth to the top of the layer. Figure 5.1 presents the four frequency distributions used for the examples introduced in Chapter 4. Frequency distributions f1, f2, and f3 were used for case ND1 and frequency distribution f4 was used for case ND2. The wavelength distributions are also presented in Figure 5.1.

Note that for case ND1, frequency distribution f2 has 50 points linearly distributed in the frequency domain and there are only 5 of these points that sampled soils between 10 and 80 meters depth based on their wavelengths. This indicates that there is a significant difference in the information available for different depths. Even if a few points satisfactorily describe a certain area of the curve, it is relevant to note that the rms error weights more heavily areas where there are a lot of points. For instance, the rms for frequency distribution f2 will weight more heavily the match between the experimental and theoretical dispersion curves for the frequencies that tested the top 10 meters

(represented by 45 points) than for the frequencies that tested between 10 and 80 meters (represented by 5 points). The frequency distribution f4 utilized in case ND2 shows a distribution in wavelength, which corresponds to an rms error that weights more similarly different areas of the dispersion curve.

Since the weight that the rms gives to different areas of the dispersion curve depends on the points used to represent it, for a specific V_s profile the resulting rms is different if the number of dispersion points and/or their frequency distribution are varied. This can be illustrated with a few profiles, like the ones shown in Figure 5.2, which were introduced in Chapter 4. Profile 24 has the layers of the real profile of case ND1, profile 29 has the layers of the real profile of case ND2, profile 31 has all layers with the same thickness, and profile 37 has layers with thickness increasing with depth. The last two profiles include appropriate layer interfaces to match the real interfaces of both ND1 and ND2. The V_s values estimated for these profiles are presented in Figure 5.3.

To see the effect of the frequency distribution on the rms value for a specific V_s profile, the inverted V_s profiles presented in figure 5.3 (a) for case ND1 with frequency distribution f1 are used to calculate the rms value with frequency distributions f2, f3, and f4. Equivalently, the inverted V_s profiles presented in figure 5.3 (b) for case ND2 with frequency distribution f4 are used to calculate the rms value with frequency distributions f1, f2, and f3. The different rms obtained are presented in tables 5.1 (a) and 5.1 (b).
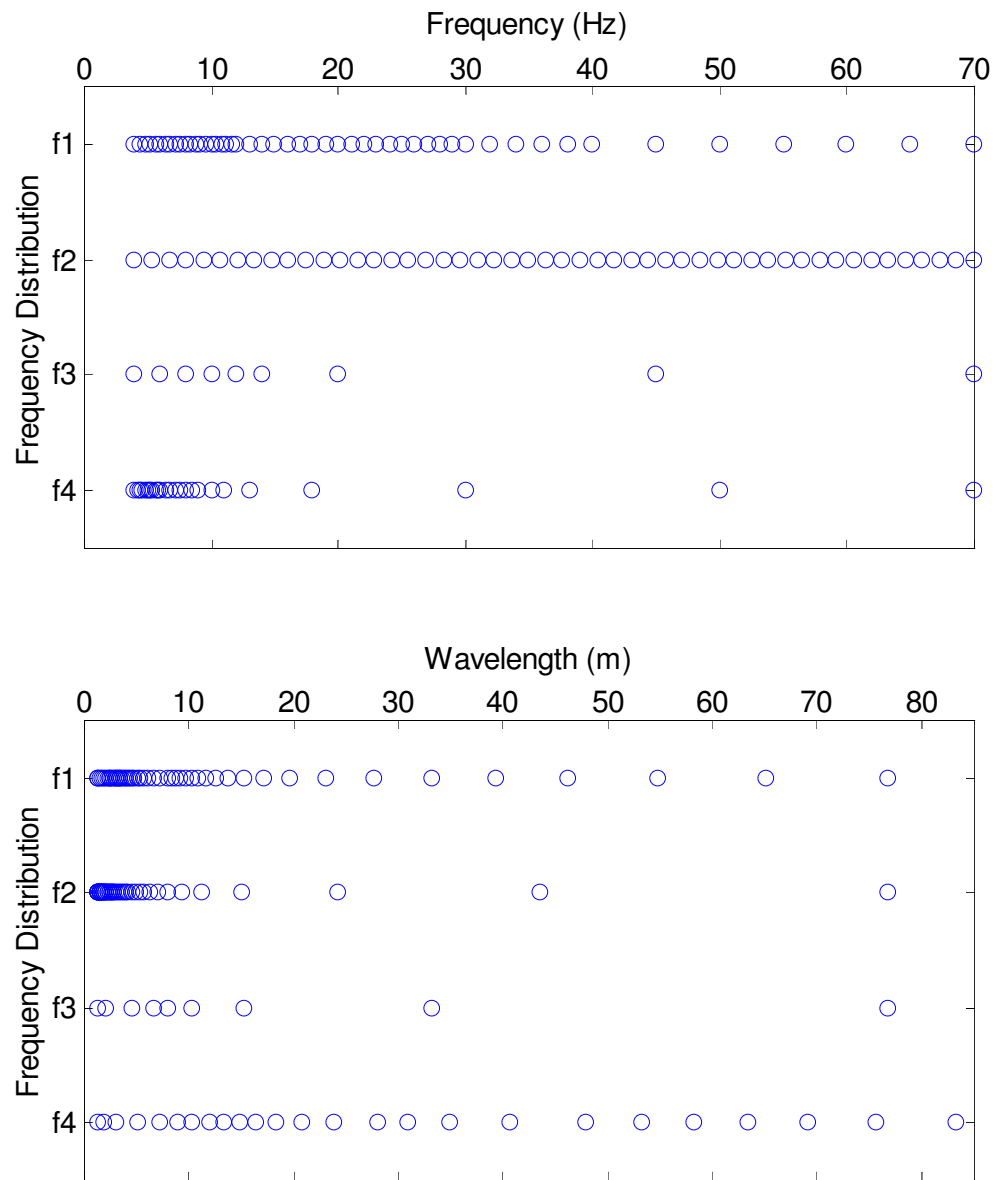
Figure 5.1 Frequency and wavelength distributions f1, f2, f3, and f4

24	29	31	37
5	5	2.5	2.5
		2.5	2.5
5	10	2.5	5
		2.5	
10		2.5	5
		2.5	
	5	2.5	5
		2.5	
		2.5	10
		2.5	
		2.5	
		2.5	
		2.5	10
		2.5	
		2.5	
		2.5	
		2.5	10
		2.5	
		2.5	
		2.5	

Figure 5.2 Layered profiles 24, 29, 31, and 37

119
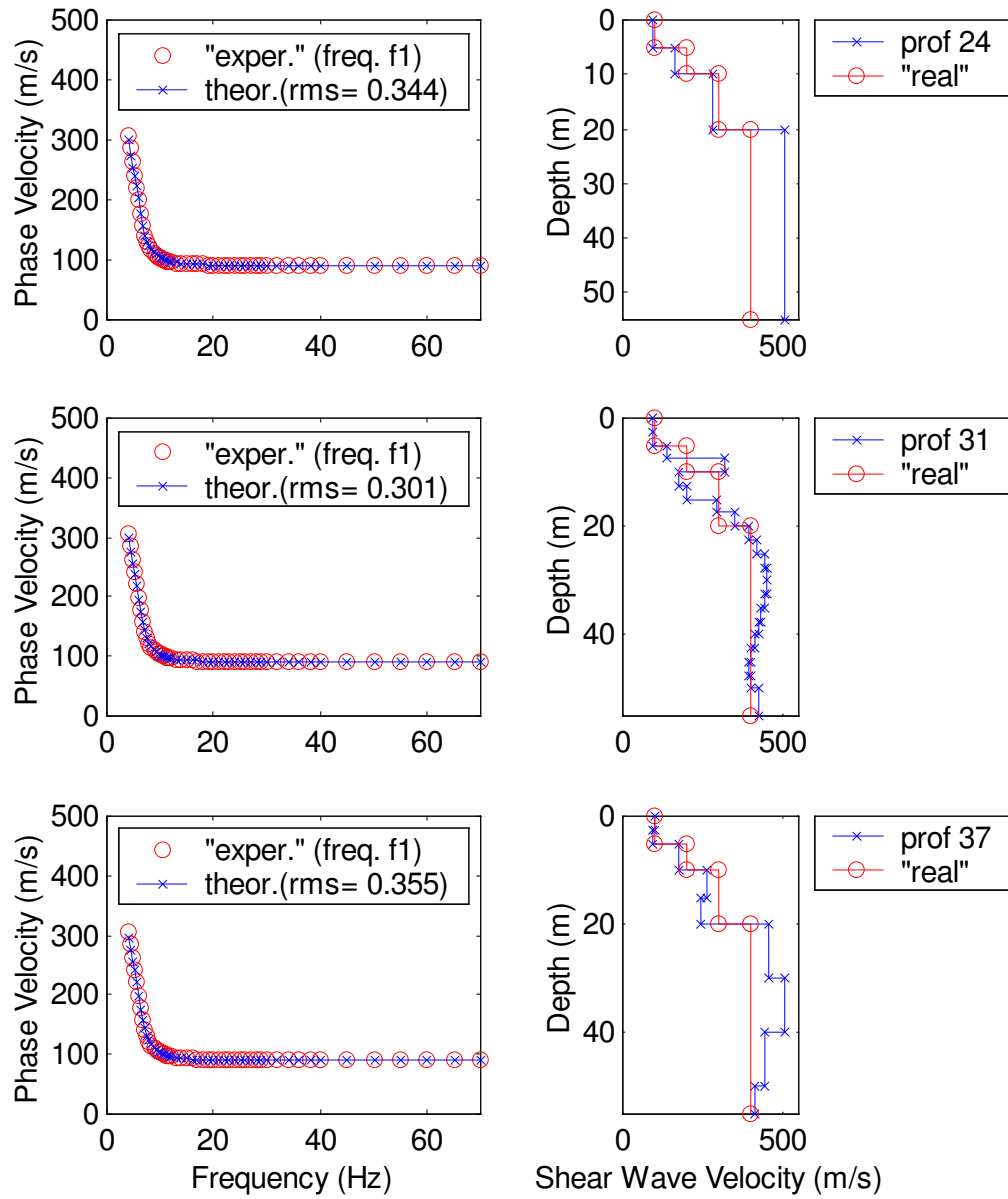
Figure 5.3(a) Inversion results for case ND1 with frequency distribution f1, for profiles 24, 31, and 37
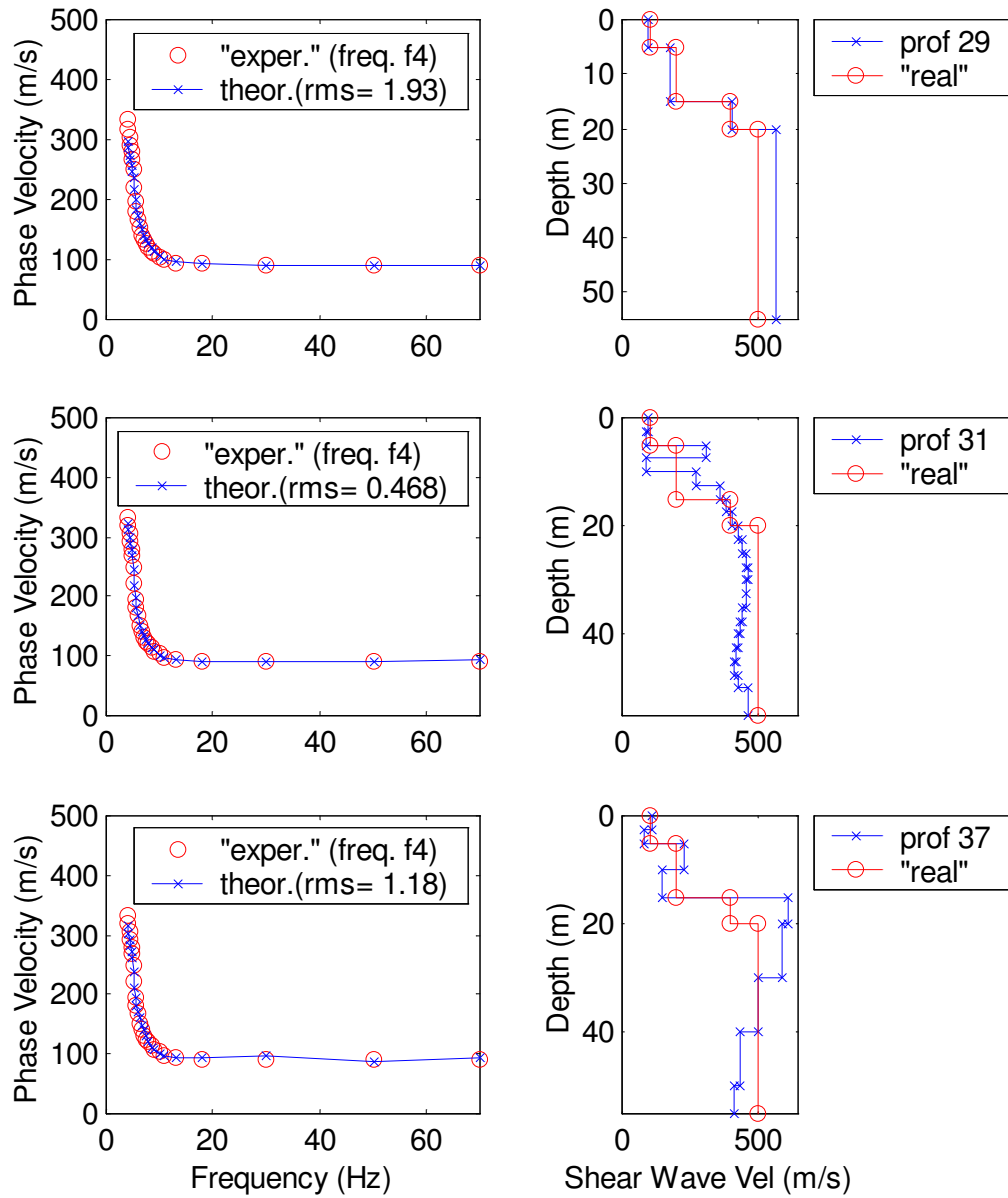
Figure 5.3(b) Inversion results for case ND2 with frequency distribution f4, for profiles 29, 31, and 37

Table 5.1(a) Direct effect of the frequency distribution on the rms error, for case ND1

ND1	24	31	37
f1	0.34	0.30	0.35
f2	0.18	0.15	0.23
f3	0.36	0.42	0.47
f4	0.62	0.55	0.63
Rms values for the V_s profile estimated with the maximum likelihood inversion using frequency distribution f1			

Table 5.1(b) Direct effect of the frequency distribution on the rms error, for case ND2

ND2	29	31	37
f1	1.19	0.46	1.44
f2	0.71	0.47	2.09
f3	1.52	0.62	0.99
f4	1.93	0.47	1.18
Rms values for the V_s profile estimated with the maximum likelihood inversion using frequency distribution f4			

The results in tables 5.1 show that the dispersion points chosen may affect significantly the value of the rms. Some of the results for ND2 show that the same V_s values might be considered acceptable or not by a 1.0 rms criterion depending on the frequency distribution used. For instance, the V_s values found for profile 29 produced an rms of 1.93 with frequency distribution f4 (the one used during the inversion process) and an rms of 0.71 for frequency distribution f2. This example emphasizes the importance of the frequency distribution, since the estimated rms error is used as a qualification on the goodness of a profile.

In order to look at the amount of experimental information available for different depths, it is illustrative to count and plot the number of waves that sampled the soil with depth. To count how many waves sampled each layer it is necessary to specify the layers used for the inversion. As an example, the profiles shown in Figure 5.2 are used for this purpose. Figure 5.4 shows the number of waves that sampled each layer depending on the frequency distribution and the profile. Figure 5.4 (a) shows case ND1 for frequency distributions f1, f2 and f3, and for profiles 24, 31 and 37. Figure 5.4 (b) shows case ND2 for frequency distribution f4, and for profiles 29, 31, and 37.

Figure 5.4 emphasizes the difference in information between layers. Part of the difference is inevitable due to the nature of the problem, since a long wavelength that tests a deep layer also tests all layers above it. Thus, there is always more information on shallower layers and less information on deeper layers. In Figure 5.4 (a), it can be noted that for frequency distribution f2, 25 out of the 50 measured waves go only through the very top

123

layer (top 2.5 meters) for profiles 31 and 37. Furthermore, only 11 out of 50 waves go through layers below 5 meters. This shows that a lot of dispersion points do not necessarily translate into a lot of information. Additionally, it does not seem reasonable to have half of the dispersion data with information only on the very top layer.

In order to look at the effect of the number of waves that sampled a layer on the inversion results a few layers were chosen. This was done because the effect of the number of waves also depends on the depth of the layer as it can be seen in Figures 5.5 to 5.7. The layers used were: (i) 0 to 2.5 m, (ii) 2.5 to 5 m, (iii) 5 to 10 m, (iv) 10 to 15 m, (v) 15 to 20 m, and the results for these layers were taken from the inversion results of all the profiles that included them.

Figure 5.5 shows the ratio of the inverted V_s to the real V_s versus the number of waves that sampled each layer. The range of values obtained for this ratio increases with depth, but there is no clear trend with the number of waves. This shows that it may be possible to reduce the number of points in the dispersion curve and still have enough data to represent the curve and get a good estimate of V_s. For instance, it seems logical that when too much data is accumulated in a single layer (for example as described above for the top layer of profiles 31 and 37 with frequency distribution f2), some of this data may be deleted without reducing the information available for the remaining layers. This can help to have a better balance of information content.
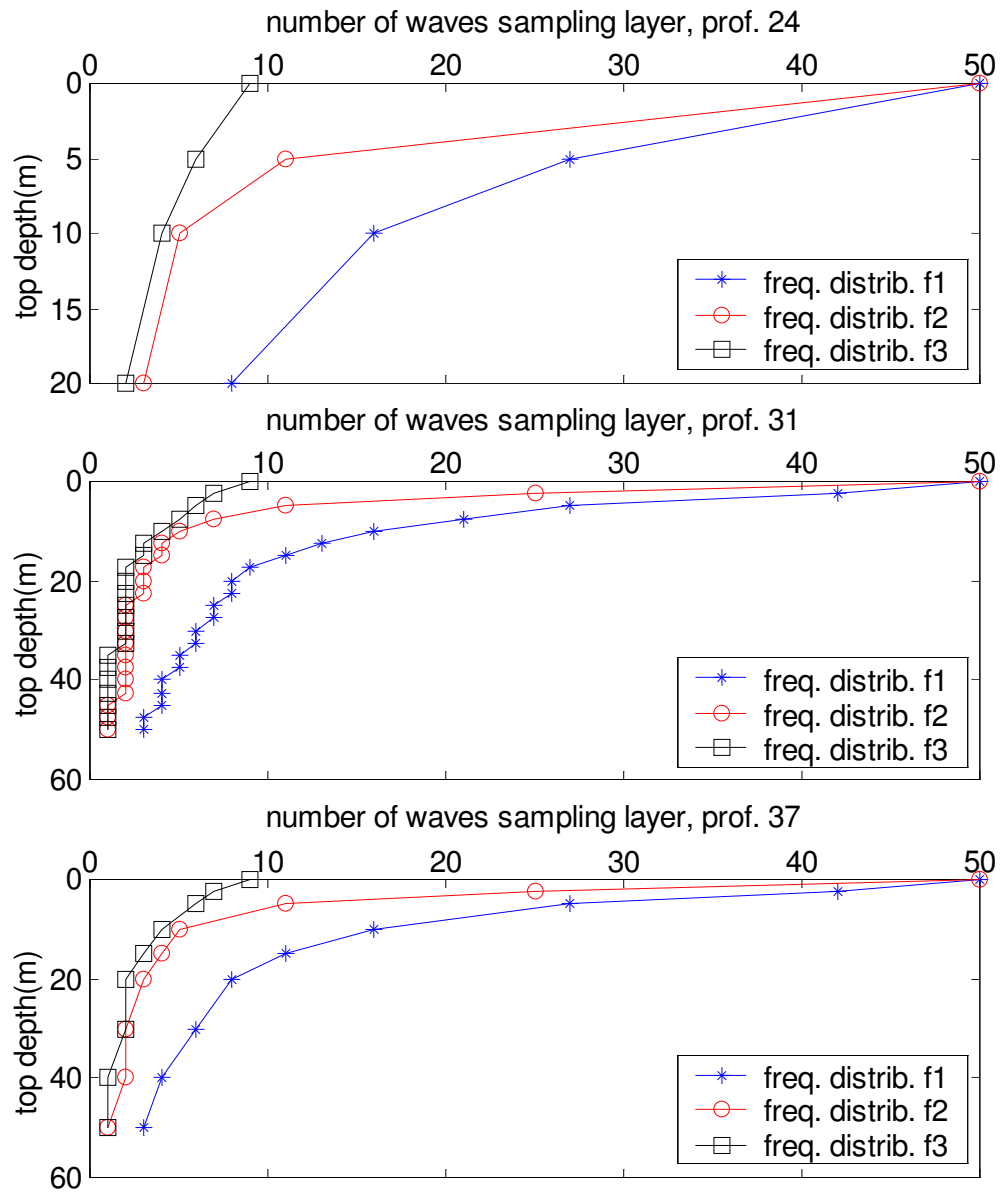
Figure 5.4(a) Number of waves per layer for case ND1 for profiles 24, 31, and 37
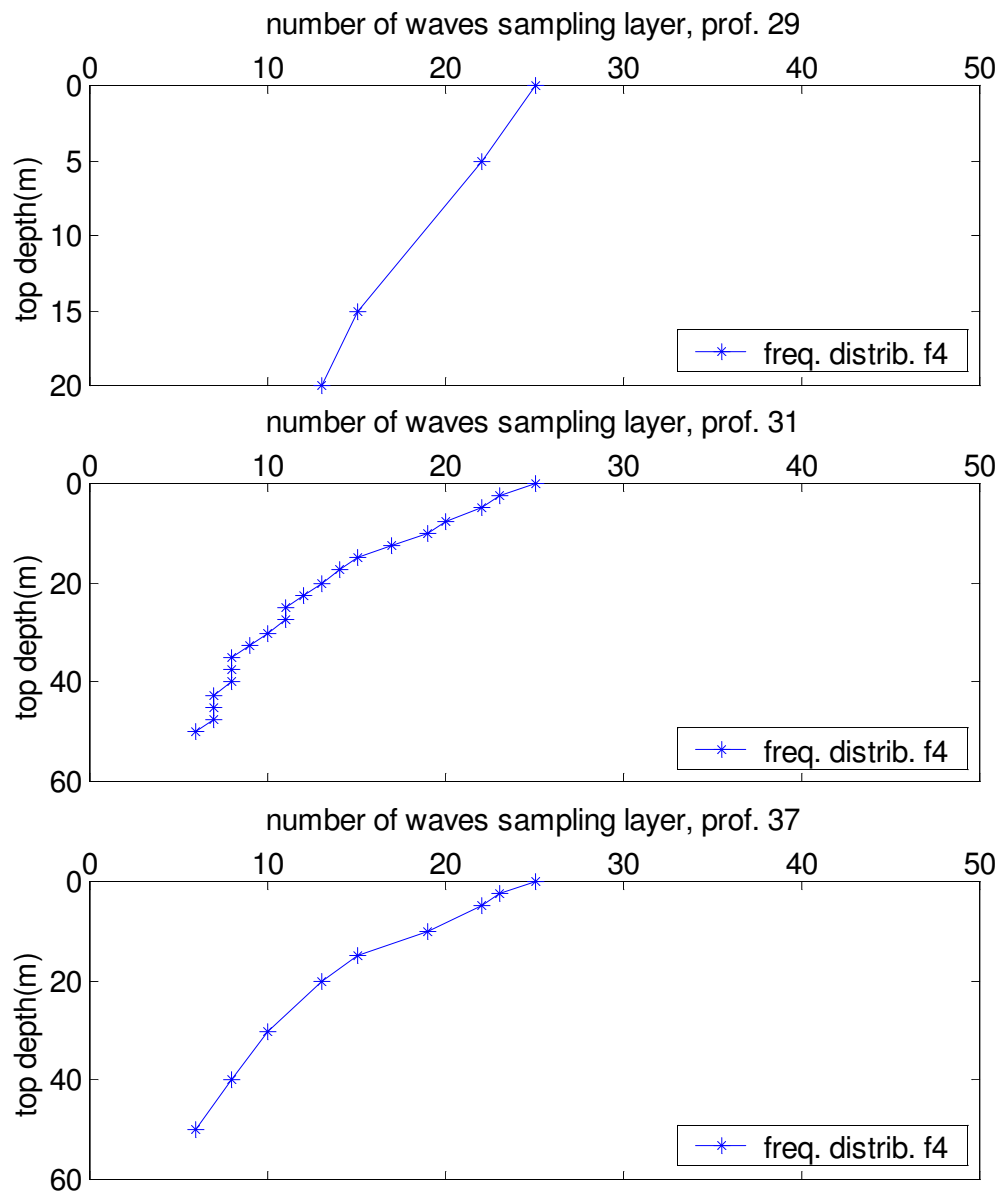
Figure 5.4(b) Number of waves per layer for case ND2, for profiles 29, 31, and 37
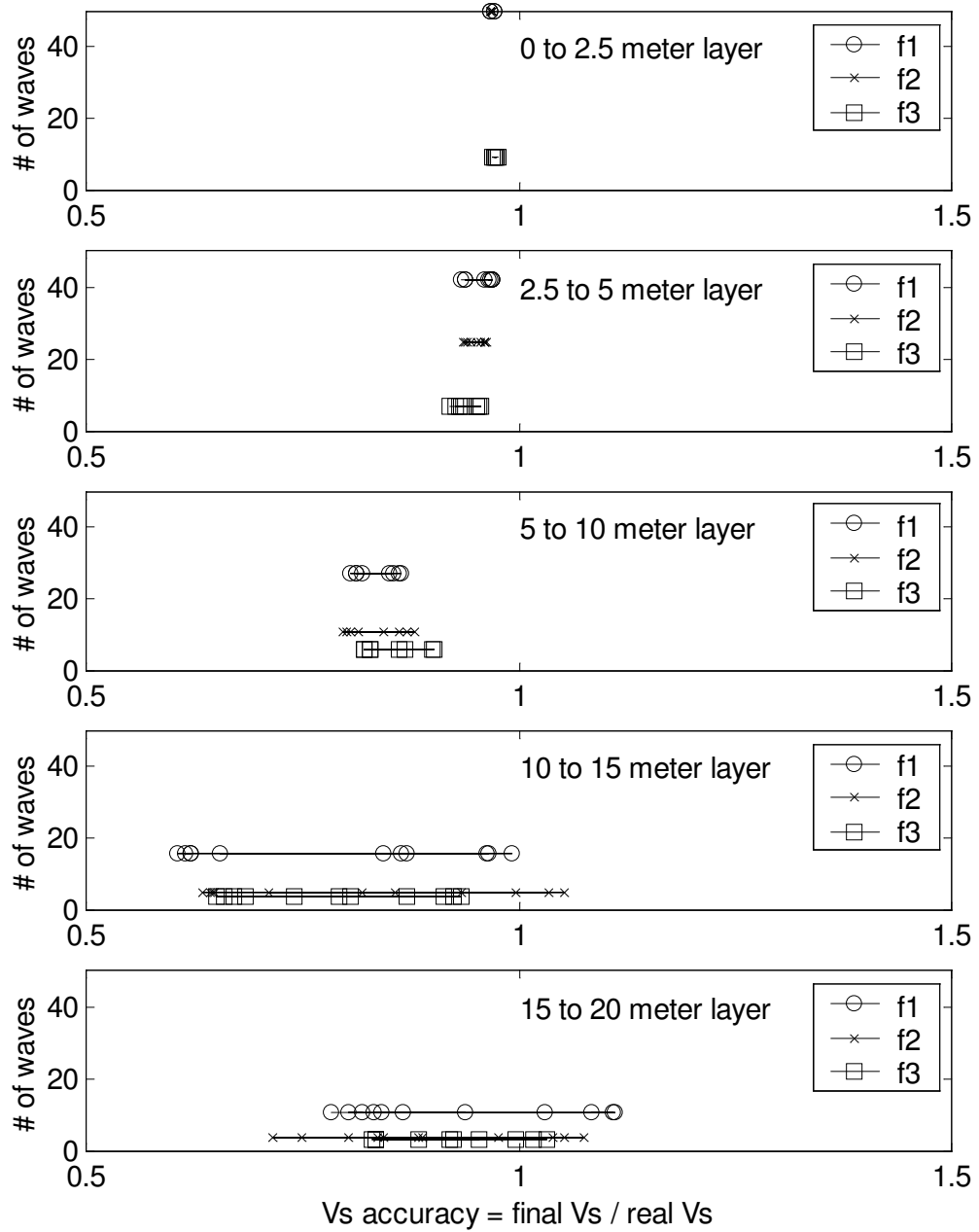
Figure 5.5 Effect of the number of waves sampling a layer on V$_s$ accuracy, for case ND1
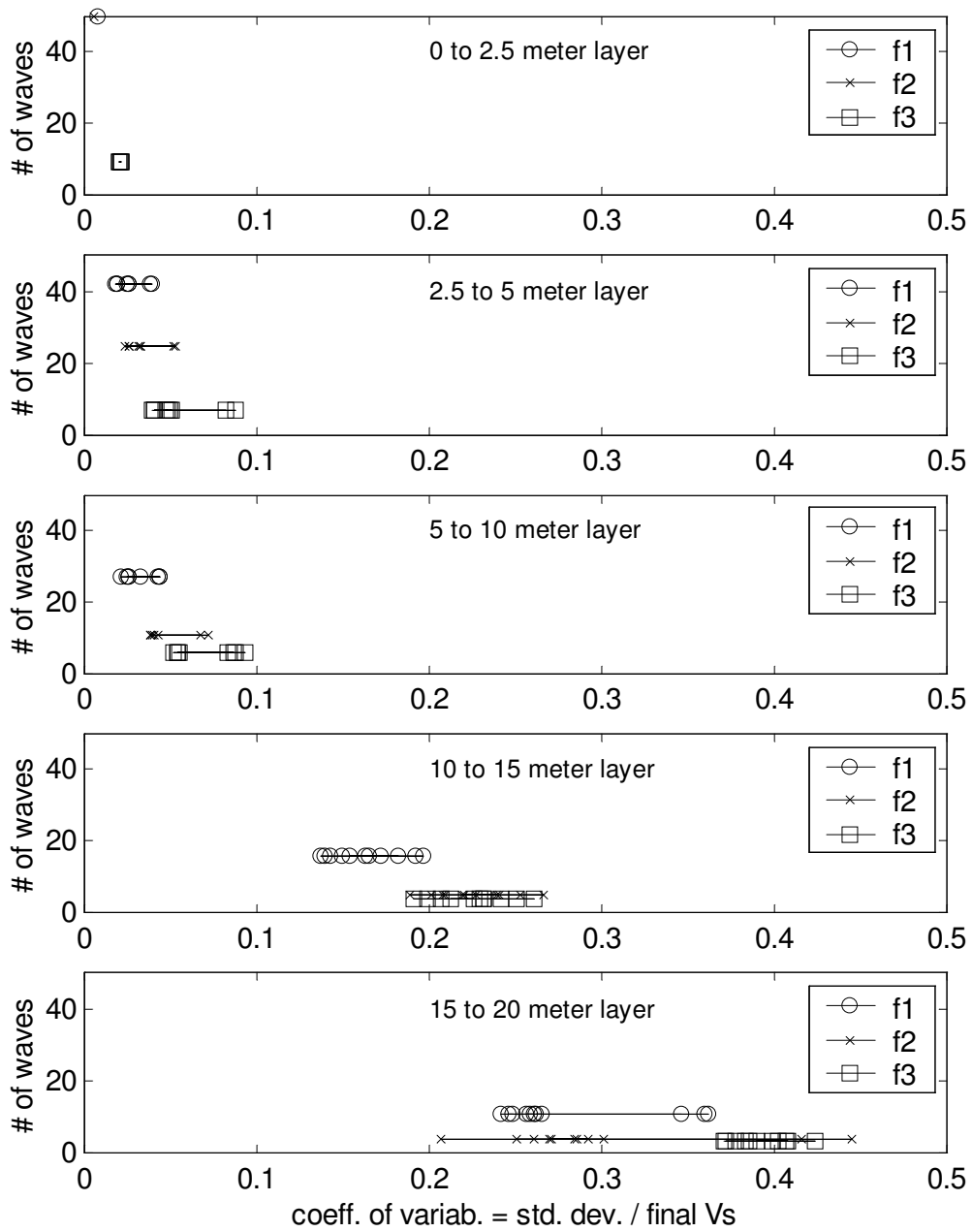
Figure 5.6 Effect of the number of waves sampling a layer on the coefficient of variability, for case ND1
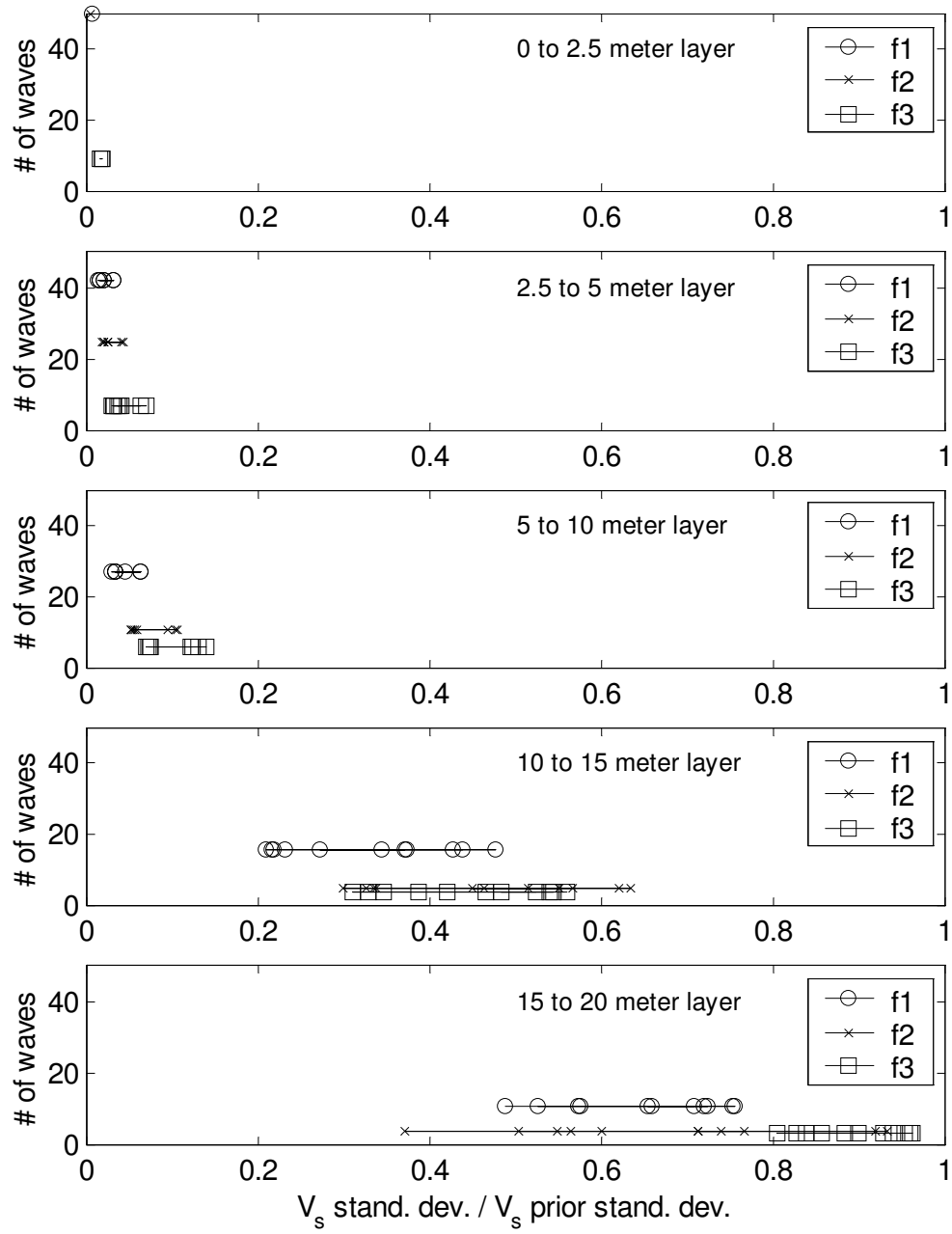
Figure 5.7 Effect of the number of waves sampling a layer on the ratio of final standard deviation of V_s to prior standard deviation of V_s, for case ND1

Additionally, representing the dispersion relation with fewer points can be very valuable because it may reduce the time required by the inversion. On the other hand, when less information is available the estimates for the uncertainties of V_s are higher as seen in Figures 5.6 and 5.7.

Figure 5.6 shows the coefficient of variability (i.e., the ratio of σ_vs to the inverted V_s) versus the number of waves that sampled each layer. It can be noted that for a specific layer the value of the coefficient of variability increases as the number of waves sampling the layer is reduced. Additionally, the coefficient also increases as the depth is increased. Figure 5.7 shows the ratio of σ_vs (standard deviations of the inverted V_s) to σ_vs_{pr} (values given prior to the inversion) versus the number of waves that sampled each layer. For a specific layer the value of σ_vs increases as the number of waves sampling the layer is reduced. Additionally, σ_vs also increases as the depth is increased. In summary, the uncertainties of V_s increase for a reduced number of waves sampling the layer and for deeper depths, which is reasonable since less information results in higher uncertainties.

Another way to study the effect of the frequency distribution is by estimating the resolution matrix, which compares the final and prior covariance matrices, as described in Chapter 4. The ideal resolution matrix would be the identity matrix (i.e., the diagonal terms equal to 1.0 and the off-diagonal terms equal to 0.0). Figure 5.8 shows the diagonal of the resolution matrix for profiles 24, 31, and 37 for frequency distributions f1, f2, and f3. It can be noted that for the very top layers all frequency distributions result in a resolution value very close to 1.0, and that the resolution for layers below 30 meters

depth is similar for all cases. In general, the plots show that the resolution of layers between 5 and 30 meters depth is highest for frequency distribution f1. Comparing this distribution with distribution f2, we see that f1 has more points for lower frequencies (longer wavelengths) and less for larger frequencies (shorter wavelengths), which helped improve the resolution for layers from 5 to 30 meters, and did not affect the resolution of the remaining layers. Distribution f3 has fewer points and the resolution of the layers between 10 and 30 meters is affected negatively. These results agree with the observations about information content and its effect on the final uncertainties of V_s.

5.2.2 Effect of Uncertainties Related to the Experimental Data

The uncertainties related to the experimental data have a direct effect on the value of the rms error, which compares the theoretical dispersion curve with the experimental curve as described in Chapter 3 in equation 3.2. For a specific theoretical V_s profile, the value of the rms error is smaller for larger uncertainties assigned to the phase velocity.

The V_s profiles shown in Figure 5.3 are used here to see this direct effect of the uncertainties of the phase velocity on the rms value. Using those exact same V_s profiles and varying only the values of the uncertainties of V_r, Tables 5.2 (a) and (b) show that the rms may change significantly when these uncertainties vary from the 3% $\mathbf{vr}_{ex}$ used during inversion to a 6% $\mathbf{vr}_{ex}$. As mentioned in Chapter 3, the 3% factor is based on data presented by Tuomi and Hiltunen (1997), which showed values between 0.2 and 6.4%.
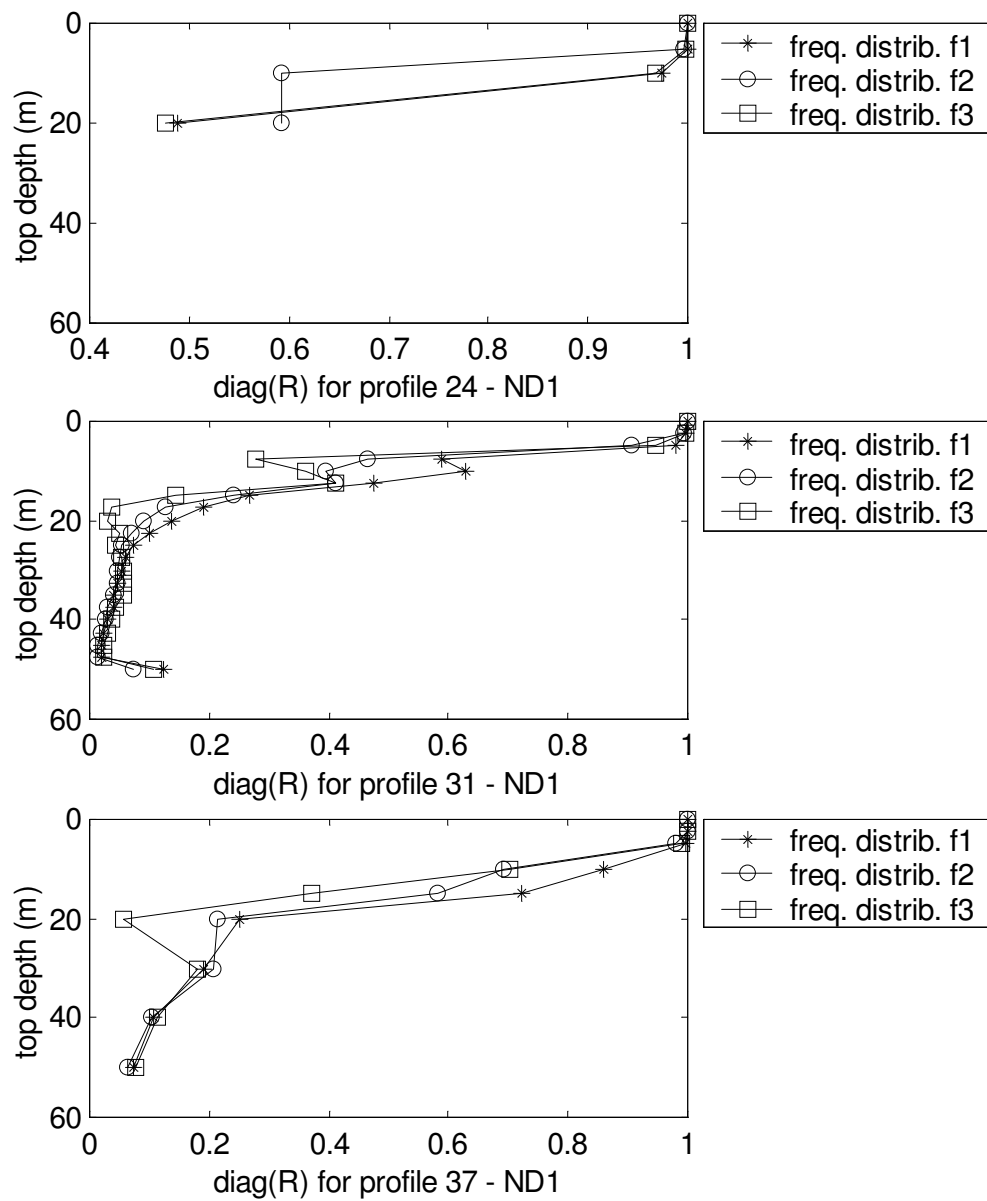
Figure 5.8 Effect of frequency distribution on the diagonal of the resolution matrix, for case ND1

Table 5.2(a) Direct effect of V_r uncertainties on the rms error, case ND1

ND1	24	31	37
$\sigma\_vr_i = 3\%\ (vr_{ex\ i})$	0.34	0.30	0.35
$\sigma\_vr_i = 6\%\ (vr_{ex\ i})$	0.17	0.15	0.18
rms values for the V_s profile estimated with the maximum likelihood inversion using frequency distribution f1			

Table 5.2(b) Direct effect of V_r uncertainties on the rms error, case ND2

ND2	29	31	37
$\sigma\_vr_i = 3\%\ (vr_{ex\ i})$	1.93	0.47	1.18
$\sigma\_vr_i = 6\%\ (vr_{ex\ i})$	0.96	0.23	0.59
rms values for the V_s profile estimated with the maximum likelihood inversion using frequency distribution f4			

As shown in Table 5.2 (b), for case ND2 using profile 29 the rms of the estimated V_s profile is 1.93, but for that exact same V_s profile the rms value is reduced to 0.96 if the uncertainties are doubled (from 3 to 6% $\mathbf{vr}_{ex}$). Since the experimental and the theoretical dispersion curves are the same ones in both cases, this should not be interpreted as a better match caused by a change in the uncertainties of V_r, but as an indication that the rms criterion cannot be completely fixed, since values assumed prior to the inversion may affect the rms value significantly.

Other than this direct effect on the rms value, the uncertainties of V_r affect the resulting V_s values and uncertainties obtained from the inversion. Figure 5.9 presents inversion results for profile 37 case ND1 for two different levels of V_r uncertainties used during inversion: 3 and 6% $\mathbf{vr}_{ex}$. It can be noted that the final profile obtained with the inversion had different V_s values and uncertainties due to the change in V_r uncertainties. Figure 5.10 shows the increase on the coefficient of variability (standard deviations of V_s / V_s) caused by an increase of the V_r uncertainties. Figure 5.10 (a) compares the coefficient of variability obtained for each layer of profile 24 when the uncertainties of V_r used during inversion are 3 and 6% vr_{ex}. Equivalently, figure 5.10 (b) and figure 5.10 (c) compare these coefficient for profiles 31 and 37, respectively.

In figure 5.10, it can be noted that the effect of increasing V_r uncertainties in the standard deviations estimated for the final V_s profile is a relatively small increase for most layers. This increase is explained because a dispersion curve with more uncertainty does not constrain the solution as much, and consequently, there are a larger number of V_s profiles

that satisfy a particular rms criterion (say rms<1.0). In conclusion, it is important to have a realistic estimate of the uncertainties of the phase velocity, because if these are too large the problem may not be sufficiently constrained by the dispersion curve and the range of potential V_s profiles might be too large. On the other hand, if the uncertainties of V_r are too small, they might constrain the problem too much, increasing the rms values and making it hard to find a V_s profile with a satisfactory rms.

5.3 Factors Related to the Initial Shear Wave Velocity Profile

5.3.1 Effect of Depths and Thicknesses of the Layers

Depending on its thickness and depth, a layer is sampled differently by the surface waves as noted on section 5.2.1, and consequently, a change in its V_s will have a different effect on the dispersion curve. The more effect a change in the V_s of a layer has on the dispersion curve, the more sensitive the dispersion curve is to that layer, and the better that layer can be resolved. This sensitivity of the dispersion curve may be examined by looking at the partial derivatives (i.e., $\partial V_r/\partial V_s$ as presented in Chapter 4) obtained for the last iteration. Figures 5.11 (a) and (b) show the partial derivatives obtained for all frequencies for each layer of profile 31 for cases ND1 and ND2 respectively. It is clear for both cases that the top layers have higher sensitivities and affect a larger range of frequencies.
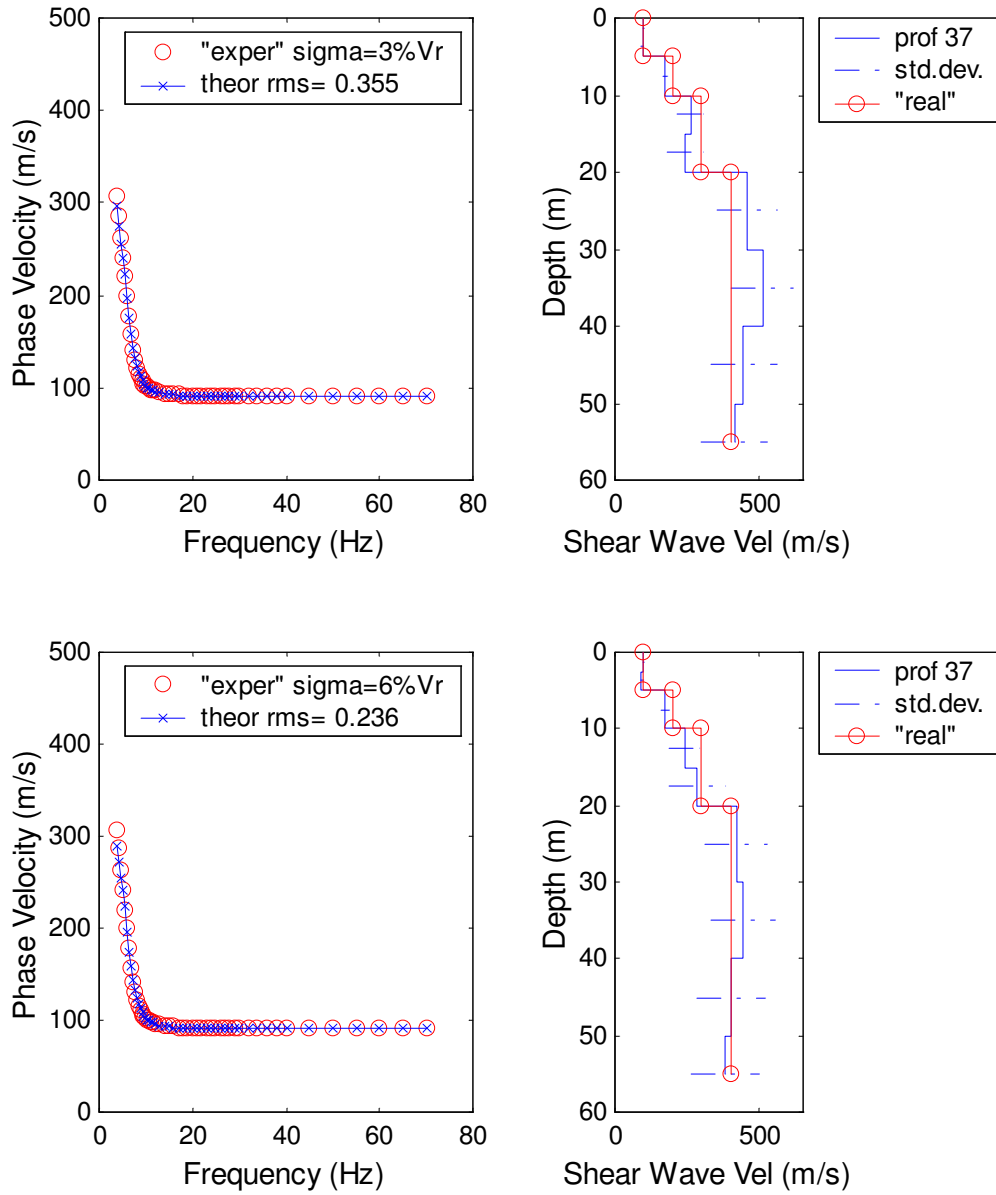
Figure 5.9 Inversion results for profile 37, for standard deviations of V_r of 3 and 6% $V_{r\ exp}$, for case ND1 with frequency distribution f1
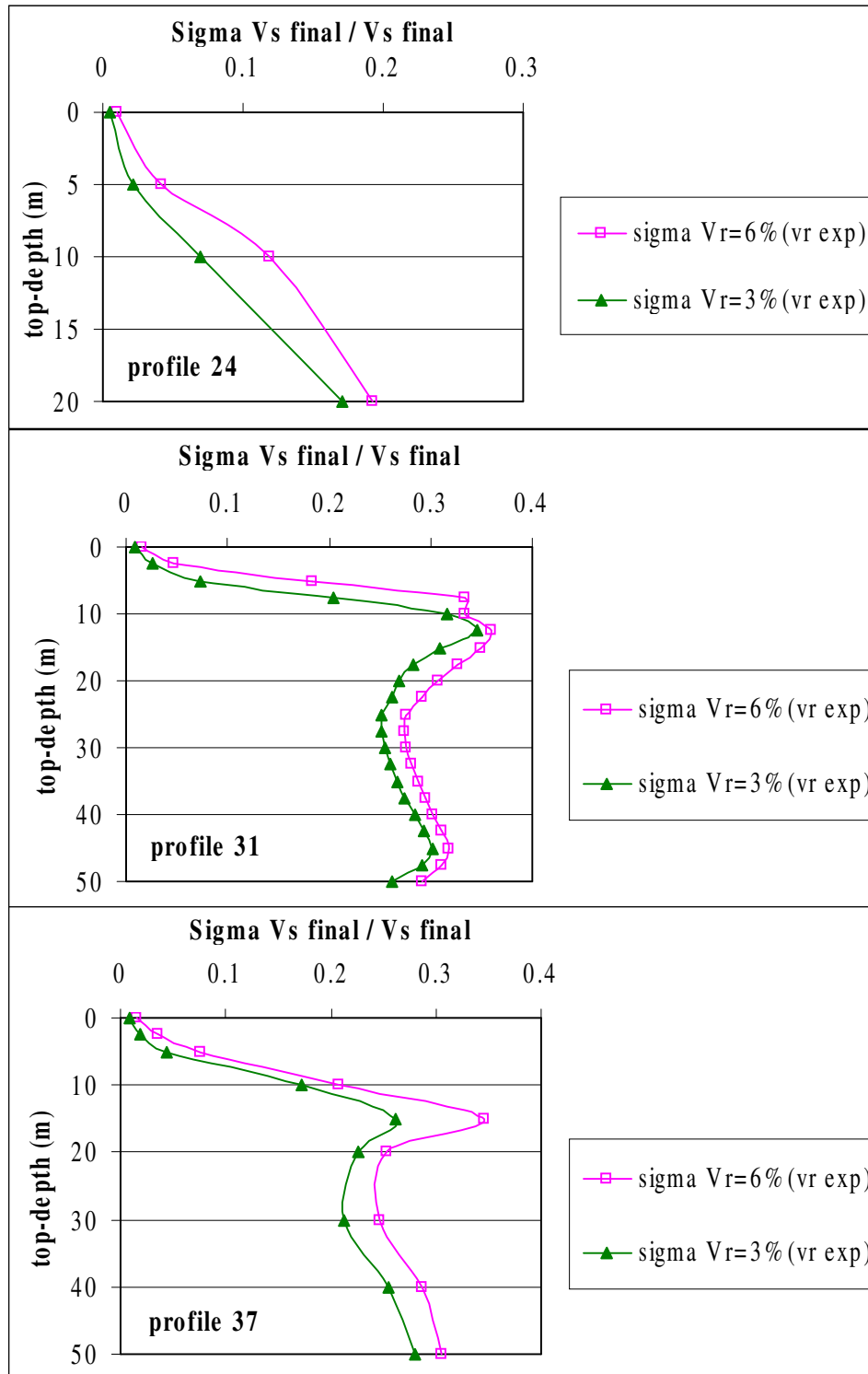
Figure 5.10 Change in coefficient of variability caused by varying standard deviations of V_r, for case ND1 profiles 24, 31, and 37
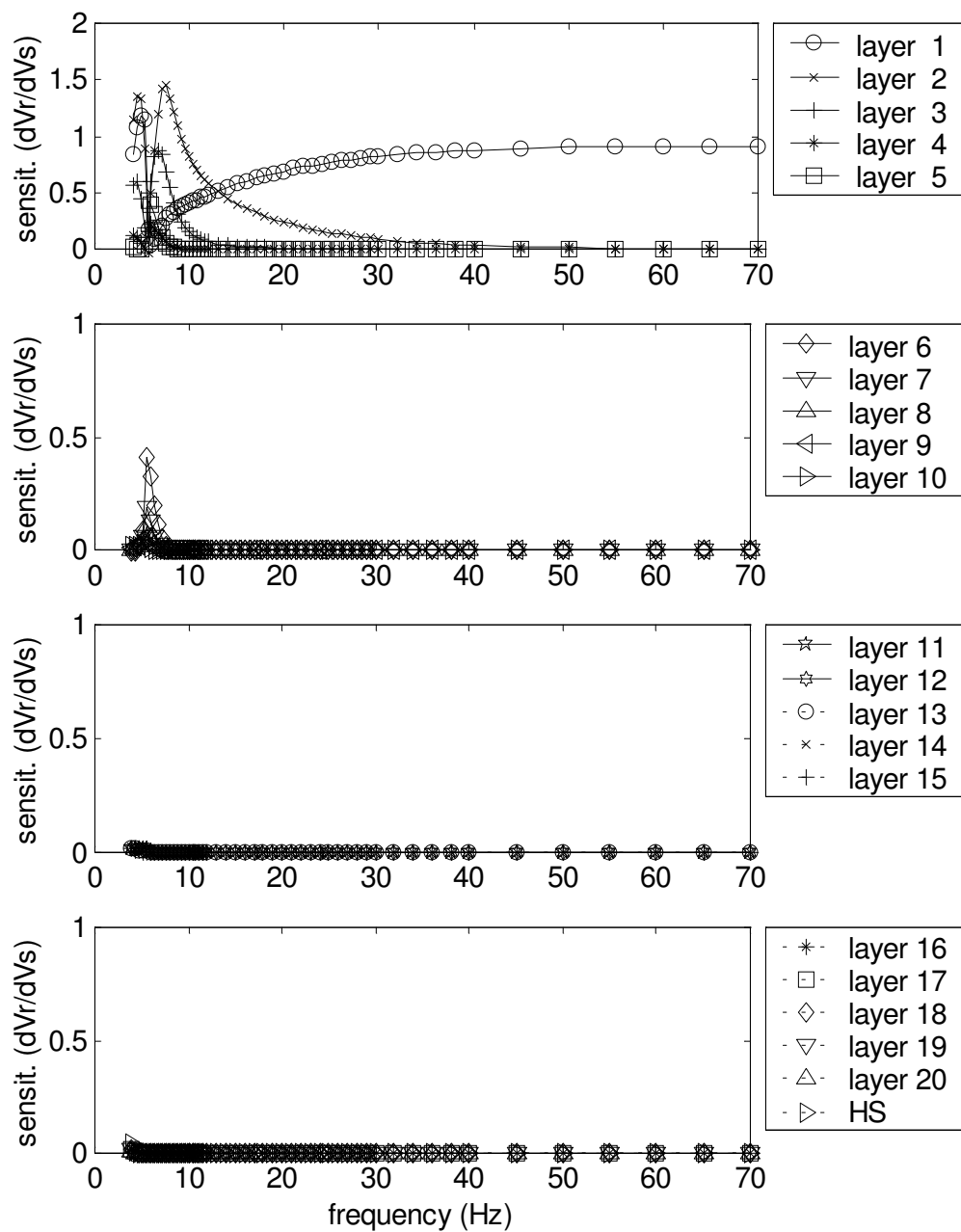
**Figure 5.11(a) Partial derivatives for all layers of profile 31,
for case ND1 with frequency distribution f1**
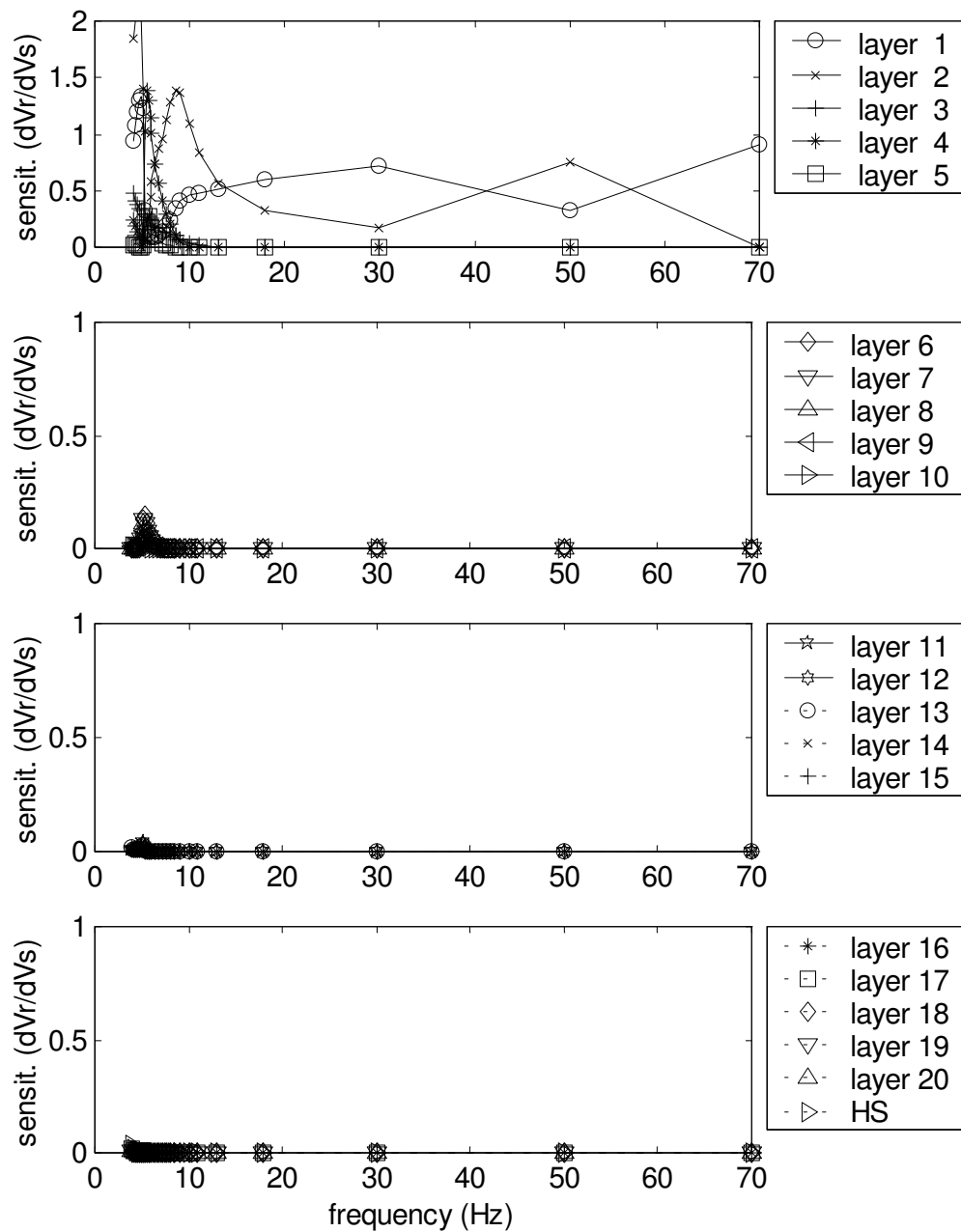
**Figure 5.11(b) Partial derivatives for all layers of profile 31,
for case ND2 with frequency distribution f4**

The sum of the partial derivatives over all frequencies is divided by the number of frequencies to obtain a mean sensitivity for each layer. This sensitivity is plotted versus the top-depth of the layers and presented for all profiles except profiles 1 to 4, in Figure 5.12. This plot shows a large decrease in the sensitivity between 0 and 10 meters, and lower sensitivities for layers below 10m.

Evaluating how sensitive the dispersion curve is to a change in the V_s of a layer, can also be done manually by changing the V_s value of the layer and observing the variation of the dispersion curve, and its effect on the rms value. Figure 5.13 shows an example where the V_s of the top layer (i.e. layer 1) of profile 31 for case ND1 was reduced by 20%. It can be noted that the rms varied from 0.301 to 5.24 and the change in the dispersion curve is clearly noticeable on the plot. Thus, the dispersion curve is very sensitive to the value of this first layer. This makes sense since the dispersion curve has a lot of information on the top layer as noted previously on section 5.2.1 (all waves travel through this top layer).

For comparison, this same V_s reduction by 20% is done to each layer of profile 31 and Figure 5.14 presents the resulting percent change in V_r. Figure 5.14 (a) presents case ND1 and figure 5.14 (b) presents case ND2. For each curve the layer specified was the only one that had the V_s changed. These plots show the same trends presented by the partial derivatives in Figure 5.11, where the top layers affect a larger range of frequencies and have a more significant effect on the phase velocity values than the deeper layers. It can be noted that for layers below the third one (i.e., below 7.5 meters depth) there is no effect on dispersion data with frequencies larger than 10Hz.
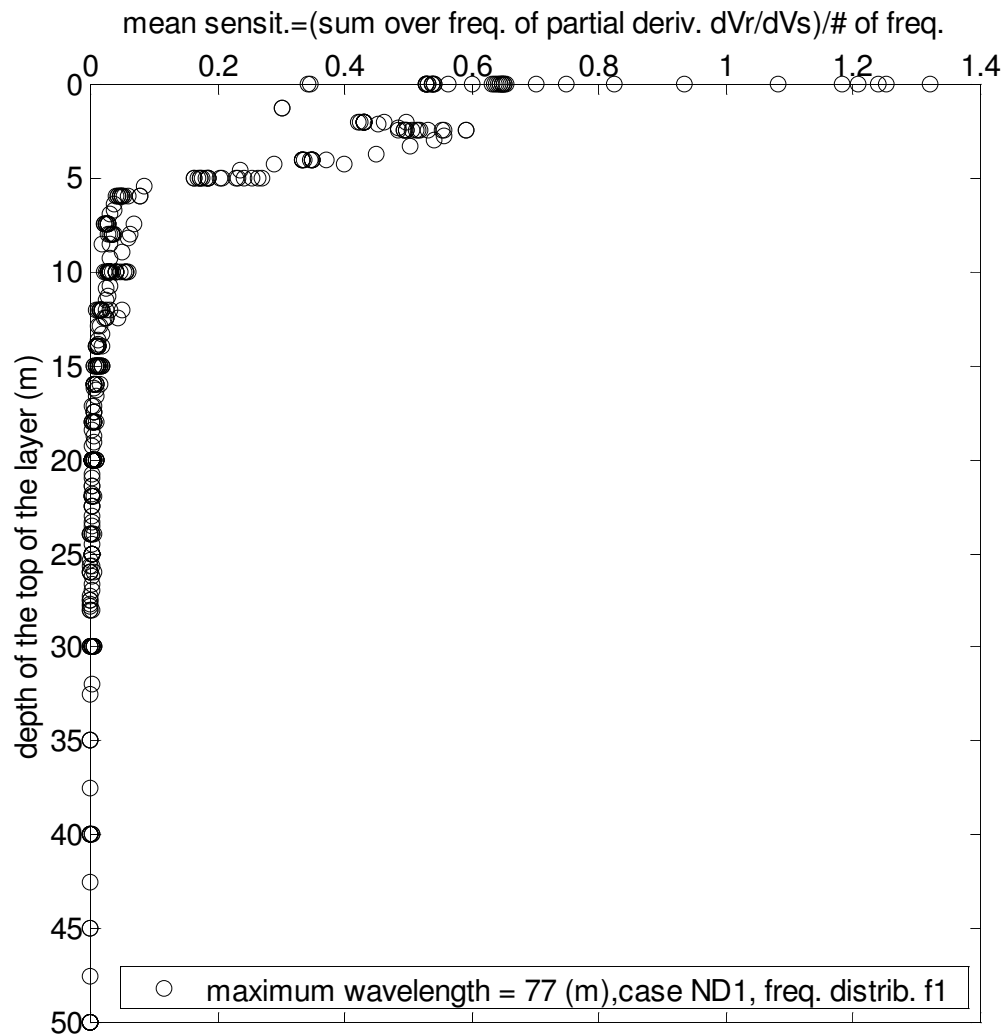
Figure 5.12 Sum over frequency of partial derivatives versus mid-depth for all layers of all satisfactory profiles for case ND1
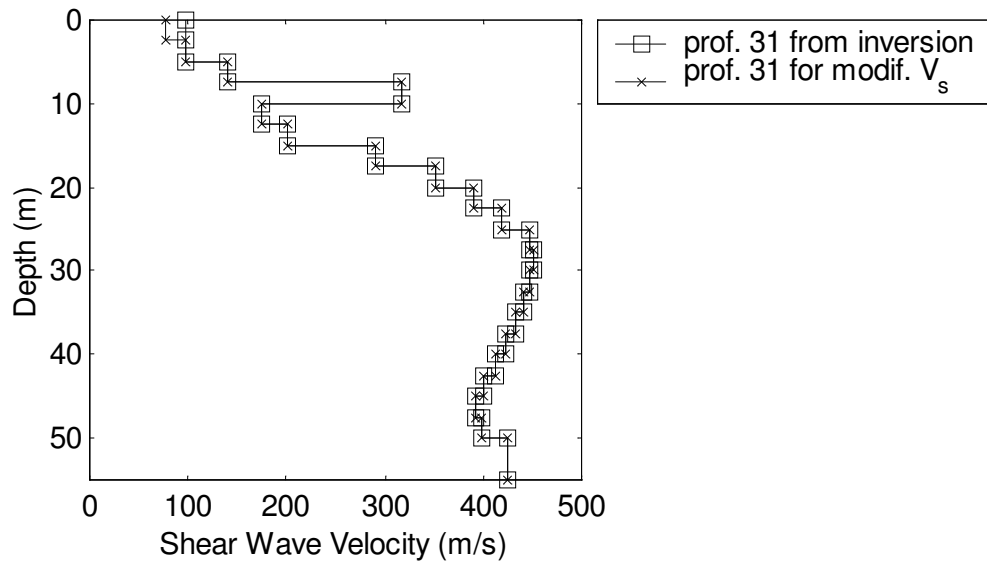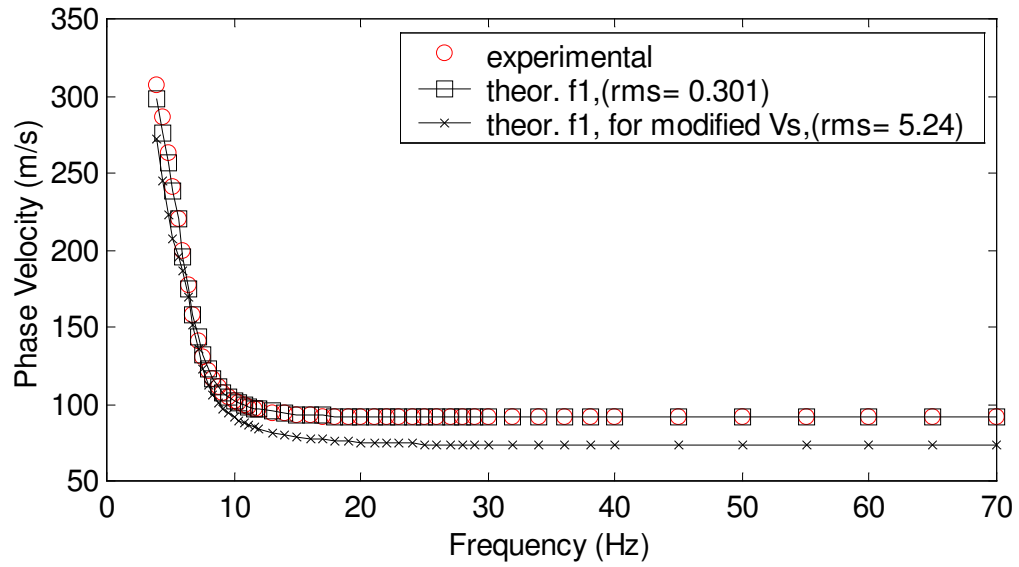
Figure 5.13 Inversion results when reducing the V_s of the first layer of profile 31 by 20%, case ND1, frequency distribution f1
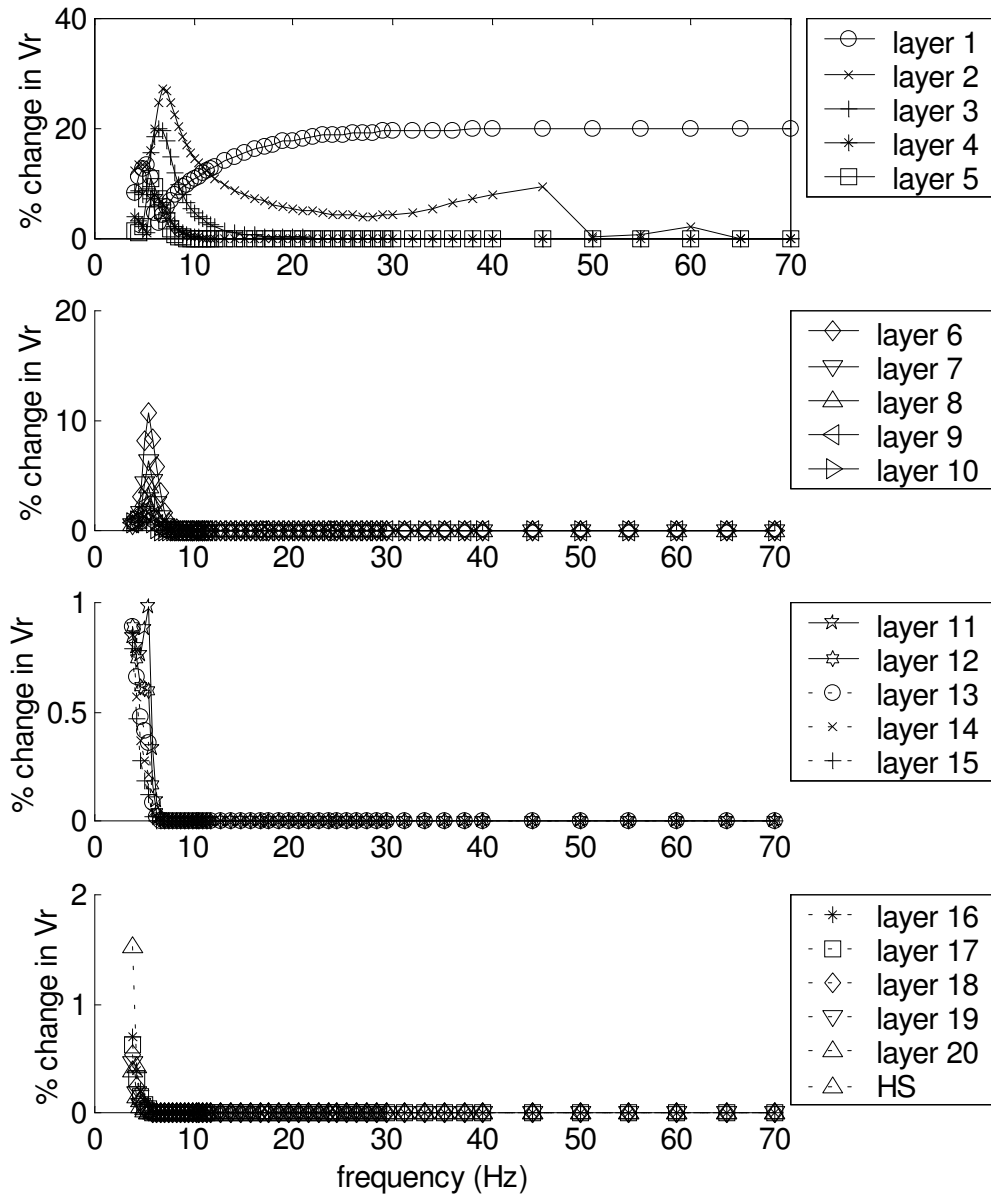
Figure 5.14 (a) Percent change in V_r caused by reducing the V_s of each layer by 20% for case ND1, frequency distribution f1, profile 31
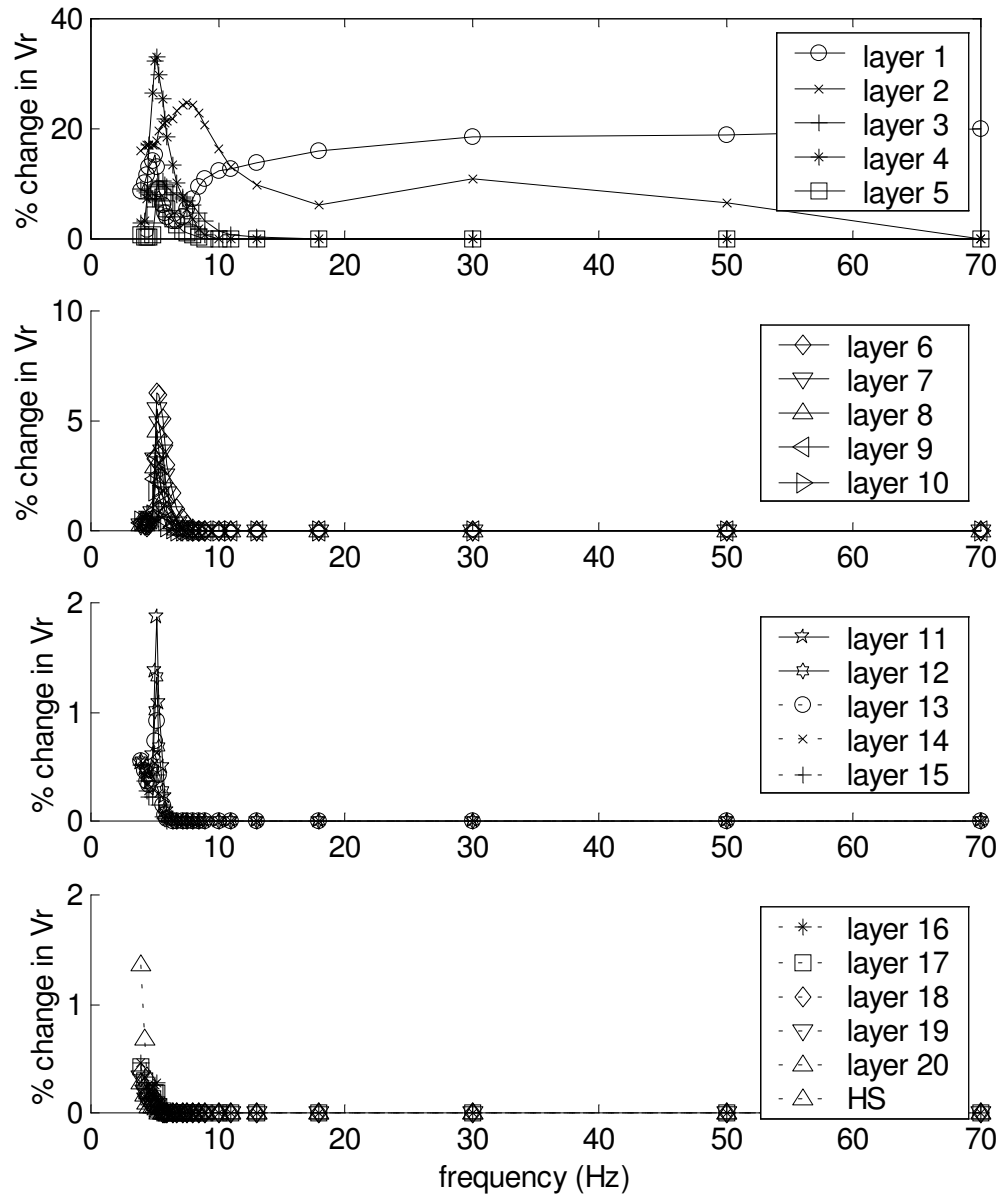
Figure 5.14 (b) Percent change in V_r caused by reducing the V_s of each layer by 20% for case ND2, frequency distribution f4, profile 31

One way to summarize the effect that the V_s change has on the dispersion curve is to look at the change on the rms which gives one number for the whole curve. Figure 5.15 shows the new rms (after reducing the V_s by 20%) divided by the original rms, and plotted versus the top-depth of each layer. Figure 5.15(a) presents case ND1 with profiles 24, 31 and 37, and figure 5.15 (b) presents case ND2 with profiles 29, 31 and 37. These plots show that the sensitivity of the dispersion curve to a change in V_s reduces with depth, which means that the deeper layers have a smaller effect on the dispersion data. Additionally, when profiles 31 and 37 are compared, it is noted that increasing the thickness with depth helps reduce the difference in sensitivities between deeper and shallower layers.

However, the sensitivity of the dispersion curve to a specific layer depends on the specific case. For example, Figure 5.15 shows that the changes in rms caused by the V_s reduction of the first and second layers of profile 31 are very different for cases ND1 and ND2. Comparing the plots for these layers in Figures 5.14(a) and 5.14(b), it can be noted that the difference is the rms change is caused mainly by the different distribution of the dispersion points. For profile ND1 there are significantly more points for frequencies above 10Hz than for profile ND2. Consequently, for profile ND2 the V_r changes for the higher frequencies (affected more by the V_s of first layer) have a smaller weight in the rms error and the V_s of the second layer ends up having a higher effect on the rms.
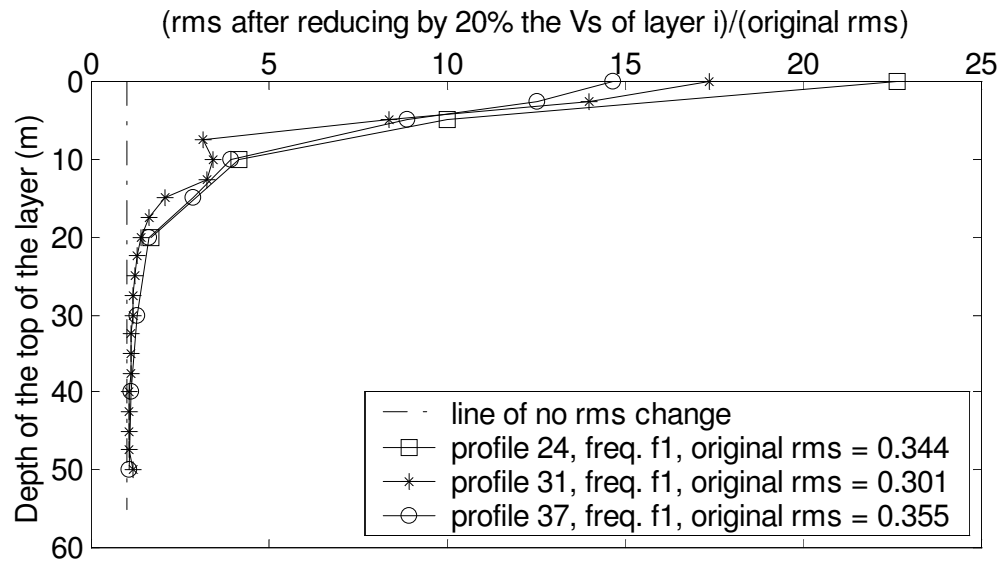
Figure 5.15(a) Change in rms caused by a reduction of V_s by 20% for case ND1, for profiles 24, 31, and 37
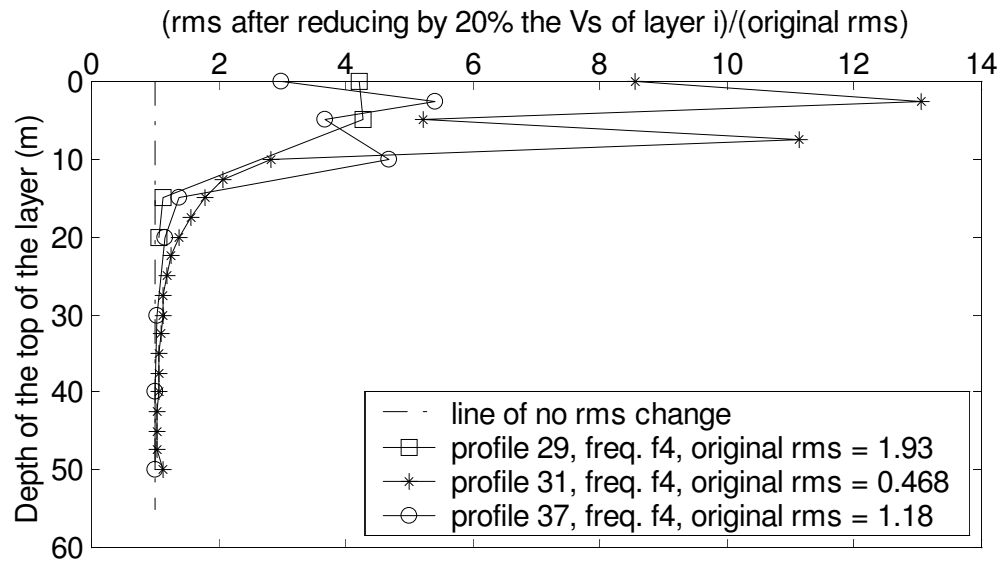
Figure 5.15(b) Change in rms caused by a reduction of V_s by 20% for case ND2, for profiles 29, 31, and 37

146

Figure 5.16 shows the V_s profiles obtained for profiles 24, 31 and 37 in case ND1, and for profiles 29, 31 and 37 in case ND2, including the standard deviations corresponding to the estimated V_s values. See that the standard deviations increase with depth markedly for the upper layers, and are very similar for the deeper layers. This is consistent with the reduction of sensitivity with depth that was discussed above, since there is a significant reduction with depth for the upper layers and for the deeper layers the sensitivities are similarly low.

The relationship between sensitivity and V_s uncertainties is observed in Figure 5.17, which includes two plots of the coefficient of variability (i.e., σ_vs/vs) versus the mean sensitivity (average of the partial derivatives for each layer). One plot includes most layered profiles obtained (excluding the ones with very high rms errors), and the other plot includes only the results for the layers used in section 5.2.1, and makes it clear that the depth of the layer has a significant influence on the sensitivity and the coefficient of variability obtained. Both plots show that the coefficient of variability increases for a decreased sensitivity. This figure also presents the coefficient of variability versus the top-depth of the layers and versus the thickness to depth ratio multiplied by the number of waves sampling the layer. As expected based on the above results, this coefficient increases with depth strongly for the shallower depths and varies slightly for the deeper layers, which have similar standard deviations. Additionally, the coefficient of variability decreases with the thickness to depth ratio multiplied by the number of waves, which means that for a specific depth a thickness increase and/or an increase in the number of waves may help lower the uncertainties of V_s.
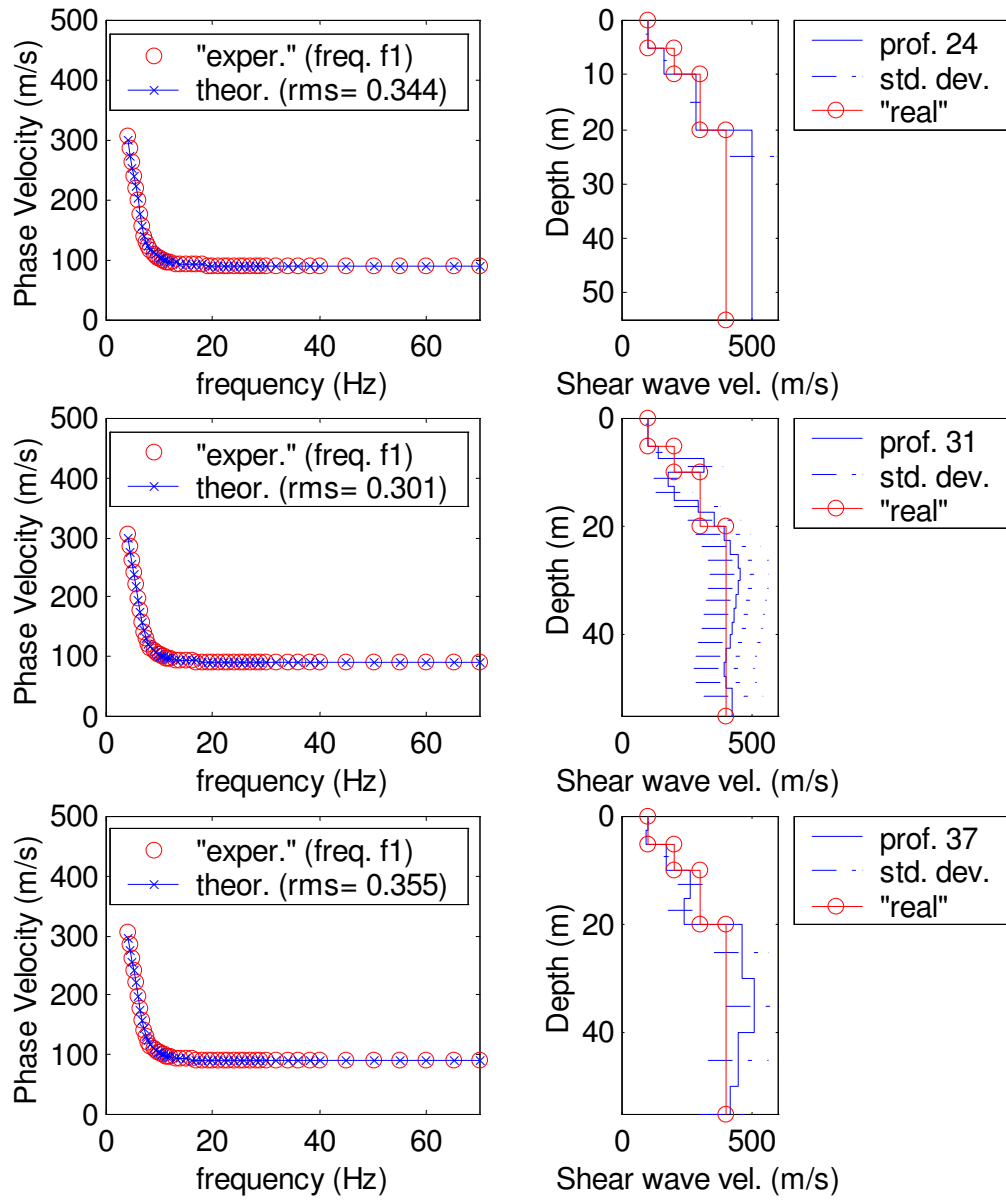
Figure 5.16(a) Inversion results for case ND1, for profiles 24, 31, and 37 (including standard deviations)
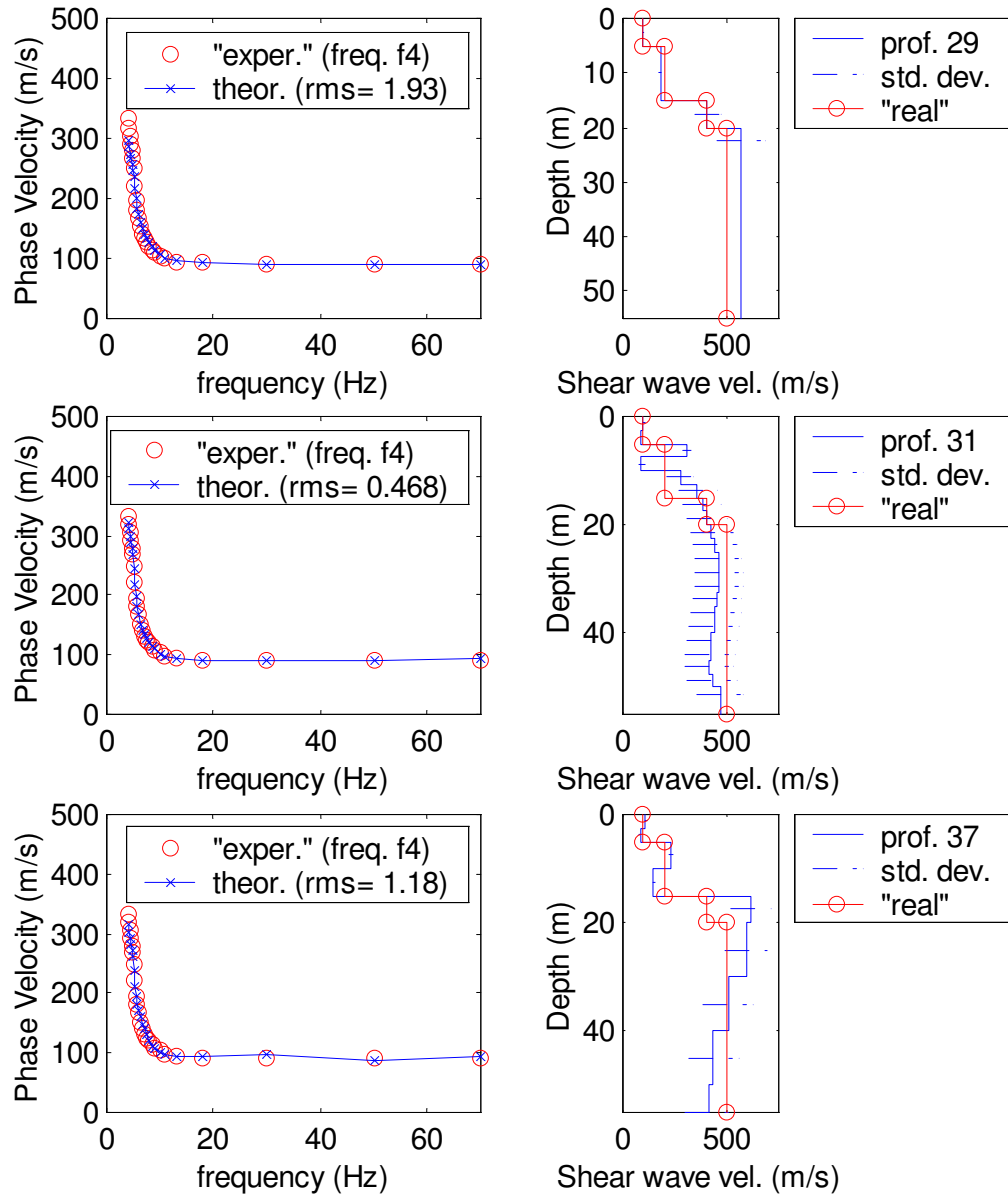
Figure 5.16(b) Inversion results for case ND2, for profiles 29, 31, and 37 (including standard deviations)
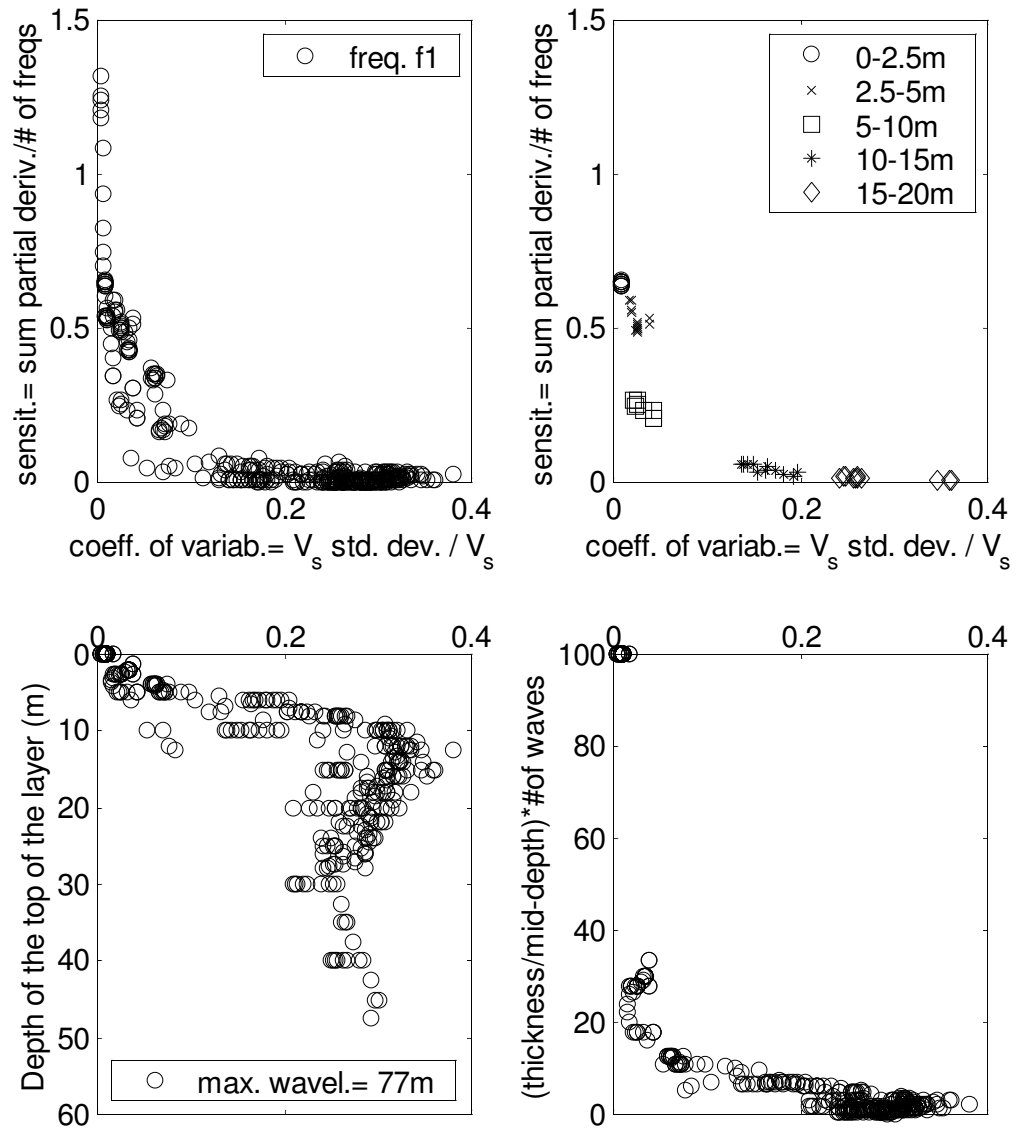
Figure 5.17(a) Coefficient of variability versus sensitivity, versus depth, and versus thickness to depth ratio for case ND1, frequency distriubution f1

150
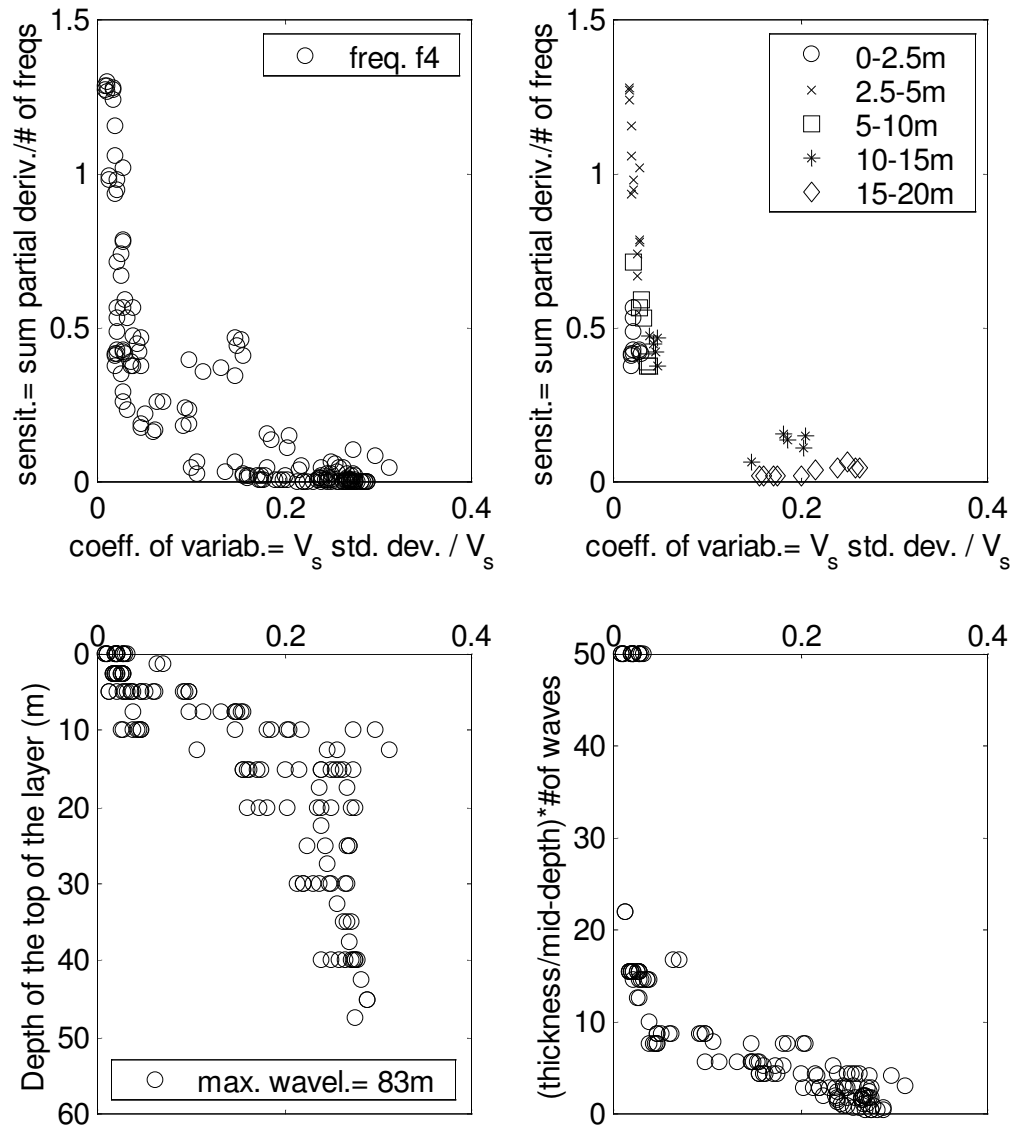
Figure 5.17(b) Coefficient of variability versus sensitivity, versus depth, and versus thickness to depth ratio for case ND2, frequency distriubution f4

151

Comparing the final uncertainties to the prior uncertainties, gives a measure of how much the data added with the inversion process improves the prior uncertainties, and gives a measure of resolution for each layer. This is done with the resolution matrix, which is based on comparing final and prior covariance matrices. As described in Chapter 4, two possible measures that help compare the resolution matrix to the identity matrix (i.e., the ideal resolution matrix) are the Dirichlet and the Backus-Gilbert spreads. The Backus-Gilbert spread penalizes more the terms of the resolution matrix that are farther from the diagonal, and the Dirichlet spread penalizes all terms equally. Figure 5.18 presents these spreads for all layered profiles of cases ND1 and ND2. The profiles with the lowest spreads are presented in Figure 5.19, except profiles 1, 2, and 39, which had low Backus-Gilbert spreads but are related to high rms errors. This emphasizes the fact that the resolution matrix does not give any weight to the fit between theoretical and experimental dispersion curves. Thus, the spreads should be compared only among profiles that are considered to produce dispersion data with a satisfactory fit.

The profile with the lowest normalized Dirichlet spread was profile 25 for both, ND1 and ND2. The profiles with lowest normalized Backus-Gilbert spread were profiles 23 and 24 for case ND1, and profile 23 for case ND2. Note in Figure 5.19 that the only case in which the profile with the lowest spread had the appropriate layer interfaces to match the real ones was for the Backus Gilbert spread in case ND1. This is something that would not be known for real experimental data, and shows that finding which layered profiles have the appropriate layer interfaces is a complicated task.
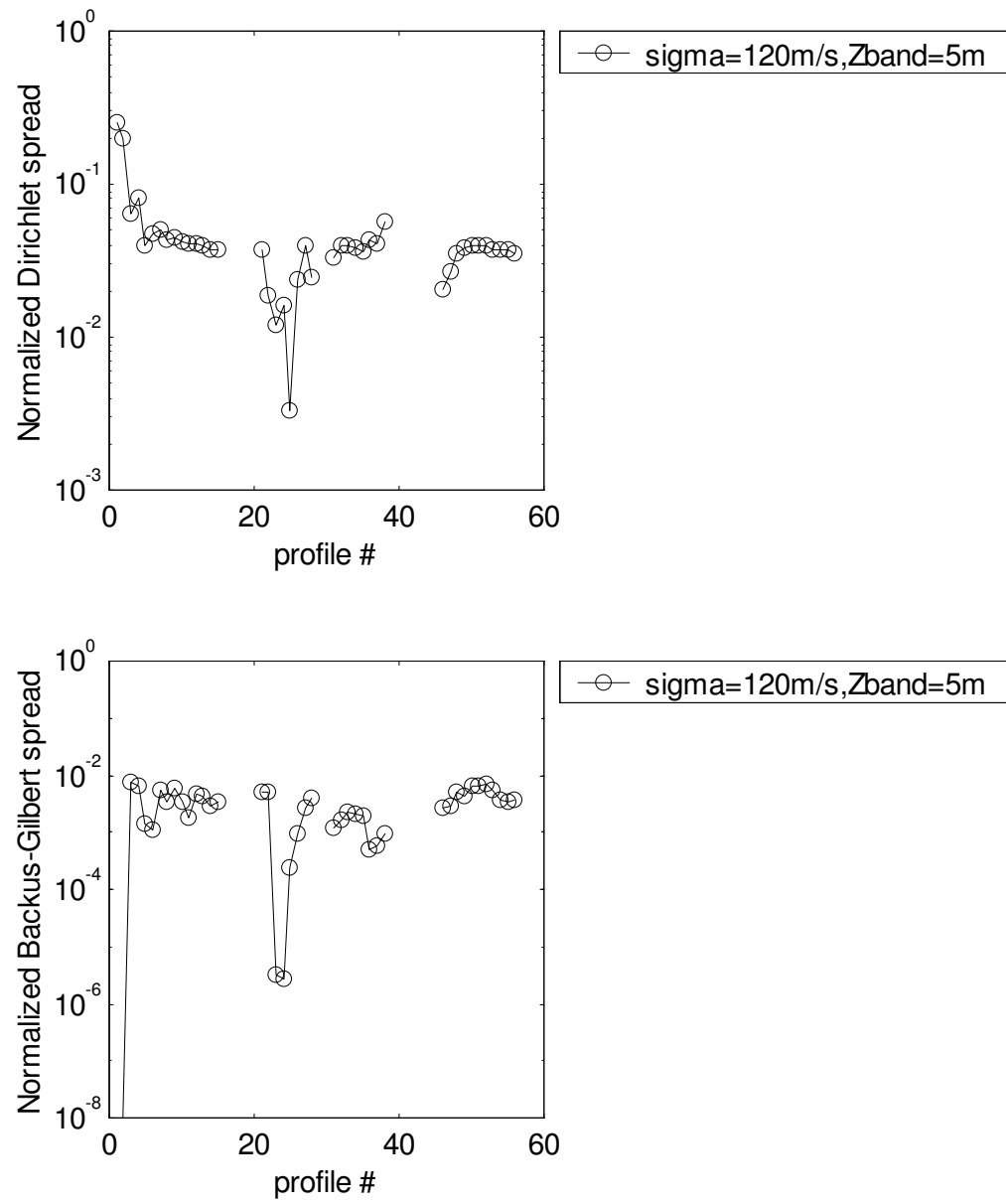
Figure 5.18(a) Spreads of the resolution matrix for case ND1, frequency distribution f1
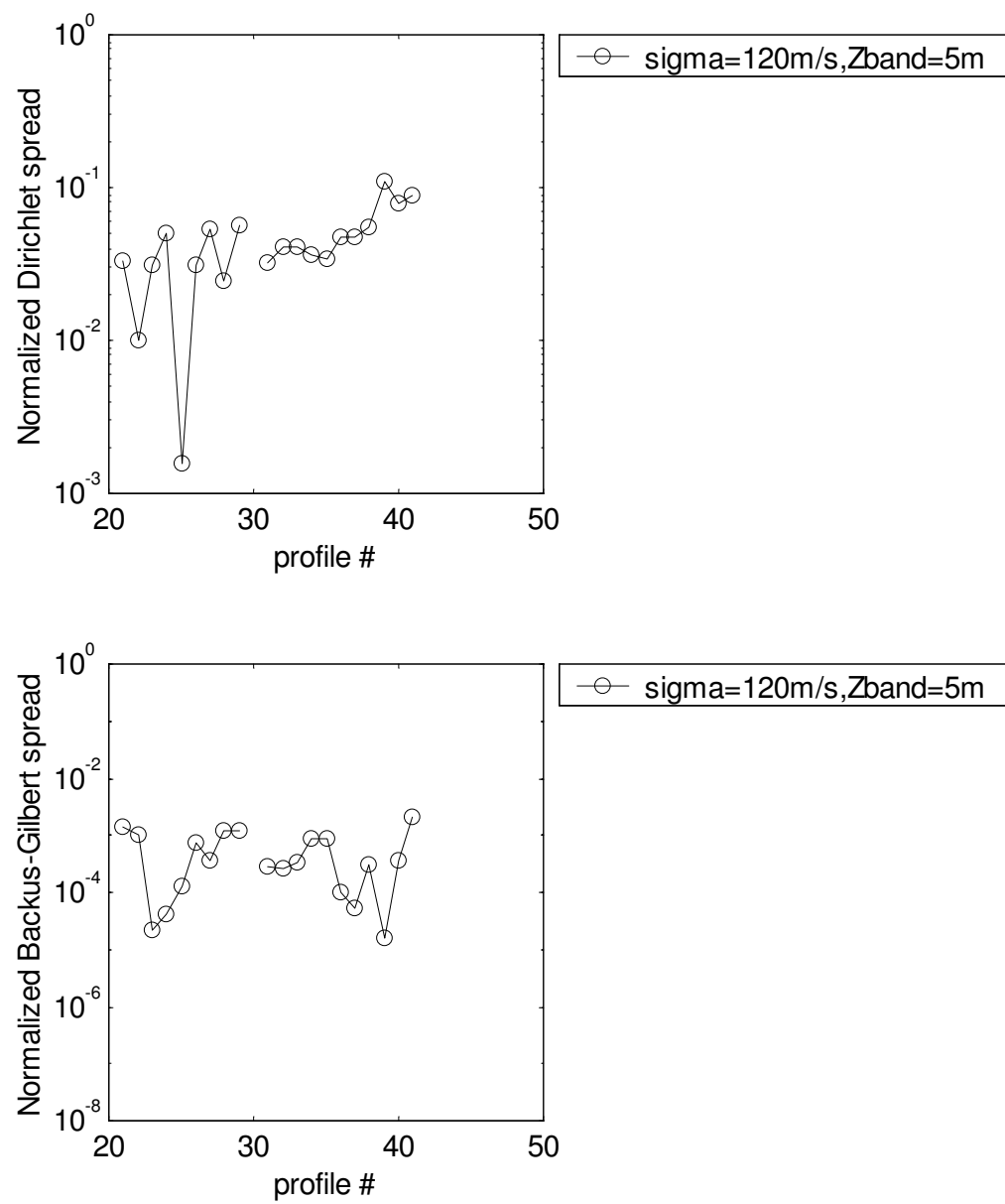
Figure 5.18(b) Spreads of the resolution matrix for case ND2, frequency distribution f4

Profile	23	24	25	real ND1	real ND2
layer thicknesses in meters	2.5	5	1.25	5	5
			1.25		
	2.5		2.5		
	5	5	2.5	5	10
			5		
	10	10	7.5	10	5

Figure 5.19 Layers of real profile and of profiles with low Normalized Dirichlet and Backus-Gilbert Spreads

The diagonal of the resolution matrix gives more information since each layer is related to one value of resolution. The configurations in Figure 5.20. were selected to observe the change in the diagonal of the resolution matrix caused by a change in the thicknesses of the layers. Figure 5.21 shows the variation of the diagonal of the resolution matrix plotted versus the top-depth of each layer. As expected the resolution values decrease with depth (i.e., expected since there is a decrease in information content with depth, a decrease of the sensitivity of the dispersion curve to a change in V_s with depth, and an increase in the uncertainties of V_s with depth).

For case ND1 in Figure 5.21(a), it can be noted that increasing the thickness of the layers with depth improves the relative resolution of the layers. The values of the diagonal become closer to one as the deeper layers are assumed thicker. Thus, the reduction in resolution may be reflected in having thicker layers with depth, which helps reduce the difference in resolution among layers. The author suggests that it is better to have a resolution decreasing with depth smoothly, as it would naturally occur due to the nature of the test, than to have some higher resolutions with jumps (for case ND1 in figure 5.21(a) see profile 27 versus 22, and profile 38 versus 32). For case ND2 in Figure 5.21(b), note that having a layer that matches the real profiles produces a smooth variation for the diagonal of the resolution, even though this configuration does not present an increase of thickness with depth (profiles 29 and 40).

Profile #	21	22	27	29	31	32	38	40
	2.5	2.5	5	5	2.5	2.5	5	5
	2.5	2.5			2.5	2.5		
	2.5	2.5	5	10	2.5	2.5	5	10
	2.5	2.5			2.5	2.5		
	2.5	5	5		2.5	5	5	
	2.5				2.5			
	2.5	5	5	5	2.5	5	5	5
	2.5				2.5			
layer thicknesses in meters					2.5	5	10	10
					2.5			
					2.5	5		
					2.5			
					2.5	5	10	10
					2.5			
					2.5	5		
					2.5			
					2.5	5	10	10
					2.5			
					2.5	5		
					2.5			

Figure 5.20 Profiles selected to compare the diagonal of the resolution matrix: 21, 22, 27, 29, 31, 32, 38, and 40
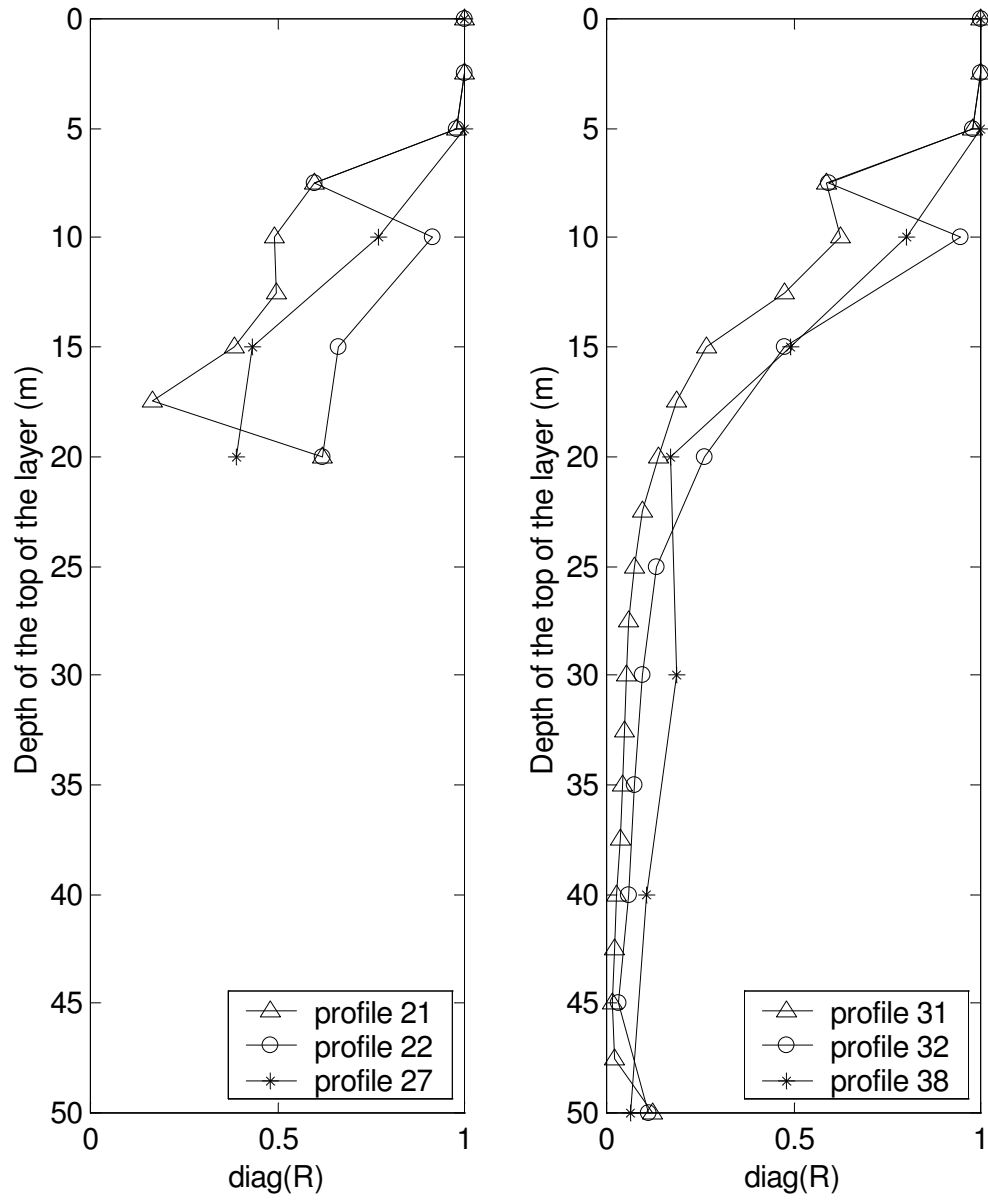
Figure 5.21(a) Diagonal of the resolution matrix for profiles 21, 22, 27, 31, 32, and 38, for case ND1.
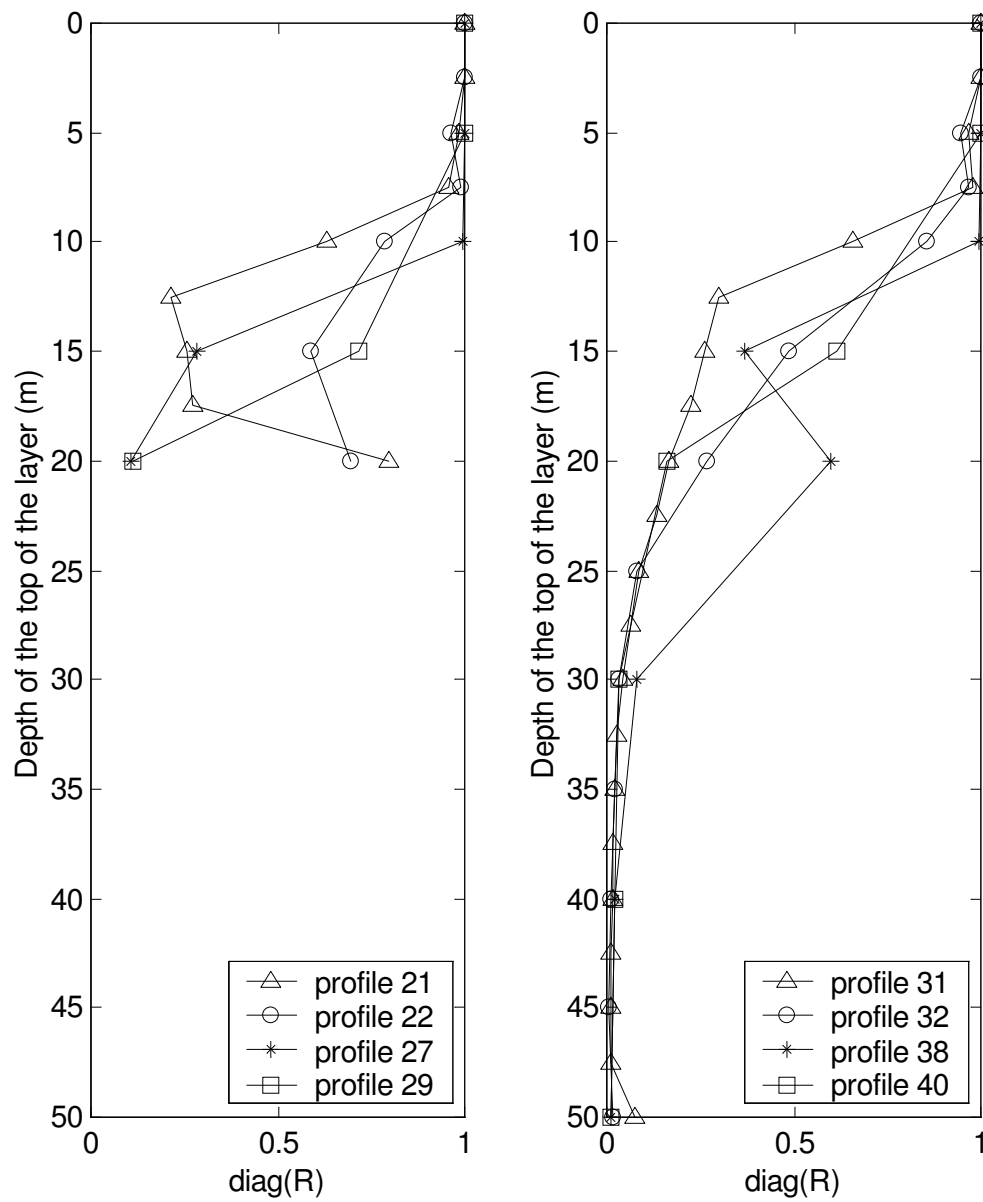
Figure 5.21(b) Diagonal of the resolution matrix for profiles 21, 22, 27, 29, 31, 32, 38, and 40, for case ND2.

Thus, the diagonal of the resolution matrix gives more information than the spreads of the resolution matrix and helps compare diverse layered configurations. Since the diagonal presents a comparison among layers of the same profile, it may help decide which thicknesses should be decreased and which increased to improve the relative resolution of the layers. Joh (1996) uses the diagonal of the resolution matrix to have a resolution value for each layer and to implement a 'layer sensitivity analysis'. He proposes that any layer with a lower resolution than the half-space should be increased in thickness, and any layer with a much higher resolution than the others should be reduced in thickness.

5.3.2 Effect of the Depth to Half-Space

Figure 5.21 may also be used to observe the effect of a deeper soil profile on top of the half space. Profiles 21, 22, 27 and 29 have the same layers for the top 20-meters than profiles 31, 32, 38, and 40 respectively (see Figure 5.20). For the deeper profiles, it is noted that the resolution decreases below 20 meters and the deeper layers have a significantly lower resolution. This is not a bad characteristic when dealing with real data because the half-space is unrealistic and the data should not be used to resolve it highly. Thus, it is preferable that the resolution of the half-space is the lowest (not like for profile 21), because it is not reasonable to resolve this layer more than the layers on top of it. In summary, a nice diagonal for a resolution matrix would show the resolution smoothly decreasing with depth, with the half space having the lowest resolution of all layers.

The depths to half-space may also be compared using the half-space sensitivity to the maximum wavelength (i.e., $\partial V_r/\partial V_s$ calculated for the V_s corresponding to the half-space and V_r corresponding to the maximum wavelength). The values for these sensitivities for all layered profiles introduced in Chapter 4 are presented in Figure 5.22. In order to compare the sensitivities, it is best to ignore the values for profiles 1 to 4 for case ND1, and the values for profiles 39 and 41 for case ND2, since they correspond to the highest rms values, respectively. It can be noted that for shallower profiles the sensitivity varies more with the type of layering than for deeper profiles. For example, for case ND1 compare profiles 21 thru 28 (twenty meters depth to half-space) with profiles 31 to 38 (fifty meters depth to half-space), and for case ND2 compare profiles 21 thru 29 (twenty meters depth to half-space) with profiles 31 to 38 and 40 (fifty meters depth to half-space). This is reasonable since the deepest the half-space the least sensitive the dispersion curve is to it. The low sensitivities found for the 50-meters deep profiles are preferred since the purpose is not to resolve this layer highly.

However, the half-space sensitivity to the maximum wavelength should not be too low because it would mean that the half-space is not being defined by the experimental data. Based on the fact that the sensitivity represents the change in V_r that would occur with a change in V_s, Joh (1996) proposes to use a minimum value criterion of 1% (or another value considered reasonable) for the half-space sensitivity to the maximum wavelength, during the analysis of the data. Additionally, Joh (1996) proposes a minimum criterion of 10% (or another value considered reasonable) for the sensitivity to the maximum wavelength of the deepest layer to be included in the final V_s profile reported.
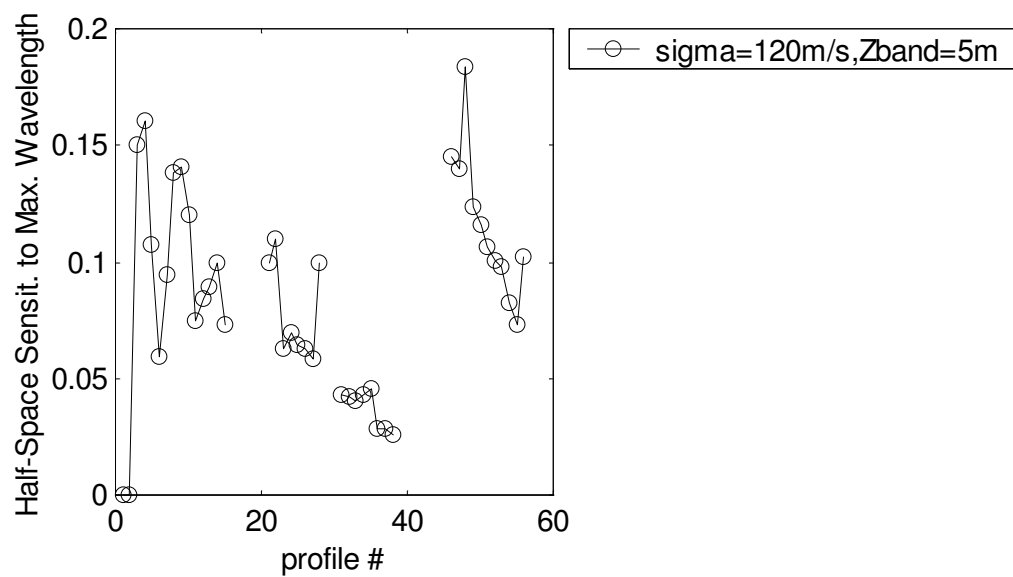
Figure 5.22(a) Half-space sensitivity to maximum wavelength for case ND1, frequency distribution f1
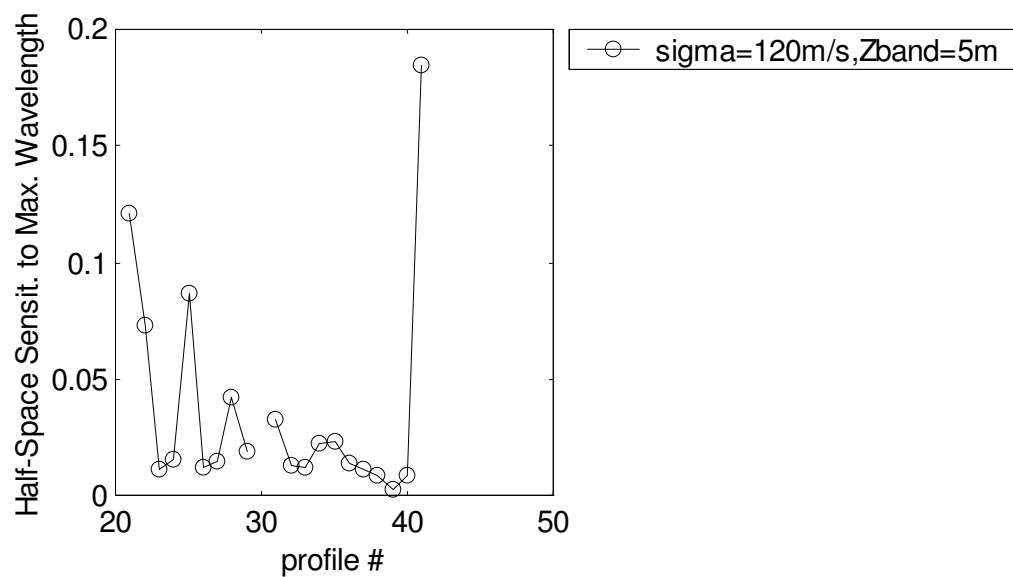
Figure 5.22(b) Half-space sensitivity to maximum wavelength for case ND2, frequency distribution f4

5.3.3 Effect of the Initial Shear Wave Velocity

The initial shear wave velocity is important due to the nonlinear nature of the problem. As mentioned previously, this nonlinear problem is solved with the maximum likelihood, which is an iterative process based on gradient methods. Thus, the inversion algorithm finds a solution by converging to a minimum close to the initial estimate of the solution. Consequently, if the initial shear wave velocities are far from the real values the algorithm may converge to a profile with a high rms.

As mentioned in Chapter 4, the initial V_s profile was based on an empirical method to get initial values that are not too far from the solution. The maximum likelihood iterative algorithm was tried with other initial estimates for the shear wave velocities. The initial estimates assumed for comparison were 100m/s for all layers (100m/s was the minimum V_s value of the real profile) and 400 m/s for all layers (400m/s was the maximum V_s value of the real profile). The change of the initial V_s values from the empirical estimates to the constant V_s values resulted in the algorithm converging to profiles with significantly higher rms errors.

As an example, for case ND1 using profiles 24, 31, and 37, Figure 5.23 presents the difference in results from having these different initial estimates. The results show that the dispersion curves for the estimated V_s profiles do not match the "experimental" dispersion curve satisfactorily for the constant V_s initial estimates.
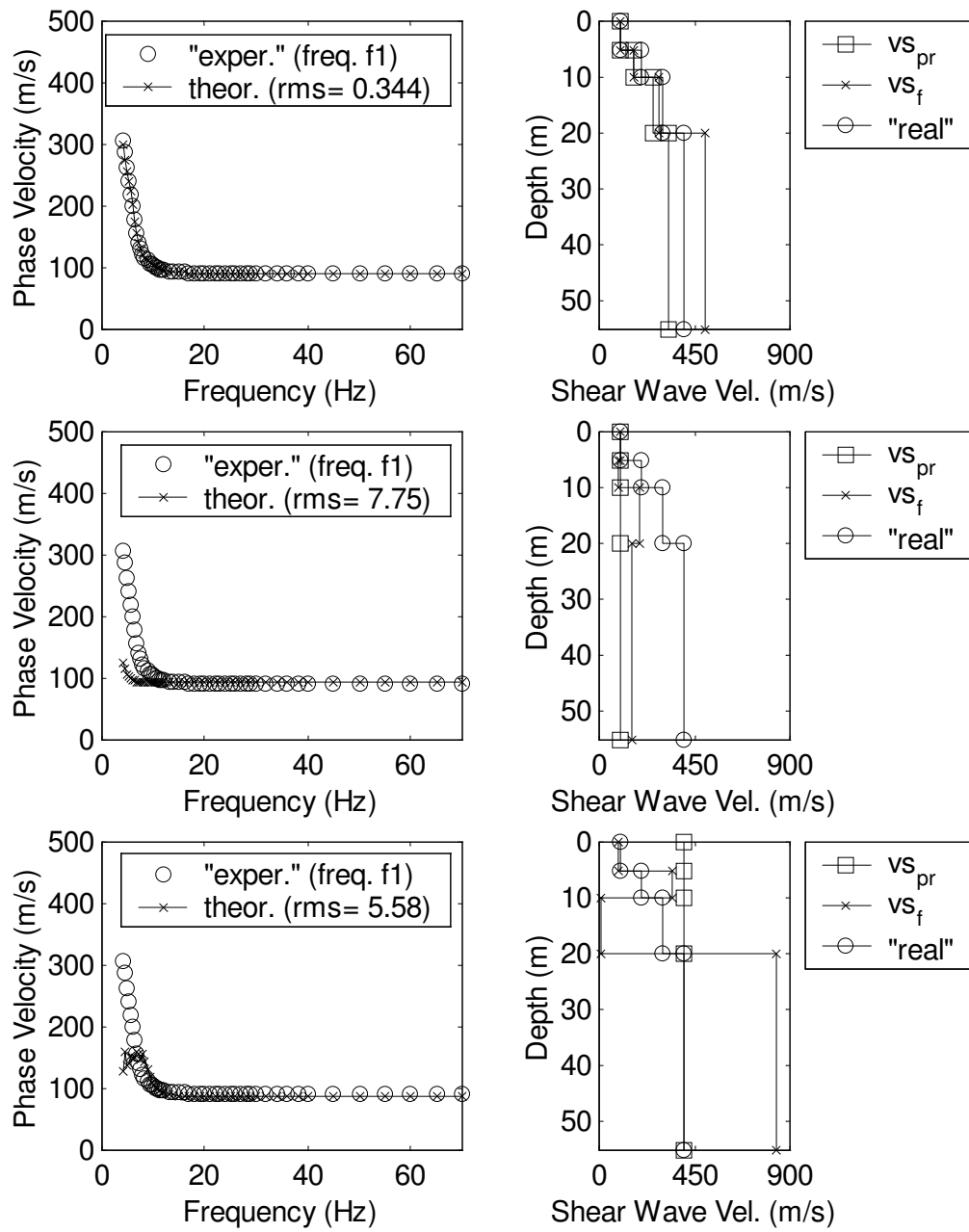
Figure 5.23(a) Inversion results for different initial V_s values for case ND1 profile 24
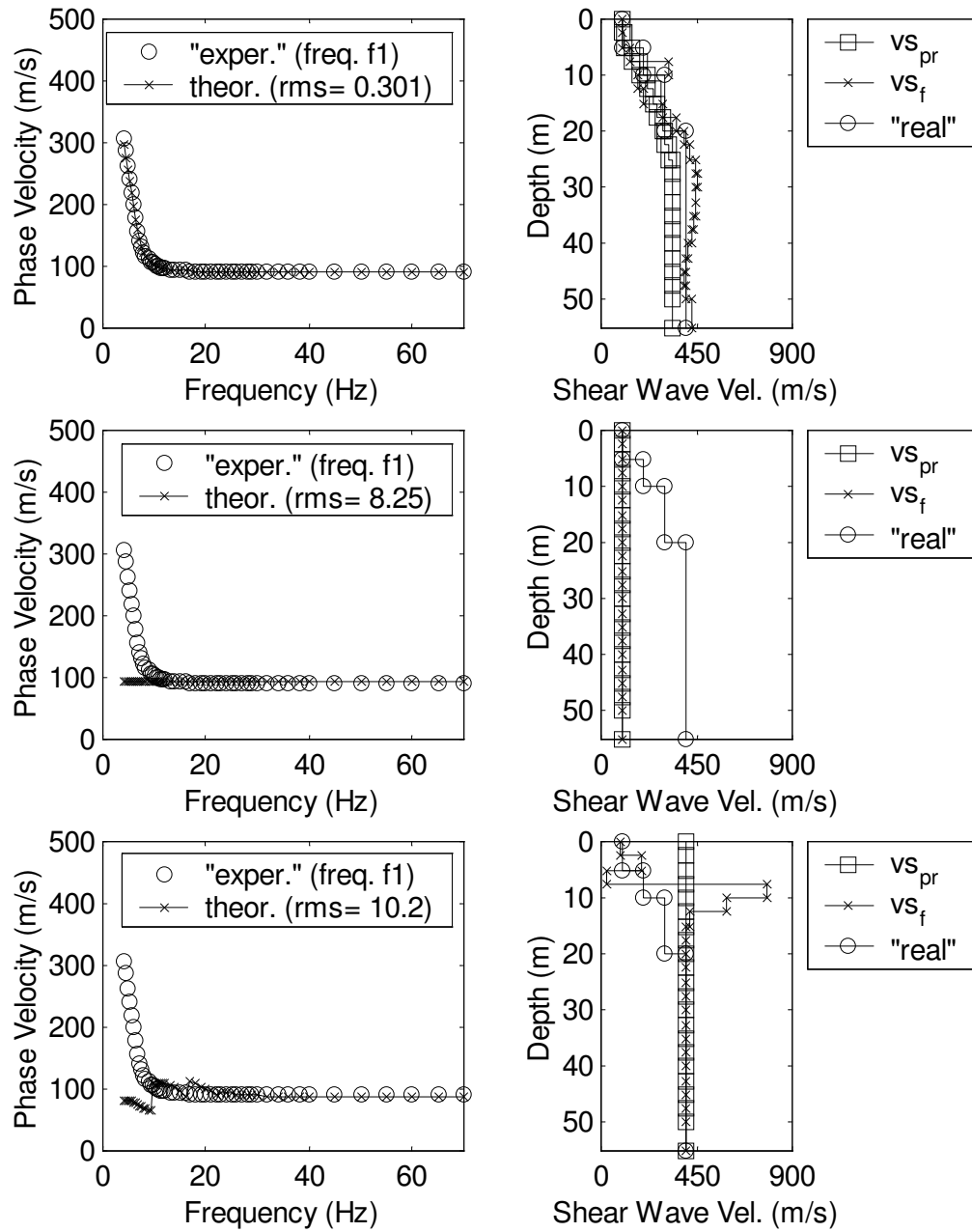
Figure 5.23(b) Inversion results for different initial V_s values for case ND1 profile 31
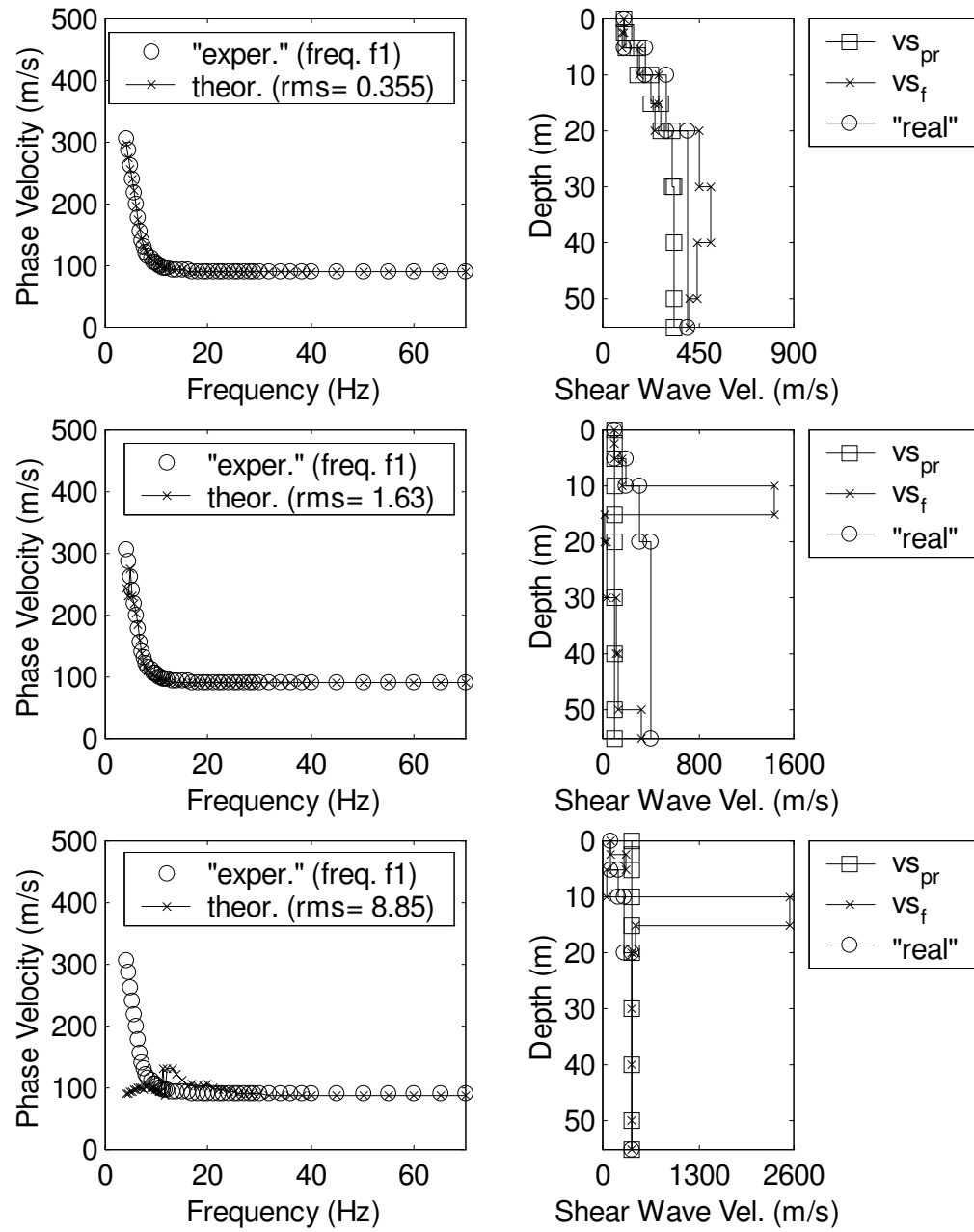
Figure 5.23(c) Inversion results for different initial V_s values for case ND1 profile 37

Thus, the empirical initial shear wave velocities present a better initial estimate, which helps the algorithm converge to a reasonable solution for the inversion problem. The results show the importance of a good initial estimate for the maximum likelihood method. This does not imply that other inversion methods that may be used for SASW can not converge for these cases with the constant initial V_s estimates.

5.3.4 Effect of Standard Deviations Related to the Initial Shear Wave Velocity

The complete set of profiles estimated for ND1 with the maximum likelihood method were presented in Figure 4.10 on Chapter 4. In that figure it was shown that all profiles had a good match to the experimental dispersion curve. Herein, figure 5.24 shows part of those results in separate plots for prior V_s standard deviations (σ_vs_{pr}) of 30 and 240 m/s. The dispersion curves are not presented since the differences among them are not significant, and it is more illustrative to look at the V_s profiles. Figure 5.24 demonstrates that the initial uncertainties of V_s have a significant influence on the range of final V_s profiles obtained. The smaller standard deviation constrains the solution more, obtaining a smaller range of V_s values, and the larger standard deviation gives more flexibility to the solution, obtaining a larger range of V_s values.

The difference in the range of profiles observed in figure 5.24 is reflected also in the estimated standard deviations for the V_s values obtained from the inversion as shown in figure 5.25.
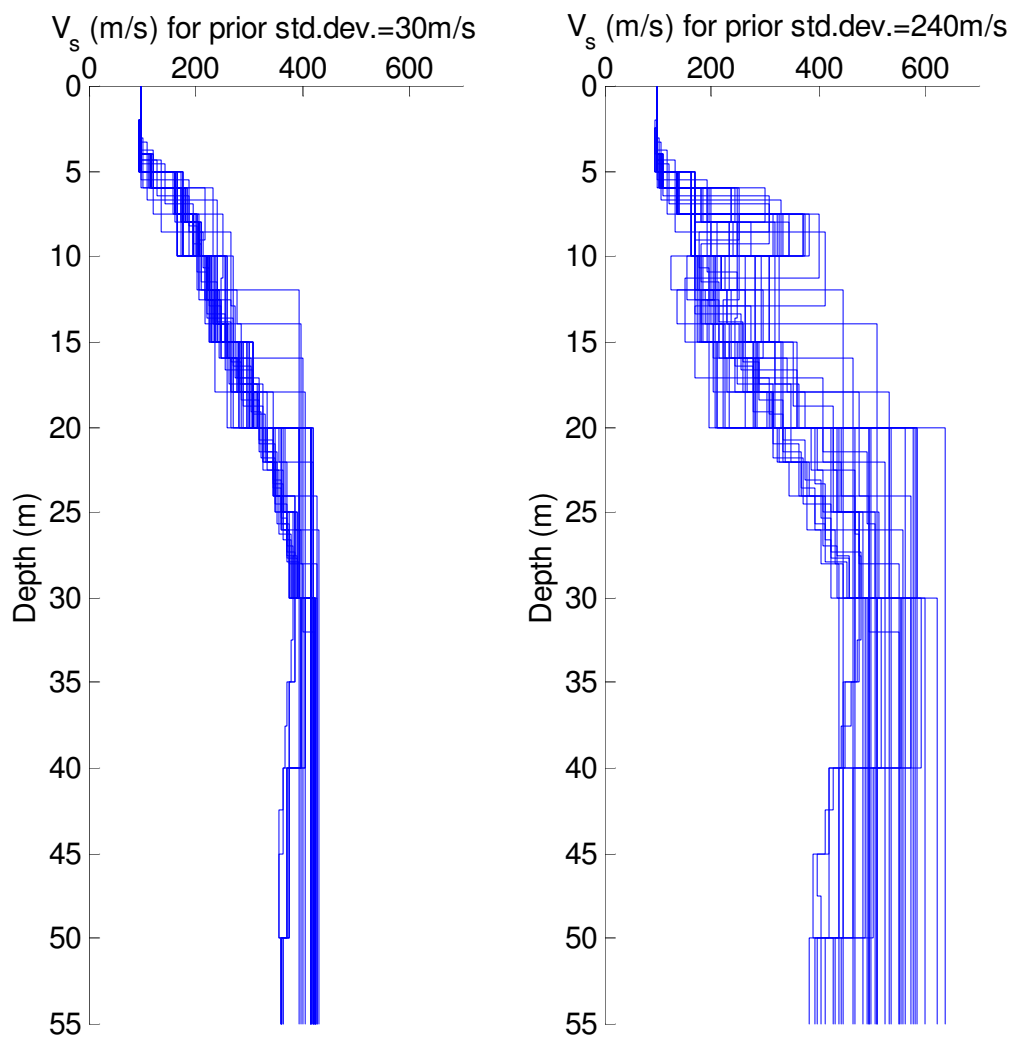
Figure 5.24 Range of estimated V$_s$ profiles obtained for prior V$_s$ standard deviations of 30 and 240m/s
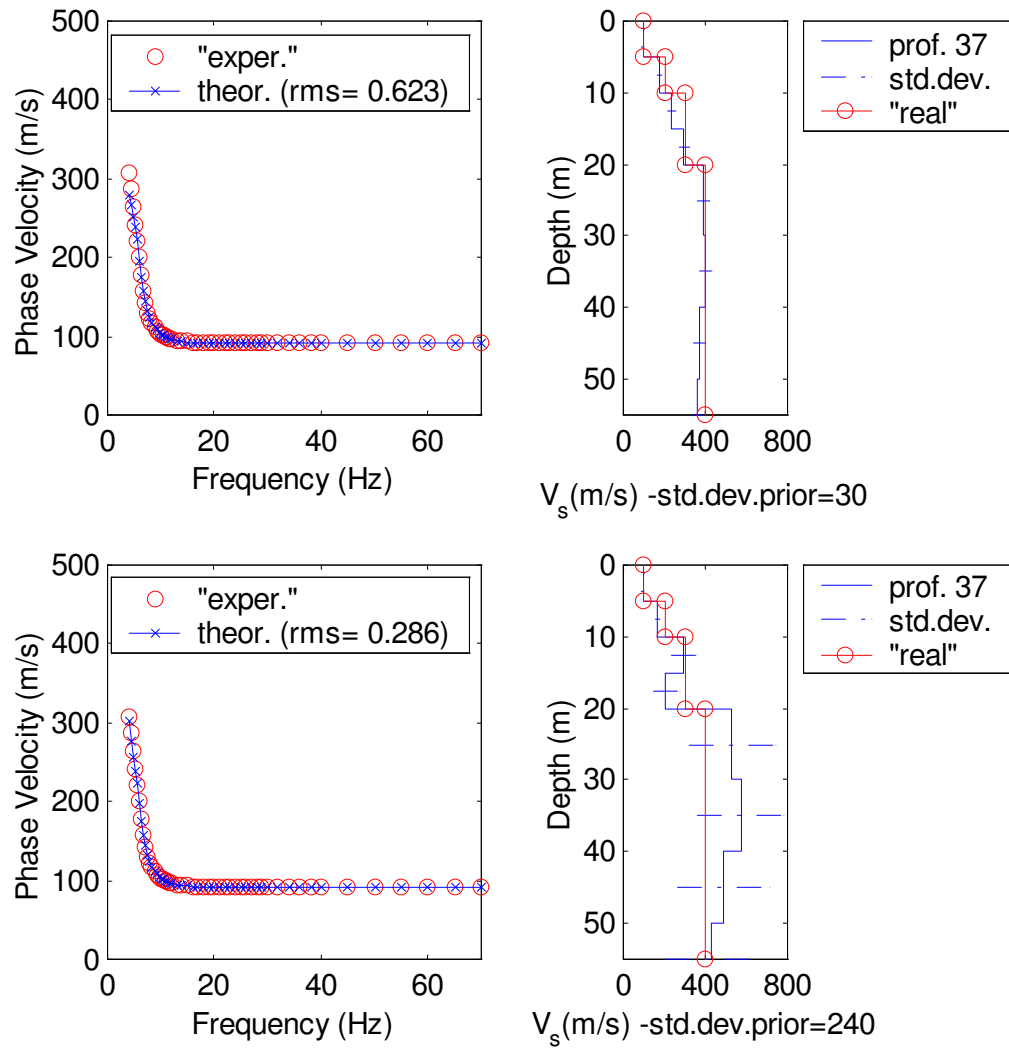
Figure 5.25 Inversion results for case ND1 profile 37, with prior V_s standard deviations of 30 and 240m/s

Figure 5.25 shows the inversion results obtained for profile 37 in case ND1, for two different initial assumptions on V_s standard deviations (i.e., 30 and 240 m/s). It is clear that the standard deviations obtained for the final V_s are significantly larger for the larger prior standard deviations (i.e., 240m/s).

Figure 5.26 presents the coefficient of variability versus the top-depth of the layers for profiles 24, 31 and 37 in case ND1, for the four different prior V_s standard deviations presented in Chapter 4 (i.e., 30, 60, 120, and 240m/s). This figure clearly shows that the prior standard deviation chosen for V_s has an important effect on the estimated uncertainties, except for the very top layers. The higher the prior assumption the higher the resulting estimate. The trends for the coefficient of variability that show a larger increase with depth for the upper layers followed by a smoother variation for the deeper layers are similar in all cases, but with more significant variations as the prior standard deviations are higher.

Figure 5.27 confirms these observations with plots that include the results for all satisfactory profiles for case ND1. This figure also presents the increase of the coefficient of variability for a decrease in sensitivity, and for a decrease in thickness to depth ratio multiplied by the number of waves sampling the layer.
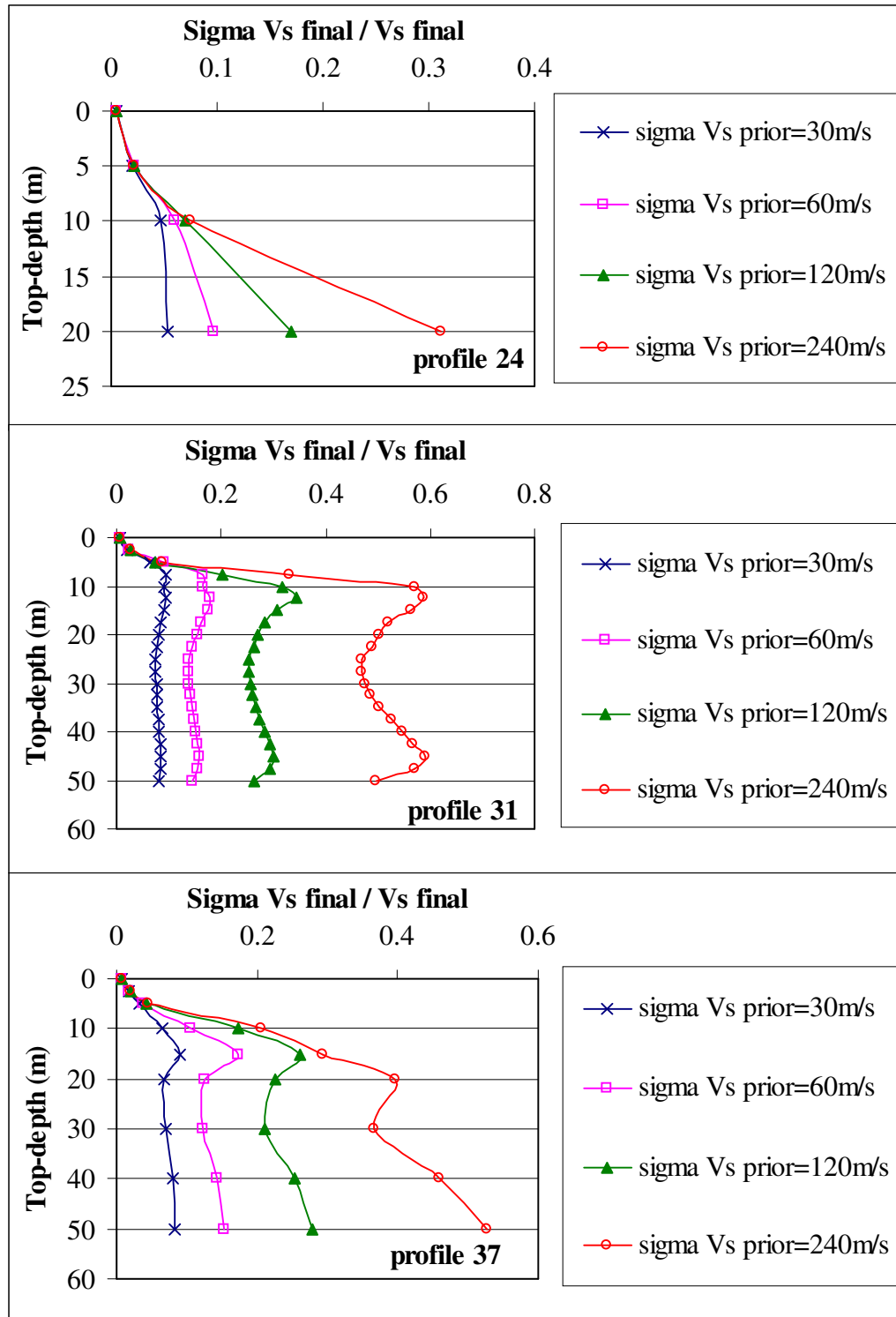
Figure 5.26 Change in coefficient of variability caused by varying the prior standard deviations of V_s, for case ND1 profiles 24, 31, and 37
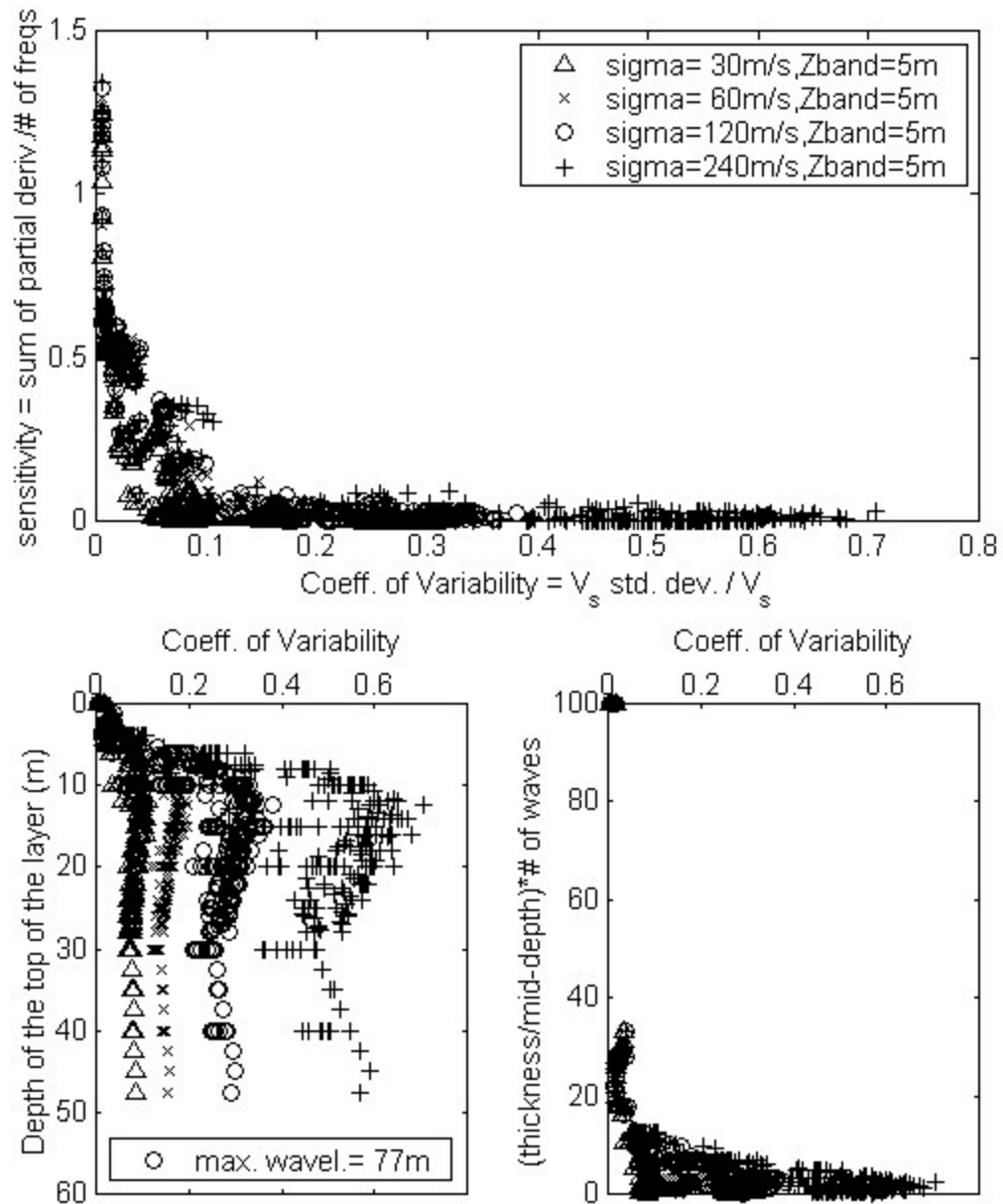
Figure 5.27 Coefficient of variability versus sensitivity, versus depth, and versus thickness to depth ratio for different prior standard deviations of V_s, for case ND1, frequency f1

Since the prior assumptions for the standard deviations of V_s (σ_vs_{pr}) have such a significant influence on the estimated V_s uncertainties, Figure 5.28 shows the ratio of the final standard deviation values to the values assumed prior to inversion. This figure emphasizes that the deeper layers have uncertainties that approach the initial guess (i.e., ratio of 1.0). If a final estimated uncertainty was estimated to be the same as the prior assumption, it would mean that there is no information added during the inversion process that helps improve the prior uncertainties. Another way to compare final and prior uncertainties is by looking at the effect on the diagonal of the resolution matrix. As noted previously, the resolution matrix is based on comparing the final and prior covariance matrices, which include final and prior uncertainties. Figure 5.29 presents the diagonal of the resolution matrix for two of the profiles included in Figure 5.28, and for the four cases of prior standard deviations of V_s.

Based on Figures 5.28 and 5.29, it can be noted that the top 5 meters have low standard deviations and are well resolved independently of the prior assumption. From 5 to 20 meters a higher prior assumption of σ_vs_{pr}, which gives more flexibility to the problem, results in lower standard deviation ratios and in better resolution values. For layers below 20 meters this trend continues but with very little difference between standard deviations an resolutions as all cases approach the value of the prior assumption (i.e., corresponding to $\sigma\_vs/\sigma\_vs_{pr}=1.0$, and diagonal of the resolution matrix=0.0).
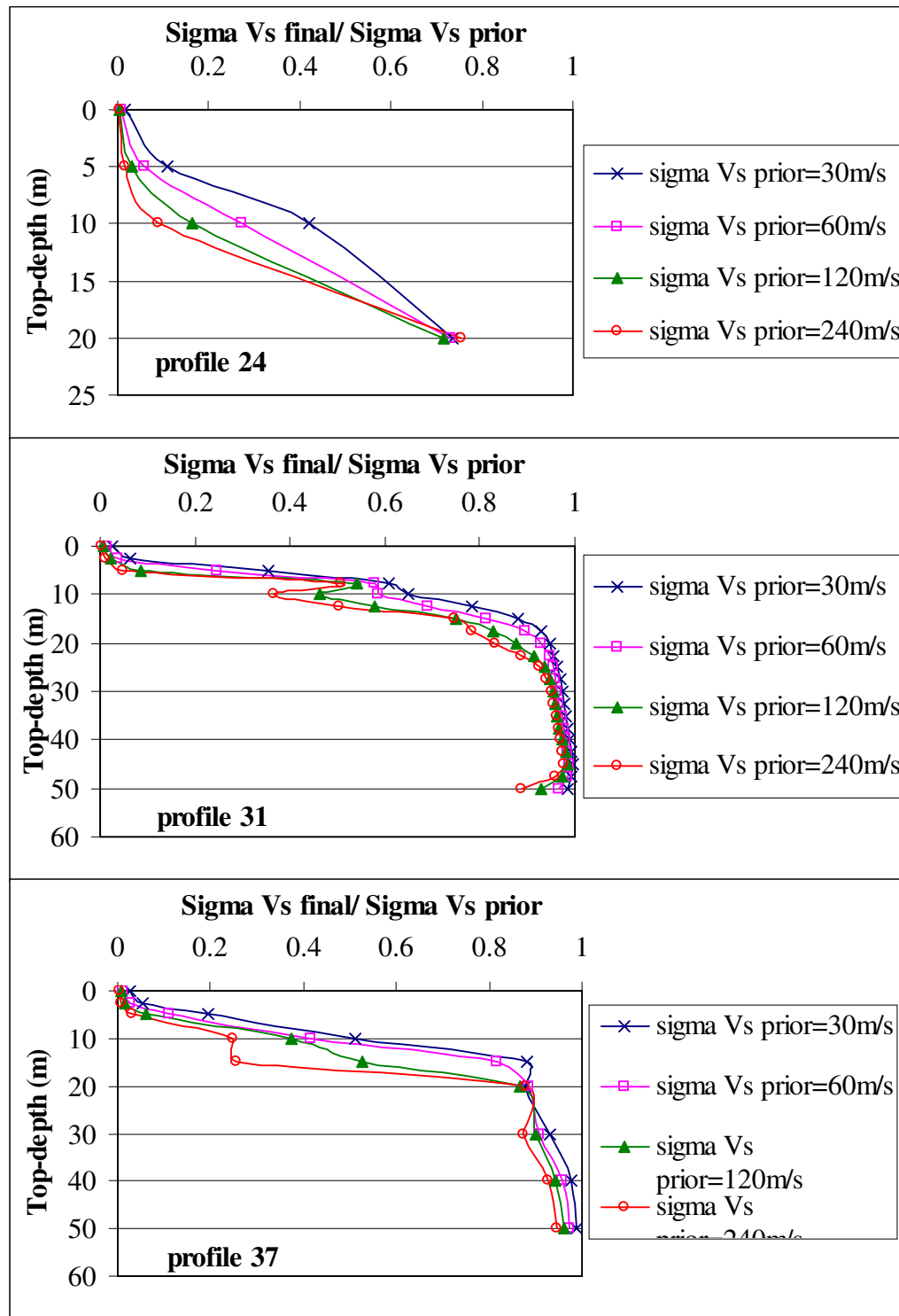
Figure 5.28 Change in the ratio of the final standard deviations of V_s to the prior standard deviations of V_s caused by varying the latter ones, for case ND1 profiles 24, 31, and 37
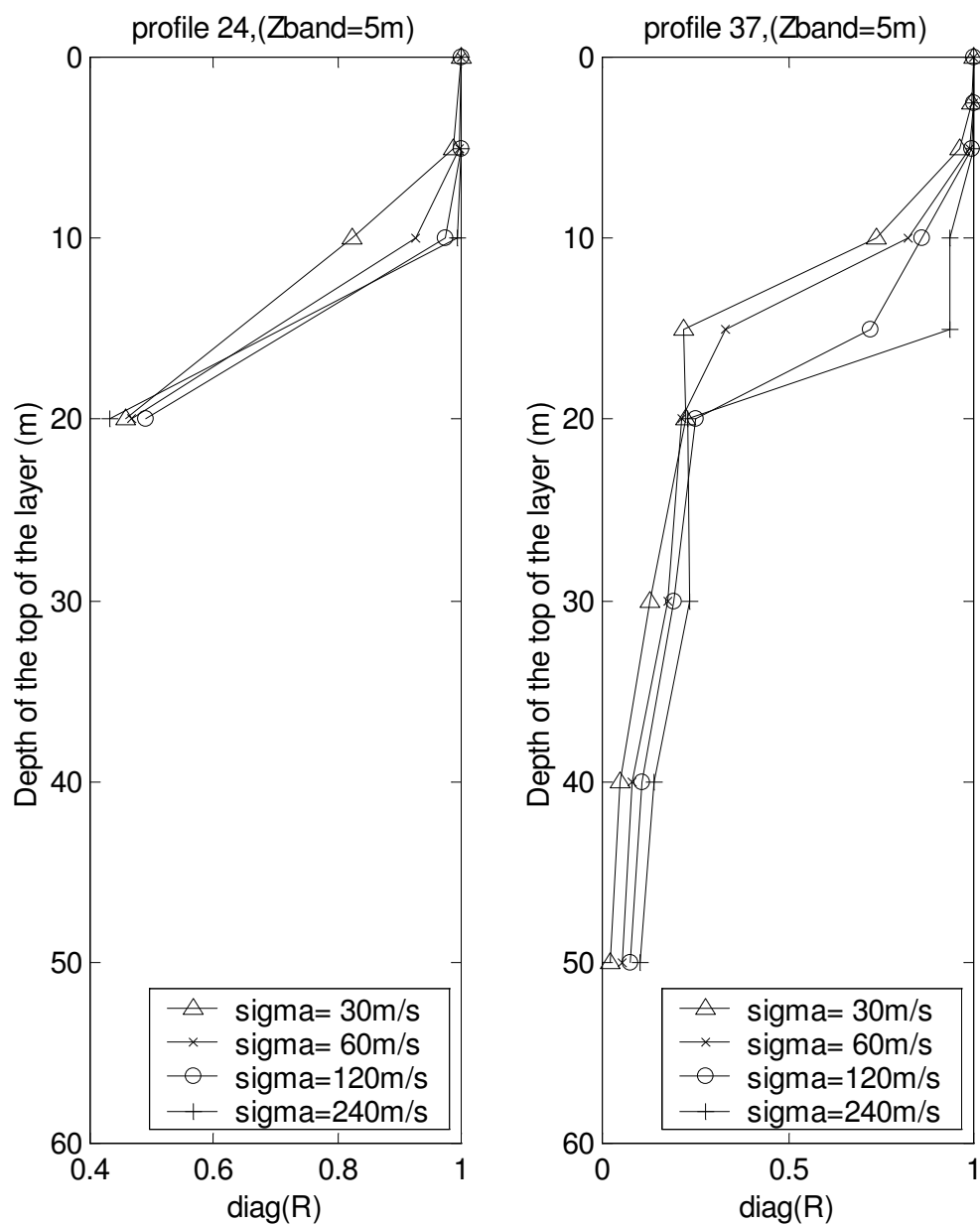
Figure 5.29 Diagonal of the resolution matrix for profiles 24 and 37, for different prior standard deviations of V_s, for case ND1.

The half-space sensitivity to the maximum wavelength is also affected by the prior standard deviations of V_s as presented in Figure 5.30. For both cases ND1 and ND2, it can be noted that higher σ_vs_{pr} values result in more variation of the sensitivity with the type of layering, and lower σ_vs_{pr} result in more similar sensitivities for profiles with the same depth to half-space. This is caused by the fact that higher σ_vs_{pr} gives more flexibility to the solution, which results in a larger range of V_s profiles as seen in Figure5.24, and a larger range of V_s profiles results in a larger range of partial derivative values (i.e., sensitivities). However, comparing profiles 31 to 38 (50 meters depth to half-space) with the rest (which vary between 12 and 32 meters depth to half-space), it is noted that as the depth to half-space is increased, its sensitivity to the maximum wavelength becomes more stable. This is due to the fact that the deeper the half space, the lower the sensitivity of the dispersion curve to it, and consequently the lower the effect that a change in the V_s profile has in the partial derivatives.

5.3.5 Effect of the Correlations Related to the Initial Shear Wave Velocity

Figure 5.31 presents part of the results shown in figure 4.10, with two separate plots that show the range of V_s profiles obtained when using Z_{band} of 1 and 15 m (see Chapter 4 for a clear explanation of how the correlations are calculated based on Z_{band}). In this case it can be noted that the larger the Z_{band} (i.e. the higher the correlations among layers) the smaller the range of V_s values obtained. Since having higher correlations among layers implies smoother profiles, it makes sense that the range of V_s values is narrower for a larger Z_{band}.
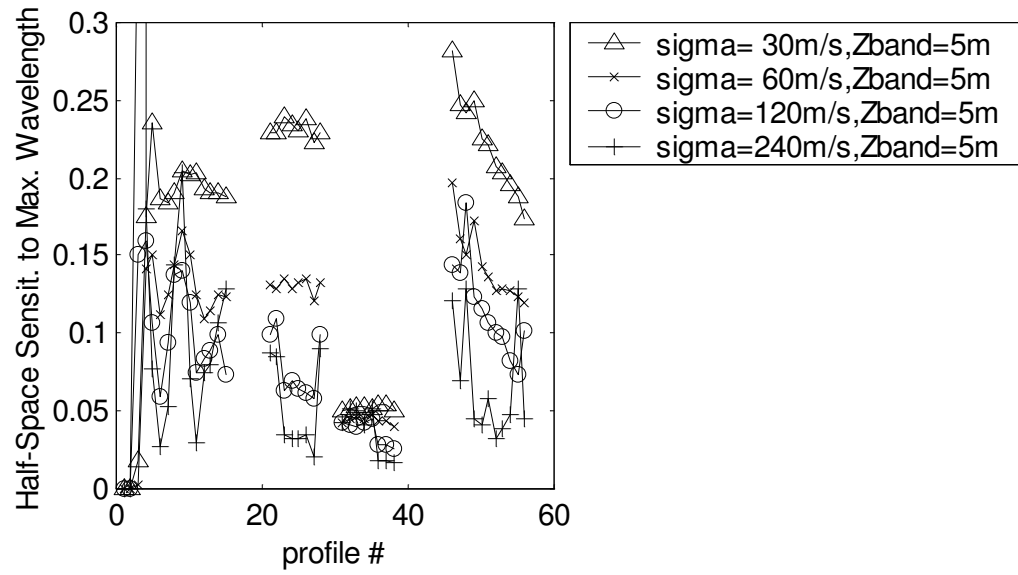
Figure 5.30(a) Half-space sensitivity for different prior standard deviations of V_s, for case ND1
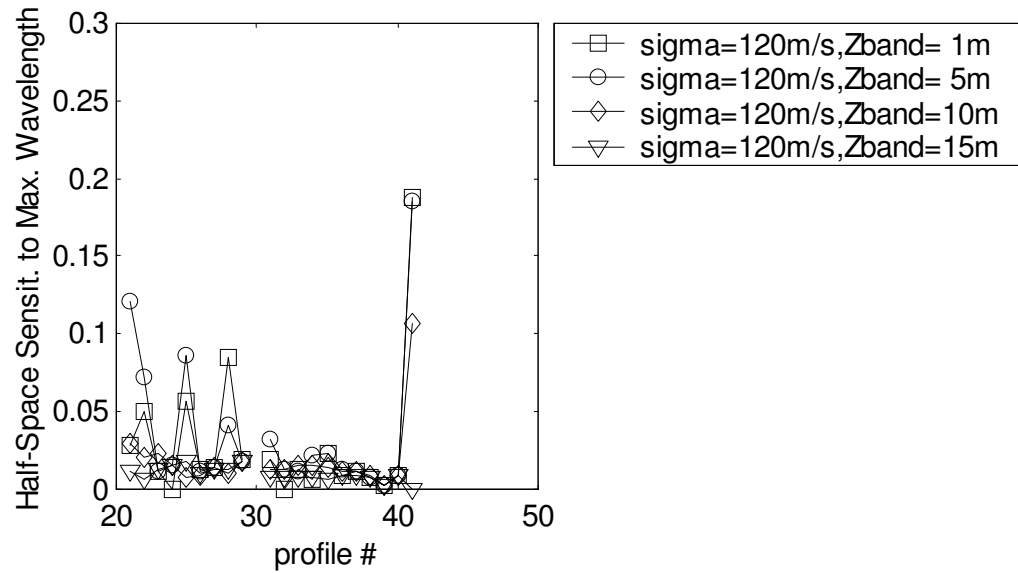
Figure 5.30(b) Half-space sensitivity for different prior standard deviations of V_s, for case ND2
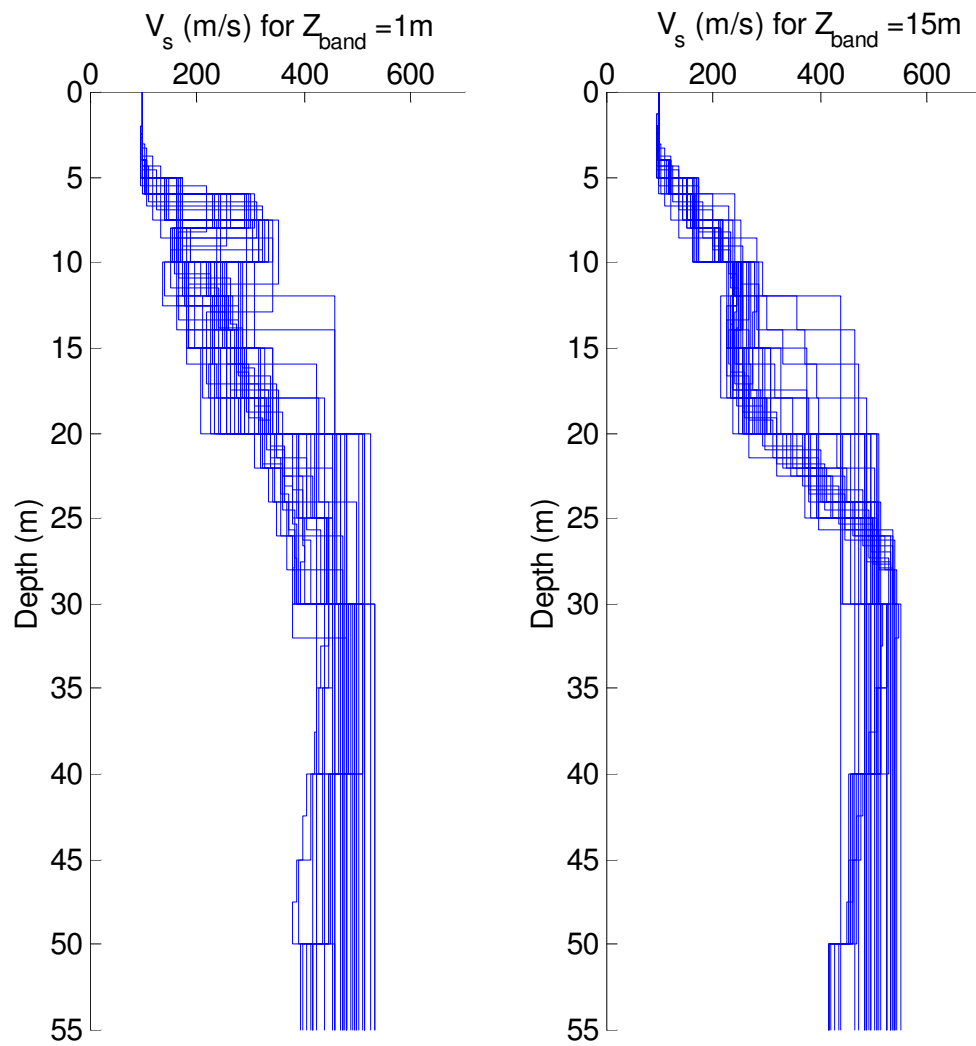
Figure 5.31 Range of estimated V_s profiles obtained for initial V_s correlations based on Z_{band} of 1 and 15m

Figure 5.32 presents the coefficient of variability versus the top-depth of the layers for profiles 24, 31 and 37 in case ND1, for the four different prior Z_{band} presented in Chapter 4 (i.e., 1, 5, 10, and 15m). This figure clearly shows that the prior correlations of V_s (given by Z_{band}) may have an effect on the estimated uncertainties. The effect is such that for a smaller Z_{band} value the resulting uncertainties for V_s are higher. The trends for the coefficient of variability show larger variations with depth for the upper layers followed by a smoother variation for the deeper layers. These variations are more significant as the Z_{band} values are lower, but below 30 meters depth the values for the coefficient of variability are similar for the different cases of Z_{band}.

These trends are confirmed in Figure 5.33, which presents plots for the coefficient of variability that include the results for all satisfactory profiles for case ND1. This figure also presents the increase of the coefficient of variability for a decrease in sensitivity, and for a decrease in thickness to depth ratio multiplied by the number of waves sampling the layer. These observations relate to the ones about the effects of the prior standard deviations of V_s, noting that a smaller Z_{band} constrains less the solution as a higher σ_vs_{pr} does.

The half-space sensitivity to the maximum wavelength is also affected by the prior correlations of V_s as presented in Figure 5.34. For both cases ND1 and ND2, it can be noted that lower Z_{band} values result in more variation of the sensitivity with the type of layering, and higher Z_{band} values result in more similar sensitivities for profiles with the same depth to half-space.
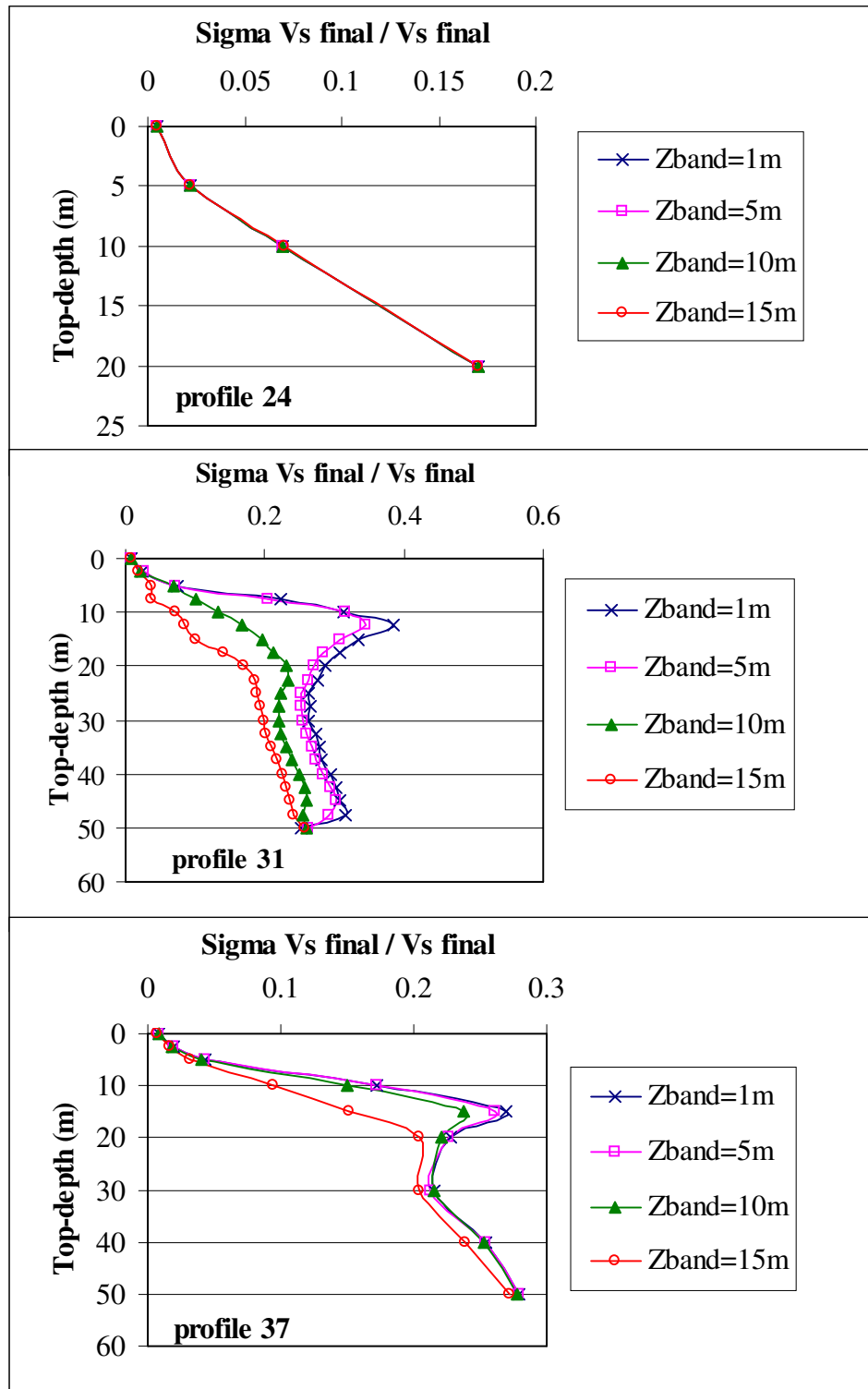
Figure 5.32 Change in the coefficient of variability for different prior correlations (given by Z$_{band}$), for case ND1 profiles 24, 31, and 37
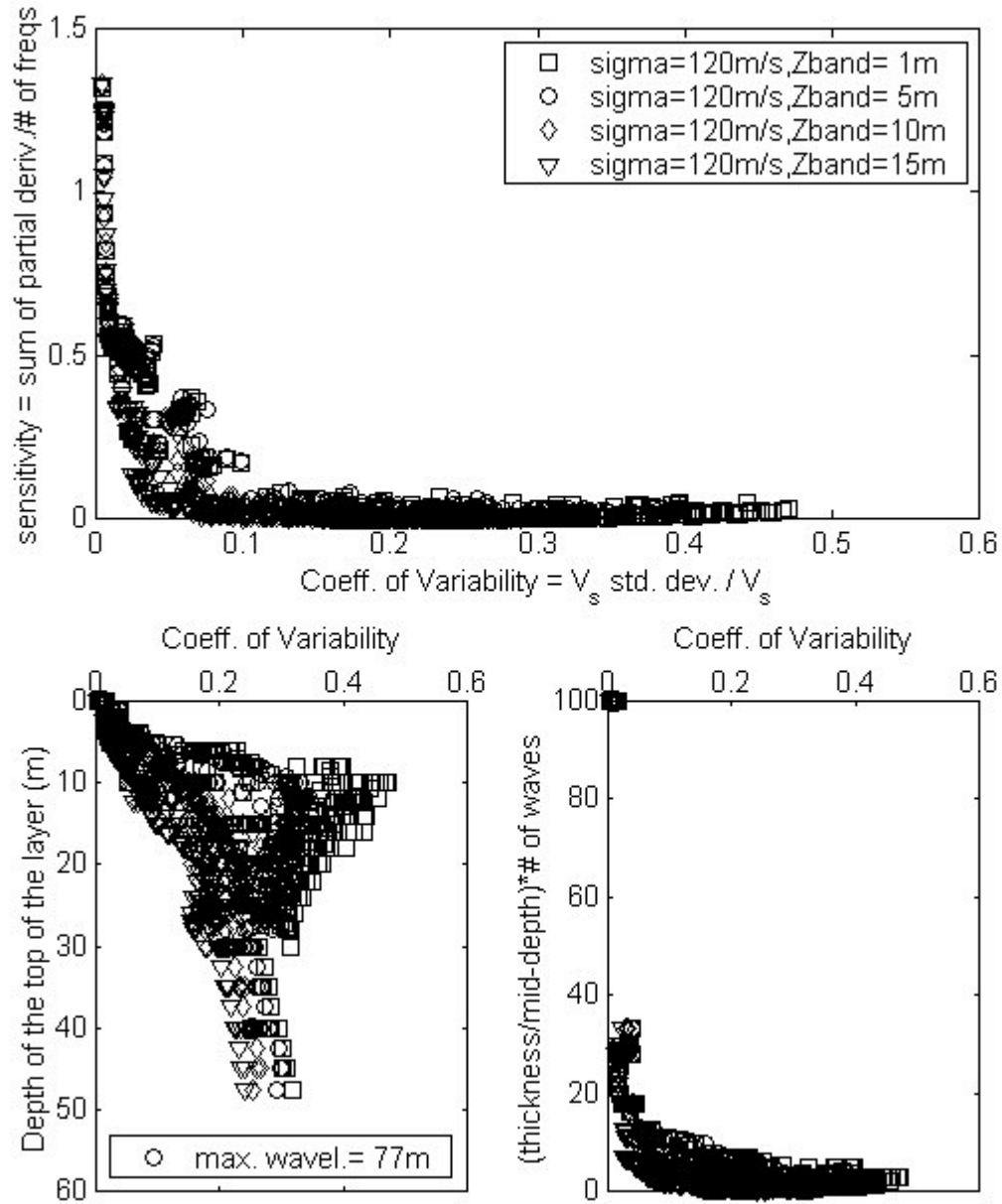
Figure 5.33 Coefficient of variability versus sensitivity, versus depth, and versus thickness to depth ratio for different prior correlations (given by Z_{band}), for case ND1, frequency f1
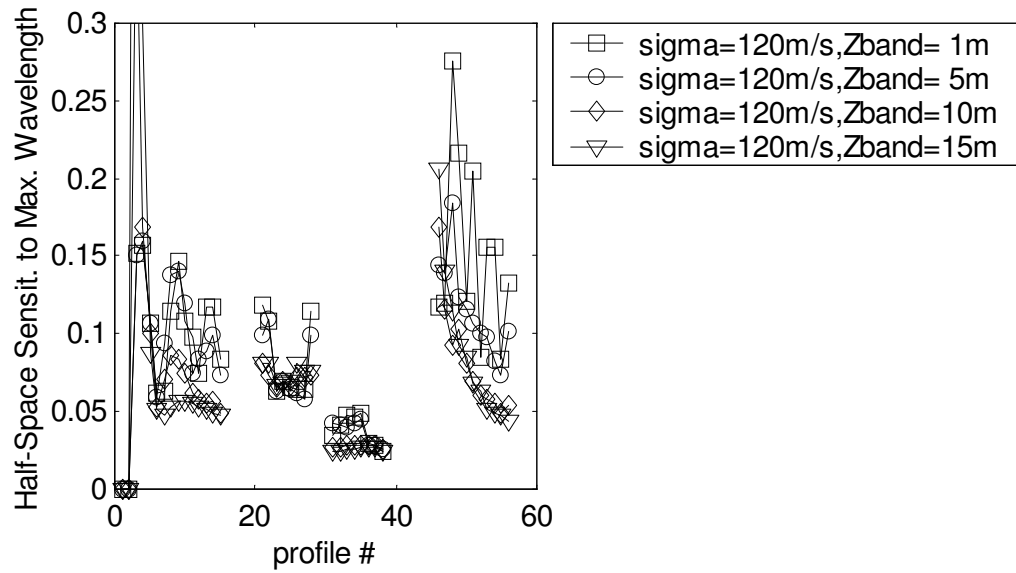
Figure 5.34(a) Half-space sensitivity for different prior correlations (given by Z_{band}), for case ND1
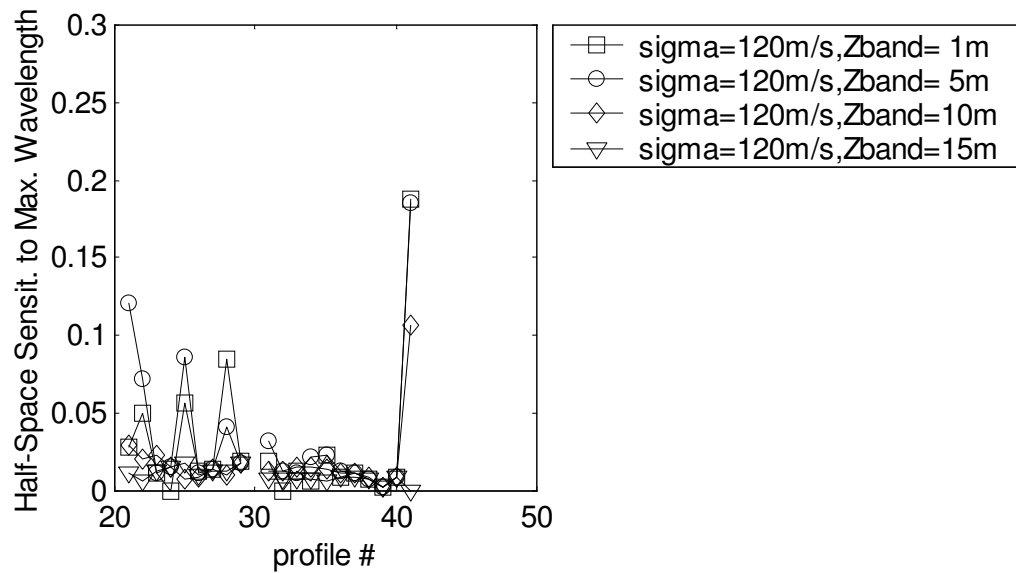
Figure 5.34(b) Half-space sensitivity for different prior correlations (given by Z_{band}), for case ND2

As mentioned for the effects of σ_vs_{pr}, this is caused by the fact that a lower Z_{band} gives more flexibility to the solution, which results in a larger range of V_s profiles as seen in Figure 5.31, and a larger range of V_s profiles results in larger differences among their partial derivatives (i.e.,their sensitivities). Like for the variation in σ_vs_{pr}, comparing profiles 31 to 38 (50 meters depth to half-space) with the rest (which varies between 12 and 32 meters depth to half-space), shows that as the depth to half-space is increased, its sensitivity to the maximum wavelength becomes more stable. As mentioned before, this is due to the fact that the deeper the half space, the lower the sensitivity of the dispersion curve to it, and consequently the lower the effect that a change in the V_s profile has in the partial derivatives. In summary, the half-space sensitivity to the maximum wavelength is affected more by the layering for a higher σ_vs_{pr}, a lower Z_{band}, and shallower profiles, and as expected the value of the sensitivity tends to decrease with a depth increase.

5.4 Summary and Conclusions

The results obtained with a theoretical inversion method such as the maximum likelihood are dependent on the characteristics of the experimental data and of the V_s profile assumed a priori. This chapter studied the effect of the following factors on the inversion results:

(i)   number and distribution of data points describing the experimental dispersion curve

The points describing the dispersion curve represent the frequencies measured at the field, and give information on the wavelengths of the surface waves that sampled the soils. It can be considered that a layer was not sampled by wavelengths shorter that the depth to the top of the layer. Counting the number of waves that sampled each layer gives an idea of the amount of experimental information available for each layer and emphasizes when there is a significant difference in the information among layers. Part of the difference is inevitable due to the nature of the problem, since a long wavelength that tests a deep layer also tests all layers above it. Thus, there is always more information on shallower layers and less information on deeper layers.

The effect on the inversion results of the number of waves that sampled a layer was studied. It was noted that the number of waves did not affect the accuracy of V_s (i.e., final V_s /real V_s), thus, a few dispersion points may be enough to represent the dispersion curve appropriately. This proves that a lot of dispersion points do not necessarily translate into a lot of information. For instance, the experimental data may have a lot of dispersion points which represent waves that tested only the top layer and very few data on the following layers. Consequently, the author suggests that it is possible to delete some of the dispersion points that present redundant data to reduce the difference in information content among layers, and consequently reduce the difference in resolution. On the other hand, the number of waves did affect σ_vs and the coefficient of variability (i.e., σ_vs /

V_s). These values increase for a reduced number of waves sampling the layer, but they increase more significantly for deeper depths. This is reasonable since it means that less information results in higher uncertainties.

Additionally, since the weight that the rms gives to different areas of the dispersion curve depends on the points used to represent it, it was noted that for a specific V_s profile the resulting rms is different for different sets of points. The dispersion points chosen to represent the curve may affect significantly the value of the rms, which emphasizes the importance of the frequency distribution, since the estimated rms error is used as a qualification on the goodness of a profile. Thus, it is suggested to look at the number of waves that tested each layer and try to have a distribution that does not weight some wavelength ranges excessively compared to others. The best option would be to produce the dispersion curve during the field test, and to use it as a reference to get additional experimental data if needed.

(ii) *uncertainties of the experimental dispersion data*

The uncertainties related to the experimental data have a direct effect on the value of the rms error. The larger the uncertainties assigned to the phase velocity the smaller the value of the rms error for a specific theoretical dispersion curve, which is generally interpreted as a better match to the experimental curve. Additionally, the uncertainties given to the experimental data also affect the results obtained from the inversion, since the larger the uncertainties the less the dispersion curve constrains the solution. Thus, it is important to

185

have a realistic estimate of the uncertainties of the phase velocity, because if these are too large the problem may not be sufficiently constrained by the dispersion curve. On the other hand, if the uncertainties of V_r are too small, they might constrain the problem too much, increasing the rms values and making it hard to find a V_s profile with a satisfactory rms. As discussed in Chapter 3, V_r uncertainties of 3% of the experimental phase velocities are considered reasonable for SASW tests.

(iii)   depths and thicknesses of the layers

Depending on its thickness and depth a layer will be sampled differently by the surface waves measured during the field test. The deeper the layer the less information there is on it, and consequently it is harder to resolve its value. The effect of a change in the V_s value of a layer on the dispersion curve shows how sensitive the dispersion curve is to that layer. A higher sensitivity means that the layer can be better resolved. Based on the data presented, it was clear that the sensitivity of the dispersion curve to a change in V_s reduces with depth, and that lower sensitivities are related to higher coefficients of variability. It was also noted that the coefficient of variability decreases with the thickness to depth ratio multiplied by the number of waves sampling the layer. Thus, increasing the thickness of a layer at a specified depth or increasing the number of waves sampling the layer may help resolve the layer better and reduce its uncertainty. For the cases presented herein, the plots show that the coefficient of variability is limited to below 25% for a thickness to depth ratio multiplied by the number of waves sampling the layer of at least 8 (see figures 5.27 and 5.33)

The diagonal of the resolution matrix may be used to compare the resolutions of the layers and vary their thicknesses (i.e., increase the thickness to increase resolution, or decrease the thickness to decrease resolution). It is suggested that the layers selected result in a resolution decrease with depth that is as smooth as possible, trying to minimize the difference in resolution among layers.

The number of waves that sample a layer depend on both its thickness and depth, and the distribution and number of points that represent the dispersion curve. Thus, for a specific set of experimental data the layers may be chosen in such a way that the difference in information available for the different layers is reduced. For instance, if only 5 waves tested soils between 10 and 80 meters (as for case ND1 with frequency distribution f2) having sixteen 2.5-meter layers from 10 to 50 meters followed by a half-space (as in layered configuration 31) gives the user of the V_s profile a false sense of resolution. To prevent this type of false impression, the author suggests that the number of waves sampling the layers should reduce with depth without having consecutive layers sampled by the same number of waves. Additionally, since the information content necessarily decreases with depth, and results in lower resolutions with depth, it is suggested that the thickness of the layers increases with depth to reflect this decrease in resolution.

(iv)   Depth to half-space

As noted above, the diagonal of the resolution matrix helps compare the resolution of the layers within a profile. Since the half-space continues to an infinite depth and the information available is for a limited depth, this unrealistic layer should have the lowest resolution of all. However, the half-space sensitivity to the maximum wavelength should not be extremely low because it would mean that the half-space is not being defined by the experimental data. Based on the fact that the sensitivity represents the change in V_r that would occur with a change in V_s, Joh (1996) proposes to use a minimum value criterion of 1% (or another value considered reasonable) for the half-space sensitivity to the maximum wavelength, during the analysis of the data.

This criterion could be complemented by a maximum value such as 10% (or another value considered reasonable), since this sensitivity should not be too high either, because the half-space would be controlling the answer too much (i.e., a very shallow half-space might affect significantly the phase velocities of the wavelengths that go thru the layers adjacent to the half-space, and their shear wave velocities might not be resolved properly). Depths to half-space that have lower sensitivity to the maximum wavelength are affected less by the prior assumptions of layering, σ_vs_{pr}, and Z_{band}, which is better to have a more stable estimate of this sensitivity. For the cases presented, the best choice for the depth to the half-space among the ones tried would be 50 meters (65% of the maximum wavelength for case ND1 and 60% of the maximum wavelength for case ND2).

(v)   *initial shear wave velocities*

The initial shear wave velocity is important due to the nonlinear nature of the problem, and also to the inversion algorithm, which is an iterative process based on gradient methods that converges to a minimum close to the initial estimate. Consequently, if the initial shear wave velocities are far from the real values the algorithm may not converge to a desirable solution. For the maximum likelihood method, simple initial guesses with constant initial V_s values resulted in the algorithm converging to final V_s profiles with high rms values for the cases presented. Thus it is suggested to employ initial V_s estimates based on the empirical method, which helped the algorithm converge to reasonable solutions to the inversion problem for the cases presented.

(vi)   *standard deviations of the shear wave velocities*

It was shown that the prior standard deviations assigned to V_s (σ_vs_{pr}) have a significant influence on the range of final V_s profiles obtained. A smaller σ_vs_{pr} constrains more the solution, and results in a smaller range of V_s values for different layered profiles. A larger σ_vs_{pr} gives more flexibility to the solution, and results in a larger range of V_s values. This is reflected in the estimated standard deviations for the V_s values obtained from the inversion. A smaller σ_vs_{pr} produces Vs profiles with smaller uncertainties, and a larger σ_vs_{pr} produces Vs profiles with larger uncertainties.

Additionally, the variation of the uncertainties of V_s could be divided in three main zones. The top zone being for the upper layers (top 5 meters in this case), where the estimated uncertainties are low, had high resolution values (i.,e, values close to 1.0), and are not affected by σ_vs_{pr}. The second zone being for the middle layers (5 to 20 meters in this case), where the uncertainties increase significantly with depth, the resolution decreases significantly with depth, and both uncertainties and resolution are significantly affected by σ_vs_{pr}. The third zone being for the bottom layers (below 20 meters), where the variation of uncertainties and resolution with depth is slighter approaching the prior assumption and a zero resolution value. These zones of variation for the uncertainties of V_s agree with the variation of the sensitivities, which presents a steep decrease with depth for the top layers and similarly low sensitivities for the bottom layers.

(vii)   correlations of the shear wave velocities

The correlations among layers also affected the final range of V_s profiles obtained and the uncertainties for the estimated V_s values. It was noted that the higher the correlations (i.e., which favors smoother the profiles) the smaller the range of V_s values obtained, and the smaller the estimated standard deviations of V_s. Again, three main zones could be observed. The top layers where the uncertainties of V_s were low and not affected by the prior correlations. The middle layers where there is a large increase in the uncertainties of V_s and a significant variation caused by the prior correlations. The bottom layers where the variation of the uncertainties of V_s is slighter.

In summary, there are a number of prior assumptions that affect the resulting V_s profile obtained from the inversion. Since these assumptions are required to perform the inversion with a local search procedure such as the maximum likelihood, it is necessary to find ways to select them objectively. For instance, among different layered profiles that result in satisfactory inversion results, which one should be chosen? Or, among different prior standard deviations and correlations for V_s, which ones should be selected? For this reason, Chapter 6 presents the Bayesian approach to model selection, which helps choose these prior assumptions by helping select the simplest model that is complex enough to fit the data. This is based on the thought that the model used to represent the V_s variation with depth should not include features that are not necessary to fit the data. The application of this approach is described utilizing the same inversion results obtained in Chapter 4 and studied in this chapter.

CHAPTER 6

BAYESIAN MODEL SELECTION

6.1 Introduction

As shown in Chapter 5, the assumptions made a priori affect the inversion results, thus, it is important to have tools to evaluate and choose this information. In this chapter, simulated data from Chapter 4 is used to implement the Bayesian model selection to help choose some of the prior information required for SASW inversion. This valuable tool for model selection based on Bayes' criterion is implemented as proposed by Malinverno (2000). The criterion helps rank the different layered configurations, the prior standard deviations of V_s (σ_vs_{pr}), and the prior correlations (given by Z_{band}), favoring the case that fits the data well enough with the simplest possible model.

6.2 Bayesian model selection applied to SASW

The application of Bayesian parameter estimation and model selection is described in detail by Malinverno (2000) and the basic concepts used herein are summarized in this section. The Bayesian approach recognizes that the solution to the inverse problem involves uncertainty, which is quantified with a probability density function (pdf). Additionally, choosing a specific parameterization (i.e., a specific layered configuration) is like making an assumption a priori, and a probability for each parameterization can be

calculated to assist on the model selection process. The probabilities related to the solution and to the parameterizations depend on prior information P which is assumed true.

In general, the inverse problem is of the form $\mathbf{vr}_{ex}=\text{r}(\mathbf{vs})+\mathbf{e}$, where $\mathbf{vr}_{ex}$ is the vector of experimental data, $\mathbf{vs}$ is the vector of model parameters which are unknown, $\mathbf{e}$ is the vector of measurement errors, and r(..) is the forward relationship that theoretically relates the parameters and the data. For parameter estimation the basic formula is Bayes' rule:

$$p(\mathbf{vs}|\mathbf{vr}_{ex},P)=\frac{p(\mathbf{vs}|P)p(\mathbf{vr}_{ex}|\mathbf{vs},P)}{p(\mathbf{vr}_{ex}|P)} \qquad\qquad \text{(eq. 6.1)}$$

where P denotes prior information,

  p($\mathbf{vs}$ | $\mathbf{vr}_{ex}$, P) is the posterior pdf of $\mathbf{vs}$ (the distribution of $\mathbf{vs}$ given $\mathbf{vr}_{ex}$ and P),

  p($\mathbf{vs}$ |P) is the prior pdf of $\mathbf{vs}$ (distribution of $\mathbf{vs}$ given P only), and

  p($\mathbf{vr}_{ex}$ | $\mathbf{vs}$, P) is the likelihood function (the pdf of $\mathbf{vr}_{ex}$ when the parameter

    vector equals $\mathbf{vs}$).

The denominator in Bayes'rule is equivalent to the integral of the numerator, and therefore it is just a normalizing factor.

Bayes' rule for parameter estimation is presented to introduce the Bayesian approach, which was used in this study for model selection. The results for parameter estimation presented and used in Chapter 4, were obtained using the formulation presented by Tarantola (1987) and described as the maximum likelihood method. It is important to note that this formulation could also be derived from Bayes' rule (Duijndam, 1988a and b).

For model selection, a pdf is formed with the posterior probabilities of K parameterization hypotheses H(k) and written using Bayes' rule:

$$p\big(H(k)\big|\mathbf{vr}_{ex}, P\big) = \frac{p\big(H(k)\big|P\big)p\big(\mathbf{vr}_{ex}\big|H(k), P\big)}{p\big(\mathbf{vr}_{ex}\big|P\big)}$$

(eq. 6.2)

This equation shows that the posterior probability of the kth parameterization $p(H(k)|\mathbf{vr}_{ex}, P)$ is proportional to its prior probability $p(H(k)|P)$ times its evidence $p(\mathbf{vr}_{ex}|H(k), P)$, since the denominator is just a normalizing factor. The evidence gives the probability of observing the data $\mathbf{vr}_{ex}$ when the parameterization is H(k), thus it plays the same role in model selection as the likelihood function in parameter estimation. Assuming that the parameterizations (e.g., different layered profiles) being compared are all equally probable a priori, they can be ranked by computing their evidences.

For a non-linear relationship between model parameters and data and where the prior and posterior pdf's are not Gaussian, the evidence used for model selection can be approximated to the one for the linear Gaussian case (Malinverno, 2000):

$$E(k) = \underbrace{\left[(2\pi)^{N_p}\left|\mathbf{C\_vs}_f(k)\right|\right]^{1/2} p\left(\mathbf{vs}_f(k)\middle|H(k),P\right)}_{\text{Ockham Factor}} \bullet \underbrace{p\left(\mathbf{vr}_{ex}\middle|\mathbf{vs}_f(k),H(k),P\right)}_{\text{Likelihood}}$$ (eq. 6.3)

where for the kth parameterization

   $E(k)$ is the evidence,

   N_p is the total number of parameters,

   $\mathbf{C\_vs}_f(k)$ is the posterior covariance matrix,

   $\mathbf{vs}_f(k)$ is the posterior mean (i.e., the value of $\mathbf{vs}$ obtained through the inversion process),

   $p(\mathbf{vs}_f(k)|H(k), P)$ is the prior pdf evaluated at the posterior mean (the prior pdf is the distribution of $\mathbf{vs}$ based on prior information only, but here the parameterization $H(k)$ is explicitly shown as prior information),and

   $p(\mathbf{vr}_{ex}|\mathbf{vs}_f(k), H(k), P)$ is the likelihood function (the pdf of $\mathbf{vr}_{ex}$ when the parameter vector equals the posterior mean).

As shown above, the evidence is composed of two terms: the Ockham factor and the likelihood. The first term favors models with fewer free parameters and the latter favors models that fit the data better. The Ockham factor will generally decrease as the parameterization has more free parameters, the likelihood will increase as the data is

better fitted, and the combination of the two, the evidence, will present a peak for the simplest parameterization that is complex enough to fit the data appropriately. Thus, this criterion evaluates which model is more appropriate to fit the data well enough with the simplest possible parameterization. If the model was more complex than needed, the solution could present elements that are not really supported by the data. To be able to implement the Bayesian criterion for model selection, the inversion results have to be obtained using a method such as the maximum likelihood, which includes prior information on the uncertainties of the parameters and the data.

The evidence can be calculated with the equation above using the following expressions for the prior pdf and the likelihood (see Appendix A Malinverno (2000) and p.30 Menke (1989)):

$$p\left(\mathbf{vs}_f(k)\big|H(k),P\right)=\frac{\left|\mathbf{C\_vs}_{pr}\right|^{-\frac{1}{2}}}{\left(2\pi\right)^{N_p/2}}\bullet\exp\left[-\frac{1}{2}\left(\mathbf{vs}_f(k)-\mathbf{vs}_{pr}\right)^T\mathbf{C\_vs}_{pr}^{-1}\left(\mathbf{vs}_f(k)-\mathbf{vs}_{pr}\right)\right]$$

(eq.6.4)

where $\mathbf{vs}_{pr}$ is the prior mean (i.e., the initial value of $\mathbf{vs}$, before the inversion), and

$\mathbf{C\_vs}_{pr}$ is the prior covariance matrix of $\mathbf{vs}$.

$$p\left(\mathbf{vr}_{ex}\big|\mathbf{vs}_f(k),H(k),P\right)=\frac{\left|\mathbf{C\_vr}\right|^{-\frac{1}{2}}}{\left(2\pi\right)^{N_d/2}}\bullet\exp\left[-\frac{1}{2}\left(\mathbf{vr}_{ex}-r(\mathbf{vs}_f(k))\right)^T\mathbf{C\_vr}^{-1}\left(\mathbf{vr}_{ex}-r(\mathbf{vs}_f(k))\right)\right]$$

(eq.6.5)

196

where $r(\mathbf{vs}_f(k))$ is the predicted data vector (theoretically calculated at $\mathbf{vs}_f$),

   $\mathbf{C\_vr}$ is the prior covariance matrix of the measurement errors ($\mathbf{e}= \mathbf{vr}_{ex}$-$r(\mathbf{vs})$), and

   N_d is the number of data points.

Thus the expression for the evidence can be written as:

$$Evidence = Ockham\_Factor \bullet Likelihood \tag{eq. 6.6(a)}$$

$$Ockham\_Factor = \frac{\left|\mathbf{C\_vs}_f\right|^{\frac{1}{2}}}{\left|\mathbf{C\_vs}_{pr}\right|^{\frac{1}{2}}} \exp\left[-\frac{1}{2}\left(\mathbf{vs}_f - \mathbf{vs}_{pr}\right)^T \mathbf{C\_vs}_{pr}^{-1}\left(\mathbf{vs}_f - \mathbf{vs}_{pr}\right)\right]$$

$$\tag{eq. 6.6(b)}$$

$$Likelihood = \frac{\left|\mathbf{C\_vr}\right|^{-\frac{1}{2}}}{(2\pi)^{\frac{N_{vr}}{2}}} \exp\left[-\frac{1}{2}\left(\mathbf{vr}_{ex} - \mathbf{vr}_{th}\right)^T \mathbf{C\_vr}^{-1}\left(\mathbf{vr}_{ex} - \mathbf{vr}_{th}\right)\right] \tag{eq.6.6(c)}$$

Note that the likelihood also compares theoretical and experimental dispersion curves like the rms does. Since the differences between experimental and theoretical data are used in the likelihood as a negative value for the exponential, the better the match, the higher the likelihood. This is different to the rms error, which is lower for better matches.

This approach can also be used to rank other prior information. In this case the parameterization used would be part of the prior information assumed to be true. For

example, to rank the prior standard deviations of V_s (σ_vs_{pr}) with the evidence, $H(k)$ would represent the hypotheses for σ_vs_{pr}, and the parameterization would be considered part of the prior information P. The evidence can be used to rank a number of σ_vs_{pr}, as long as the assumption is that all the hypotheses are equally probable a priori.

As noted by Malinverno (2000), the evidence can be normalized by dividing it by a factor equal to the sum of all evidences. Thus, to compare parameterizations (i.e., layered configurations) the normalizing factor is the sum of evidences of all different parameterizations for the same σ_vs_{pr} and same Z_{band}. In the same way, to compare σ_vs_{pr} the normalizing factor is the sum of evidences of all different σ_vs_{pr} for the same parameterization (i.e., same layered profile) and same Z_{band}. Equivalently, to compare Z_{band} the normalizing factor is the sum of evidences of all different Z_{band} for the same parameterization and same σ_vs_{pr}.

6. 3 Results and Comments

6.3.1 Selection of the layered profile

The Bayesian criterion was used to calculate the Ockham factor, the likelihood, and the evidence for the results obtained in the synthetic cases ND1 and ND2, using frequency distributions f1 and f4, respectively (see Figures 4.10 and 4.11 in Chapter 4). Figure 6.1 presents these results with the evidence for each profile normalized by dividing it by the sum of all evidences for fixed prior assumptions of σ_vs_{pr} and Z_{band}.
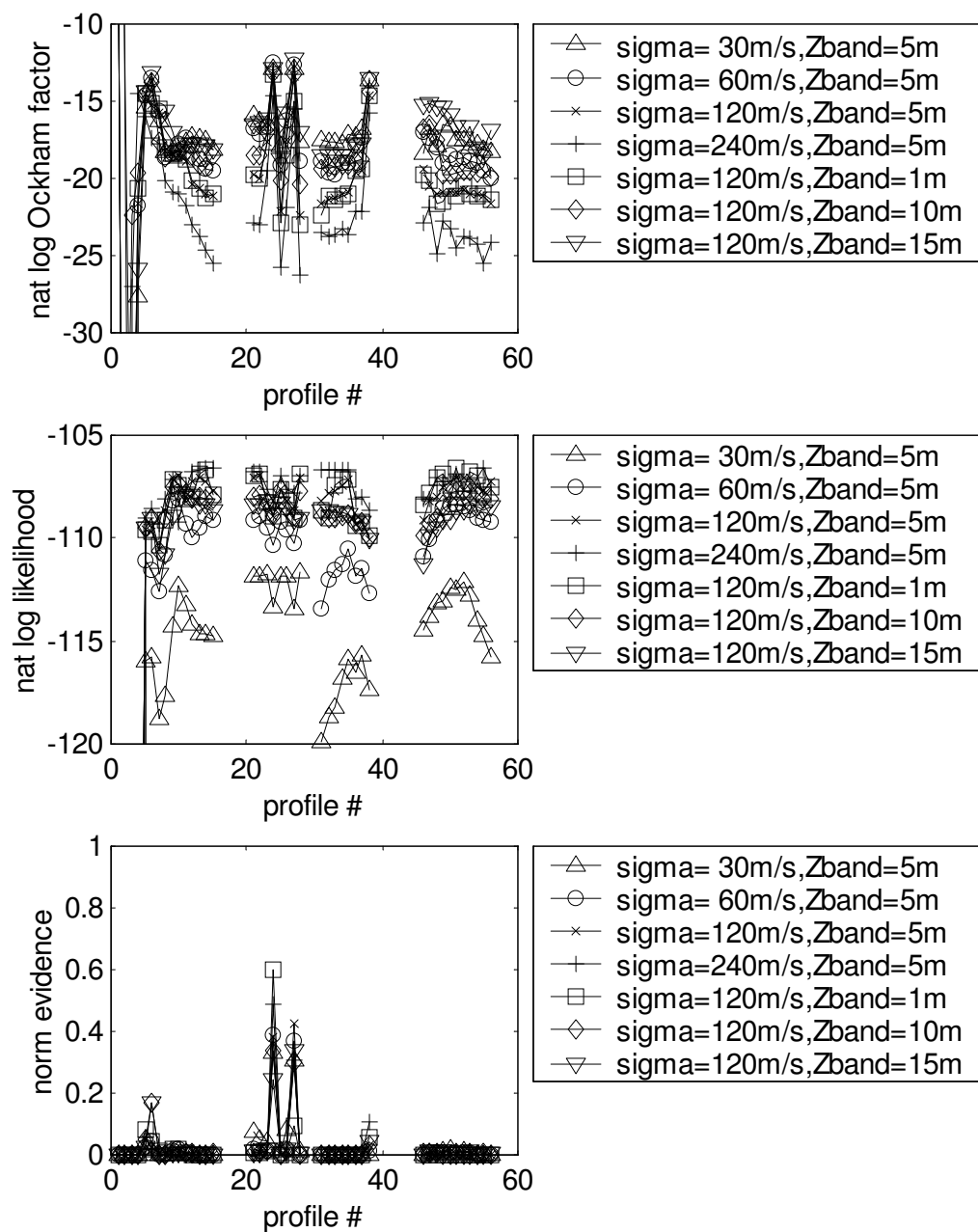
**Figure 6.1(a) Ockham factor, likelihood, and normalized evidence
to choose best layers for case ND1**
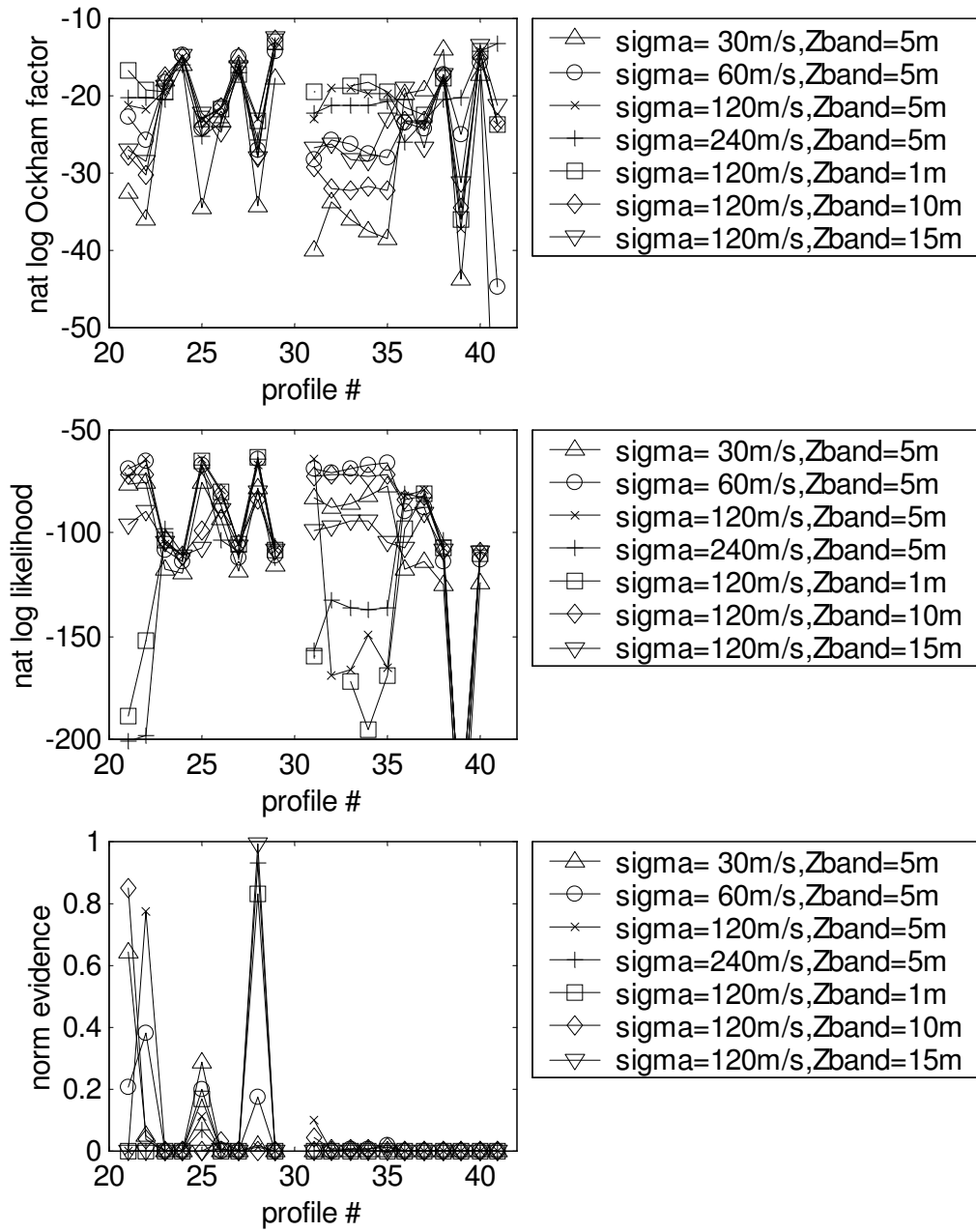
**Figure 6.1(b) Ockham factor, likelihood, and normalized evidence
to choose best layers for case ND2**

Table 6.1(a) Profiles that present evidence peaks for the different initial conditions in case ND1

profiles with evidence peaks (case ND1) for different initial conditions of σ_vs_{pr} and Z_{band}				
σ_vs_{pr}	Z_{band}	1st peak	2nd peak	3rd peak
30	5	24	27	26
60	5	24	27	6
120	5	27	24	5
240	5	24	27	38
120	1	24	27	5
120	10	24	27	6
120	15	27	24	6

Table 6.1(b) Profiles that present evidence peaks for the different initial conditions in case ND2

profiles with evidence peaks (case ND2) for different initial conditions of σ_vs_{pr} and Z_{band}				
σ_vs_{pr}	Z_{band}	1st peak	2nd peak	3rd peak
30	5	21	25	22
60	5	22	21	25
120	5	22	25	31
240	5	28	25	-
120	1	28	25	-
120	10	21	31	22
120	15	28	26	37

Figure 6.2(a)

Profile #	6	24	27	38	real
layer thicknesses in meters	5	5	5	5	5
	5	5	5	5	5
	5	10	5	5	10
	5		5	5	
	5			10	
	5			10	
				10	
				10	

Figure 6.2(a) Layers of real profile and of profiles chosen based on evidence for case ND1

Figure 6.2(b)

Profile	21	22	25	28	real
layer thicknesses in meters	2.5	2.5	1.25	1.25	5
			1.25	1.25	
	2.5	2.5	2.5	2.5	
	2.5	2.5	2.5	2.5	10
	2.5	2.5	5	2.5	
	2.5	5		2.5	
	2.5			2.5	
	2.5	5	7.5	5	5
	2.5				

Figure 6.2(b) Layers of real profile and of profiles chosen based on evidence for case ND2

Based on figure 6.1, table 6.1 shows which profiles present evidence peaks for the different initial conditions of σ_vs_{pr} and Z_{band}. To help interpret these results, figure 6.2 presents the layered configurations for the profiles that obtained the highest evidence values. These configurations were introduced in Chapter 4 and are repeated here for easier reference. All other profiles are presented in Chapter 4 in figures 4.2, 4.3, 4.4, 4.5, 4.8, and 4.9.

In table 6.1(a), the list of the peaks for case ND1 shows that the profile with the most top peaks ("1 st peaks" in the table) is profile 24. Thus, for this synthetic case the evidence helps choose the actual configuration of the real profile (Figure 6.2(a)). As discussed in Chapter 5, for a real case it would be advised to choose a depth to half space of around 50 meters based on the half-space sensitivity to the maximum wavelength. This is because in a real case the experimental data should not be used to resolve highly the half-space since it is an unrealistic layer. However, for the synthetic example all layered configurations introduced previously were evaluated and the evidence was highest for the simplest configuration that presented a satisfactory fit to the data, which is the result wanted.

The second profile that presents high evidence values for case ND1 is number 27 as noted in Table 6.1(a). This profile is the simplest one after profile 24, and also includes layers appropriate to represent the real profile (Figure 6.2(a)). Additionally, among the 50-meters deep profiles (31 to 38) the profile with the highest evidence was profile 38, which is the simplest one of these that could represent the true profile, and among the 30-meters deep profiles (1 to 15) profile 6 had the highest-evidence, which is the most

appropriate of these to represent the true profile (Figure 6.2(a)). This example shows how the model selection based on the Bayesian criterion is a valuable tool to analyze the inversion results obtained for SASW. As described previously, the Ockham factor favors hypotheses with fewer free parameters and the likelihood favors hypotheses that fit the data better. The evidence combines the Ockham factor and the likelihood and is greatest for the simplest model that produces a satisfactory fit to the data.

It can be noted that in Figure 6.1(a) the evidence peaks obtained for case ND1 are basically the same peaks observed for the Ockham factor, consequently favoring simpler profiles. Thus, the likelihood did not have an important influence in this case, which makes sense because the matches between experimental and theoretical dispersion curves were all satisfactory with low rms errors (all errors were under 0.75, for all cases except for profiles 1 to 4)

In table 6.1(b), the list of the peaks for case ND2 shows that the profile with the most top peaks ("1 st peaks" in the table) is profile 28, with 3 peaks. However, this profile is closely followed by profiles 21 and 22 with 2 top peaks each. Also it is noted that profile 25 has 4 secondary peaks. Thus, for this synthetic case the evidence does not choose the actual configuration of the real profile (Figure 6.2(b)).

It can be noted that in Figure 6.1(b) the evidence peaks obtained for case ND2 are basically the same peaks observed for the likelihood. Thus, in this case, the profiles favored by the evidence are not necessarily the simpler ones, but the ones with theoretical

204

dispersion curves that present better matches to the experimental dispersion curve. It is reasonable that the likelihood has an important influence in this case because the matches between experimental and theoretical dispersion curves were variable, with rms errors between 0.32 and 3.3 (for all cases except for profiles 39 and 41). This range of values is significantly larger than the range of values for case ND1, which means that in case ND2 there is more difference in the goodness of the fit among different profiles.

The fact that the selection of the profile is influenced by the fit to the experimental data is an important characteristic of the Bayesian approach. Note that other tools used to compare different layered configurations in Chapter 5, such as the diagonal of the resolution matrix and the partial derivatives, do not take into account the goodness of the fit. Figure 6.3 presents the rms errors obtained for the profiles with high evidence values in case ND2, and for the layered configuration of the real profile (i.e., profile 29). Note that for profile 29 the rms is around 2.0 for all cases of σ_vs_{pr} and Z_{band}, and that considerably better rms values are obtained for the other profiles, since for each of the other profiles at least three cases of σ_vs_{pr} and Z_{band} result in rms values below 1.0. Thus, profile 29 could not be chosen by the evidence due to the higher rms values that are related to it. These results emphasize the difficulties in finding the actual profile, since the configuration matching the layers of the real profile in this perfect synthetic example converged to V_s values that resulted in higher rms errors.
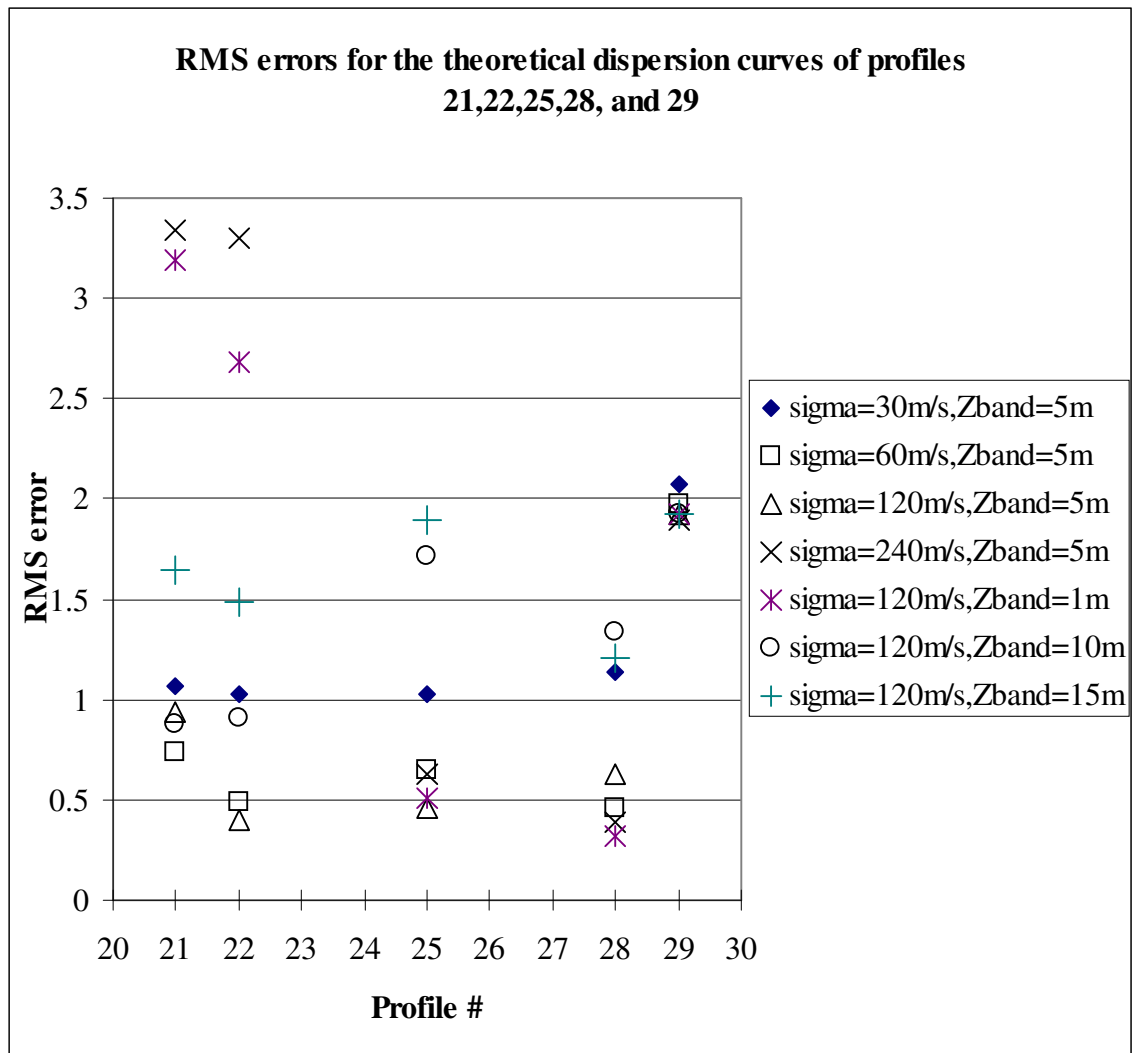
Figure 6.3 RMS errors for profiles with high evidence and for layered configuration of the real profile, for case ND2

6.3.2 Selection of the prior standard deviations of V_s

Other than evaluating which profile contains the best set of layers, the evidence can help choose prior information such as the V_s standard deviations. Figure 6.4 presents how the prior standard deviations (σ_vs_{pr}) affect the values of the Ockham factor, the likelihood, and the evidence. In this case, the evidence is normalized by dividing it by the sum of all evidences for a fixed set of layers and a fixed Z_{band} (this was done for all layered configurations introduced in Chapter 4). The number of top peaks obtained for each case of σ_vs_{pr} is summarized in table 6.2.

For case ND1 in figure 6.4 (a), it can be noted that as σ_vs_{pr} increases the Ockham factor decreases and the likelihood increases. The Ockham factor decreases because a larger σ_vs_{pr} constrains less the solution, and results in final values that depart more from the initial ones, which produces a lower Ockham factor. The reason is that if two profiles are equally good to fit the data, the one that departs less from what is expected a priori is preferred, and this is reflected with a higher Ockham factor for the profile with the posterior pdf more similar to the prior pdf. Additionally, for case ND1, a larger σ_vs_{pr} constrains less the solution and results in a better fit, which is reflected in a higher likelihood.
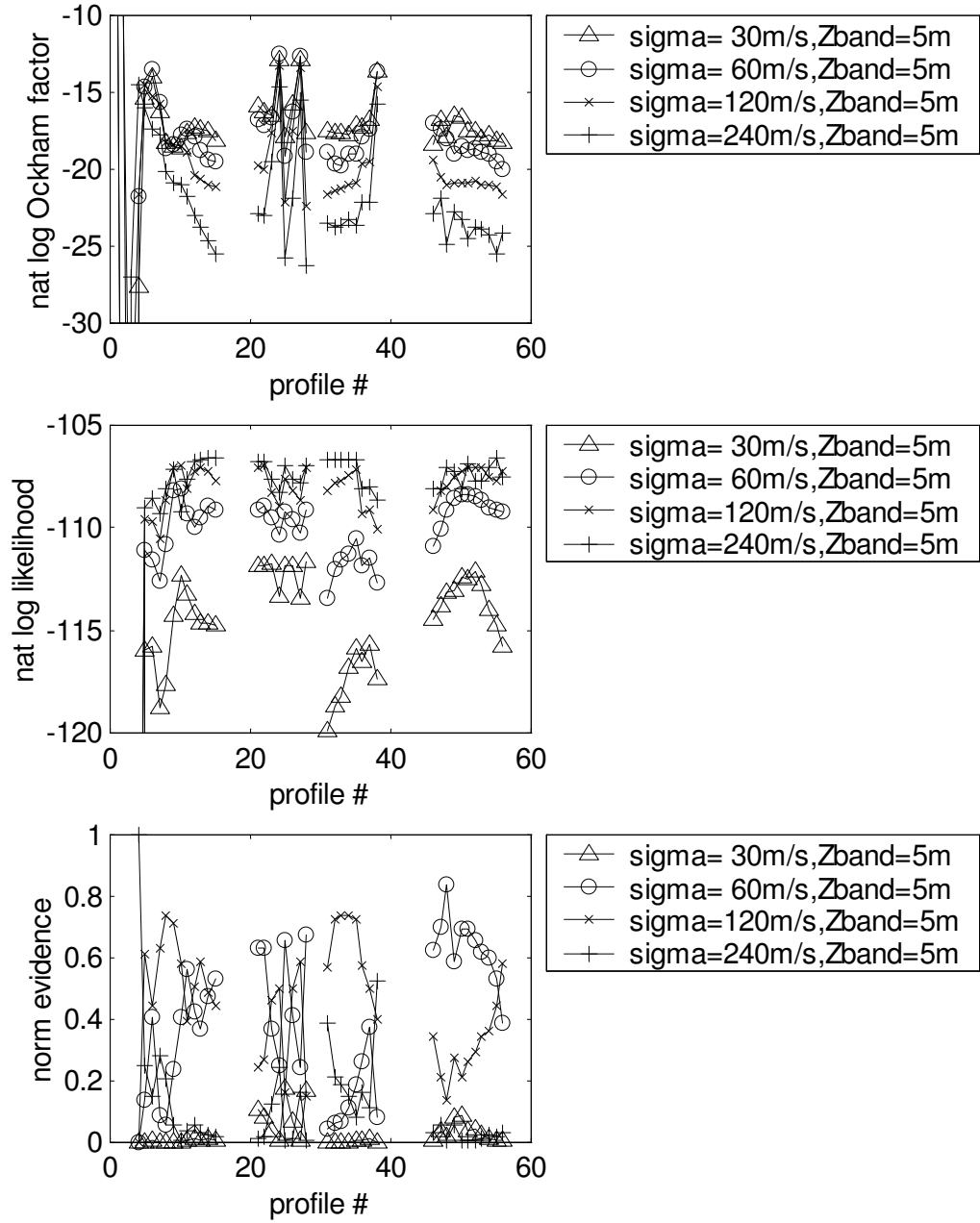
Figure 6.4(a) Ockham factor, likelihood, and normalized evidence to choose best σ_vs_{pr} for case ND1

208
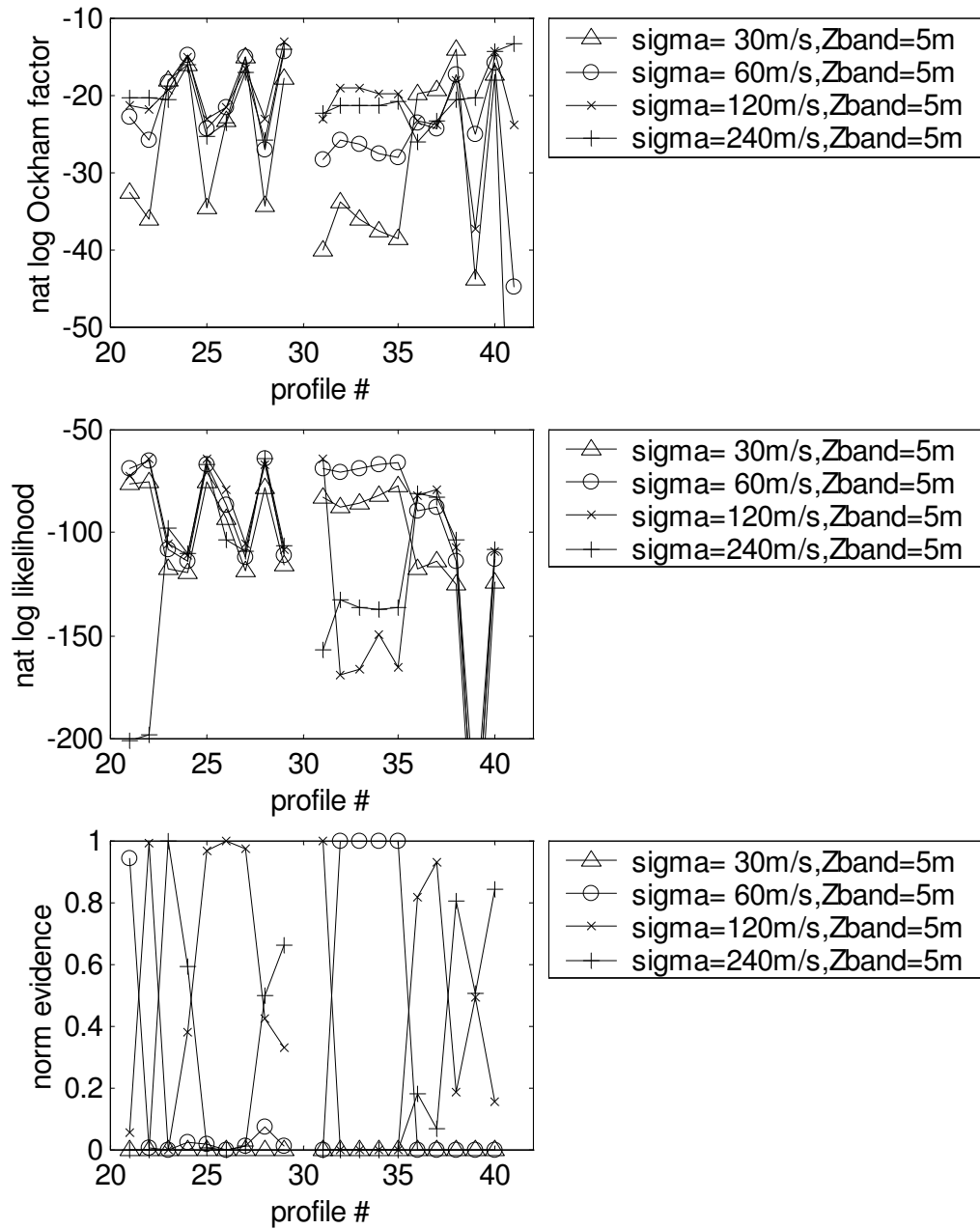
Figure 6.4(b) Ockham factor, likelihood, and normalized evidence to choose best σ_vs$_{pr}$ for case ND2

Table 6.2(a) Total number of evidence peaks for each case of σ_vs$_{pr}$, case ND1

CASE ND1, Z$_{band}$=5m	
σ_vs$_{pr}$	total # of peaks
30	0
60	16
120	21
240	2

Table 6.2(b) Total number of evidence peaks for each case of σ_vs$_{pr}$, case ND2

CASE ND2, Z$_{band}$=5m	
σ_vs$_{pr}$	total # of peaks
30	0
60	5
120	7
240	7

The plot of the evidence in figure 6.4(a) shows that the highest evidence values are found for σ_vs_{pr} values of 60 and 120m/s and that the evidence does not favor very low (30m/s) or very high (240m/s) uncertainty values. As noted in Table 6.2(a), 60 m/s presented 16 peaks and 120 m/s presented 21 peaks. Thus, a σ_vs_{pr} of 120m/s is preferred in most cases. Additionally, looking at the preferred layered configurations, 24 and 27, it is noted that for these configurations the preferred value is 120m/s.

The trends observed in case ND1 for the Ockham factor and the likelihood do not occur for case ND2. This is due to the inversion results varying significantly from case to case, which is reflected in the larger range of rms errors obtained. This means that for this case a lower σ_vs_{pr} does not necessarily result in a profile closer to what was expected a priori and a larger σ_vs_{pr} does not necessarily result in a better fit. For example, in Figure 6.3, it can be noted that for profiles 21 and 22 the rms errors are above 3.0 for the largest σ_vs_{pr} (i.e., 240m/s), which is significantly higher than the rms for lower values of σ_vs_{pr} utilized with the same Z_{band} (i.e., 5m). However, for profile 28 the rms error found using the largest σ_vs_{pr} is below 0.5 and very close to the lowest rms for that profile.

 Consequently, for case ND2 (figure 6.4(b)), there are no clear trends for the change in Ockham factor and likelihood caused by a change in σ_vs_{pr}. Note that the values of σ_vs_{pr} that present top values for the evidence are almost the same ones that present top values for the likelihood. Thus, the fit has a more significant influence than the simplicity of the profile and its closeness to the prior assumptions. As shown in table 6.2(b), most peaks are obtained for the higher values of σ_vs_{pr} (i.e., 120 and 240m/s). This makes

sense since for case ND2 the real profile has a higher V_s contrast among layers, and consequently needs more flexibility to vary from the initial V_s values than for case ND1 (the initial V_s values come from a smooth initial V_s profile obtained with the empirical estimated based on the dispersion curve).

The evidence peaks for the preferred layered configurations show that for profile 28 the preferred value for σ_vs_{pr} is 240m/s, for profile 22 the preferred value is 120m/s, and for profile 21 the preferred value is 60m/s. As mentioned before, this method helps choose among values that are considered equally probable a priori. Thus, if there is data other than the dispersion curve available to help constrain the problem, the prior standard deviations of V_s should reflect the actual level of confidence in the prior V_s values.

6.3.3 Selection of the prior correlations of V_s

The evidence can also help choose prior information such as the V_s correlations given by Z_{band} (as described in Chapter 4). Figure 6.5 presents how the prior correlations (given by Z_{band}) affect the values of the Ockham factor, the likelihood, and the evidence. In this case, the evidence is normalized by dividing it by the sum of all evidences for a fixed set of layers and a fixed σ_vs_{pr} (this was done for all layered configurations introduced in Chapter 4). The number of top peaks obtained for each case of Z_{band} is summarized in table 6.3.
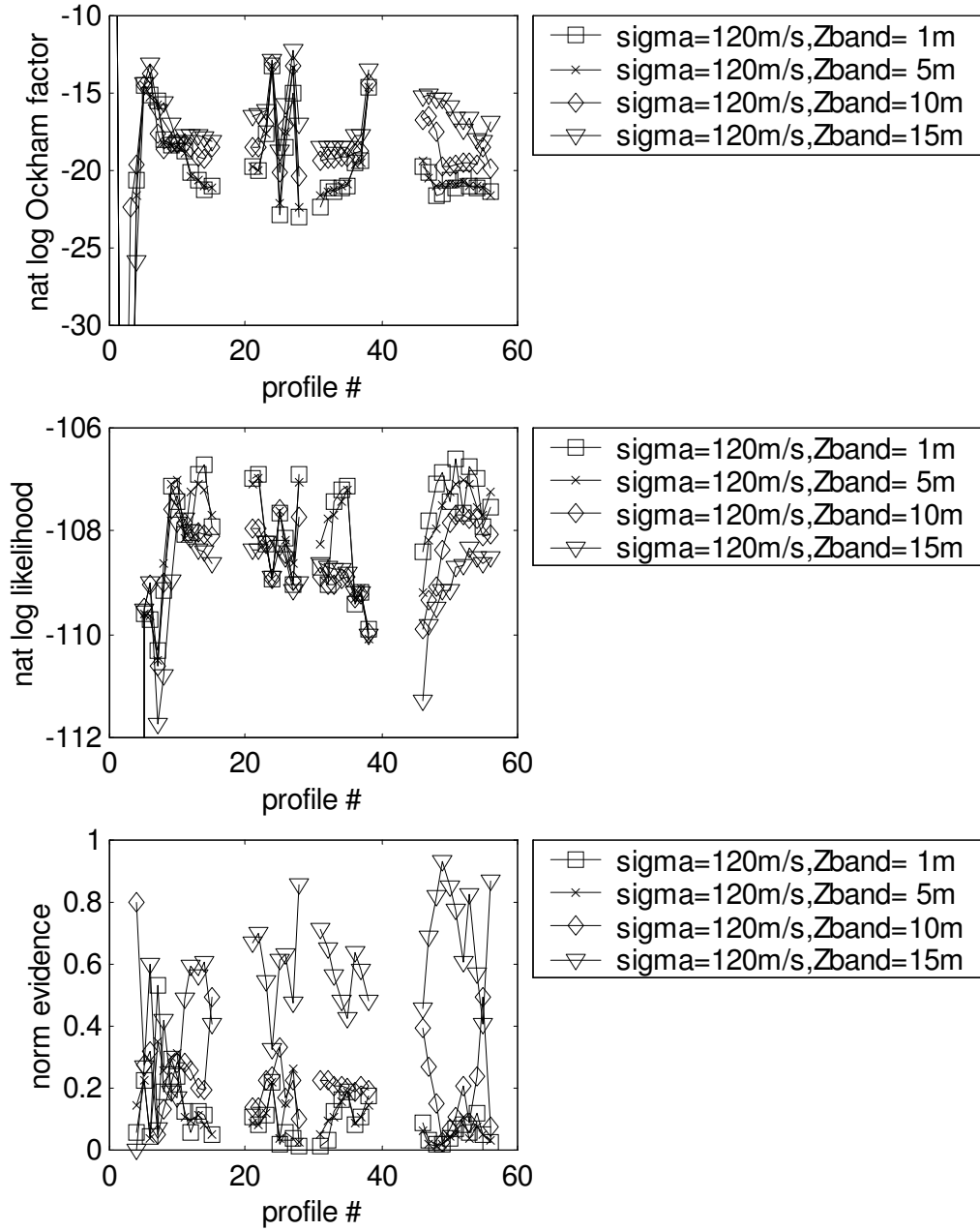
Figure 6.5(a) Ockham factor, likelihood, and normalized evidence to choose best Z$_{band}$ for case ND1

213
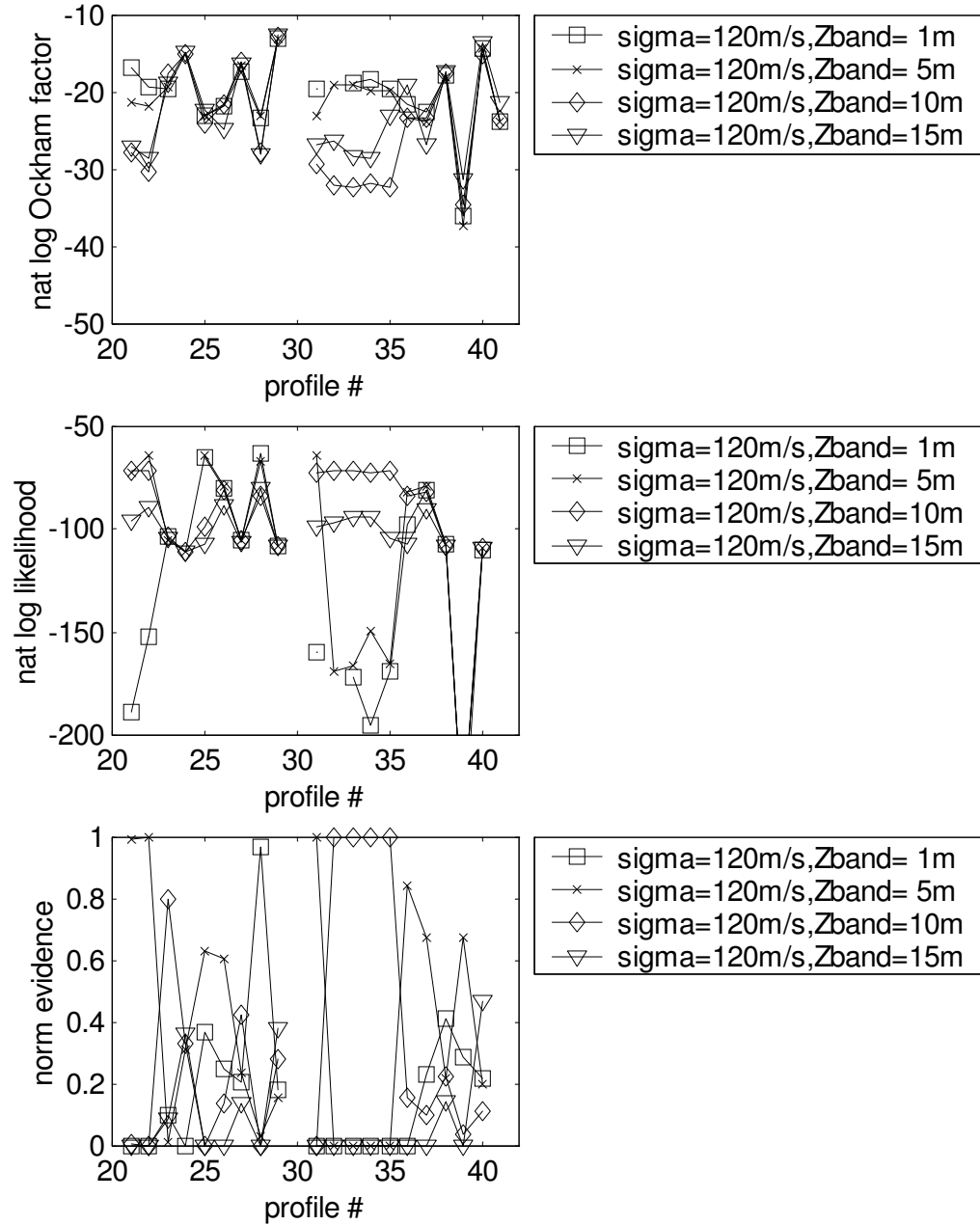
Figure 6.5(b) Ockham factor, likelihood, and normalized evidence to choose best Z_{band} for case ND2

Table 6.3(a) Total number of evidence peaks for each case of Z_{band} , case ND1

CASE ND1, σ_vs_{pr}=120m/s	
Z_{band}	total # of peaks
1	1
5	2
10	4
15	32

Table 6.3(b) Total number of evidence peaks for each case of Z_{band} , case ND2

CASE ND2, σ_vs_{pr}=120m/s	
Z_{band}	total # of peaks
1	2
5	8
10	6
15	3

For case ND1, in figure 6.5(a), it can be noted that as Z_{band} increases the Ockham factor increases and the likelihood decreases. Thus, the tendencies are the opposite than for σ_vs_{pr} (figure 6.4(a)), which makes sense because a higher correlation (higher Z_{band}) constrains more the solution as a lower σ_vs_{pr} does, and a lower correlation (lower Z_{band}) lets the solution vary more and thus go farther from what is expected a priori as a higher σ_vs_{pr} does. The plot of the evidence in figure 6.5(a) shows that the highest evidence values are found for a Z_{band} value of 15m and that the evidence does not favor low correlation values. As noted in Table 6.3(a), a Z_{band} of 15m presented 32 peaks out of 39 cases. Thus, a Z_{band} of 15m is preferred in most cases, including the preferred layered configurations, 24 and 27.

The trends observed in case ND1 for the Ockham factor and the likelihood do not occur for case ND2. As mentioned in the previous section, this is due to the inversion results varying significantly from case to case. Thus for this case a higher correlation does not necessarily result in a profile closer to what was expected a priori and a lower correlation does not necessarily result in a better fit. For example, in Figure 6.3, it can be noted that for profiles 21 and 22 the rms errors are above 2.5 for the lowest Z_{band} (i.e., 1m), which is significantly higher than the rms for higher values of Z_{band} utilized with the same σ_vs_{pr}(i.e., 120m/s). However, for profile 28 the rms error found using the lowest Z_{band} is below 0.5 and the lowest for that profile.

As shown in table 6.3(b), most peaks are obtained for the middle values, with 8 peaks for a Z_{band} of 5m and 6 peaks for a Z_{band} of 10m. This makes sense since for case ND2 the

real profile has a higher V_s contrast among layers, and needs more flexibility (i.e., given by lower correlations among layers, which allow higher contrast among layers) to vary from the initial V_s values than for case ND1.The evidence peaks for the preferred layered configurations show that for profile 28 the preferred value for Z_{band} is even lower (i.e.,1m), and for profiles 21 and 22 the preferred value is 5m.

6.3.4 Selected models

Based on the results obtained for the evidence, the best model for case ND1 is profile 24 with prior standard deviations for V_s of 120m/s and prior correlations given by a Z_{band} of 15m. The inversion results obtained for this case are presented in Figure 6.6(a). Additionally, this figure presents the inversion results for the other model that obtained high evidence values. This model corresponds to profile 27 with prior standard deviations for V_s of 120m/s and prior correlations given by a Z_{band} of 15m. The V_s values and standard deviations shown in figure 6.6(a) correspond to coefficients of variability (i.e., σ_vs/vs) below 20%. These values are lower than the values estimated based on the results obtained for case ND1 with the Monte Carlo algorithm as described in Chapter 3. This is reasonable since a higher rms criterion results in a higher range of V_s profiles and consequently in larger coefficients of variability (the values for the coefficients of variability in Chapter 3 were based on 85 V_s profiles with rms errors between 0.68 and 1.5, which are higher values than the rms values of 0.342 and 0.357 shown in figure 6.6(a)).
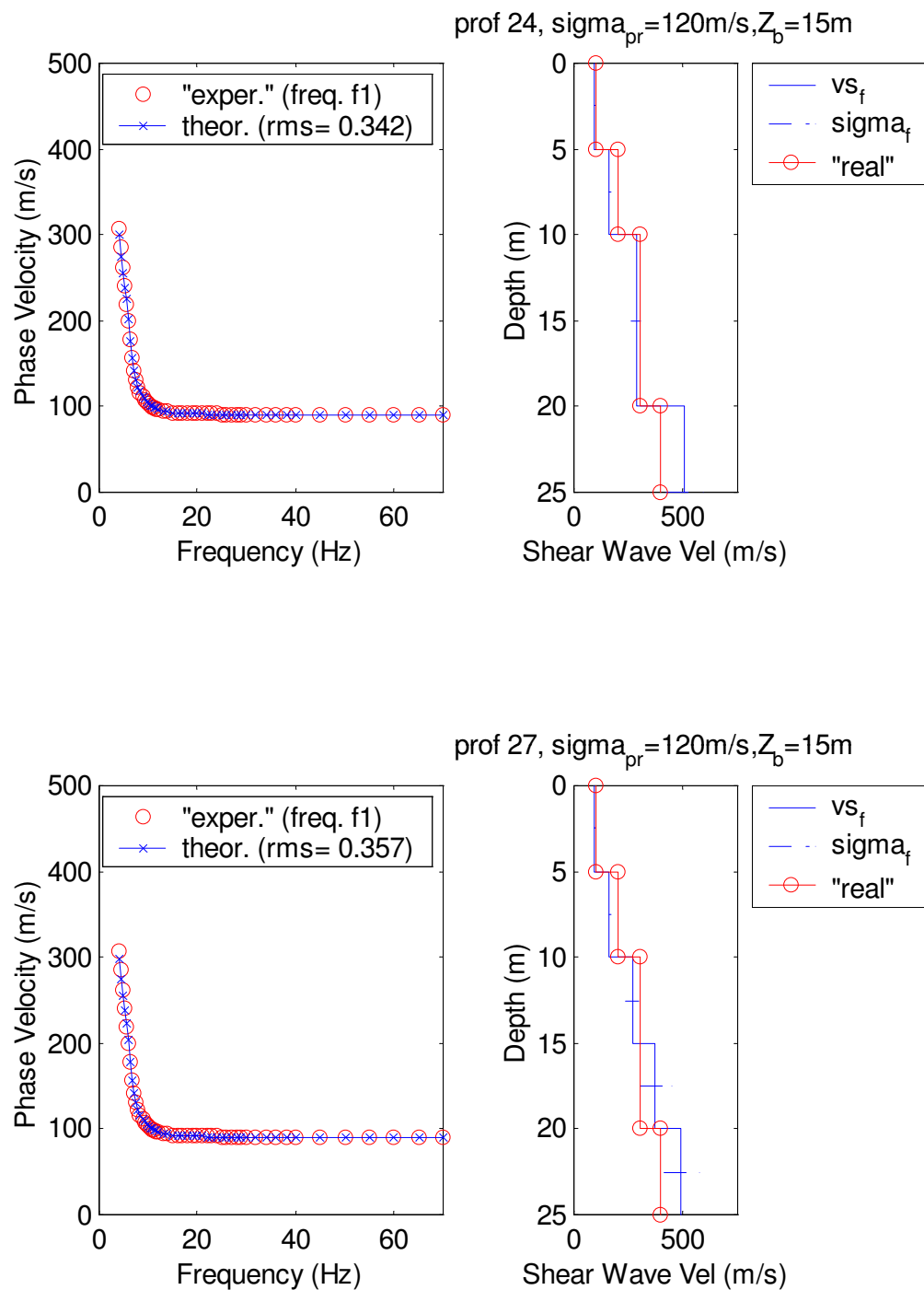
Figure 6.6(a) Inversion results for profiles 24 and 27 (σ_vs$_{pr}$ =120m/s, Z_{band}=15m) for case ND1
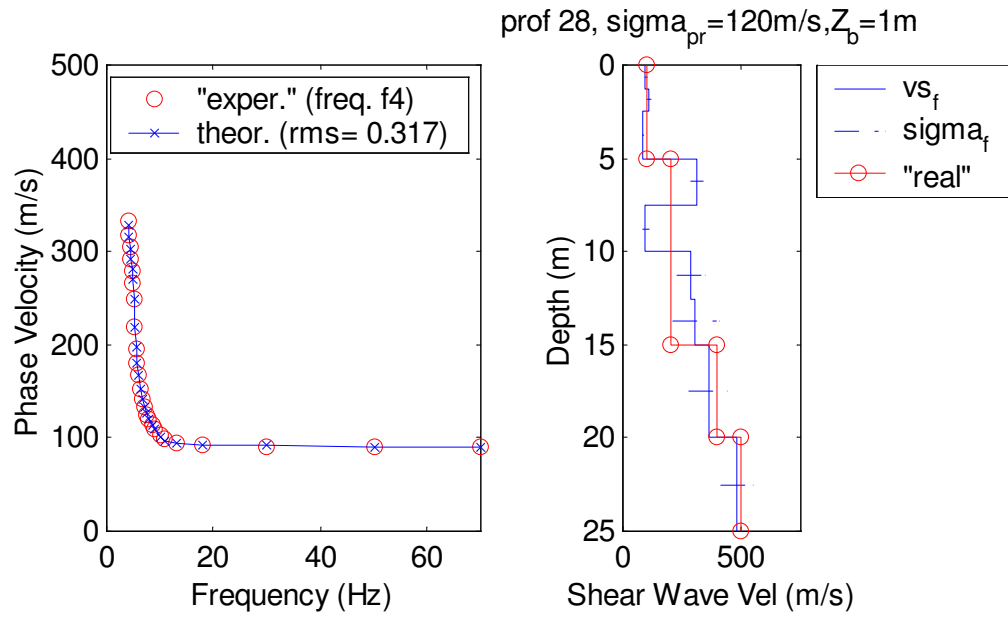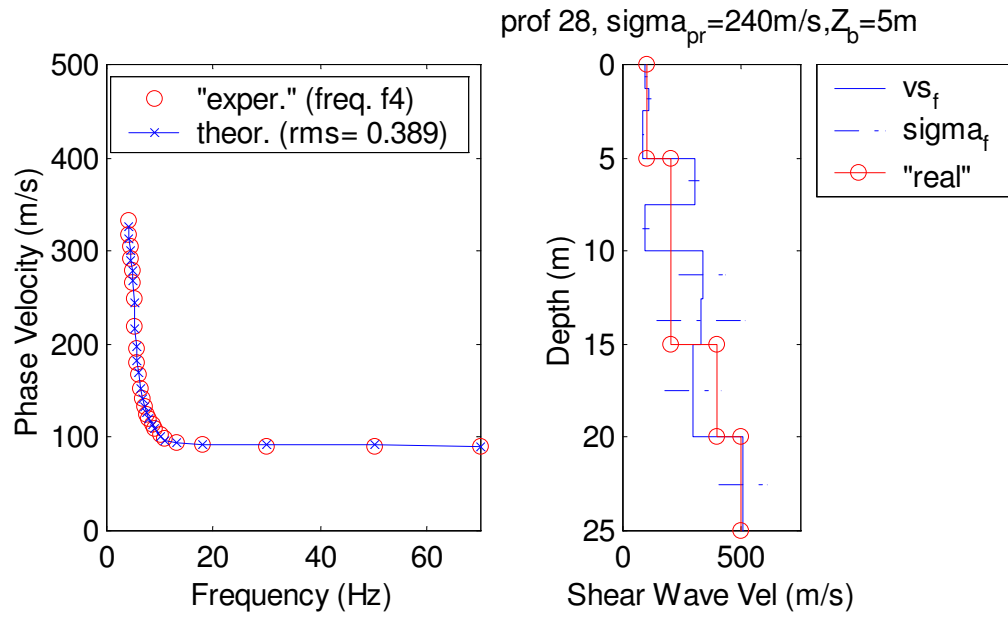
Figure 6.6(b) Inversion results for profile 28 (σ_vs_{pr} =240m/s, Z_{band}=5m and σ_vs_{pr} =120m/s, Z_{band}=1m) for case ND2
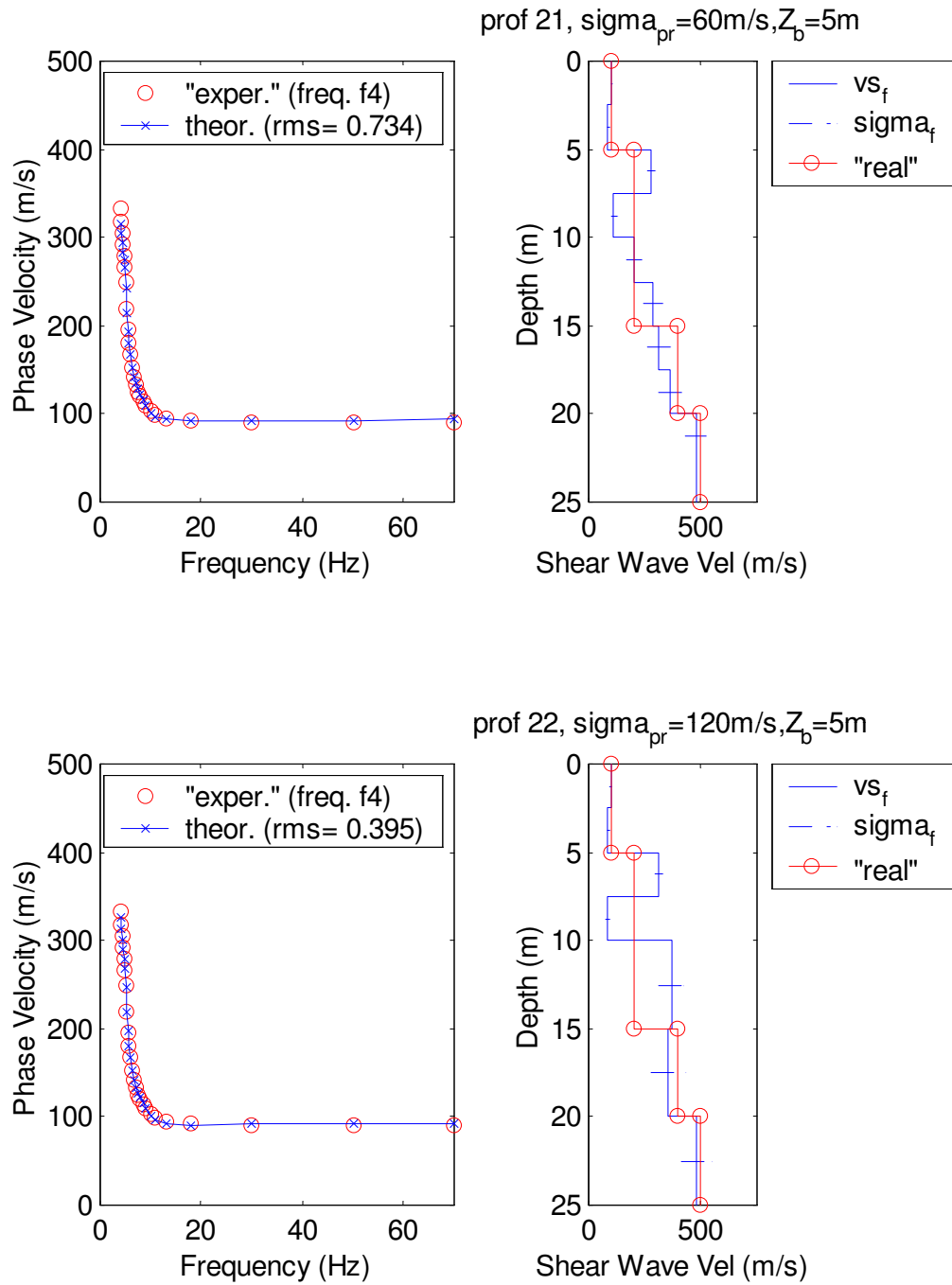
Figure 6.6(c) Inversion results for profiles 21 (σ_vs_{pr} =60m/s, Z_{band}=5m) and 22 (σ_vs_{pr} =120m/s, Z_{band}=5m) for case ND2

For case ND2, the best model based on evidence is profile 28. The preferred prior standard deviations of V_s for this profile were 240m/s, accompanied by a Z_{band} of 5m. The preferred prior correlations for this profile corresponded to a Z_{band} of 1m, accompanied by a σ_vs_{pr} of 120m/s. Among these two cases, the first one is selected because it has a higher normalized evidence in Figure 6.1(b) than the second (i.e., highest normalized evidence for the selection of the layered configuration). Additionally, a Z_{band} of 5m was selected for most cases in case ND2. The inversion results obtained for both of these cases are presented in Figure 6.6(b).

Additionally, figure 6.6(c) presents the inversion results for the other models that obtained high evidence values. These are profiles 21 and 22, the first with prior standard deviations for V_s of 60m/s, the second with prior standard deviations for V_s of 120m/s, and both with prior correlations given by a Z_{band} of 5m. Note that the results obtained for case ND1 in figure 6.6(a) are much closer to the real profile than the results obtained for case ND2 in figures 6.6(b) and 6.6(c). This emphasizes that the inversion algorithm had a harder time solving the V_s values for the case with a higher V_s contrast.

It is relevant to note that the case that combines the selected prior values of σ_vs_{pr}=240m/s and Z_{band}=1m for profile 28 in case ND2 was not evaluated when looking at the evidence, and results in a higher rms error than the two combinations selected by the evidence:

RMS error=1.27 for σ_vs_{pr}=240m/s and Z_{band}=1m,

RMS error =0.39 for σ_vs_{pr}=240m/s and Z_{band}=5m, and

RMS error =0.32 for σ_vs_{pr}=120m/s and Z_{band}=1m.

Thus, the selection of prior standard deviations and correlations for V_s is inevitably related, and for a real case it is suggested that all combinations of the values assumed for comparison are evaluated and ranked with the evidence.

6.4 Conclusions

The numerical examples presented in Chapter 4 were employed in this chapter to implement the Bayesian criterion to compare different parameterizations (i.e., layered configurations) and prior information (i.e., standard deviations and correlations of V_s), and select among them. This is accomplished by calculating the evidence, which combines the Ockham factor and the likelihood. The first favors simpler models, and the second favors hypotheses that fit the data better. Thus, the evidence helps find the simplest model that satisfactorily fits the data.

In case ND1, the Ockham factor had an important influence on the evidence and the simplest profiles had the highest values. This was due to the fact that most inversion results presented similarly good fits for the dispersion curves with rms values below 0.75. Consequently, the selected profile for this case was the layered configuration with the exact layers of the real profile. In case ND2, the likelihood controlled which profiles had the highest evidence values and the profiles that presented dispersion curves with better fits to the experimental data were preferred. This was due to the fact that the inversion

results did not have similar fits to the data, with the range of rms values going from 0.32 to 3.3. Thus, the configuration chosen was one with low rms error.

Additionally, the evidence was used to evaluate the assumed prior standard deviations of V_s. For ND1 the preferred values were in the middle of the range used (60 and 120m/s), and for ND2 the preferred values were to the higher end of the range used (120 and 240 m/s). This is reasonable, since the profile with a higher V_s contrast (ND2) needs more flexibility (i.e., given by higher initial uncertainties) to vary from the initial guess. Equivalently, the evidence was used to evaluate the assumed prior correlations of V_s. For ND1 the preferred value was for the highest correlations used (Z_{band}=15 m), and for ND2 the preferred values were towards the middle of the range used (Z_{band}=5 and 10 m). Again, it is reasonable that the profile with a higher V_s contrast (ND2) needs more flexibility (i.e., given by lower correlations) to vary from the initial guess.

The simplest way to compare the inversion results is by looking at the rms error. However, when there are a large number of cases that fit the data satisfactorily under a specified rms criterion (i.e., rms<1.0) the selection of the best case is not obvious. Choosing the lowest rms of all may not be appropriate since it may imply choosing a model that includes characteristics that are not necessary to fit the data. The two cases presented showed the two significant sides of the Bayesian approach, since in one case the selection was controlled by the Ockham factor choosing the simplest model among similar fits and in the other case the selection was controlled by the goodness of the fit. Based on these results, the Bayesian model selection was shown to be a valuable method,

that has the ability to select the simplest profile that produces a good fit to the data. Other tools that help compare the inversion results such as the resolution matrix and the partial derivatives used in Chapter 5, do not take into account a good fit to the data. Additionally, these tools help compare different layered configurations but do not help compare among different assumptions of the prior standard deviations and correlations of V_s.

CHAPTER 7

EVALUATION OF INVERSION PROCEDURE WITH REAL DATA

7.1 Introduction

The methods employed with the simulated data in Chapters 4, 5, and 6 are applied in this chapter to SASW real experimental data. The experimental data used was obtained at Shelby Forest (Memphis, Tennessee) in July 2000, and more details about this site may be found in Hebeler (2001). This site has the advantage that there is additional shear wave velocity data available from other in situ tests. However, it is important to clarify that this data is not used herein as additional data before performing the inversion, but as data available to compare the type of results that may be obtained from SASW tests.

The steps of the inversion procedure for SASW based on the maximum likelihood method and complemented with model selection tools are utilized for this real experimental case. Thus, the inversion is a complete process that includes from the preparation of the data necessary for the inversion algorithm to the final selection and presentation of the V_s profile. The use of diverse tools to choose the information required for the inversion is very valuable to decrease the subjectivity of this process.

7.2 Experimental Dispersion Data

7.2.1 Number and Distribution of Points Describing the Experimental Dispersion Data

The decisions made during the field test, such as sensor setup and source will affect the information obtained in the experimental dispersion curve. Details on all the aspects involved in obtaining an accurate and representative dispersion curve can be found in Hebeler (2001), where the experimental results from 11 field tests performed in Memphis, Tennessee, during the summer of 2000 are presented. One of these field tests was performed in Shelby Forest and is the real experimental data employed here to evaluate the inversion method and tools presented. There were 15 sensors used during the field test, which were located at distances from the active source of: 8, 10, 12, 15, 18, 22, 28, 34, 42, 50, 60, 70, 80, 95, 110 ft (i.e., 2.4 3.0 3.7 4.6 5.5 6.7 8.5 10.4 12.8 15.2 18.3 21.3 24.4 29.0 33.5m). The active source was harmonic and the 60 individual frequencies used were: 4.375, 5.000, 5.625, .., 15.000, 16.250, 17.500, .., 35.000, 37.500, 40.000, ..,60.000 Hz, and can be observed in Figure 7.1 together with the experimental dispersion curve obtained for this field test.
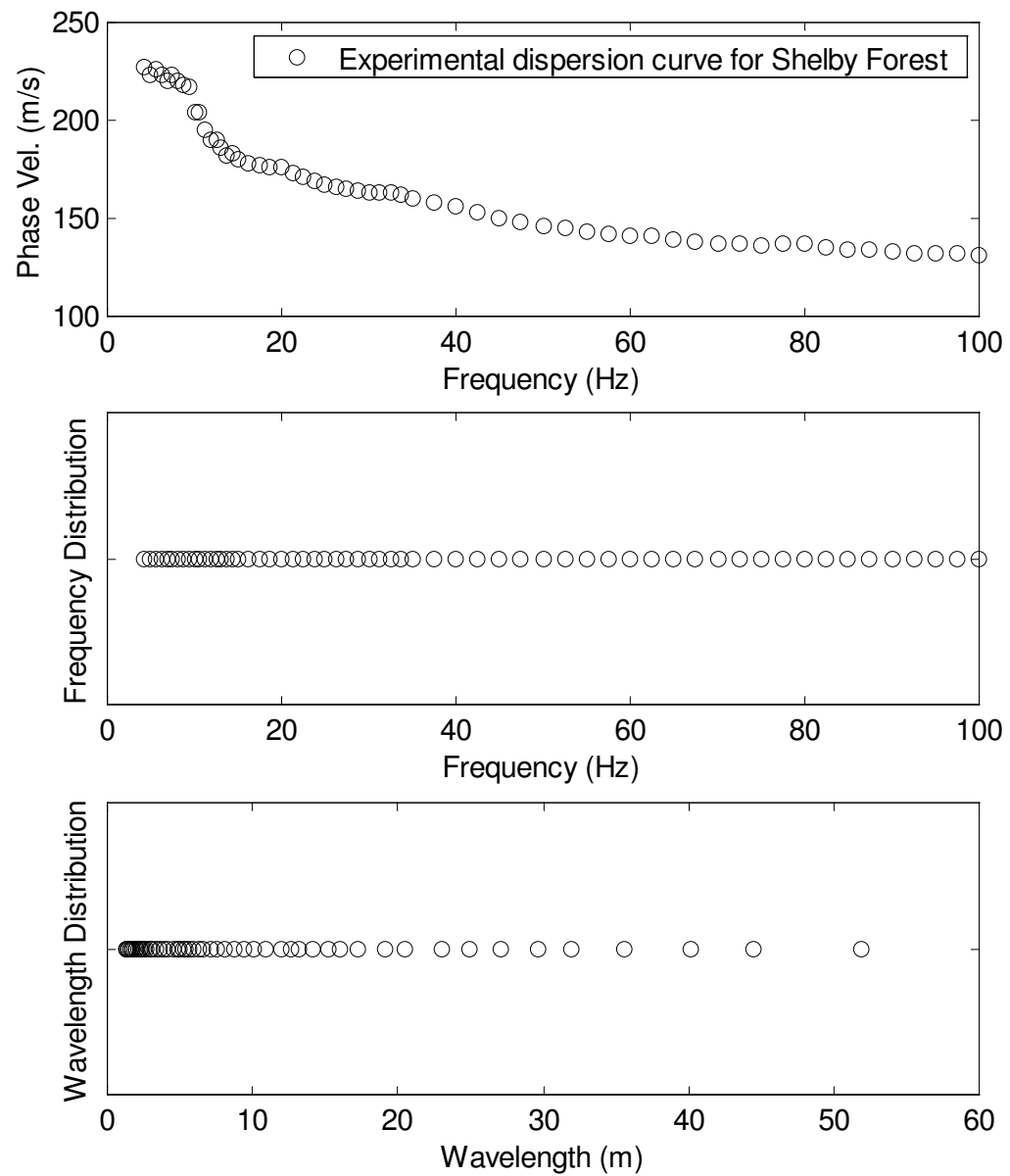
Figure 7.1 Experimental dispersion curve for Shelby Forest, Memphis, Tennessee

From this dispersion curve the wavelength distribution is calculated (wavelength=phase velocity/frequency) and also plotted in Figure 7.1. As discussed in Chapter 5, it can be considered that a layer was not sampled by wavelengths shorter than the depth to the top of the layer. Thus, based on the wavelengths obtained, it can be noted that out of 60 wavelengths only 20 sampled soils below 10 meters depth, only 10 sampled soils below 20 meters depth, and only 5 sampled soils below 30 meters depth. Thus, one would expect the deeper layers to have a lower resolution since there is less experimental information for them. Accordingly, it makes sense to have thicker layers with depth to reflect the decrease in resolution, and to choose the layers of the profile based on the wavelengths that sampled the soil as done in section 7.3.1.

Figure 7.2 shows a reduced experimental dispersion curve for Shelby Forest, with 36 instead of 60 dispersion points. As suggested in Chapter 5, some of the dispersion points are deleted to reduce the difference in information content among layers. Note that the 24 points deleted correspond to high frequencies and short wavelengths (i.e., the lowest frequency of the dispersion points deleted was 23.75 Hz and the longest wavelength was 7.13 meters). The dispersion curve represented by the 60 points obtained at the field is still used here to obtain the main inversion results, and the reduced curve with 36 points is used for comparison purposes only.
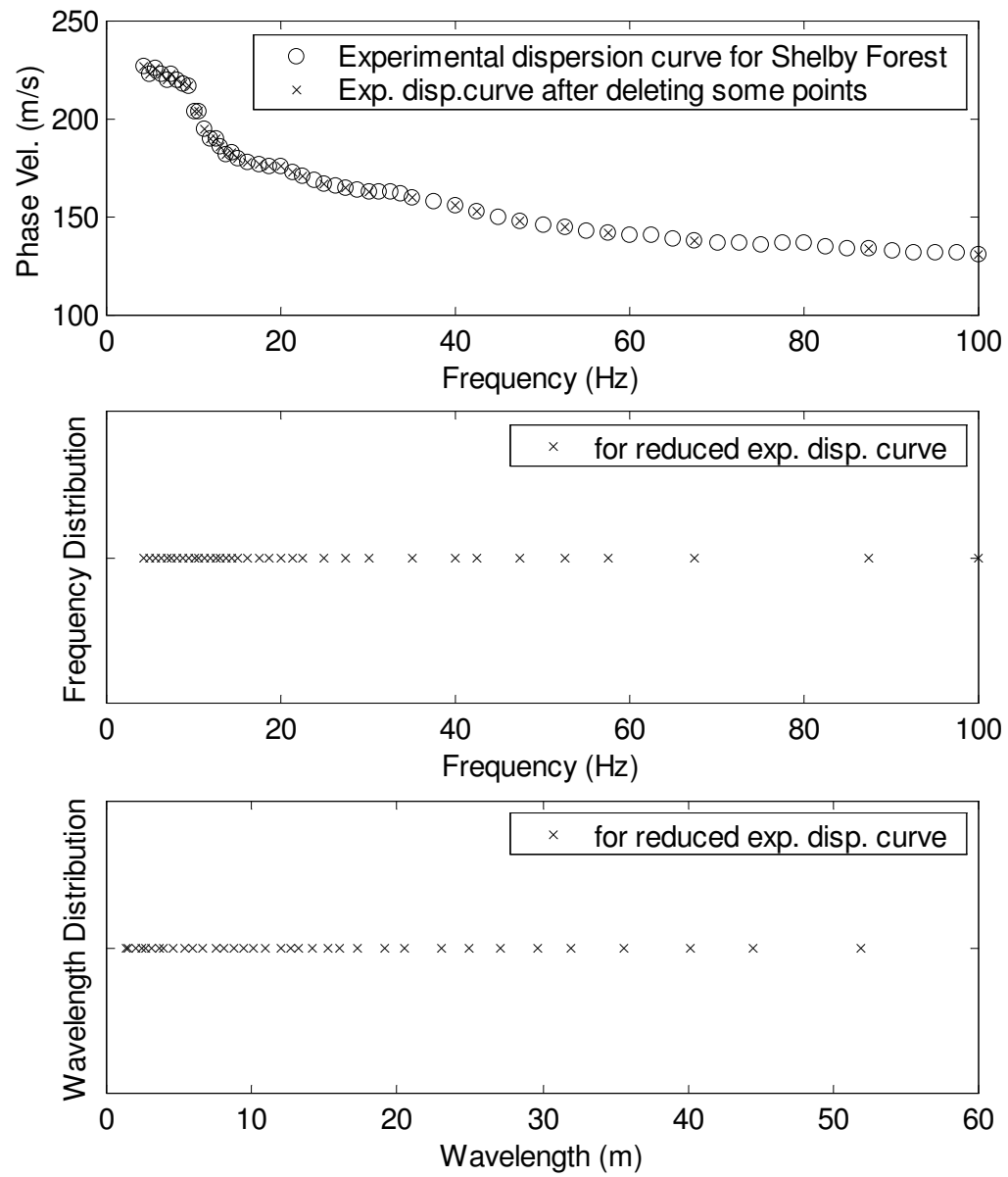
Figure 7.2 Reduced dispersion curve for Shelby Forest (36 points instead of 60)

7.2.2 Uncertainties Related to the Experimental Dispersion Data

As discussed in Chapter 5, the uncertainties related to the experimental data have an effect on the value of the rms error, and on the results obtained from the inversion. A dispersion curve with more uncertainty does not constrain the solution as much, and consequently, there are a larger number of V_s profiles that satisfy a particular rms criterion (say rms<1.0). In Chapter 3 it was noted that V_r uncertainties of 3% of the experimental phase velocities are considered reasonable for SASW tests, and this is the value used herein.

7.3 Prior Information

7.3.1 Depth and Thicknesses of the Layers

As suggested in Chapter 5, one way to evaluate a good relation between the thickness and depth of the layers of a profile and the number and distribution of the dispersion points is by counting the number of waves that sampled the soil with depth. In this case the number and distribution of the dispersion points is given by the field test (Figure 7.1), and the profiles chosen are presented in Figure 7.3. The depth to Half-Space was chosen such that 3 out of 60 waves sample soils in it (i.e., actually the number of waves is close to 2 waves since one of them has a wavelength of 40.2m and the half-space starts at 40m). This depth was chosen to have some data define the half-space but most data used for solving layers

on top of the half-space. A depth to half-space of 40 meters corresponds to ¾ of the maximum wavelength measured (52 meters), and is later evaluated by looking at the half-space sensitivity to the maximum wavelength as discussed in Chapter 5.

In Figure 7.3, it can be noted that the thickness of the layers increases with depth. The only exception is from the top layer to the next one in profile r2. This was done to have a top layer with a thickness that is not less than the minimum wavelength (1.31 m in this case) as recommended by Joh (1996). Additionally, this follows the recommendation from Chapter 5, which suggests that the number of waves sampling a layer should reduce with depth without having consecutive layers sampled by the same number of waves. The second layer may be thinner than the first since there are a good number of waves that sampled it.

Figure 7.4 shows the number of waves that sampled each layer for these profiles. In this figure, it can be noted that the difference in the number of waves that sampled two contiguous layers is at least two. This was done on purpose, choosing profiles with an increase in thickness with depth that was enough to have at least a difference of two waves from one layer to the next. It is inevitable to have more waves test the top layers and consequently a better resolution for those. Thus, it is reasonable to have an increase in thickness, which helps reduce the difference in information available for the diverse layers.

Figure 7.3 Layered profiles chosen to be used for the inversion analysis
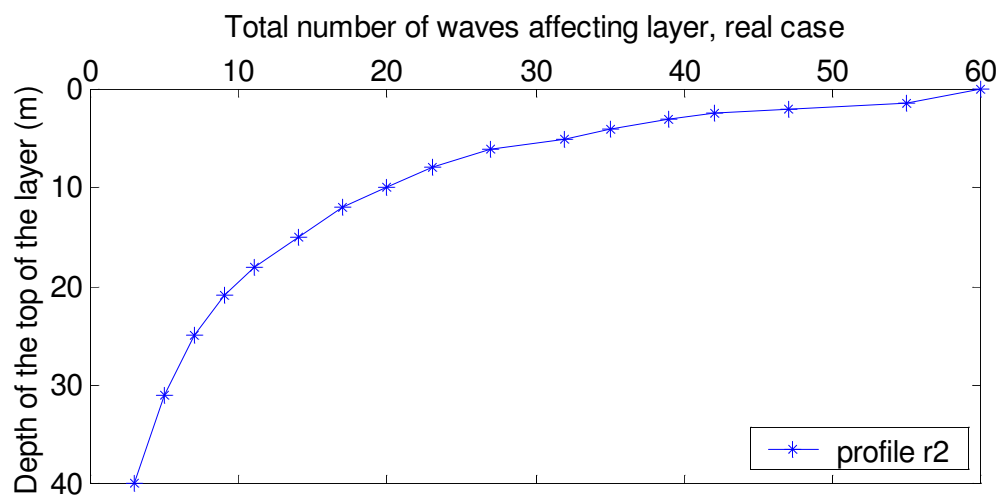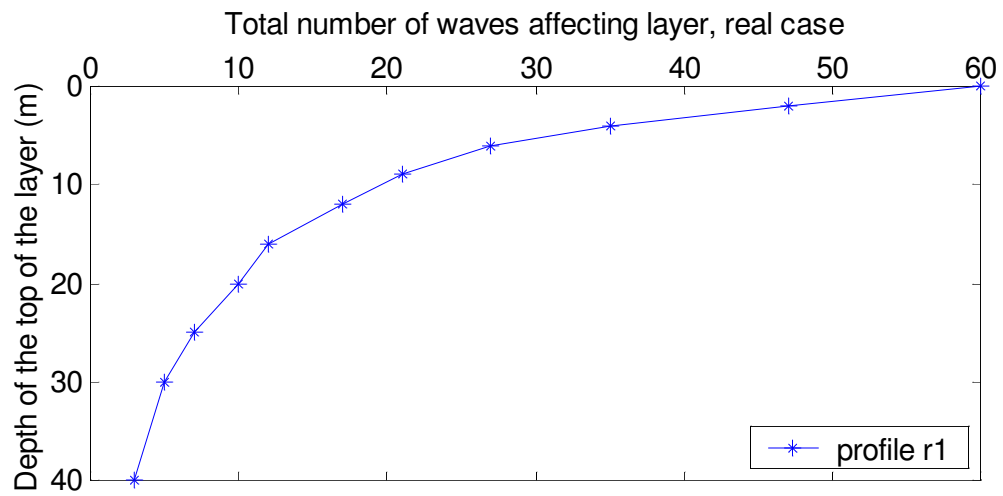
Figure 7.4 Number of surface waves that tested each layer
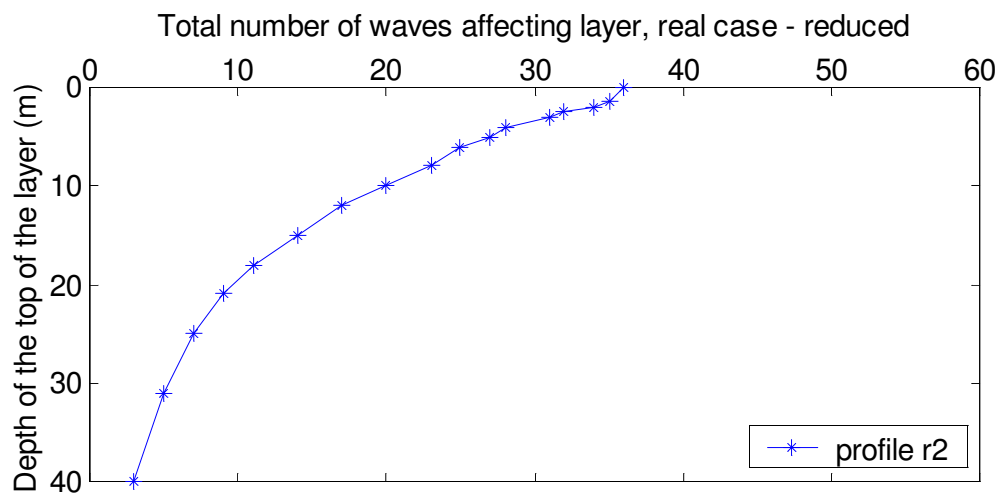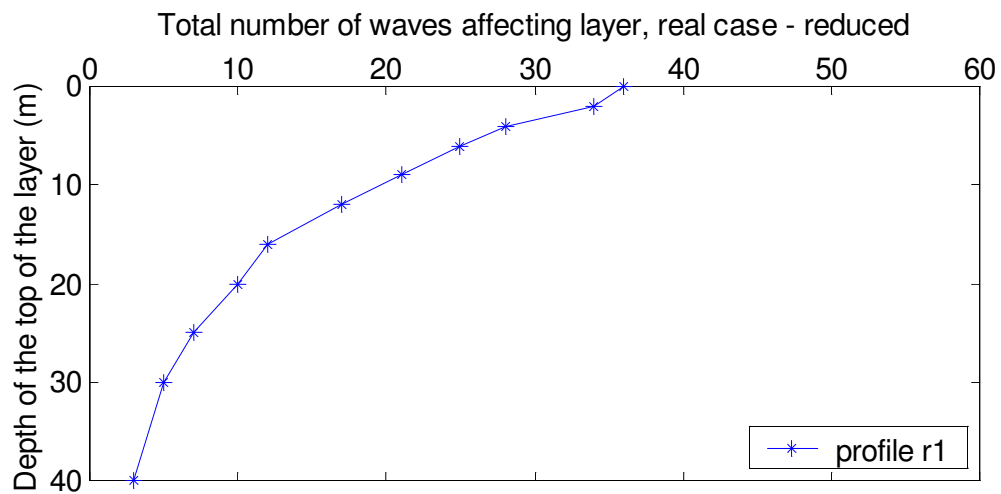
Figure 7.5 Number of surface waves that tested each layer when using the reduced dispersion curve

Figure 7.5 shows the number of waves that sampled each layer for the case of the reduced experimental curve presented in Figure 7.2. This plot reflects that the number of waves testing the layers varied only for the very top layers, reducing the difference in information available for the top layers and for the bottom layers. For profile r2, some of the top layers have now a difference of only one wave between contiguous layers, which still agrees with the suggestion of not having consecutive layers sampled by the same number of waves.

7.3.2 Initial Shear Wave Velocities

Since the maximum likelihood method requires a starting point that is not too far from the solution to the problem to guarantee convergence, a good approach is to obtain an empirical estimate of the shear wave velocities as discussed in Chapter 4. To obtain this estimate, V_r is multiplied by a factor of 1.1 to obtain V_s and an equivalent depth (z) is found by multiplying the wavelength (λ, where $\lambda=V_r/f$) by a scaling factor. Since the best scaling factor to find z depends on the variation of the shear modulus with depth (see Chapter 2), the approach proposed in Chapter 4 is to try a number of scaling factors (0.2, 0.25, 0.3.., 0.8) and choose the one that results in the V_s profile with the theoretical dispersion curve closest to the experimental dispersion curve (i.e., with the lowest rms). The details on how this empirical estimate is done can be found in Chapter 4.

For the profiles introduced in Figure 7.3, the initial V_s values found were based on a scaling factor of 0.25, which was the one that resulted in the best fit of the dispersion data. The empirical estimate of the variation of V_s with depth and the V_s profiles based on this empirical estimate are presented in Figure 7.6. The Poisson's ratio and the unit weight of the soil used to describe the V_s profiles were 0.4 and 1.8 g/cm^3, respectively, assuming dense sands. As mentioned in previous chapters, these assumptions have an insignificant effect on the inversion process and the derived shear wave velocity profile.

7.3.3 Uncertainties related to the Initial Shear Wave Velocities

The prior covariance matrix includes prior standard deviations (σ_vs_{pr}) and correlations (given by Z_{band}). In Chapter 4, it is described how the covariance matrix is obtained, and the same steps are followed here. The prior standard deviation is taken as a constant value (i.e., equal for all layers) and 5 different cases are looked at: 30, 60, 120, 180, and 240m/s. The correlations among layers are based on Z_{band} values as described in Chapter 4. The Z_{band} value is taken as constant for each case and also five cases are proposed: 1, 5, 10, 15, and 20m.

These suggested values are a starting point and are evaluated employing the Bayesian approach as described in Chapter 5 and used in this chapter. If for the case at hand an extreme value is preferred another value may be tried. For instance, if a standard deviation of 240m/s is chosen it may be appropriate to try a higher value. Additionally, if

the best prior standard deviations for V_s are 60 and 120m/s, a reasonable option is to run the inversion for an intermediate value such as 90 m/s to compare the results.

7.4 Inversion and Evaluation of Results

7.4.1 Inversion Results

The maximum likelihood method as described in Chapter 4 was used to perform the inversion of the experimental dispersion curve and obtain potential shear wave velocity profiles with theoretical dispersion curves that match the Shelby Forest experimental dispersion curve. The theoretical dispersion curves were found using the effective dispersion curve given by the forward algorithm presented by Lai and Rix (1998). This curve includes the effect of all modes of propagation. For the synthetic examples in previous chapters only the fundamental mode was used. However, for a real case it is more appropriate to take into account the effect of all modes on the dispersion curve, since these may have an important influence in the dispersion data as discussed in Chapter 2.

Figure 7.7 shows 50 V_s profiles obtained for 50 different initial models that correspond to: (i) two different sets of layers (profiles r1 and r2); (ii) five different cases of prior standard deviation (σ_vs_{pr} of 30, 60, 120, 180, and 240m/s); and (iii) five different cases of prior correlation (Z_{band} of 1, 5, 10, 15, and 20m).
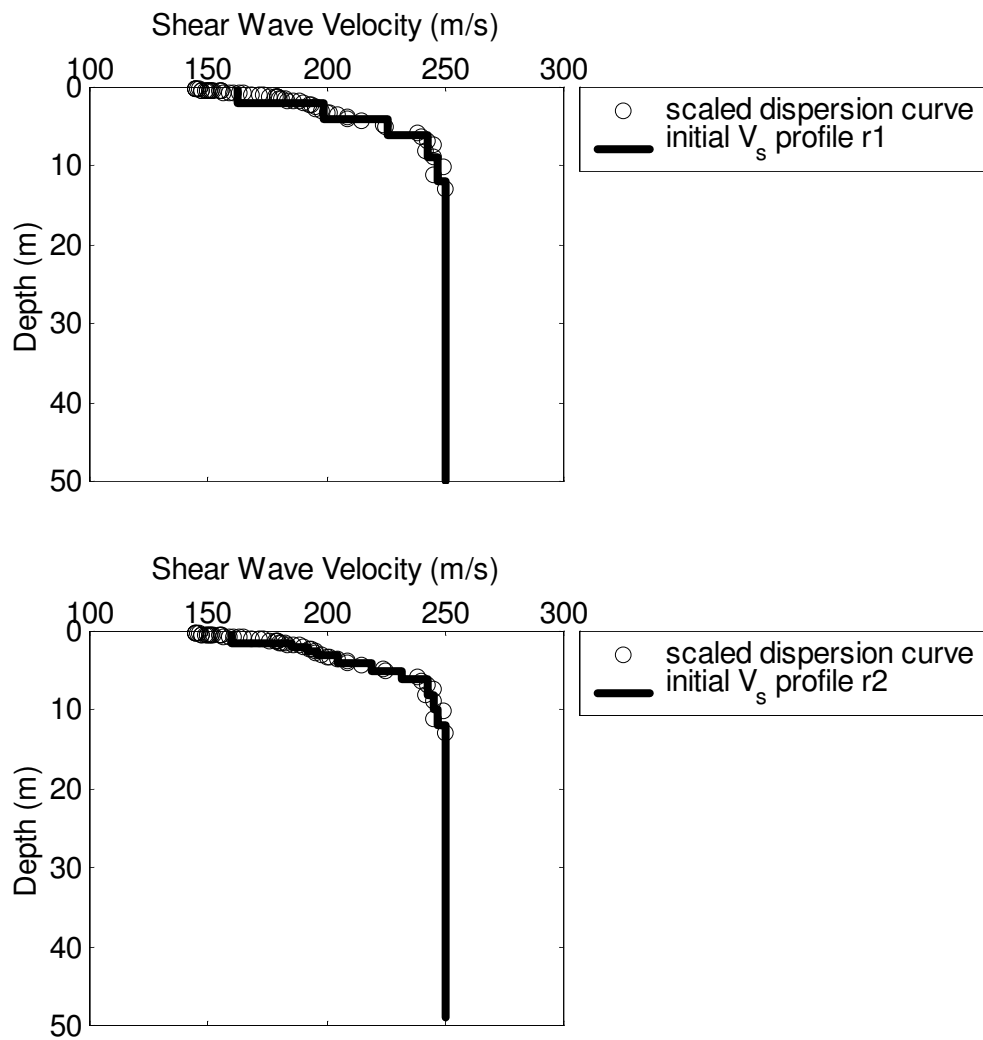
Figure 7.6 Empirical estimate of the V_s variation with depth and initial V_s profiles based on this estimate
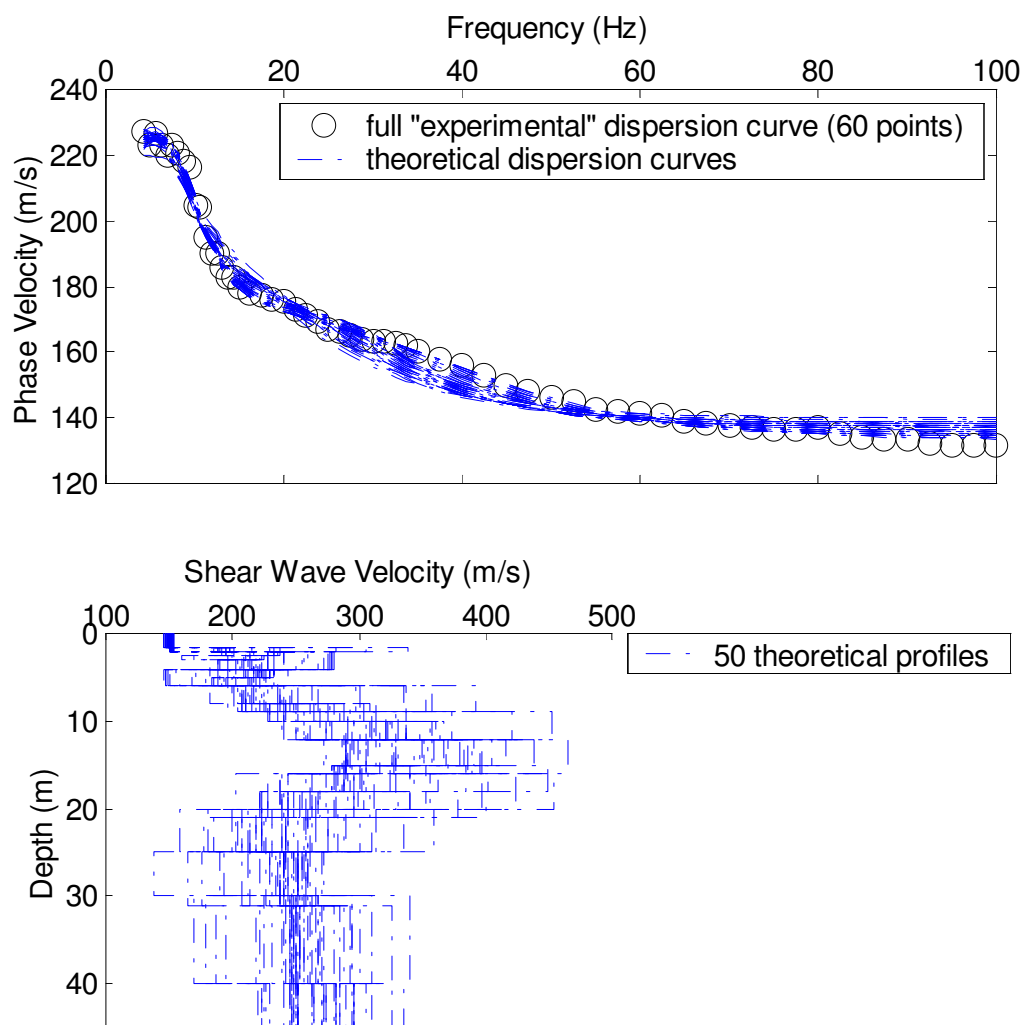
Figure 7.7 Fifty final shear wave velocity profiles obtained from inversion

For profile r1 the average time to perform the inversion for each case of initial conditions was 46 minutes in a Pentium II - 500 MHz processor. Thus, the 25 cases took around 19 hours to run. For profile r2 the average time to perform the inversion for each case of initial conditions was 94 minutes and running the 25 cases took around 39 hours.

Like in Chapter 4, the purpose of showing all the final V_s profiles in the same plot is to have an overview of the range of V_s values caused by the variation of the initial model, noting that the maximum likelihood method converged to a different V_s profile for each different initial model. The rms values of all profiles shown in Figure 7.7 vary between 0.29 and 1.21, with most profiles having an rms value below 1. As noted in Chapter 4, the range of V_s profiles illustrates that many different profiles can match the experimental dispersion curve with a low rms. Thus, it is the information added a priori, that helps find a single answer (i.e., a single answer is obtained for a specific set of values given to the prior information).

In Chapter 5, it was shown that the prior standard deviations and correlations have an influence on the standard deviatons (σ_vs) of the estimated V_s profiles. Figure 7.8 presents the inversion results obtained for profile r2 for 3 different cases of σ_vs_{pr} and Z_{band} as an example of the effect of these prior assumptions on the inversion results. This figure shows that σ_vs_{pr} has a stronger influence on the final estimated standard deviations than Z_{band}. Figure 7.9 presents the ratio of the estimated standard deviations to the prior assumption. This figure shows that Z_{band} also has a significant effect.
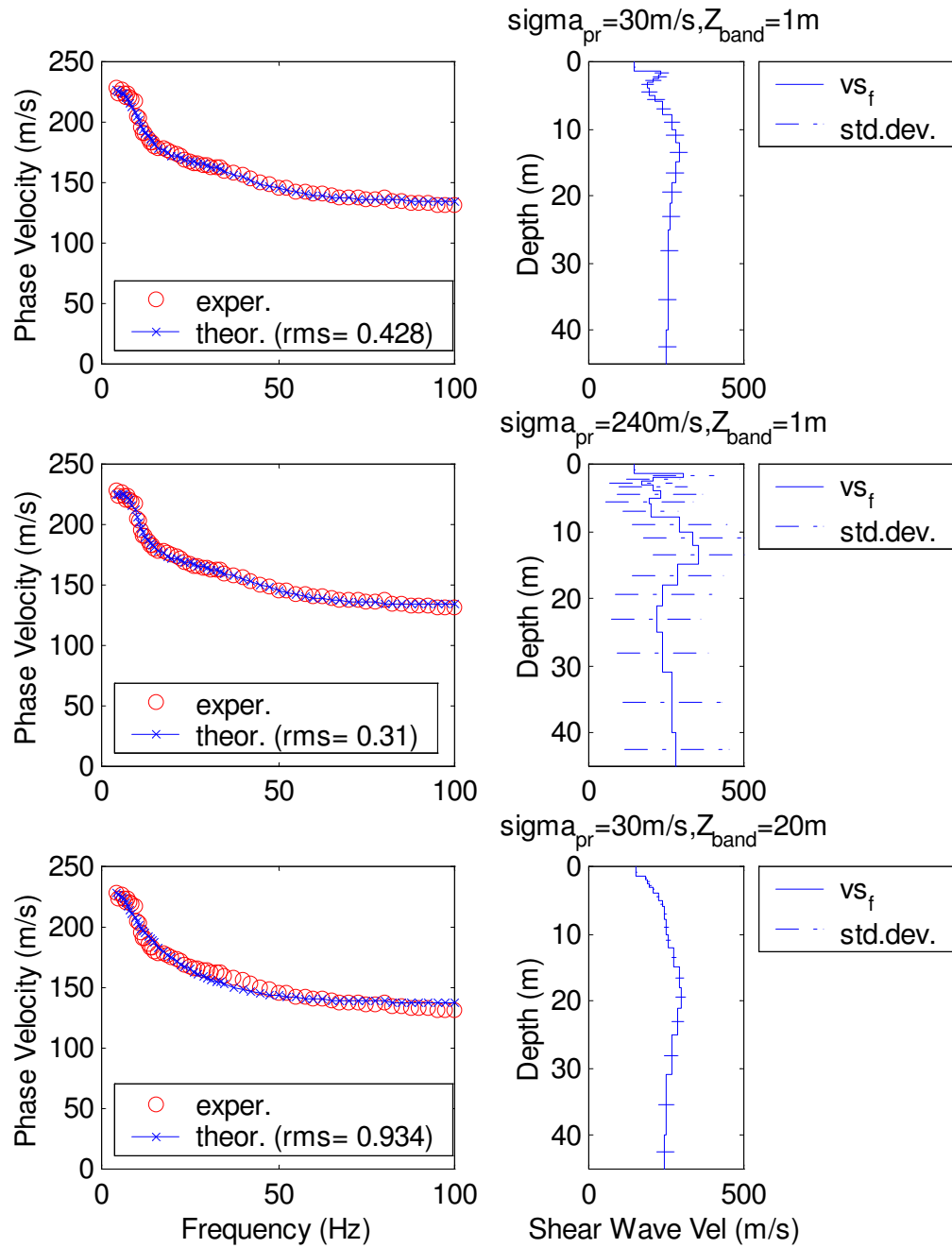
Figure 7.8 Example of the effect of prior standard deviations and correlations on the standard deviations of the final Vs profile
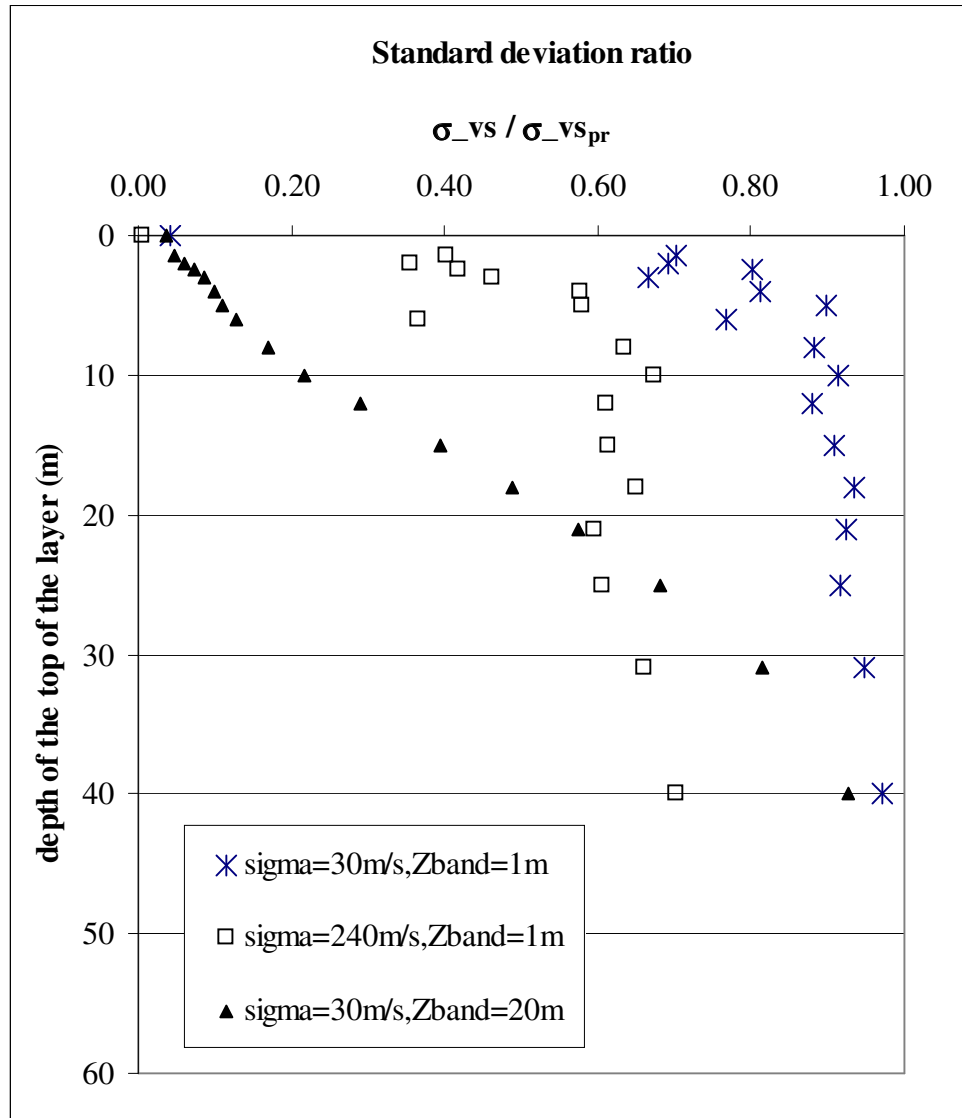
Figure 7.9 Example of the effect of prior standard deviations and correlations on the standard deviation ratio σ_vs/σ_vs_pr

In figure 7.9, note that for σ_vs_{pr}=30m/s the change of Z_{band} from 1m to 20m (i.e., the increase in the correlation values) results in a different trend for the change of σ_vs/σ_vs_{pr} with depth. The top layer and the half-space have similar values, but the variation of σ_vs/σ_vs_{pr} is smooth for the highly correlated layers, which makes these values lower for most layers. Note also that for Z_{band}=1m the change in σ_vs_{pr} from 30 to 240m/s results in a decrease of σ_vs/σ_vs_{pr} for all layers. In this case, the trend of the change of σ_vs/σ_vs_{pr} with depth is similar, but presents lower values for the higher σ_vs_{pr}. This shows that for the higher σ_vs_{pr}, which gives more flexibility to the profile, the final standard deviation were significantly higher but represented a smaller ratio of the prior assumed value. This example shows the importance of the prior assumptions which would preferably be defined based on available data for the site. When no data is available, the Bayesian criterion implemented in the next section helps choose the values that present the simplest model with a satisfactory fit to the data.

Figure 7.10 presents the rms values for the profiles in Figure 7.7. This figure shows that the rms varies with the prior standard deviation and with the prior correlation. The higher the standard deviation the lower the rms, and the lower the correlation the lower the rms. Thus, the initial conditions that gave more flexibility to the problem (with higher prior standard deviation and lower correlation among layers) resulted in lower error values. Another fact that can be observed in Figure 7.10 is that for profile r2 the rms values are lower than for profile r1. This profile produced only rms values below 1, and only 7 values out of 25 above 0.6, whether for the profile r1 all rms values were above 0.6. Thus, profile r2 converged to V_s configurations that produce better fits for the dispersion data.
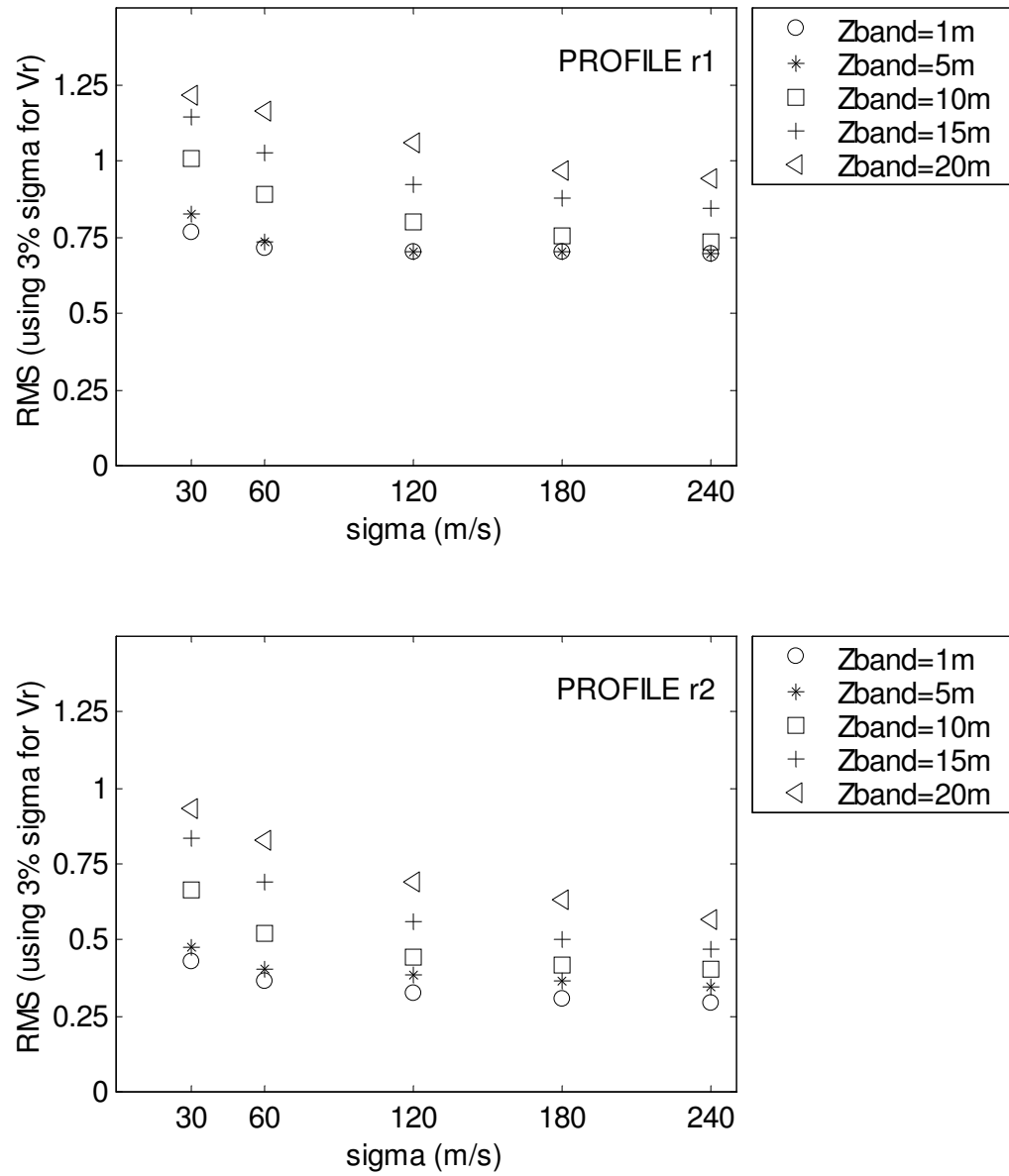
Figure 7.10 RMS error of the 50 profiles obtained from inversion

7.4.2 Bayesian Model selection

As done in Chapter 6, the Bayesian criterion was used to calculate the Ockham factor, the likelihood, and the evidence. Figure 7.11 presents these results with the evidence for each profile normalized by dividing it by the sum of evidences for fixed prior assumptions of σ_vs_{pr} and Z_{band}. As described previously, the Ockham factor favors simplicity and the likelihood favors better fits. The evidence combines the Ockham factor and the likelihood and should be greatest when the data is fitted satisfactorily with the simplest profile.

Note that the Ockham factor is lower for higher σ_vs_{pr} (better seen in Figures 7.12 and 7.13), which agrees with the fact that in general the higher the σ_vs_{pr} the less simple the profile. For Z_{band} the trend of the Ockham factor is variable depending on the value of σ_vs_{pr} (better seen in Figures 7.12 and 7.13). For this real experimental case, the differences in the Ockham factor were not significant compared to the differences in likelihood (Figure 7.11), due to the better fit in the dispersion curves produced for the V_s profiles found with the layered configuration presented by profile r2. Consequently, the profile with the highest evidence is profile r2 (Figure 7.11), which in this case is the one that has more layers (i.e., 16 layers, compared to 10 layers for profile r1).
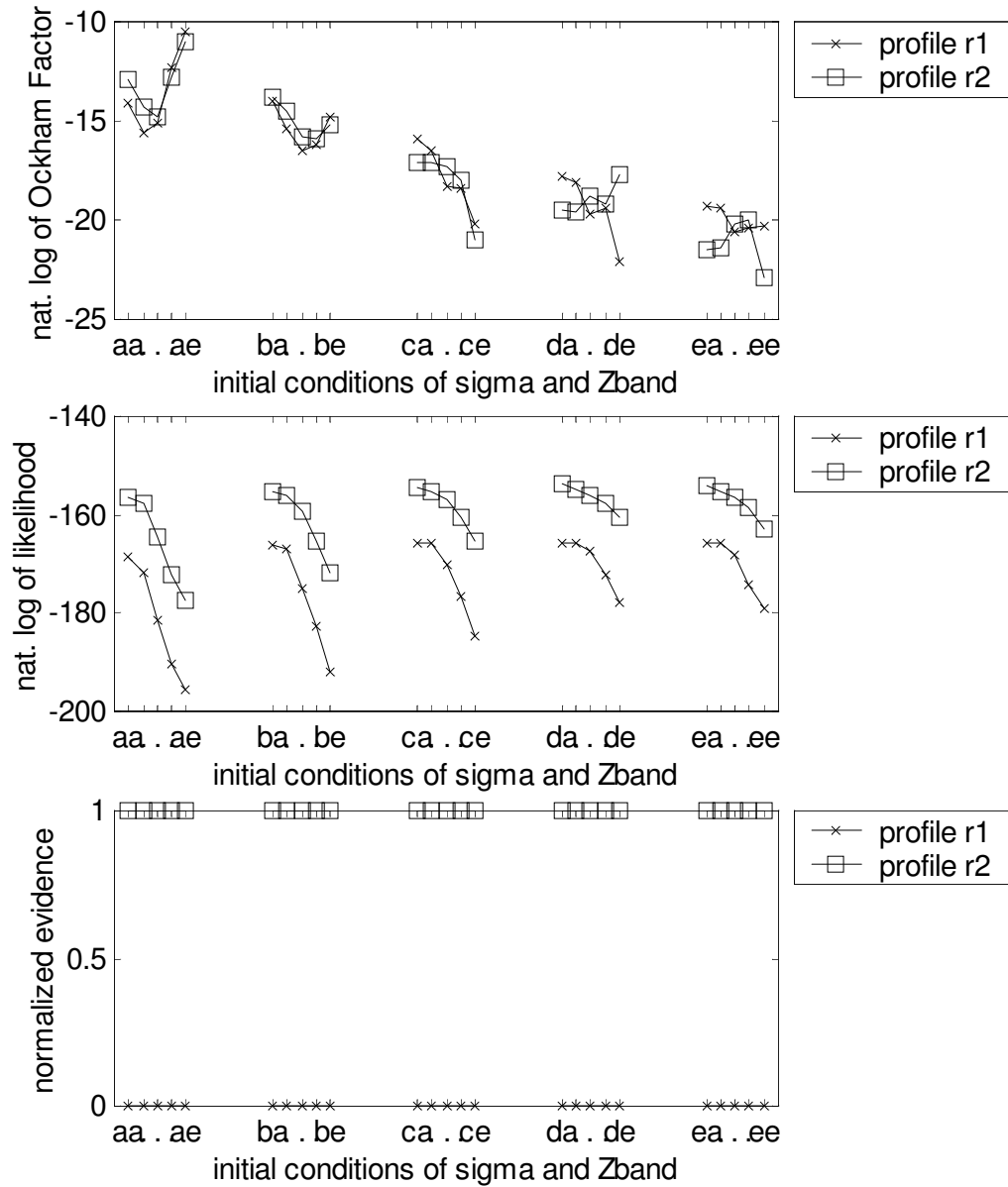
Figure 7.11 Ockham factor, likelihood, and evidence to choose the best profile
The convention for initial conditions is:
the first letter is for sigma (σ_vs$_{pr}$) with a=30,b=60,c=120,d=180, and e=240 m/s
the second letter is for Zband (Z_{band}) a=1,b=5,c=10,d=15, and e=20 m
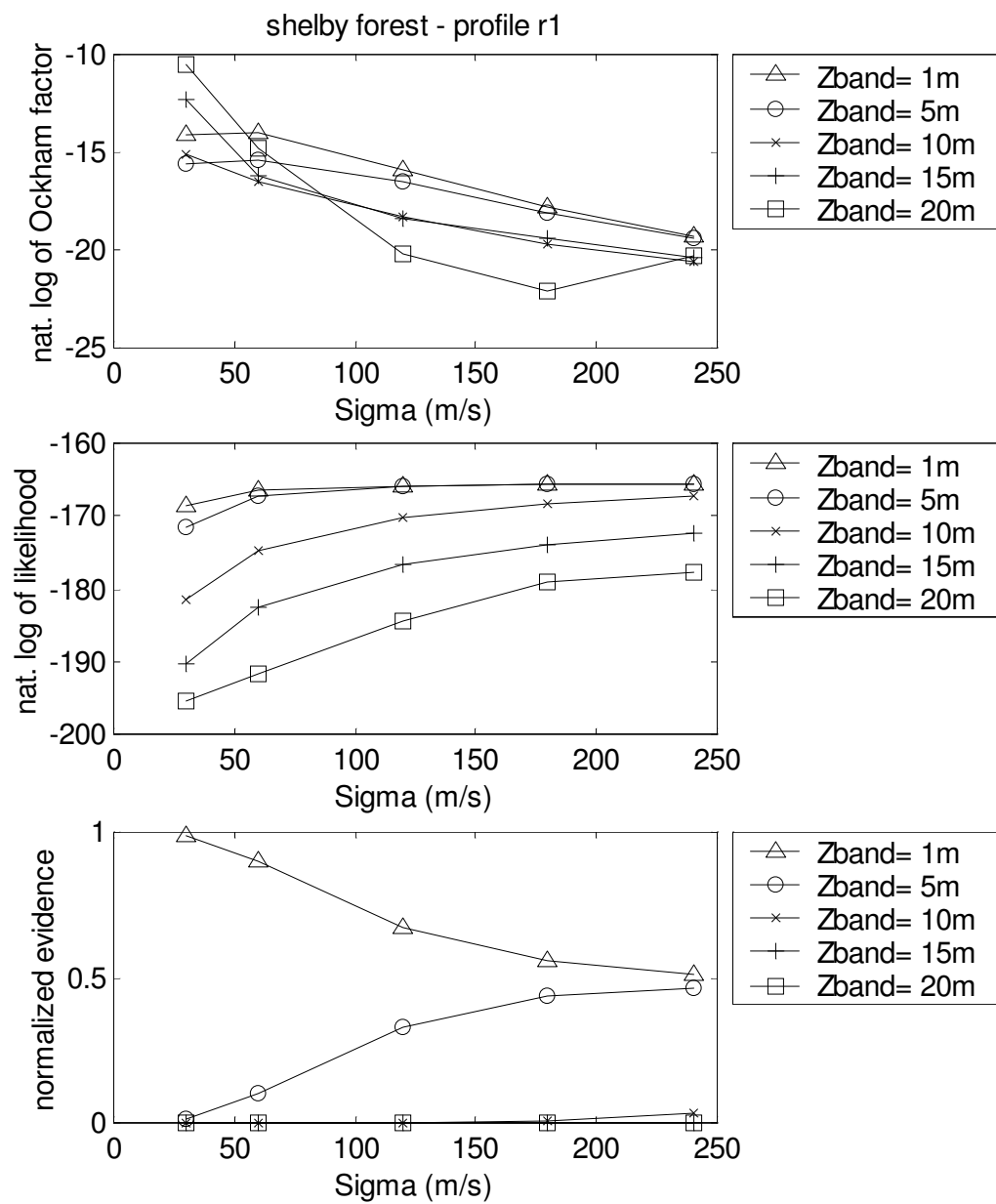
Figure 7.12(a) Ockham factor, likelihood, and evidence to choose the best Z_{band} (i.e., correlation) for profile r1
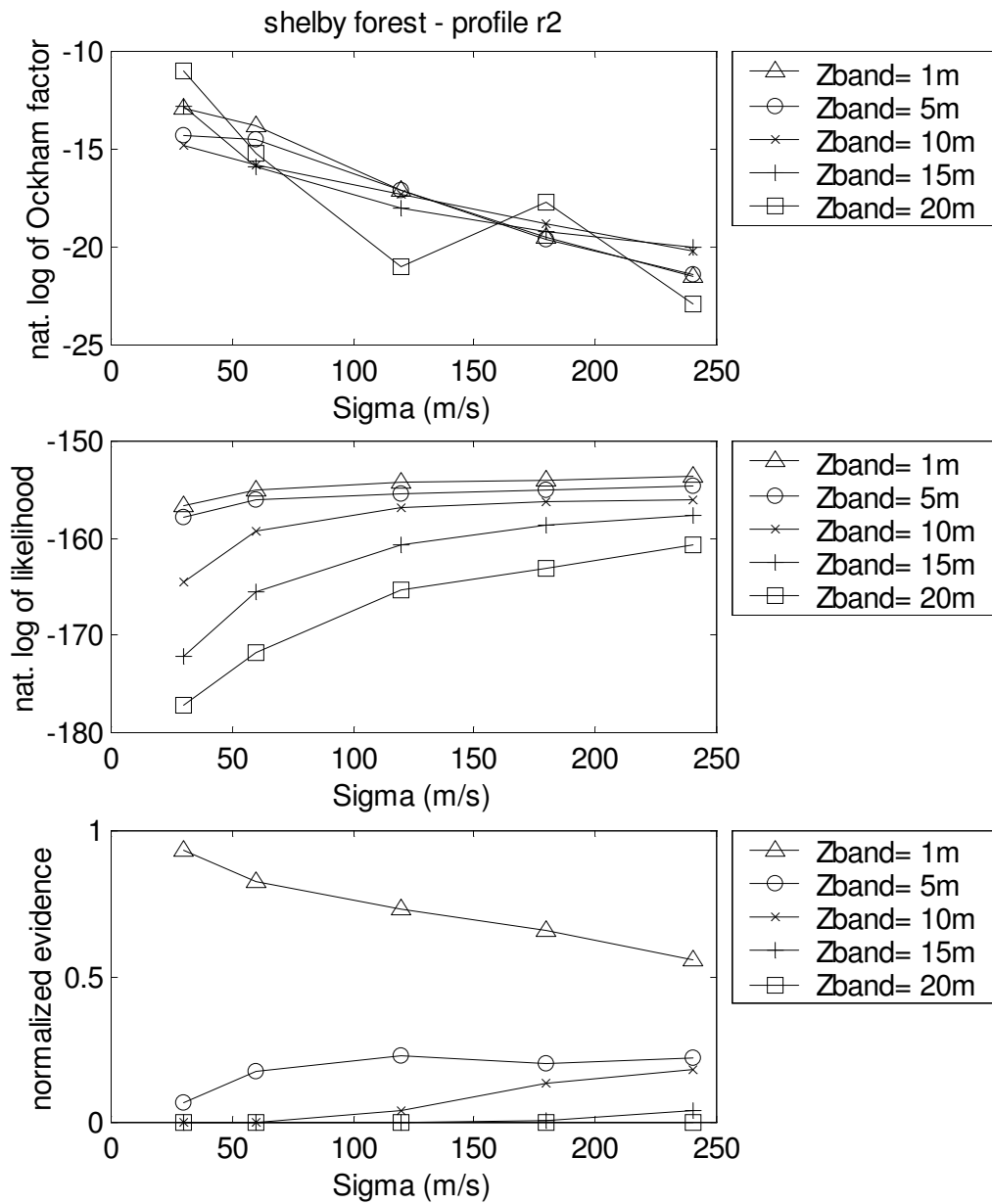
Figure 7.12(b) Ockham factor, likelihood, and evidence to choose the best Z_{band} (i.e., correlation) for profile r2
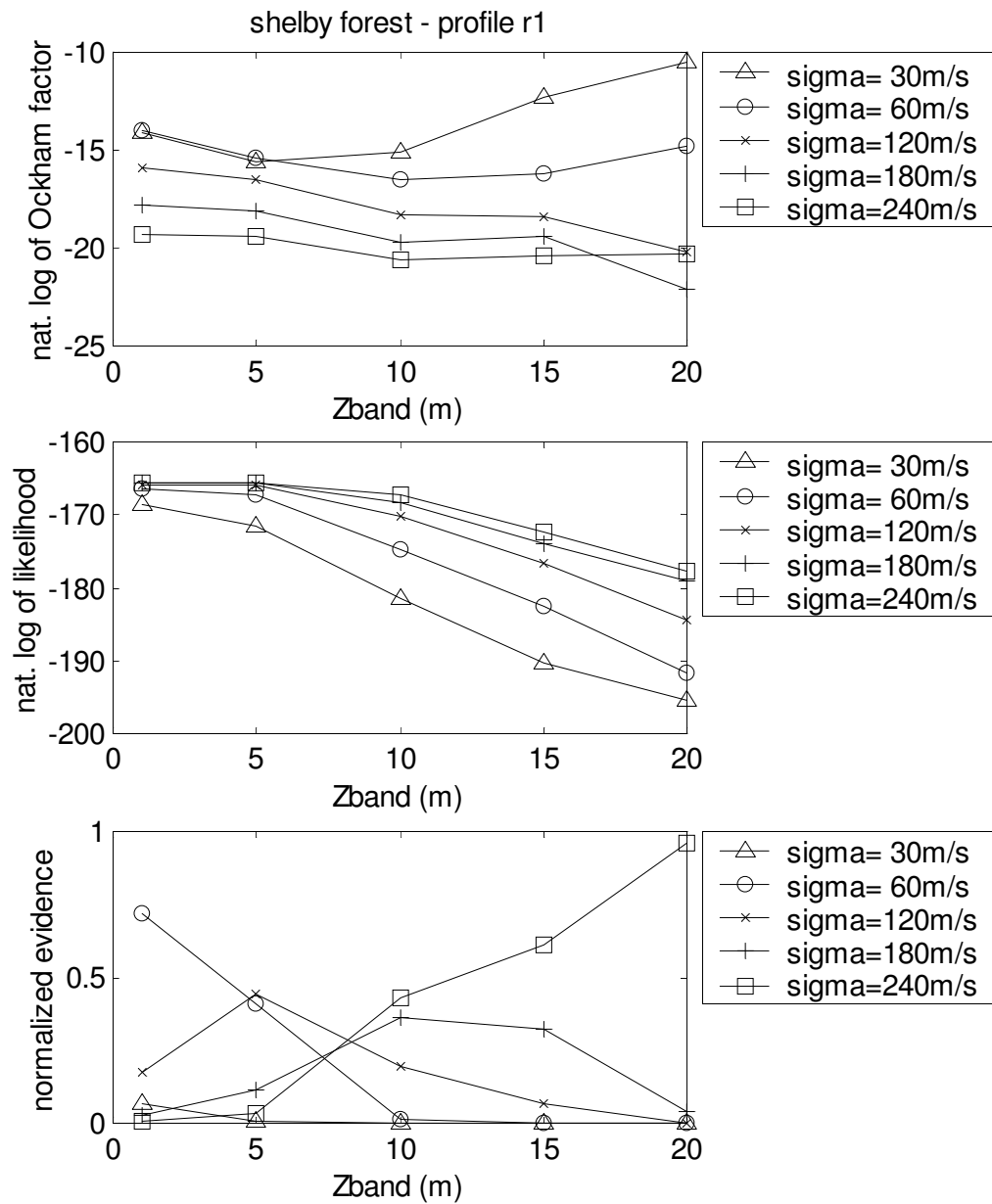
**Figure 7.13(a) Ockham factor, likelihood, and evidence to choose
the best prior standard deviation for profile r1**
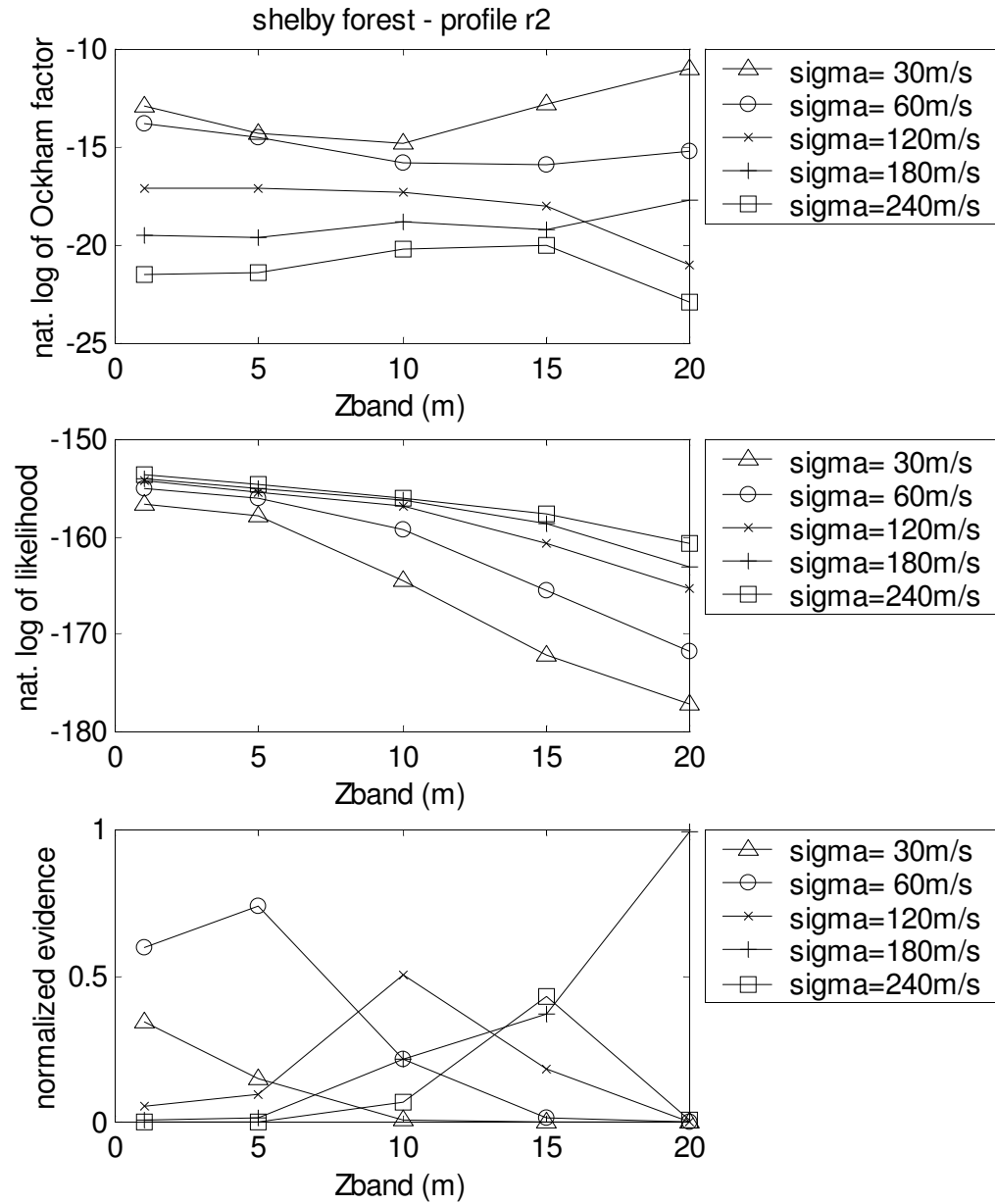
Figure 7.13(b) Ockham factor, likelihood, and evidence to choose the best prior standard deviation for profile r2

Figure 7.12 shows the Ockham factor, the likelihood and the resulting normalized evidence for each case to compare the values of Z_{band}. In this case, the evidence is normalized by dividing it by all evidences for a fixed profile and a fixed σ_vs_{pr}. For all cases the lowest Z_{band} value of 1 meter is preferred based on evidence. This value is the one that gives the least correlation and practically no correlation at all, since a Z_{band} of 1meter implies insignificant correlation for layers that have its centers distanced more than 1 meter, which is the case for most layers of the profiles presented.

Figure 7.13 shows the Ockham factor, the likelihood and the resulting normalized evidence for each case to compare the values of σ_vs_{pr}. In this case, the evidence is normalized by dividing it by all evidences for a fixed profile and a fixed Z_{band}. It can be noted that the preferred σ_vs_{pr} varies with Z_{band}, with a general trend of a higher σ_vs_{pr} preferred for a higher Z_{band}. This means that for a higher correlation, which constrains more the solution, it is better to choose a higher uncertainty, which helps give more flexibility to the solution. Table 7.1 summarizes the results of Figures 7.12 and 7.13. Since the Z_{band} chosen was clearly 1m, the best σ_vs_{pr} is chosen for this value. Thus, the σ_vs_{pr} chosen is 60m/s for both profiles.

The V_s profile chosen for layered configuration r2 with Z_{band} of 1m and σ_vs_{pr} of 60m/s is one of the cases with very low rms but not the lowest (Figure 7.10). As said before, the likelihood favors better fits and the Ockham factor favors simplicity, which makes the Bayesian approach more complete to chose the best model than just looking at the rms (i.e., the fit). The resulting V_s profiles for the initial conditions of σ_vs_{pr} and Z_{band} chosen

are presented in Figure 7.14. As concluded previously, from these two profiles the chosen by the Bayesian model selection is r2.

For the reduced dispersion curve (Figure 7.2) the resulting V_s profiles for r1 and r2 with the initial conditions of σ_vs_{pr} =60m/s and Z_{band} =1m are shown in figure 7.15. The differences in V_s between the resulting V_s profiles when using the reduced dispersion curve and when using all the data are presented in Table 7.2. For profile r1, the differences for all layers are below 8% of V_s. For profile r2, all layers present difference of 2% of V_s or less except the second layer, which presents a difference of 6% of V_s. This shows that deleting 24 points out of 60 may be feasible. Additionally, it may help in speedness and a larger number of layered models and/or initial conditions may be tried.

7.4.3 Resolution of Model Parameters

In Chapter 5, the diagonal of the resolution matrix was shown to be a valuable tool to look at the relative thicknesses of the layers of a profile. Figure 7.16 shows the diagonal of the resolution matrix for the initial conditions of σ_vs_{pr} =60m/s and Z_{band} =1m, chosen with the Bayesian criterion in the previous section (profiles shown in Figure 7.14). The resolutions for most layers of profile r1 are higher and decrease with depth with fewer jumps than for profile r2.

Table 7.1(a) Evidence results to select σ_vs_{pr} and Z_{band} for profile r1

PROFILE R1	
σ_vs_{pr}	Z_{band} **with highest evidence**
30	1
60	1
120	1
180	1
240	1
Z_{band}	σ_vs_{pr} **with highest evidence**
1	60
5	120
10	240
15	240
20	240

Table 7.1(b) Evidence results to select σ_vs_{pr} and Z_{band} for profile r2

PROFILE R2	
σ_vs_{pr}	Z_{band} **with highest evidence**
30	1
60	1
120	1
180	1
240	1
Z_{band}	σ_vs_{pr} **with highest evidence**
1	60
5	60
10	120
15	240
20	180
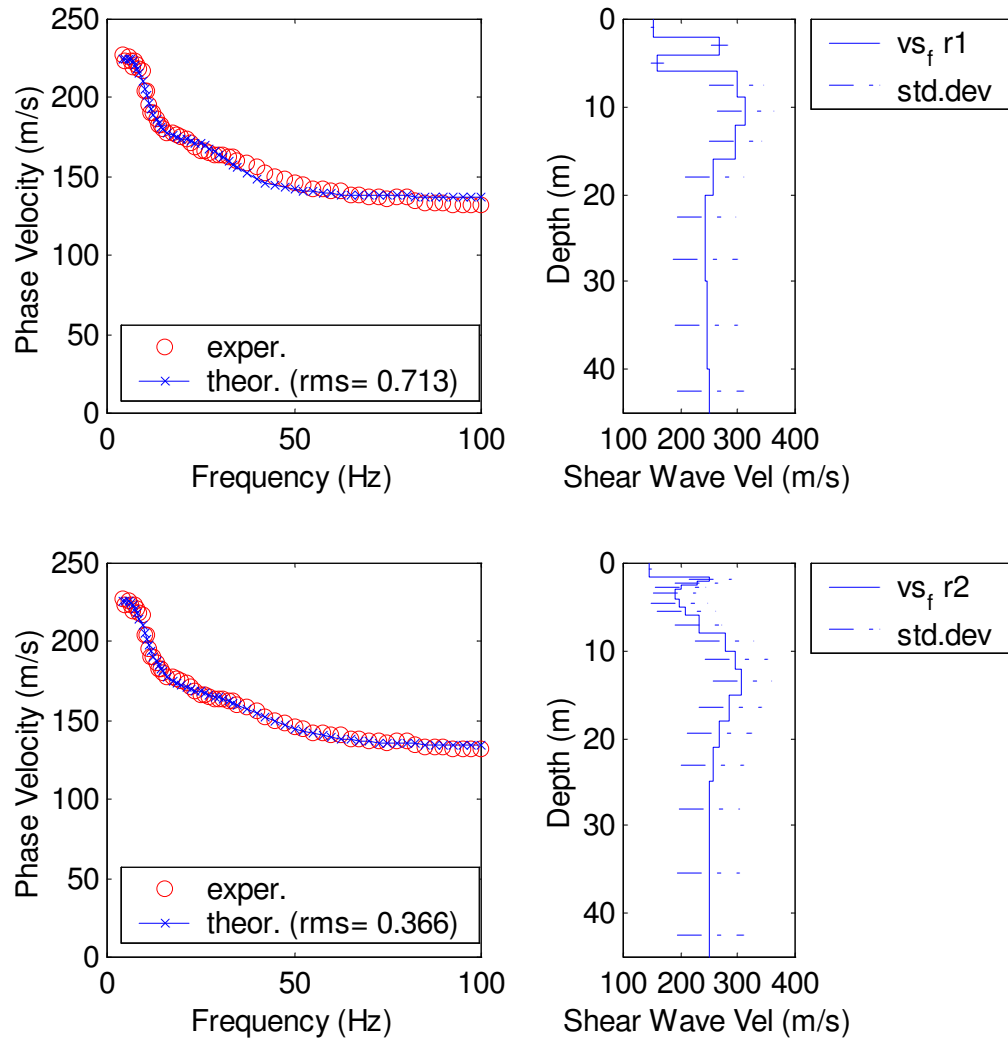
Figure 7.14 Shear wave velocity profiles obtained with chosen initial conditions
$(\sigma\_vs_{pr}=60m/s, Z_{band}=1m)$
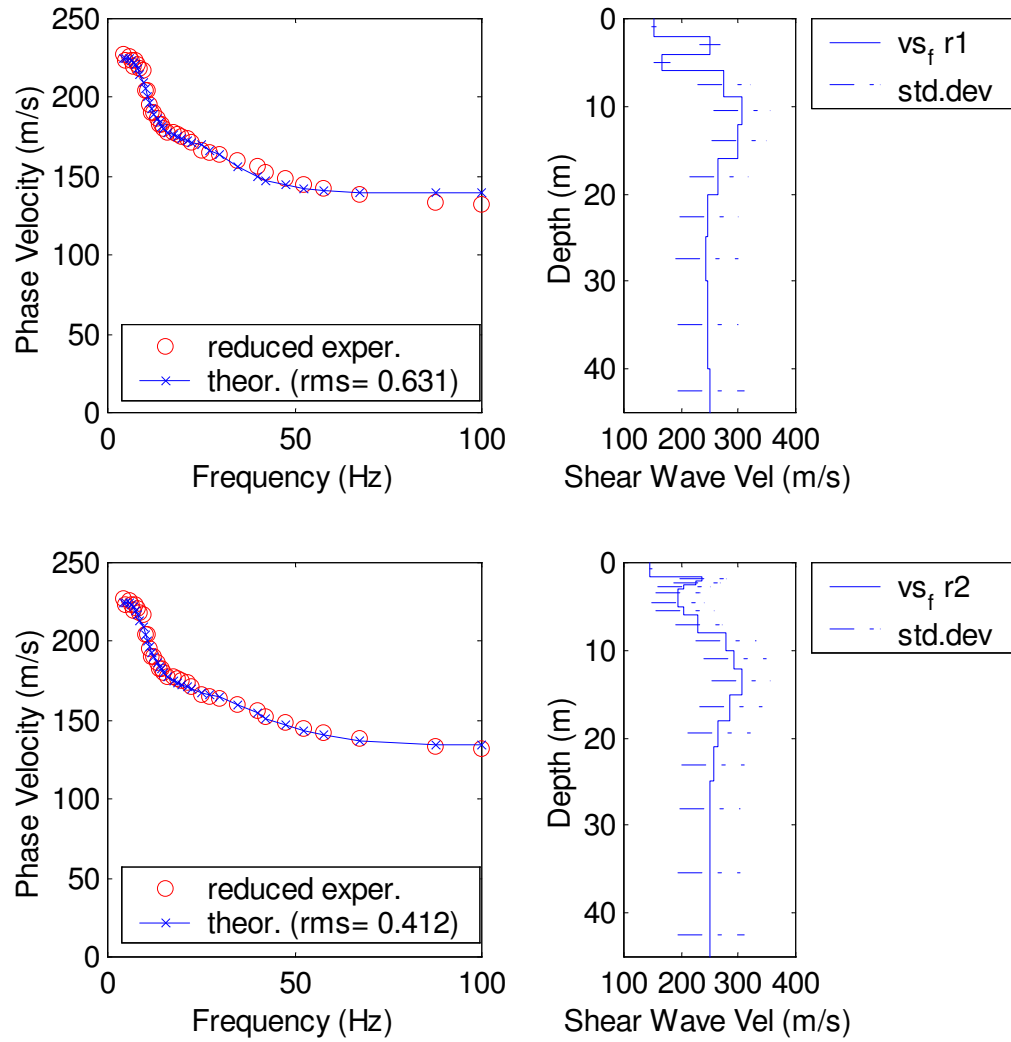
Figure 7.15 Shear wave velocity profiles obtained with chosen initial conditions (σ_vs_{pr}=60m/s, Z_{band}=1m), when using the reduced dispersion curve

Table 7.2(a) Differences in Vs for profile r1, caused by a reduction in the number of points representing the dispersion curve

Top-depth (m) PROFILE r1	V_s value for full dispersion curve	V_s value for reduced dispersion curve	$(V_{s(full\ curve)}-V_{s(reduced\ curve)})/V_{s(full\ curve)} *100\%$
0	150.8	152.4	-1%
2	268.3	251.5	6%
4	158.4	166.9	-5%
6	297.6	274.2	8%
9	312.6	305.8	2%
12	295.1	300.2	-2%
16	258.2	265.4	-3%
20	243.5	247.4	-2%
25	243.0	244.6	-1%
30	245.2	246.0	0%
40	251.3	251.2	0%

Table 7.2(b) Differences in Vs for profile r2, caused by a reduction in the number of points representing the dispersion curve

Top-depth (m) PROFILE r2	V_s value for full dispersion curve	V_s value for reduced dispersion curve	$(V_{s(full\ curve)}-V_{s(reduced\ curve)})/$ $V_{s(full\ curve)} *100\%$
0	146.8	147.1	0%
1.5	251.5	237.6	6%
2	227.6	227.3	0%
2.5	200.0	204.1	-2%
3	189.3	193.4	-2%
4	197.6	194.1	2%
5	209.3	206.2	1%
6	231.9	230.2	1%
8	276.6	277.8	0%
10	295.7	293.5	1%
12	306.0	305.5	0%
15	286.2	286.5	0%
18	267.3	265.5	1%
21	255.7	256.0	0%
25	249.8	248.5	1%
31	249.3	248.4	0%
40	251.6	251.3	0%
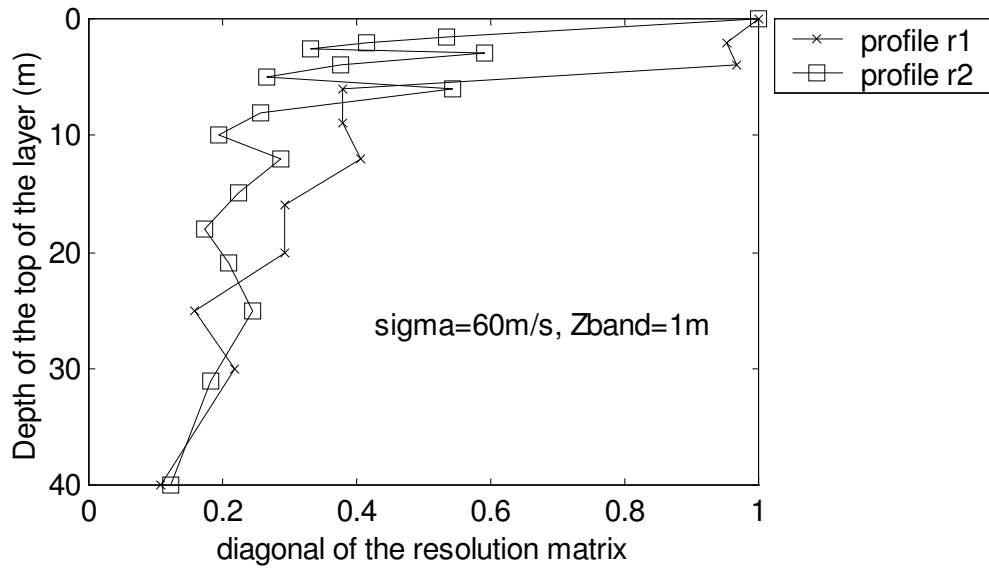
Figure 7.16 Diagonal of the resolution matrix for the shear wave velocity profiles obtained with the chosen initial conditions (σ_vs_{pr}=30m/s, Z_{band}=1m)
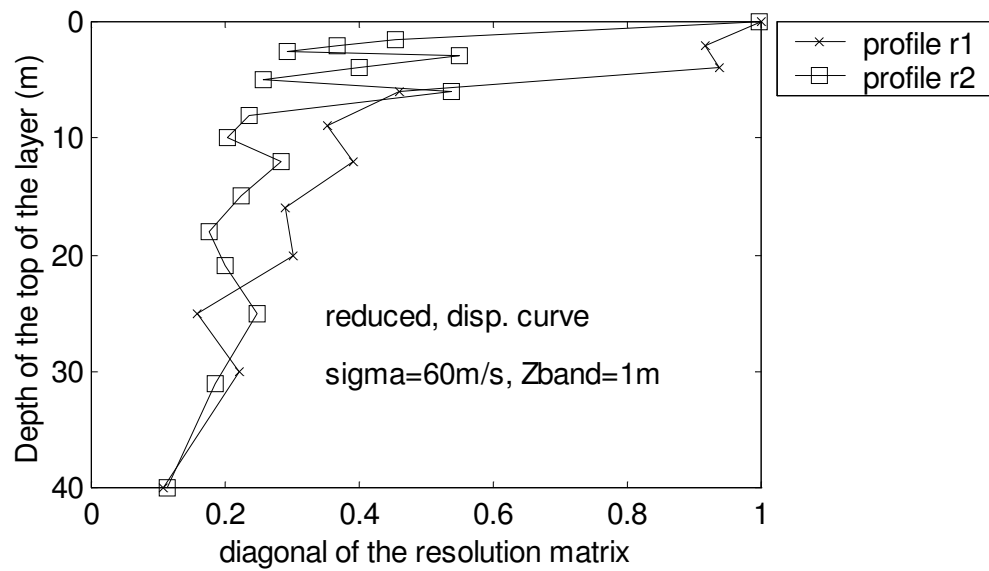
Figure 7.17 Diagonal of the resolution matrix for the shear wave velocity profiles obtained with the chosen initial conditions when using the reduced dispersion curve

As mentioned in Chapter 5 and suggested by Joh (1996), the most important characteristics are to have relatively similar resolutions among layers and a half-space with the lowest resolution value. Both profiles have these characteristics, except for the top layers with significantly higher resolution values:

♦ For profile r2, except for the top layer which cannot be much thinner due to the restriction of the minimum wavelength, the values of resolution are between 0.1 and 0.6.

♦ For profile r1 the top 3 layers have resolutions between 0.9 and 1.0 and the rest of the layers have resolutions between 0.1 and 0.5. Thus, the top layers could be replaced by thinner layers to decrease the difference in resolution among layers. However, since r2 is the profile chosen by the Bayesian approach and has a significantly lower rms, in this case it is not considered necessary to try a new profile based on modifying profile r1.

Figure 7.17 presents the diagonal of the resolution matrix for the profiles shown in Figure 7.15, which were obtained with the reduced dispersion curve. Comparing this plot with the plot in Figure 7.16, it is observed that the differences between the diagonal of the resolution obtained for the case with the reduced dispersion curve and for the case with the complete dispersion curve are not significant.

7.4.4 Half-Space Sensitivity to Maximum Wavelength

In Chapter 5, the half-space sensitivity to the maximum wavelength was shown to be a valuable tool to decide the appropriate depth to the half-space, as suggested by Joh (1996). In this case, both profiles were chosen with the same depth to half-space and it is important to check the values of the sensitivities. Figure 7.18 shows that the values of the half-space sensitivity to maximum wavelength varies slightly with Z_{band} except for the highest value of Z_{band}, which makes it vary significantly. It can also be noted that the sensitivity decreases with an increase in σ_vs_{pr}. For the profiles chosen the values fall within a reasonable range except for the highest value of Z_{band}, meeting the "higher than 1%" criterion suggested by Joh (1996).

7.4.5 Final V_s profile obtained and comparison with results from other field tests

The final V_s profile obtained is presented in Figure 7.19. The half-space is not reported since the surface waves have a limited depth of testing. The layers used are a discretization of a continuum and are not intended to be defined layer interfaces. Note that the standard deviation estimated for most layers is relatively high when compared with the initial assumption of 60m/s.
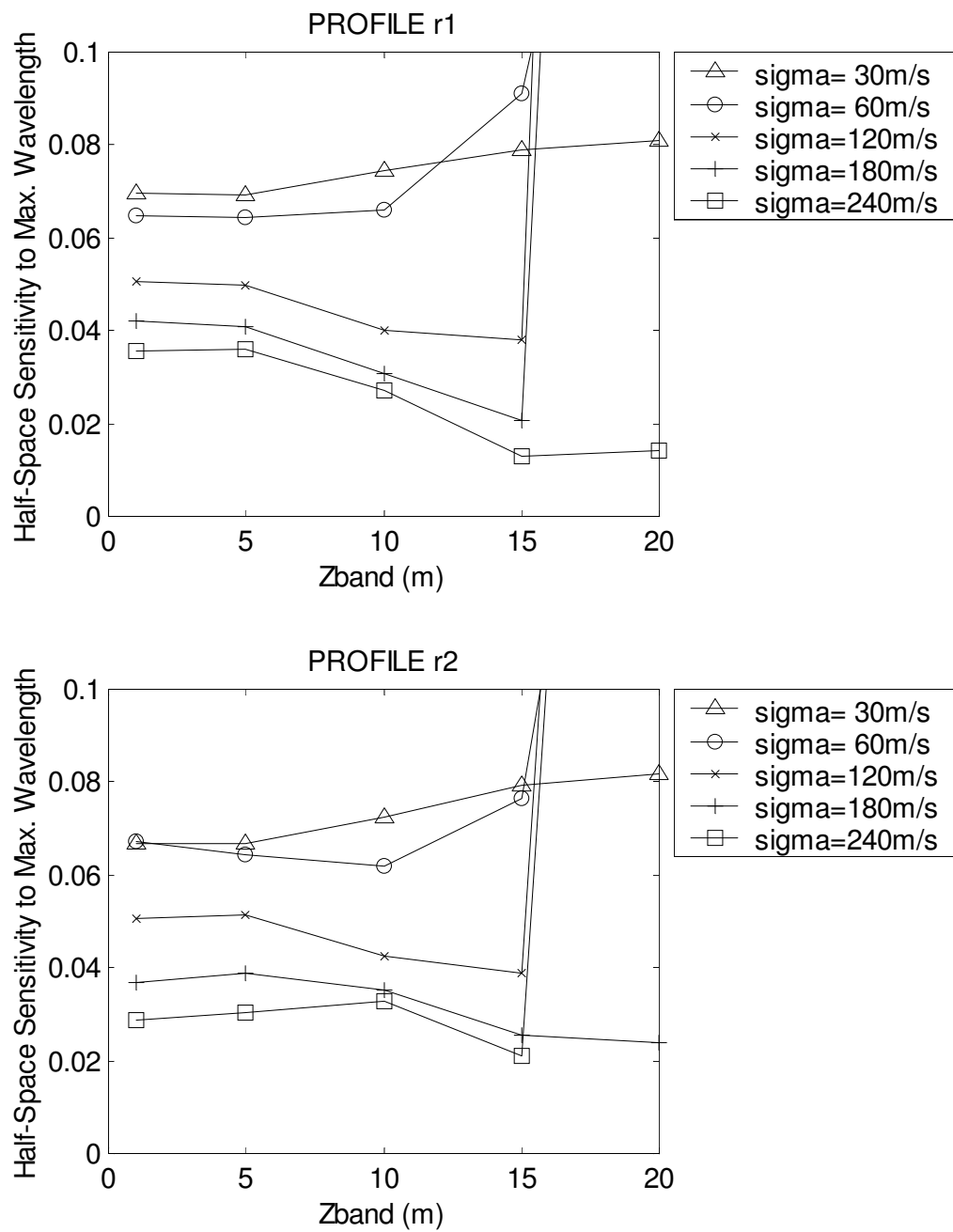
Figure 7.18 Half-space sensitivity to maximum wavelength
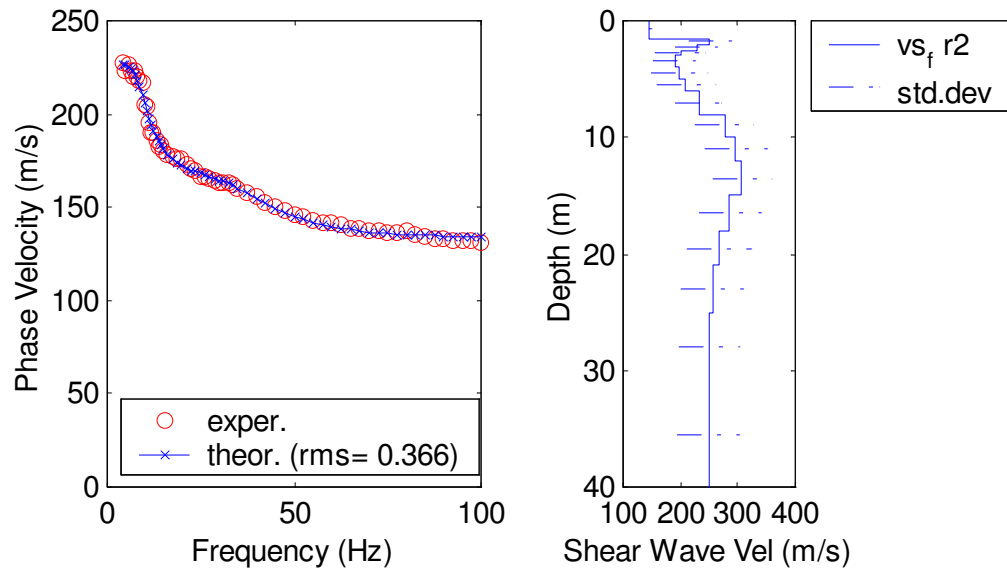
depth of top of layer (m)	depth of bottom of layer (m)	final V_s (m/s)	final V_s std. dev. (m/s)
0	1.5	147	1
1.5	2	252	36
2	2.5	228	37
2.5	3	200	44
3	4	189	37
4	5	198	47
5	6	209	51
6	8	232	41
8	10	277	52
10	12	296	54
12	15	306	51
15	18	286	53
18	21	267	55
21	25	256	53
25	31	250	52
31	40	249	54
40		252	56

Figure 7.19 Selected final shear wave velocity profile r2

Figure 7.20 presents the final V_s profile compared with V_s data obtained from other in-situ tests. The data from these other field tests was taken from Hebeler (2001) and include data from five SCPT soundings, one seismic refraction/reflection survey, and one downhole measurement. The agreement of the SASW profile with the values from the other tests is for the most part good. The most significant difference between the SASW profile presented and the data from the other tests is the high velocity layer at around 20 meters depth. The chosen profile for SASW does not include such high velocities.

This is due to the reasoning that without data from other field tests or any previous information on a site (which was the assumption here to estimate the V_s profile), it is not appropriate to report a profile with high velocity contrasts, when these contrasts are not required to fit the experimental data appropriately. For this reason the Bayesian criterion is utilized to choose the V_s profile, because it chooses the simplest one that fits the data satisfactorily. Thus, if there is data available the prior information could be based on these data to constrain the problem, but if the SASW tests are performed to find new data, it does not make sense to choose a profile with strong features that are not needed to fit the data. Doing this might give the false impression that these features are defined by the SASW experimental data when they are not.
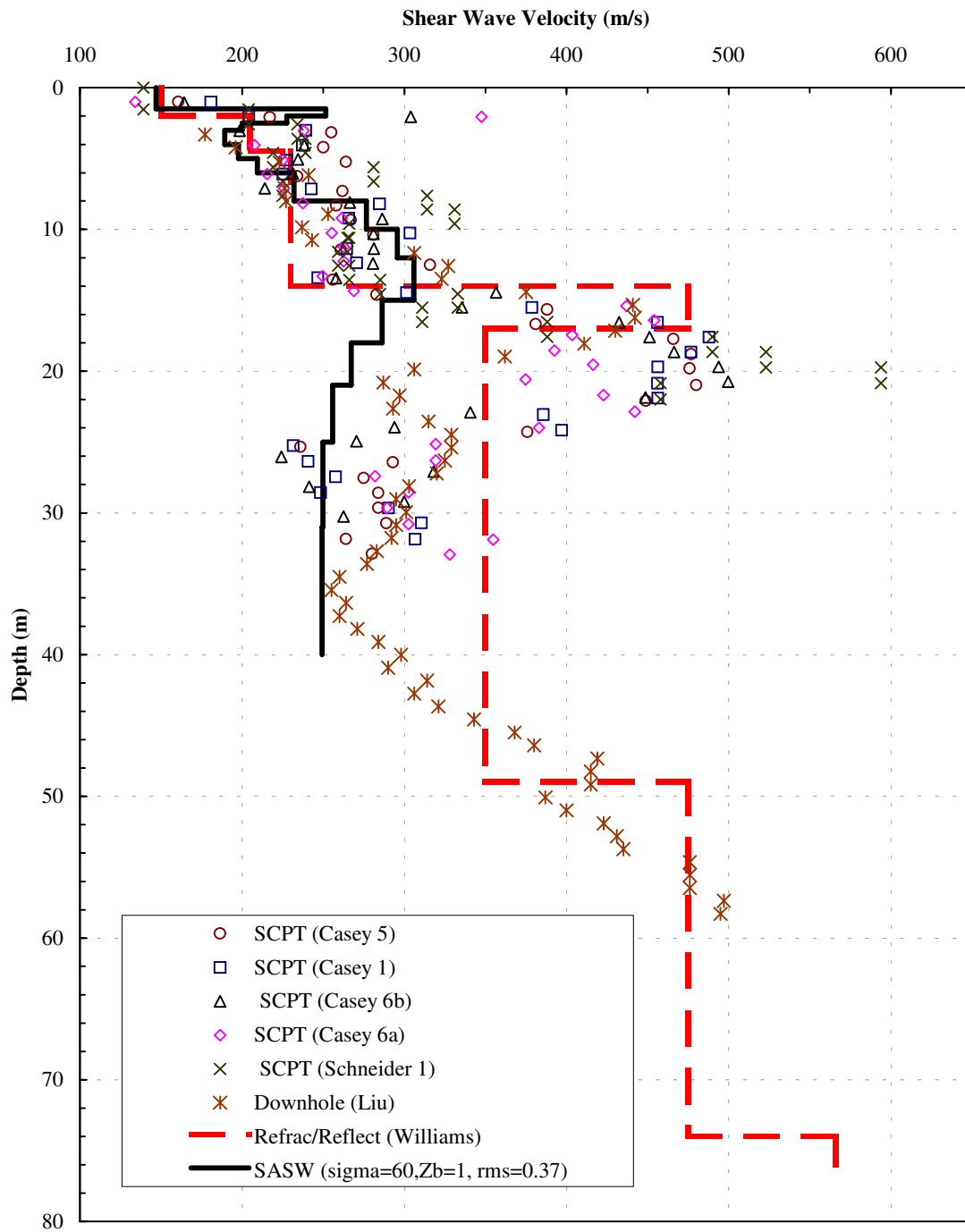
Figure 7.20 Selected final shear wave velocity profile r2 compared to data from other in-situ tests
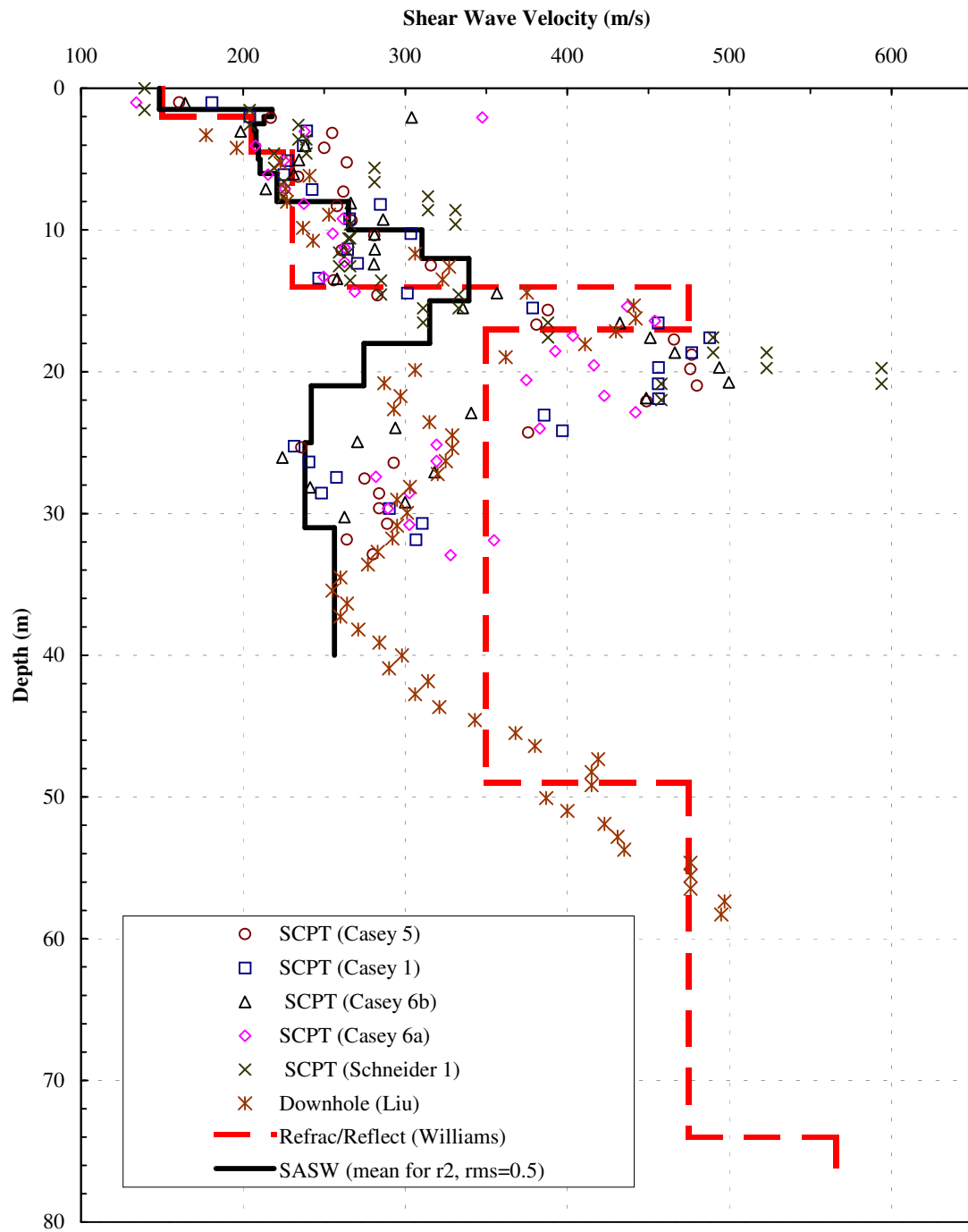
Figure 7.21 Mean shear wave velocity profile r2 compared to data from other in-situ tests, (mean based on results for 25 cases, corresponding to five σ_vs_{pr} and five Z_{band})

As mentioned before, there are many profiles that may fit the dispersion data under a specified rms criterion. Looking at the whole range of SASW profiles presented for the 50 initial models (Figure 7.7), there are V_s profiles with higher velocities than the chosen V_s profile. This whole set of profiles gives the idea of a higher velocity zone between 10 and 20 meters, with some profiles having V_s values up to 400 and 450 m/s, which are comparable to the velocities found with other tests. The mean profile of the 25 cases presented for r2 is shown in Figure 7.21. Note that this mean profile goes to higher velocities than the selected profile at around 15m depth, but it still does note include the high velocities given by other tests at around 20m depth.

7.5 Conclusions

The methods for inversion and selection of prior information presented in previous chapters were successfully used in this Chapter with real experimental data obtained in Shelby Forest (Memphis, Tennessee).

Based on the synthetic examples from previous chapters and on the real example from this chapter it is clear that trends and best values for prior information vary. Consequently, it is not possible to have recommended values that work for all cases. However, the tools that may be used to choose these values can be recommended. In this way, the prior information is not selected in a purely empirical way, but with a methodology such as the Bayesian approach, which helps choose appropriate values for

each specific case. This approach becomes more practical as trying more cases of layered profiles, standard deviations, and correlations becomes easier and less time consuming day by day with the use of faster computers.

As noted in this chapter and in previous ones, a large number of V_s profiles may fit the experimental data satisfactorily. For this reason, it is clear that SASW is not the appropriate method to find specific velocity contrasts between layers. Localized features of a velocity profile are better found with localized tests such as SCPT and Downhole methods. However, SASW can give a fast estimate of the values of shear wave velocities present at a site, and tests larger volumes of soils than localized methods.

CHAPTER 8

CONCLUSIONS AND RECOMMENDATIONS

8.1 Conclusions

This research focused on the inversion of SASW dispersion curves to obtain shear wave velocity profiles. It is common to present the inverted V_s profile as a unique profile without showing a range of possible solutions or some type of error bars, such as the standard deviations of the V_s values of each layer. Additionally, the person performing the inversion usually assumes the prior information required to constrain the problem based on his or her own judgment. Implementing an inversion method that includes estimates of the standard deviations of the V_s profile and finding tools to choose the prior information objectively were the main purposes of this research.

To perform SASW inversion, one global and one local search procedures were presented and employed with synthetic data: a pure Monte Carlo method and the maximum likelihood method. The synthetic data was produced with the same forward algorithm used during inversion. This implies that all uncertainties are caused by the nature of the SASW inversion problem alone since there are no uncertainties added by experimental errors in data collection, analysis of the data to create the dispersion curve, layered model to represent a real 3-D soil stratification, or wave propagation theory.

The pure Monte Carlo method was chosen to study the non-uniqueness of the problem by looking at a range of acceptable solutions (i.e., V_s profiles) obtained with as few constraints as possible. It is important to note that this method requires large amounts of time to obtain V_s profiles with low rms error. Based on the variety of shapes found for V_s profiles with satisfactory rms, the non-uniqueness of SASW inversion was evident, concluding that the dispersion curve does not constrain the solution sufficiently to determine a unique V_s profile or to resolve specific velocity contrasts between layers. Consequently, if the best fitting profile is reported, it may mislead the user of the V_s profile to believe in specific V_s contrasts that are unnecessary to fit the experimental data. Thus, in examining the entire set of satisfactory profiles, it was of interest to determine if the V_s values of each layer were normally distributed and if the mean and the standard deviation were valid parameters to characterize all satisfactory V_s profiles that meet the chosen rms error criterion. This was confirmed by plotting the data in normal probability plots. For this reason, the mean and standard deviation were chosen to present the range of solutions obtained with Monte Carlo inversion, and the use of a least-squares method such as the maximum likelihood was considered appropriate.

The estimated coefficients of variation for the profiles with rms<1.5 for the most constraining V_s limits were between 20% and 30%, except for the very top layers, where lower values were obtained. These uncertainties are the ones caused by the nature of the SASW inversion problem alone.

The maximum likelihood method was also chosen because it is a statistical approach, which enables one to estimate the uncertainties of the resulting model parameters and to apply the Bayesian criterion as a model selection tool. Two synthetic examples were implemented for several frequency distributions of the dispersion data, different initial models obtained by varying the number and thicknesses of the layers, and different values of the standard deviations and correlations of the shear wave velocities. The results obtained showed that the inversion converged to different estimates of the V_s profile for different initial models, and that a close match to the experimental dispersion curve can be obtained with a large number of V_s profiles. For this reason, it is important to recognize that the dispersion curve does not have the information to resolve individual layers and the solution is highly dependent on the prior information added to constrain it. Consequently, it is of interest to identify objective techniques to choose this prior information, and the final layered V_s profile should be interpreted as a discrete model, which is one possible representation of the real V_s variation with depth and should include uncertainties for the estimated V_s values.

Based on the results from the maximum likelihood method, the effect of a number of factors that influence the resulting V_s profile obtained from the inversion of SASW data was studied. These factors can be divided in two main types: (i) characteristics related to the experimental dispersion curve and (ii) characteristics related to the initial shear wave velocity profile. Since assigning these characteristics is required to perform the inversion, it is necessary to find ways to select them objectively. A summary of the reasons for the

effects of these factors and some guidance on how to most appropriately select their values is presented below.

(i) Characteristics related to the experimental dispersion curve

♦ *number and distribution of data points describing the experimental dispersion curve*

The points describing the dispersion curve represent the frequencies measured in the field, and give information on the wavelengths of the surface waves that sampled the soils. It can be considered that a layer was not sampled by wavelengths shorter that the depth to the top of the layer. Counting the number of waves that sampled each layer gives an idea of the amount of experimental information available for each layer and emphasizes the difference in information content among layers. Part of the difference is inevitable due to the nature of the problem, since a long wavelength that penetrates a deep layer also has significant particle motion in all layers above it.

It is recommended to examine the dispersion data in the wavelength domain and to select a distribution that does not weight some wavelength ranges excessively compared to others. The best option would be to calculate the dispersion curve during the field test and use it as a reference to acquire additional experimental data for the wavelengths needed. Having a distribution that weights more

similarly different wavelengths ranges is important not only to have similar amounts of information for different depths as noted above, but also because the rms error weights equally all dispersion points used to represent the dispersion curve. This means that wavelengths ranges represented by a large number of dispersion points are weighted more heavily in the error calculation than wavelength ranges represented by only a few points. This is an important issue because the effect of the distribution of the points on the value of the rms error may be significant and this error is a measure of the goodness of a V_s profile.

♦   *uncertainties of the experimental dispersion data*

The uncertainties assigned to the experimental data affect the results obtained from the inversion because the larger the uncertainties, the less the dispersion curve constrains the solution. Thus, it is important to have a realistic estimate of the uncertainties of the phase velocity. Conversely, if the uncertainties of V_r are too small, they might constrain the problem too much, increasing the rms error values and making it difficult to find a V_s profile with a satisfactory rms error. As discussed in Chapter 3, based on experimental data presented by Tuomi and Hiltunen (1997), V_r uncertainties of 3% of the experimental phase velocities are considered reasonable for SASW tests.

(ii) Characteristics related to the initial shear wave velocity profile

First, it is important to clarify that the values related to the shear wave velocity profile (i.e., thicknesses and depths of the layers, depth to half-space, initial V_s values, and prior standard deviations and correlations for V_s) should be based as much as possible on independent data available for the site. If there are different values for the prior information that need to be compared, it is assumed that all cases presented are equally probable, and the main purpose is to select the simplest V_s profile that includes an estimate of the standard deviations of V_s, and presents a satisfactory fit to the experimental data. Additionally, the suggestions given below have the purpose of producing a V_s profile with characteristics that reduce the difference in information content between layers and result in more similar resolutions for all layers.

♦ *depths and thicknesses of the layers*

Depending on its thickness and depth, a layer will be sampled differently by the surface waves measured during the field test. Thus, the number of waves that sample a layer depend on both its thickness and depth and the distribution and number of points that represent the dispersion curve. For a specific set of experimental data the layers may be chosen in such a way that the difference in information available for the different layers is reduced. It is recommended that

the number of waves sampling the layers should reduce with depth without having consecutive layers sampled by the same number of waves.

Since the information content necessarily decreases with depth, the deeper the layer the less information there is on it and the more difficult it is to resolve its V_s value. A lower resolution is reflected in a higher coefficient of variation. It was noted that the coefficient of variation decreases with the thickness to depth ratio multiplied by the number of waves sampling the layer. Thus, increasing the thickness of a layer at a specified depth or increasing the number of waves sampling the layer may help resolve the layer better and reduce its uncertainty. For the cases presented, the plots show that the coefficient of variation is limited to below 25% for thickness to depth ratio multiplied by the number of waves sampling the layer of at least 8.

As suggested by Joh (1996), the diagonal of the resolution matrix may be used to compare the resolution of the layers and vary their thicknesses (i.e., increase the thickness to increase resolution, or decrease the thickness to decrease resolution). He suggests that the thickness of the layers increases with depth to reflect the decrease in resolution with depth and that the layers selected result in a resolution variation with depth that minimizes the difference in resolution among layers as much as possible.

It is recommended that different profiles that comply with the above suggestions be compared with the Bayesian criterion for model selection. The Bayesian criterion is a valuable tool to compare and choose among different layered configurations. This criterion ranks the configuration giving preference to the simplest profile with a satisfactory match to the experimental dispersion data.

♦ *Depth to half-space*

The half-space should be sampled at least by one of the waves measured in the field and contained in the experimental dispersion data. Thus the depth to half-space should be less than than the maximum wavelength. Additionally, since the half-space continues to an infinite depth and the information available is for a limited depth, this unrealistic layer should have the lowest resolution of all and should not be included in the reported V_s profile. Other than having the lowest resolution, the half-space sensitivity to the maximum wavelength may be used to check the appropriateness of the depth to the half-space. This sensitivity should not be extremely low because this would mean that the half-space is not well defined by the experimental data. Based on the fact that the sensitivity represents the change in V_r that would occur with a change in V_s, Joh (1996) proposes to use a minimum value criterion of 1% (or another value considered reasonable) for the half-space sensitivity to the maximum wavelength. This criterion could be complemented by a maximum value such as 10% (or another value considered reasonable) The sensitivity should not be too high to avoid having the half-space

control the solution (i.e., a very shallow half-space might affect significantly the phase velocities of the wavelengths that penetrate the layers adjacent to the half-space, and their shear wave velocities might not be resolved properly).

♦ *initial shear wave velocities*

The initial estimate of the shear wave velocity profile is important due to the nonlinear nature of the problem because the inversion algorithm, which is an iterative process based on gradient methods, requires a good intial estimate to converge properly. Consequently, if the initial shear wave velocities are far from the actual, (but unkown) values, the algorithm may not converge to a desirable solution. For the maximum likelihood method, simple initial estimates with constant initial V_s values resulted in the algorithm converging to final V_s profiles with high rms values for the cases presented. Thus, it is suggested to employ initial V_s estimates based on the empirical method, which help the algorithm converge to reasonable solutions to the inversion.

♦ *standard deviations and correlations of the shear wave velocities*

It was shown that the prior standard deviations (σ_vs_{pr}) and correlations (given by Z_{band}) assigned to V_s have a significant influence on the range of final V_s profiles obtained and on the standard deviations of the estimated V_s values. A lower σ_vs_{pr} and a higher Z_{band} (i.e., which favors smoother profiles) constrain more the

solution, resulting in a smaller range of V_s values for different layered profiles and in smaller estimated standard deviations for V_s. A higher σ_vs_{pr} and a lower Z_{band} give more flexibility to the solution, resulting in a larger range of V_s values, and in larger estimated standard deviations for V_s. The estimated standard deviations for shallow layers are not affected by their value prior to inversion, but for the deeper layers the standard deviations of the solution approach this initial guess. It is relevant to note that if the final estimated uncertainty is the same as the prior assumption there was no information in the inversion process that helped reduce the prior uncertainties.

Since this prior information required to constrain the solution to the inverse problem affects the resulting V_s profile, it is important to have a tool that helps choose this information. The Bayesian criterion is a valuable tool to compare and choose among different values for the prior standard deviations and correlations given to V_s. This criterion ranks the prior information giving preference to the prior values that result in the simplest profile that presents a satisfactory fit to the data. Thus, the Bayesian criterion should be implemented to compare different parameterizations (i.e., layered configurations) and prior information (i.e., standard deviations and correlations of V_s), that are considered equally probable and select among them. The model selection is accomplished by calculating the evidence, which combines the Ockham factor and the likelihood. The first favors simpler models, and the second favors hypotheses that fit the data better. Thus, the evidence helps find the simplest model that satisfactorily fits the data.

The Bayesian criterion was used for the synthetic results obtained with the maximum likelihood method and was shown to be a valuable tool to compare different parameterizations (i.e., layered configurations) and prior information (i.e., standard deviations and correlations of V_s), and select among them. This was accomplished by calculating the evidence, which combines the Ockham factor and the likelihood. The first favors simpler models, and the second favors hypotheses that fit the data better.

The maximum likelihood method of inversion was also used with real experimental data obtained in Shelby Forest (Memphis, Tennessee). Initially, the distribution of the dispersion data was used to select two layered configurations for the real case by examining the number of waves that sampled each layer. Then, the Bayesian criterion was succesfully used to select the simplest profile that presented a satisfactory fit to the data among 50 cases corresponding to two layered configurations, five values of prior V_s standard deviations, and five values of prior correlations for V_s. This was complemented with the comparison of the resolution of the layers, and the half space sensitivity to the maximum wavelength, which were appropriate for the selected case.

Based on the synthetic and the real examples, it was clear that trends and best values for prior information vary. Consequently, it is not possible to have recommended values that work for all cases. However, the tools that may be used to choose these values can be recommended. In this way, the prior information is not selected in a purely empirical way, but is chosen with a methodology such as the Bayesian approach, which helps choose

appropriate values for each specific case. This approach becomes more practical as trying more cases of layered profiles, standard deviations, and correlations becomes easier and less time consuming with the use of faster computers.

In summary, the common and simple way to compare the inversion results is by looking at the rms error. However, when there are a large number of cases that fit the data satisfactorily under a specified rms criterion (i.e., rms<1.0), the selection of the best profile is not obvious. Choosing the lowest rms value may not be appropriate because it may imply choosing a model that includes characteristics that are not necessary to fit the data. The Bayesian model selection was shown to be a valuable method that has the ability to select the simplest profile that produces a good fit to the data. This is based on the concept that the model used to represent the V_s variation with depth should not include features that are not necessary to fit the data. Other tools that help compare the inversion results such as the resolution matrix and the partial derivatives do not take into account the simplicity of the profile or the fit to the data. These tools are appropriate to compare different layered configurations but do not help compare among different assumptions of the prior standard deviations and correlations of V_s. Thus, the layered configurations may be chosen using the criteria mentioned for information content, for the resolution of the layers, and for the sensitivity of the half-space to the maximum wavelength, and the configurations that meet these criteria may be compared with the Bayesian approach. Additionally, this criterion will help compare among the prior standard deviations and correlations for V_s.

Finally, it is essential to remember that a large number of V_s profiles may fit the experimental data satisfactorily. For this reason, it is clear that SASW is not the appropriate method to find specific velocity contrasts between layers. However, SASW is able to produce data that gives an estimate of the range of V_s values for the soils tested. The advantage of surface wave test is that it can be performed in a short period of time due to its non-invasive nature, tests larger volumes of soils than localized methods, and gives reasonable estimates of the shear wave velocities. However, if localized features of the V_s profiles are needed, localized tests such as SCPT and Downhole methods are more suited for those tasks.

8.2 Recommendations

For the synthetic examples and the real case presented it was shown how the reduction in the number of points that represent the dispersion curve is a viable option that does not necessarily decrease the accuracy of the inversion results obtained. Representing the dispersion relation with fewer points may reduce the time required by the inversion due to the smaller matrix of partial derivatives to be calculated in each iteration. The time savings can be significant especially when evaluating different parameterizations and prior information. Thus, it is recommended that future work should study this issue in more detail to implement a method that would help select the points used to represent the dispersion curve in order to optimize their distribution with as few points as possible.

The points that represent the dispersion characteristics of a site needs to be selected carefully to have: (i) sufficient data to include all important features of the dispersion curve, and (ii) a good balance of information content to resolve the V_s of the layers based on similar amounts of information and have a fairly weighted rms error that gives a good measure of the fit between theoretical and experimental data. The suggestion given here to compare the information content of different layers was based on counting the number of waves that sampled each layer. For future work, it is recommended to calculate the dispersion curve in the field and compare the information content for different wavelength ranges to determine if additional dispersion data should be obtained at the field. This becomes feasible with the increasing speed of computers and the reduction in processing times and would be an excellent way of adding dispersion data to assure a better distribution of information content throughout the entire profile.

Based on the large amount of V_s profiles that were found to fit a dispersion curve satisfactorily, the non-uniqueness of the solution was evident, which emphasizes the importance of finding other ways to constrain the solution. It would be very valuable to obtain data during the SASW field test to better constrain the problem. For instance, Tokimatsu (1997) suggests the use of measurements for the horizontal displacements in addition to the measurement of the vertical displacements.

For the Monte Carlo method implemented in this research, the limits established for V_s constrain the range of results obtained. Unfortunately, it was very difficult to explore a sufficient number of possibilities with the flexibility given by the widest limits due to

time constraints. The wider the V_s limits the higher the number of trials required to appropriately explore the model space and the longer the amount of time and computer resources necessary. In the best case scenario (i.e., most constraining V_s limits) it took twenty five 24-hour days to generate only 14 profiles with rms<1 with a Pentium II 500MHz processor. Due to the rapid improvement in computers, the processing time will be reduced in the future. Consequently, it is recommended to use a Monte Carlo type method as a viable inversion procedure, performing a thorough search of a sufficiently large model space. The implementation and use of a global search procedure would be of interest since the search for the minimum error would look for the global minimum and not for a local one.

An important next step in this research is to implement a user-friendly program. This program should include the entire inversion process from the initial estimate of the V_s profile to the use of model selection tools to compare various values for the prior information and select among them. The program should include options to help assume and compare prior information. When the final V_s profile is reported, it is important to be aware of the non-uniqueness of the solution by including error bars for the V_s values (i.e., such as the standard deviations presented here). It is also recommended to include the Bayesian criterion to select the simplest profile that fits the data satisfactorily, since reporting features that are not necessary to fit the data gives the false impression that these features are determined by the experimental data when they are not. The V_s profile reported is should be considered to be one possible representation of the real V_s variation with depth.

REFERENCES

Constable, S.C., Parker, R. L., and Constable, C.G., 1987. "Occam's Inversion: A Practical Algorithm for Generating Smooth Models from Electromagnetic Sounding Data", *Geophysics*, Vol. 52, p 289 - 300.

Curtis, A. and Lomax, A., 2001. "Tutorial: Prior Information, Sampling Distributions, and the Curse of Dimensionality", *Geophysics*, Vol. 66, No. 2, p. 372 - 378.

Ganji, V., Gucunski, N., and Nazarian, S., 1998. "Automated Inversion Procedure for Spectral Analysis of Surface Waves", *Journal of Geotechnical and Geoenvironmental Engineering*, Vol. 124, No. 8, p 757 - 770.

Gucunski, N. and Woods, R.D., 1991. "Inversion of Rayleigh Dispersion Curve in SASW Test", *5th International Conference on Soil Dynamics and Earthquake Engineering*, Kalsruke, Germany, p 127 – 138.

Gucunski, N. and Woods, R.D., 1992. "Numerical Simulation of the SASW Test", *Soil Dynamics and Earthquake Engineering*, Vol. 11, p 213 – 227.

Haskell, N.A., 1953. "The Dispersion of Surface Waves on Multilayered Media", *Bulletin of the Seismological Society of America*, Vol. 43, p 17 - 34.

Hebeler, G.L., Orozco M.C., and Rix G.J., 2001. "Site Characterization in the New Madrid Seismic Zone Using Advanced Surface Wave Methods," *Proceedings, Tenth International Conference on Soil Dynamics and Earthquake Engineering*, Philadelphia, PA, October.

Hisada, Y., 1994. "An Efficient Method for Computing Green' s Functions for a Layered Half-Space with Sources and Receivers at Close Depths", *Bulletin of the Seismological Society of America*, Vol. 84, No. 5, p 1456 - 1472.

Joh, S., 1996. "*Advances in Data Interpretation Technique for Spectral-Analysis-of-Surface-Waves (SASW) Measurements*" PhD dissertation, University of Texas at Austin.

Kausel, E. and Roësset, M., 1981. "Stiffness Matrices for Layered Soils", *Bulletin of the Seismological Society of America*, Vol. 71, No. 6, p 1743 - 1761.

Kennett, B.L.N., 1983. "*Seismic Wave Propagation in Stratified Media*", Cambridge University Press, UK, p 342.

Lai, C.G. and Rix, G.J., 1998. "*Simultaneous Inversion of Rayleigh Phase Velocity and Attenuation for Near-Surface Site Characterization*", Georgia Institute of

Technology, School of Civil and Environmental Engineering, *Report No. GIT-CEE/GEO-98-2*.

Lines, L.R. and Treitel S., 1984. "Tutorial: A Review of Least-Squares Inversion and Its Application to Geophysical Problems", *Geophysical Prospecting*, Vol. 32, p 159 - 186.

Malinverno, A., 2000. "A Bayesian Criterion for Simplicity in Inverse Problem Parametrization", *Geophysical Journal International*, Vol. 140, p 267 - 285.

Nazarian, S. and Desai, M.R., 1993. "Automated Surface Wave Method: Field Testing", *Journal of Geotechnical Engineering*, Vol. 119, No. 7, p 1094 - 1111.

Rix, G.J., Hebeler, G.L., and Orozco, M.C., 2002. "Near-Surface V_s Profiling in the New Madrid Seismic Zone Using Surface-wave Methods," *Seismological Research Letters*, June.

Rix, G.J. and Lai, C.G.., 1998. "Simultaneous Inversion of Surface Wave Velocity and Attenuation", *Geotechnical Site Characterization*, Proceedings of the First International Conference on Site Characterization, Atlanta, April 19-22, edited by Robertson, P. K. and Mayne, P. W.

Rix, G.J., Lai C.G., Orozco M.C., Hebeler G.L., and Roma V., 2001. "Recent Advances in Surface Wave Methods for Geotechnical Site Characterization," *Proceedings, XV International Conference on Soil Mechanics and Geotechnical Engineering*, Instanbul.

Rix, G.J., Lai, C.G., and Spang Jr., A.W., 2000. "In Situ Measurement of Damping Ratio Using Surface Waves", *Journal of Geotechnical and Geoenvironmental Engineering*, Vol. 126, No. 5, p 472 - 480.

Rix, G.J. and Leipski, E.A., 1991. "Accuracy and Resolution of Surface Wave Inversion", *Recent Advances in Instrumentation, Data Aquisition, and Testing in Soil Dynamics*, Geotechnical Special Publication No. 29, ASCE.

Roësset, J.M., Chang, D.W., and Stokoe, K.H. II, 1991. "Comparison of 2-D and 3-D Models for Analysis of Surface Wave Tests", *5th International Conference on Soil Dynamics and Earthquake Engineering*, Kalsruke, Germany, p 111 – 126.

Santamarina, J.C. and Fratta, D., 1998. "*Introduction to Discrete Signals and Inverse Problems in Civil Engineering*" ASCE Press.

Sen, M. and Stoffa, P.L., 1995. "*Global Optimization Methods in Geophysical Inversion*", Advances in Exploration Geophysics 4, series editor: A.J. Berkhout, Elsevier.

Scales, J.A. and Tenorio, L., 2001. "Tutorial: Prior Information and Uncertainty in Inverse Problems", *Geophysics*, Vol. 66, No. 2, p. 389 - 397.

Stokoe, K.H., Rix, G.J., and Nazarian, S., 1989. "In Situ Seismic Testing with Surface Waves", *Proceedings, XII International Conference on Soil Mechanics and Foundation Engineering*, p 331 - 334.

Stokoe, K.H., Wright, S.G., Bay, J.A., and Roësset, J.M.,1994. "Characterization of Geotechnical Sites by SASW Method", *Geophysical Characterization of Sites*, Edited R.D.Woods, International Science Publisher, New Hampshire.

Tarantola, A., 1987. "*Inverse Problem Theory: Methods for Data Fitting and Model Parameter Estimation*", Elsevier.

Thomson, W.T., 1950. "Transmission of Elastic Waves through a Stratified Solid Medium", *Journal of Applied Physics*, Vol.21, p 89 - 93.

Tokimatsu, K., 1997. "Geotechnical Site Characterization Using Surface Waves", *Earthquake Geotechnical Engineering*, Ishihara (ed.), Balkema, Rotterdam, p 1333 – 1368.

Tokimatsu, K., Kuwayama, S., Tamura, S., and Miyadera, Y, 1991. "Effects of Multiple Modes on Rayleigh Wave Dispersion Characteristics", *Soils and Foundations*, Vol. 31, No. 2, p 153 - 163.

Tokimatsu, K., Shinzawa, K., and Kuwayama, S., 1992b. "Use of Short-Period Microtremors for Vs Profiling", *Journal of Geotechnical Engineering*, Vol. 118, No. 10, p 1544 - 1558.

Tokimatsu, K., Tamura, S., and Kojima, H, 1992a. "Effects of Multiple Modes on Rayleigh Wave Dispersion Characteristics", *Journal of Geotechnical Engineering*, Vol. 118, No. 10, p 1529 - 1543.

Tuomi, K.E., and Hiltunen, D.R., 1997. "Experimental Evaluation of the Uncertainty of the SASW method", *Proceedings, XIV International Conference on Soil Mechanics and Foundation Engineering*, Hamburg, Germany, Sept 6-12, p 611-614.

Ulrych, T.J., Sacchi, M.D., adn Woodbury, A., 2001. "Tutorial: A Bayes Tour of Inversion: a Tutorial", *Geophysics*, Vol. 66, No. 1, p 55 - 69.

Vrettos, C., 2000. "Waves in Vertically Inhomogeneous Soils", *Wave Motion in Earthquake Engineering*, Chapter 7, WIT Press, p 247 - 282.

Wiggins, R.A., 1972. "The General Linear Inverse Problem: Implication of Surface Waves and Free Oscillations for Earth Structure", *Reviews of Geophysics and Space Physics,* Vol. 10, No. 1, p 251 – 285.

Xia, J., Miller, R.D., and Park, C.B., 1999. "Estimation of Near-Surface Shear-Wave Velocity by Inversion of Rayleigh Waves", *Geophysics*, Vol. 64, No. 3, p 691 - 700.

Yuan, D. and Nazarian, S., 1993. "Automated Surface Wave Method: Inversion Technique", *Journal of Geotechnical Engineering*, Vol. 119, No. 7, p 1112 - 1126.

VITA

Mrs. Orozco was born in Evanston, Illinois, but lived most of her life in Bogota, Colombia. She has a B.S. in Civil Engineering (CE) from Universidad de los Andes (Bogota), where she graduated with a 4.4/5.0 GPA. This was the best GPA of her graduating class and of at least seven previous graduating classes. As an undergraduate she was a teaching assistant for surveying practices, materials' lab, and soil mechanics' lab. She also worked as an engineering assistant at a geotechnical consulting firm.

After obtaining her BS, she was offered a National Science Foundation (NSF) Graduate Fellowship and went to Northwestern University where she completed her M.S. in Geotechnical engineering obtaining a 4.0/4.0 GPA. She worked with Dr. Richard Finno on her master thesis, which focused on compaction grouted micropiles.

She moved to Atlanta, where she worked for GeoSyntec Consultants and was involved in a variety of projects, mostly related to permit applications for Municipal Solid Waste Landfills. Some of her tasks were to design reinforced soil walls, to manage a pilot program for blast densification of sand, to work on geotechnical site characterization, to perform settlement calculations, and to run 2-D and 3-D slope stability analyses.

After this, Mrs. Orozco went to Georgia Tech, where she earned a Ph.D. in Geotechnical engineering with a 3.9/4.0 GPA. The first two years she was supported by her NSF Fellowship. Her doctoral work focused on the inversion analysis of surface wave test data and was guided and partially supported by Dr. Glenn Rix. Additionally, she received the President's Fellowship from Georgia Tech.